Organic-geochemical studies of microbial lipids and carbon flow in oxygen-deficient marine environments

Dissertation
zur Erlangung des Doktorgrades
der Naturwissenschaften
- Dr. rer. nat. -

Am Fachbereich Geowissenschaften
der Universität Bremen

vorgelegt von

Sitan Xie

Bremen
September 2012

1. Gutachter: Prof. Dr. Kai-Uwe Hinrichs
2. Gutachter: Prof. Dr. Gesine Mollenhauer

Date of defense: September 27, 2012

“积土成山，风雨兴焉；积水成渊，蛟龙生焉；积善成德，而神明自得，圣心备焉。故不积跬步，无以至千里；不积小流，无以成江海.....”

——荀子《劝学篇》

TABLE OF CONTENTS

Thesis Abstract I

Zusammenfassung III

List of Abbreviations V

Chapter I Introduction 1
I.1 General Introduction 2
I.2 Methods 15
I.3 Objectives of this Thesis 23
I.4 Contribution to Publications 24
I.5 References 25

Chapter II Distribution of eukaryotic and bacterial intact polar lipids in the oxygen minimum zone of the Eastern Tropical North Pacific Ocean 37
II.1 Abstract 38
II.2 Introduction 38
II.3 Experiments 40
II.4 Results and Discussion 42
II.5 Conclusions 55
II.6 Acknowledgements 55
II.7 References 56

Chapter III Distribution of glycerol ether lipids in the oxygen minimum zone of the Eastern Tropical North Pacific Ocean 63
III.1 Abstract 64
III.2 Introduction 64
III.3 Experiments 68
III.4 Results and Discussion 71
III.5 Conclusions 82
III.6 Acknowledgements 83
III.7 References 83

Chapter IV Turnover of microbial lipids in the deep biosphere and activity of benthic archaeal populations 91
IV.1 Abstract 92
IV.2 Introduction 93
IV.3 Methods 95
IV.4 Calculations for Modeling Work 97
IV.5 Results and Discussion 104
IV.6 Acknowledgements 113
IV.7 References 114

IV.S1. Supporting Figures 118

Chapter V Ethane- and propane-producing potential and molecular characterization of an ethanogenic enrichment in anoxic estuarine sediment 123
V.1 Abstract 124
V.2 Introduction 124
V.3 Material and Methods 127
V.4 Results 132
V.5 Discussion 144
V.6 Conclusions 150
V.7 Acknowledgements 150
V.8 References 150
V.S1. Supporting Tables 156
V.S2. Supporting Figures 166

Chapter VI Concluding Remarks and Outlook 169
IV.1 Summary and Conclusions 170
IV.2 Outlook 173
IV.3 References 174

Acknowledgements 179

Thesis Declaration 183

THESIS ABSTRACT

In order to get a better understanding of microbes' role in marine element cycles, organic-geochemical studies targeting microbial lipids and metabolic products in oxygen-deficient oceanic water column and sediments were carried out.

Intact polar membrane lipids (IPLs) as biomarker for living biomass have been established as a tool in microbial ecology and already successfully used in a variety of surface ecosystems. In the Eastern Tropical North Pacific Ocean (ETNP), the oxygen minimum zone (OMZ) presents between 100~800 m depths characterized by dissolved oxygen concentration of less than 20 μM. IPLs were predominant by eukaryotic and bacterial IPLs. Intact polar isoprenoid glycerol dialkyl glycerol tetraethers (IP GDGTs), the biomarker for living Archaea, were detected after purification of the total lipids extract (TLE) using preparative HPLC. Glycolipids which are mainly derived from photosynthetic membranes were dominant in the euphotic zone. With increasing depth, phospholipids and betaine lipids (BL) became dominant components in the OMZ and deep oxycline layers. In the surface layers where light and oxygen could penetrate, photosynthetic organisms, such as photosynthetic algae and cyanobacteria, produced abundant glycolipids. Glycolipids were decreased quickly with increasing depth probably due to remineralization. In the oxygen minimum zone, eukaryotic and bacterial organisms which could survive under oxygen limitation condition accumulated and produced abundant phospholipids and BL. Ratios between phosphorous-containing lipids and their corresponding non-phosphorous-containing substitute lipids, e.g., SQDG/PG and BL/PC (SQDG: sulfoquinovosyldiacylglycerol, PG; phosphatidylglycerol, PC: phosphatidylcholine) were high at depths where phosphate was abundant suggesting that not only phosphate limitation but also the microbial community inhabiting in the oceanic water impact enrichment of substitute lipids. Archaeal IP GDGTs peaked in the upper layers of the OMZ, which exhibited different from peaks of most glycerol ether core lipids (glycerol ether lipids without head groups representing fossil signal) in the deeper depths of the OMZ indicating that IP GDGTs represented an in-situ contribution from the planktonic archaeal community whereas core lipids were exported downward and accumulated in the mid OMZ with a longer residence time.

After exported to the sediment, IPLs derived from the upper water column would either rapidly degrade or bury as fossil components. Degradation kinetics of IPLs could influence the interpretation of abundant observed archaeal IPLs in the deep biosphere. Based on a radiotracer

experiment and a new comprehensive modeling work, half-life of model archaeal IPL increased with depth from 20 to 310 kyrs, which was relatively longer than the microbial community turnover times of 1.6 to 73 kyrs. It is suggested that a substantial fraction of the archaeal IPLs in marine sediments were fossil components of past microbial populations. Based on the observed IPL concentration and their degradation kinetics, the in-situ synthesis rates of archaeal IPL fell into a range of 1000 pg ml^{-1} yr^{-1} to 0.2 pg ml^{-1} yr^{-1} from surface to 1 km depth. Such a result is equivalent to the annual production of 7×10^{5} to 140 archaeal cells ml^{-1} sediment. Due to the high fossil proportion of archaeal IPLs of probably more than 80%, previously estimated subseafloor living biomass were probably too high. Therefore, the abundant archaeal IPL in subsurface sediments may not reflect a dominant archaeal community of deep biosphere.

Ethane and propane as metabolic products of microorganisms are widely detected in the anoxic cold marine sediments. Through a test of several C-2 and C-3 compounds for their alkane-producing potential in anoxic Wadden Sea sediment, alkane production could be observed from ethylene, ethanethiol and propanethiol. Among these three substrates, ethylene had the maximum conversion efficiency for alkane production. Compared to the incubation with sterilized sediment, methanogens were involved in the alkane production. The initial H_2 concentration required to stimulate ethanogenesis from ethylene was lower than 0.01% H_2. After 80-days of incubation, an ethane-producing enrichment with ethylene as the substrate was used for molecular characterization. *Methanocalculus* and sequences belonging to the *Methanomicrobiales* were the dominant groups in the archaeal 16S rRNA gene library and the *mcrA* gene library, respectively. *Methanocalculus* is a candidate responsible for ethanogenesis from ethylene.

ZUSAMMENFASSUNG

Für ein besseres Verständnis der mikrobiellen Rolle in marinen Elementkreisläufen umfasst diese Arbeit organisch-geochemische Studien, die sich mit mikrobiellen Lipiden und Stoffwechselprodukten in den sauerstoffarmen Bereichen der Wassersäule sowie Sedimenten beschäftigen.

Die Untersuchung von intakten polaren Lipiden (IPLs), als Biomarker für lebende Biomasse, stellt eine etablierte Methode der mikrobiellen Ökologie dar und wurde bereits in unterschiedlichen Ökosystemen erfolgreich angewandt. Die sauerstoffarme Zone (OMZ, von engl., oxygen minimum zone) im östlich tropischen Nord Pazifik liegt zwischen 100-800 m Wassertiefe mit Sauerstoffkonzentrationen kleiner 20 µM. Die IPL Analysen zeigten, dass diese durch eukaryotische und bakterielle IPLs dominiert wurden. Während intakten polaren isoprenoid Glycerol Dialkyl Glycerol Tetraethern (IP GDGTs), als Indikator für lebende archaeelle Biomasse, erst nach einer Aufreinigung des Totalen Lipid Extraktes mittels präparativer HPLC detektiert werden konnten. In der euphotische Zone dominierten glykosidische Lipide, welche von photosynthetischen Organismen stammen. Dagegen stellten Phospholipide und Betainlipide (BL) die Hauptkomponenten der OMZ und der Oxykline im Tiefenwasser dar. Dies lässt darauf schließen, dass im Oberflächenwasser, unter Anwesenheit von Licht und Sauerstoff, photosynthetische Organismen wie Algen und Cyanobakterien glykosidische Lipide produzieren. Die Abnahme der glykosidischen Lipide mit zunehmender Tiefe ist wahrscheinlich der Remineralisation zuzuordnen. Im Gegensatz stellen in der OMZ Eukaryoten und Bakterien, welche unter sauerstoff-limitierten Bedingungen überleben können und dort vermehrt anzutreffen sind, die Quelle der Phospholipide und BL dar. Verhältnisse zwischen phosphorhaltigen Lipiden und ihrer entsprechenden nicht-phosphorhaltigen Vertreter, z.B., SQDG/PG and BL/PC (SQDG: Sulfoquinovosyldiacylglycerol, PG; Phosphatidylglycerol, PC: Phosphatidylcholine) mit hohen Werten in Wassertiefen mit hohem Phophatgehalt deuten darauf hin, dass sowohl die Limitation in Phosphat als auch die mikrobielle Gemeinschaft der Wassersäule eine Anreicherung der nicht-phosphorhaltigen Lipide verursacht. Die Verteilung der IP GDGTs zeigte Maxima in den oberen Bereichen der OMZ. Diese weicht vom Auftreten der meisten Glycerol Ether Kernlipide (Glycerol Ether Lipide ohne Kopfgruppe als Indikator eines fossilen Signals) ab, welche ihr Hauptvorkommen in den größeren Wassertiefen der OMZ aufweisen. Dies zeigt, den in situ Eintrag von IP GDGTs durch die planktische archaeelle Gemeinschaft, wobei die Kernlipide in

die mittlere OMZ exportiert werden und dort akkumulieren.

Nach dem Export der IPLs aus den oberen Bereichen der Wassersäule in das Sediment, werden diese schnell abgebaut oder werden als fossile Komponenten überliefert. Dabei kann die Abbaukinetik von IPLs die Interpretation von vorhandenen archaeellen IPLs in der tiefen Biosphäre beeinflussen. Basierend auf einem radioaktivem Tracer Experiment und einer neuen umfassenden Modellierung steigt die Halbwertszeit der modellierten archaeellen IPLs mit der Tiefe von 20 000 auf 310 000 Jahren, welches länger ist als die Umsatzrate der mikrobiellen Gemeinschaft von 1 600 bis 73 000 Jahren. Dies deutet darauf hin, dass ein entschiedener Anteil der archaeellen IPLs in marinen Sedimenten fossilen Komponenten aus vergangenen mikrobiellen Populationen angehört. Unter Hinzunahme der beobachteten IPL Konzentrationen und ihrer Abbaukinetik ergeben sich in situ Syntheseraten der archaeellen IPLs von 1000 pg ml^{-1} yr^{-1} bis zu 0.2 pg ml^{-1} yr^{-1} von der Oberfläche bis zu 1 km Tiefe. Dieses Ergebnis entspricht einer jährlichen Produktion von 7×10^{5} zu 140 archaeellen Zellen ml^{-1} Sediment. Aufgrund des hohen Anteils an fossilen IPLs von ca. 80% erscheinen vorherige Annahmen zur lebenden Biomasse der tiefen Biosphäre zu hoch. Daher spiegelt die Verteilung der archaeellen IPLs in tiefen Sedimenten womöglich nicht die von Archaeen dominierte Gemeinschaft der tiefen Biosphäre wider.

Ethan und Propan als mikrobielle Stoffwechselprodukte sind in anoxischen und kalten marinen Sedimenten weit verbreitet. Die potentielle Alkanproduktion wurde anhand von diversen C-2 und C-3 Substraten an anoxischen Sedimenten aus dem Wattenmeer getestet. Dabei konnte eine Alkanproduktion durch Ethylen, Ethanthiol und Propanthiol festgestellt werden. Von diesen drei Substraten besaß Ethylen die höchste Umsatzeffizienz. Im Vergleich zur Inkubation der sterilisierten Sedimente wurde die Alkanproduktion auf Methanogene zurückgeführt. Dabei lagen die Anfangskonzentration von H_2 für die Stimulierung der Ethanogenese durch Ethylen unter 0,01%. Nach einer Inkubationszeit von 80 Tagen wurde dieser Inkubationsansatz mit dem Substrat Ethylen einer molekularen Charakterisierung unterzogen. Als dominante Gruppen konnten unter Verwendung der archaeellen 16S rRNA gene library sowie der *mcrA* gene library *Methanocalculus* und Sequenzen der *Methanomicrobiales* identifiziert werden. In diesem Fall stellt *Methanocalculus* ein Kanditat für die Ethanogenese mittels Ethylen dar.

LIST OF ABBREVIATIONS

1Gly	Monoglycosyl
2Gly	Diglycosyl
16S rRNA	Small subunit of ribosomal ribonucleic acid with a sedimentary unit of 16
α	Alpha particles or alpha-proteobacteria
a_{TOC}, b_{TOC}	Intercept and slope of log k-log t plot for TOC degradation
a', b'	Intercept and slope of log k'-log t plot for IPL degradation
AEG	Acyletherglycerol
Anammox	Anaerobic oxidation of ammonium
APCI	Atmospheric pressure chemical ionization
AR	Archaeol or diphytanoldiether
AS	Arabian Sea
β	Beta particles or beta-proteobacteria
BB	Bay of Bengal
BD	Below detection
BES	2-bromoethanesulfonic acid
BIS	Black Sea
BL	Betanie lipids
BL DGCC	Betaine lipid diacylglyceryl carboxyhydroxymethylcholine
BL DGTA	Betaine lipid diacylglyceryl hydroxymethyl-trimethyl-β-alanine
BL DGTS	Betaine lipid diacylglyceryl trimethylhomoserine
Bq	Becquerel
Branched GDGTs	Branched glycerol dialkyl glycerol tetraethers
BS	Baltic Sea
γ	Gamma rays or gamma-proteobacteria
C	Gene library coverage
$Cell_{pro\text{-}TOC}$	Cell production rate converted from IPL production rate ($IPL_{pro\text{-}TOC}$)
Cer	Ceramides
C_{46} GTGT	Glycerol trialkyl glycerol triethers
CH_3-S-CoM	Methylthioethanesulfonic acid
CH_3CH_2-S-CoM	Ethylthioethanesulfonic acid
Ci	Curie
CoB-SH	Coenzyme B
CoM-SH	Coenzyme M
CoM-S-S-CoB	Heterodisulfide of coenzyme M and coenzyme B
Core lipids	Glycerol ether core lipids
CPM	Counted decays per minute
Cren	Crenarchaeota
$\delta^{13}C$	Stable carbon isotopic value
DAG	Diacylglycerol
DEG	Dietherglycerol

DGDG	Diglycosyldiacylglycerol
DHVE-8 group	Deep sea hydrothermal vent Euryarchaeota group 8
DIC	Dissolved inorganic carbon
DMS	Dimethylsulfide
DOM	Dissolved organic matter
DPG	Diphosphatidylglycerol
DPM	Decays per minute
DPS	Decays per second
ε	Epsilon-proteobacteria
ENP	Eastern North Pacific
ESI	Electrospray ionization
ESP	Eastern South Pacific
ESPC	Eastern South Pacific off Chile
ESPP	Eastern South Pacific off Peru
ESTNP	Eastern Subtropical North Pacific
ETNP	Eastern Tropical North Pacific Ocean
Eury	Euryarchaeota
GA	Gulf of Alaska
GDD-Cren	Isoprenoid GDDs contain one glycerol moiety less than crenarchaeol
GDGT-0	GDGT with acyclic biphytane moieties
GDGT-Cren	Crenarchaeol
GDGT-Cren Iso	Crenarchaeol isomer
GlcDGD	Glucosyl-diphytanylglyceroldiether
Gly-Cer	Glycosylceramides
H-1020	A tentatively identified H-shaped GDGT
H_4MPT	Tetrahydromethanopterin
HS-CoM	Mercaptoethanesulfonic acid
IB-GDGTs	Hybrid isoprenoid/branched GDGTs
IP GDGTs	Intact polar GDGTs
[IPL_0]	IPL concentration at surface sediment
IPL_{deg}	IPL degradation rate
IPL_{pro}	IPL production rate
$IPL_{pro\text{-}TOC}$	Modeling IPL production rate based on TOC degradation
IPLs	Intact polar membrane lipids
[IPL_t]	IPL concentration at time t
IPL_{input} Rate	Modeling IPL production rate according to power function
Isoprenoid GDDs (iso-GDDs)	Isoprenoid glycerol dialkanol diethers
Isoprenoid GDGTs (iso-GDGTs)	Isoprenoid glycerol dialkyl glycerol tetraethers
k_{TOC}	TOC degradation rate constant
k'	IPL degradation rate constant
LSC	Liquid Scintillation Counting

mbsf	Meters below sea floor
mcrA	Methyl-coenzyme M reductase A
MGDG	Monoglycosyldiacylglycerol
NPIW	North Pacific Intermediate Water
OB-GDGTs	Overly branched GDGTs
OH-AR	*sn*-2-hydroxyarchaeol
OH-eAR	Extended hydroxyarchaeol
OH-GDDs	Hydroxylated isoprenoid GDDs
OH-GDGTs	Hydroxylated isoprenoid GDGTs
OMZ	Oxygen minimum zone
OUTs	Operational taxonomic units
PA	Phosphatidic acid
PC	Phosphatidylcholine
PCA	Principal Component Analysis
PCR	Polymerase chain reaction
PDME	Phosphatidyl-(N, N)-dimethylethanolamine
PE	Phosphatidylethanolamine
PG	Phosphatidylglycerol
PG	Persian Gulf
PI	Phosphatidylinositol
Pla	Planctomycetes
PM	Particulate matter
PME	Phosphatidyl-(N)-methylethanolamine
POC	Particulate organic carbon
POM	Particulate organic matter
PS	Phosphatidylserine
PUFA	Polyunsaturated fatty acids
Q-TOF	Time-of-Fight mass spectrometer
Redox	Reduction-oxidation
RS	Red Sea
SB-GDGTs	Sparsely branched GDGTs
SQ	Sulfoquinovosyl
SQDG	Sulfoquinovosyldiacylglycerol
SRB	Sulfate-reducing bacteria
SST	Sea surface temperature
SWACM	Southwest African Continental Margin
t	Time
Δt	Short time interval
$t_{1/2}$	Half-life of IPL
$t_{initial}$	Initial ages of sediment, an expression of organic matter reactivity at water-sediment interface
TEA	Terminal electron acceptor
TLEs	Total lipids extracts

TN	Total nitrogen
TOC	Total organic carbon
[TOC_0]	TOC concentration at time zero
[TOC_t]	TOC concentration at time t
WBS	Western Bering Sea
Z_m	Mean maximal mixed-layer
Z_e	Euphotic layer

Chapter I

Introduction

I.1. GENERAL INTRODUCTION

The ocean plays a crucial role on the global carbon cycle. Microbes inhabiting in the ocean control the ocean's carbon flux. In order to investigate the distribution of microbial communities and their metabolism in the ocean, organic-geochemical studies of microbial lipids and carbon flow in oxygen-deficient water column (e.g., oxygen minimum zones, OMZs) and sediments (e.g., anoxic surface sediment and deep biosphere) were carried out in this thesis. In this introduction chapter, firstly, the role of the ocean in the global carbon cycle will be generally introduced. Secondly, the microbial control of oceanic carbon flux will also be presented. Thirdly, the geological settings and microbial processes in the oxygen minimum zones (OMZs) and deep biosphere will be introduced subsequently. Additionally, the presence of light hydrocarbons as microbial metabolic products in anoxic marine sediment will be summarized.

I.1.1. The role of the ocean in the global carbon cycle

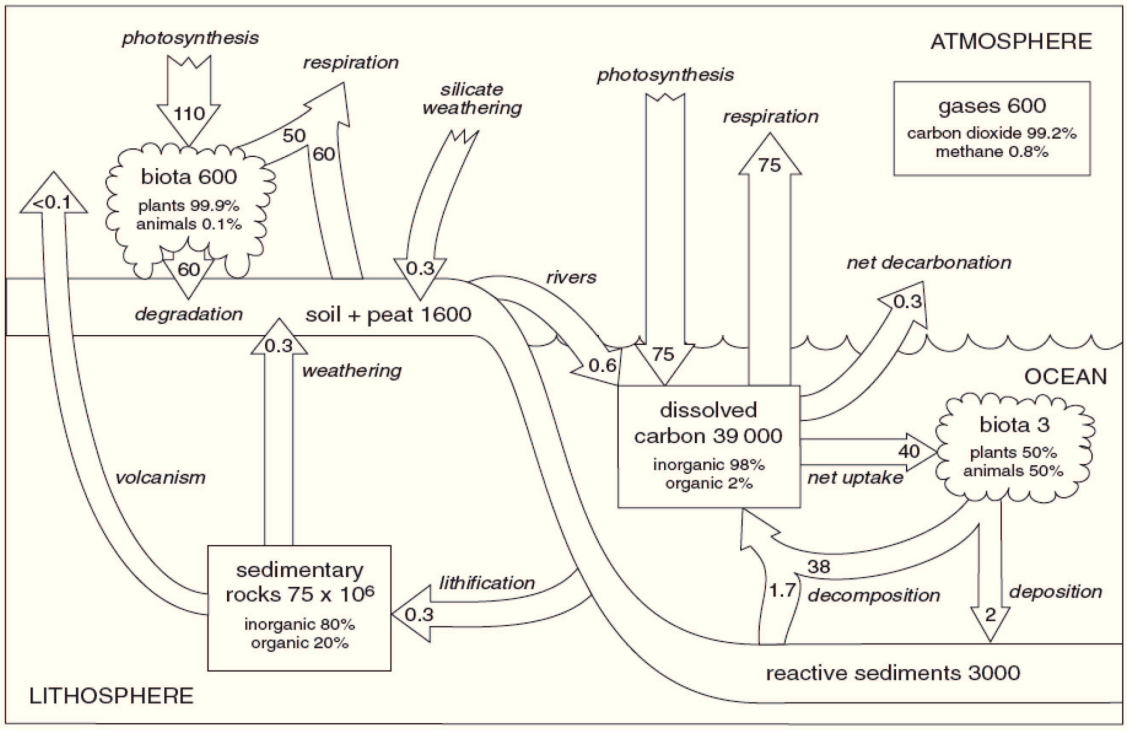

Fig. I.1. Simplified sketch of the preindustrial carbon cycle. The sizes of the main reservoirs (boxes) and annual fluxes (arrows) are given in Gt carbon (10^{15} g). Information is compiled from previous studies, e.g., Bolin et al. (1979, 1983), De Vooys (1979), Kempe (1979), Mopper and Degens (1979), Siegenthaler and Sarmiento (1993), Sundquist (1993), Arthur (2000) and Falkowski et al. (2000). Figure is taken from Killops and Killops (2005).

The global carbon cycle consists of two subcycles, geochemical and biochemical cycles. Geochemical subcycle contains the largest reservoir of carbon (75×10^6 Gt of C; Fig. I.1), sedimentary rocks, with the residence times up to millions of years (Killops and Killops, 2005). This long-term geochemical cycle involves the carbon exchange between sedimentary rocks and the ocean, atmosphere, biota and soils (Berner, 1999; Killops and Killops, 2005). The biochemical subcycle is smaller (40×10^3 Gt of C), which involves carbon exchange within the surficial reservoirs, including the ocean, fresh water, atmosphere, soils and biosphere (Berner, 1999; Killops and Killops, 2005). Turnover time of the carbon in biochemical subcycle is up to thousand years (Des Marais, 1997; Killops and Killops, 2005). Although the geochemical subcycle hosts 99.95% of the total carbon on the Earth, a large proportion of the carbonate and all the organic matter in this cycle are actually originated from the smaller biochemical subcycle (Killops and Killops, 2005).

The ocean plays a crucial role on the global carbon cycle. The marine part of the biochemical subcycle contains 50 times higher dissolved inorganic carbon (DIC) than that of the atmosphere (Falkowski et al., 2000; Killops and Killops, 2005). The fact that the ocean hosts one of the largest parts of the total carbon inventory suggests that the ocean determines atmospheric CO_2 concentrations, not vice versa (Falkowski et al., 2000; Marinov and Sarmiento, 2004). When atmospheric CO_2 dissolves in the ocean, CO_2 is found in three main forms of DIC (CO_2, CO_3^{2-}, HCO_3^-) through a sequence of reversible reactions. Conversion of DIC to organic carbon is mainly performed by phytoplankton through photosynthesis in the euphotic zone of the ocean (Fig. I.2). Only 25% of the carbon transports from the surface into the interior of the ocean (Falkowski et al., 1998; Laws et al., 2000), where it is subsequently oxidized by heterotrophic respiration. Finally, less than 1% of the organic matter produced in the euphotic zone can be exported and buried in the marine sediments (Suess and Müller, 1980; Killops and Killops, 2005), and fuel benthic life there.

I.1.2. Microbial control of oceanic carbon flux

The ocean hosts half of the global primary production on the Earth (Falkowski et al., 1998; Field et al., 1998). A large fraction of primary production is in the form of dissolved organic matter (DOM) through various mechanisms. This part of the primary production is almost taken up by Bacteria and Archaea (Fig. I.3; Azam and Ammerman, 1984; Ducklow and Carlson, 1992).

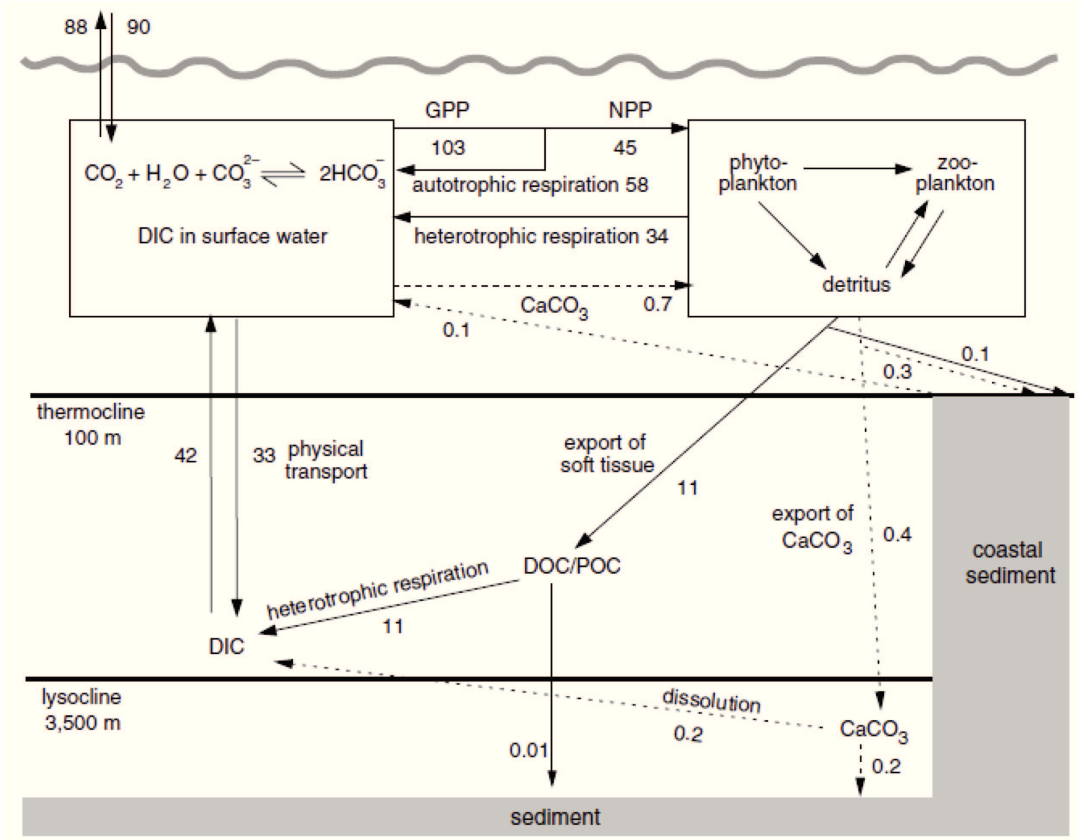

Fig. I.2. Summary of the carbon cycle in the ocean. After dissolving in the ocean, CO_2 is found in three main forms of DIC (CO_2, CO_3^{2-}, HCO_3^-). DIC is converted to organic carbon by phytoplankton photosynthesis in the upper ocean. Large fraction of organic carbon is respired by heterotrophic respiration and returned to the atmosphere, while only 25% sinks into the interior of the ocean (Falkowski et al., 1998; Laws et al., 2000). This vertical transport of organic carbon is known as "soft-tissue pump" (Volk and Hoffert, 1985). Besides converted to organic carbon, minor component of DIC in the surface layer are utilized by phytoplankton and zooplankton to form $CaCO_3$ shells, which sink into the deeper ocean. Half of the $CaCO_3$ in the deep ocean is re-dissolved and joins the DIC pool (known as "carbonate pump"; Milliman, 1993), while the other half buries in the deep sediments. The soft-tissue combined with carbonate pumps are the full "biological pump" (Volk and Hoffert, 1985; Marinov and Sarmiento, 2004). Additionally, "solubility pump" also contributes to the higher DIC concentration in the ocean interior. "Solubility pump" is the process that cool and dense water mass (especially in the North Atlantic and in the Southern Ocean confluence) controls the sequestration of atmospheric CO_2 in the ocean interior (Falkowski et al., 2000), since CO_2 is more soluble in cold and high salinity water. Figure is taken from Prentice et al. (2001).

Most of the DOM is respired to CO_2 by heterotrophy respiration, while a fraction is assimilated by organisms and returned into the food chain (Fig. I.3). The sinking aggregates, e.g., fecal pellets, macroaggregates and marine snow, are a dominate vehicle for exporting organic matter to the

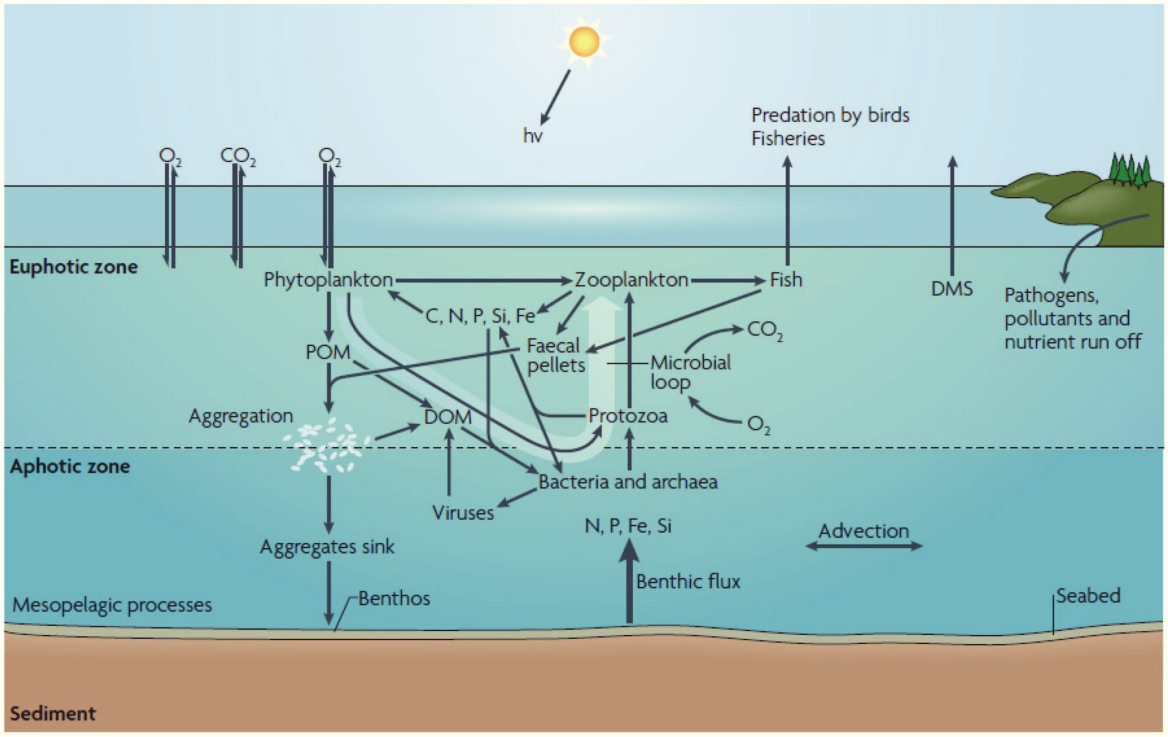

Fig. I.3. Microbial control of oceanic carbon flux. DMS, dimethylsulfide; hv, light; POM, particulate organic matter. Figure is taken from Azam and Malfatti, 2007.

deep ocean (Azam and Malfatti, 2007). A fraction of organic matter transports to the deep-sea sediments, where they are recycled by detrital-feeding benthic organisms. The uptake of organic matter by microorganisms is a major carbon-flow pathway in the ocean (Williams, 1981; Azam, 1998; Williams, 1998; Azam and Malfatti, 2007). Therefore, investigation of microbial processes in the marine environment will provide us a better understanding of the marine carbon cycle, and how these carbon flux patterns might respond to the global change.

I.1.3. Oxygen minimum zones (OMZs)

I.1.3.1. The OMZs in the modern ocean

The oxygen minimum zones (OMZs) are the oceanic water column characterized by dissolved oxygen concentrations of less than 20 µM at depths between ~100 and ~800 m. In the modern ocean, the total surface of the OMZs is 30.4 millions of km^2, which accounts for ~8% of the total oceanic area (Paulmier and Ruiz-Pino, 2009). In the open ocean, there are four well

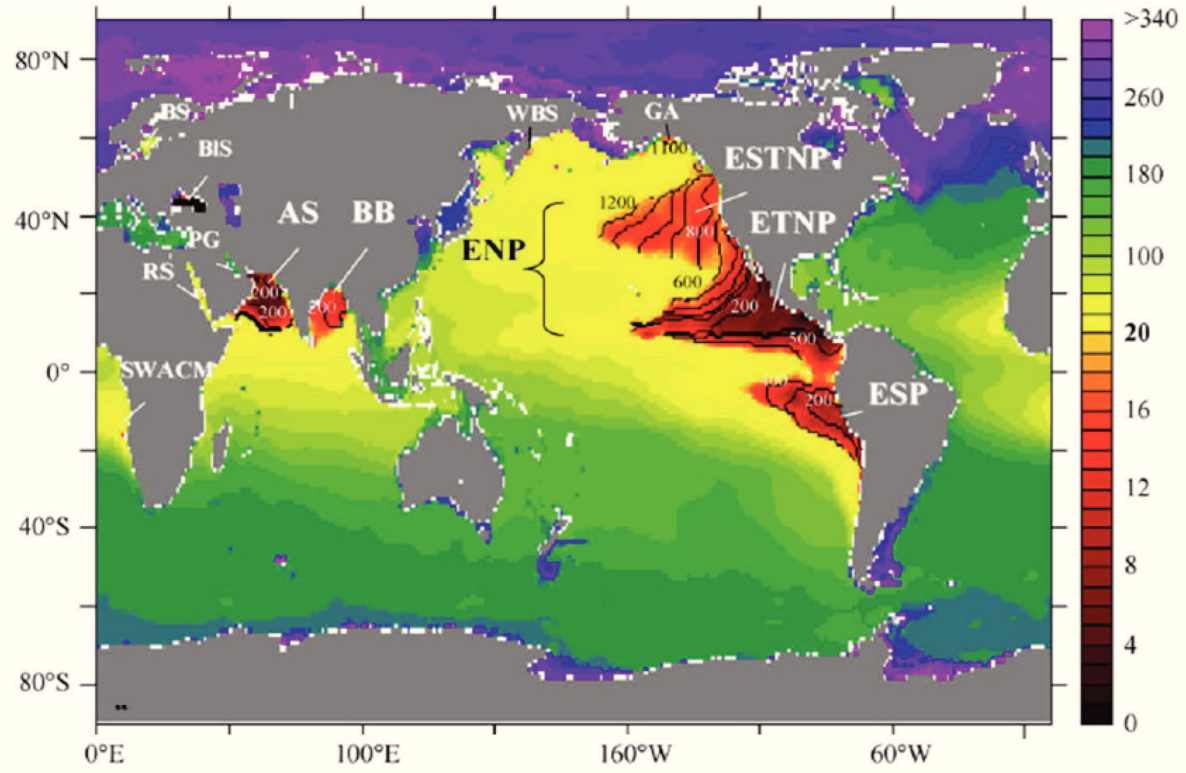

Fig. I.4. The distribution of the OMZs (in red) in the modern ocean. The color bar refers to O_2 concentration (μM). The isolines indicate the upper boundary (m) of the OMZ. Abbreviations of permanent OMZs: AS, Arabian Sea; BB, Bay of Bengal; ENP: Eastern North Pacific; ETNP, Eastern Tropical North Pacific; ESTNP, Eastern Subtropical North Pacific; ESP, Eastern South Pacific. Abbreviations of seasonal OMZs: WBS, Western Bering Sea; GA, Gulf of Alaska. Others: BS, Baltic Sea; BlS, Black Sea; RS, Red Sea; PG, Persian Gulf; SWACM, Southwest African Continental Margin. Figure is taken from Paulmier and Ruiz-Pino (2009).

known permanent OMZs: Eastern South Pacific (ESP), Eastern North Pacific (ENP), Arabian Sea (AS) and Bay of Bengal (BB) (Fig. I.4; Paulmier and Ruiz-Pino, 2009).

The OMZs can be formed when the oxygen demand required for respiration exceeds that is available in poorly ventilated regions (Wright et al., 2012). As oxygen concentrations decrease, the amount of anaerobic microorganisms will increase, which leads to an energy diversion from aerobic into anaerobic metabolism according to a defined order of terminal electron acceptors (TEA; Fig. I.5, label 1; Diaz and Rosenberg, 2008; Wright et al., 2012). Anaerobic microbial metabolism results in production of greenhouse gases, such as nitrous oxide and methane, as well as loss of fixed nitrogen (Wright et al., 2012). The chemical gradients observed in the water column of the OMZs (Fig. I.5, label 1) are also found in the interior of the ocean, which are in the form of sinking organic particles (Fig. I.5, label 2 and 3; Alldredge and Silver, 1988). Oxygen is

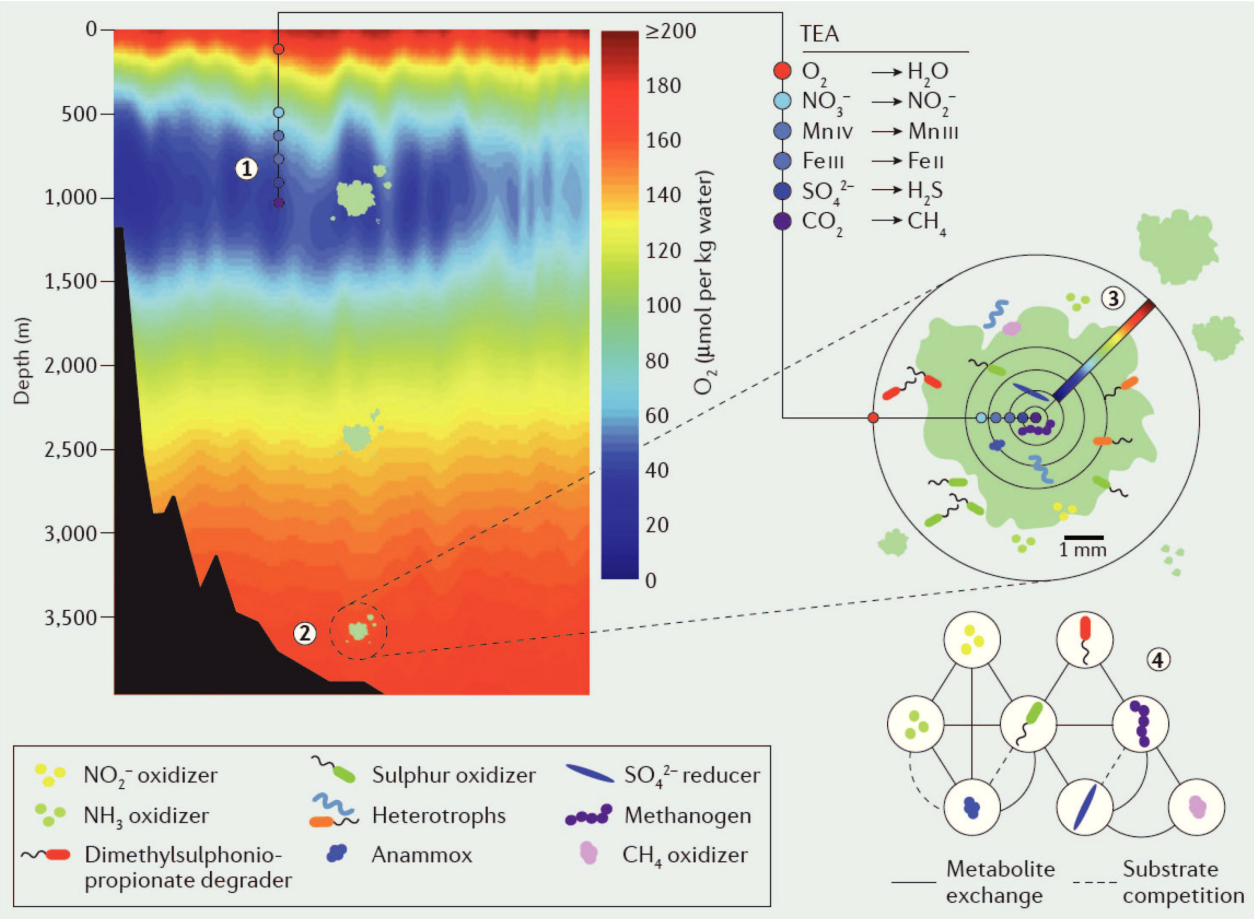

Fig. I.5. Microbial processes in the water column of the OMZs. TEA: terminal electron acceptor. Figure is taken from Wright et al. (2012).

continuously depleted within these particles (Alldredge and Cohen, 1987). Millimeters thick of microhabitats accumulate around large particles, and involve in a series of suboxic or anoxic processes due to the formation of microscale oxyclines (Fig. I.5, label 3; Karl et al., 1984; Alldredge and Cohen, 1987; Woebken et al., 2007). Overall, biological process in which sequential reactions are carried out by different organisms can be found in the microbial pathways (Fig. I.5, label 4) that drive the carbon cycle (Paulmier et al., 2006; Walsh et al., 2009), nitrogen cycle (Codispoti et al., 2001; Kuypers et al., 2003; Gruber, 2008; Lam and Kuypers, 2011) and sulfur cycles (Walsh et al., 2009; Canfield et al., 2010) in the OMZs and also in deeper waters where oxygen concentration increases again.

Due to the global warming, expansion of the OMZs occurred during the past fifty years (Stramma et al., 2008; Keeling et al., 2010), which is going to spread in the coming decades as a

consequence of continuously raise in air and seawater temperatures (Taylor et al., 2007; Paulmier an Ruiz-Pino, 2009). OMZs expansion would have a profound effect on the global carbon cycle, nitrogen cycle, and unpredicted climate changes. Therefore, studies focused on microbial processes in the OMZs will help us to better understand marine element cycles, and how marine organisms can adapt to oxygen limitation environments (Karstensen et al., 2008).

I.1.3.2. The OMZ of the Eastern Tropical North Pacific Ocean (ETNP)

The Eastern Tropical North Pacific Ocean (ETNP) off Mexico and Central America hosts one of the largest oxygen minimum zones (OMZs) in the open ocean (Fig. I.4) at depths between 100 m to 600~800 m (Paulmier and Ruiz-Pino, 2009). Sea surface temperature (SST) of ETNP is around 26°C, and decreases with increasing water depth, about 4°C at 1200 m (Taylor et al., 2007). Rapid oxygen consumption via respiration of organic matter exported from the highly productive upper water column, together with a sharp permanent pycnocline that prevents ventilation of more oxygenated deep waters result in the occurrence of the strong OMZ in the ETNP (Fiedler and Talley, 2006). In the OMZ of the ETNP, the oxygen content of surface water is around 200 μM and drops rapidly to less to 30 μM within euphotic zone due to biological respiration, O_2 maintains lower than 20 μM in the main body of the OMZ, but elevated O_2 is observed in the deep oxycline layer (> 800 m) because of the presence of more oxygenated deep waters (Fig. I.6). In general, the OMZ of the ETNP could be roughly compartmentalized into four horizons based on O_2 concentrations: an euphotic and upper oxycline zone (200 μM > O_2 > 20 μM), the upper OMZ (20 μM > O_2 > 2 μM), the mid or core OMZ (O_2 < 2 μM), and the deep oxycline layer below mid OMZ (> 2 μM) where O_2 levels begin to rise (see *Chapter II and III* for details)

In the OMZs of the ETNP, the highest abundance of zooplankton, phytoplankton and prokaryotes are observed in the euphotic zone (Saltzman and Wishner, 1997; Podlaska et al., 2012). Zooplankton and prokaryotes have secondary peaks in the mid OMZ (Saltzman and Wishner, 1997; Podlaska et al., 2012). Among prokaryotes, Bacteria are more abundant than Archaea throughout the water column (Fig. I.7; Podlaska et al., 2012). High heterotrophic potential are mirrored in nitrate-deficient suggesting nitrate reduction by nitrate-reducing chemoorganotrophs (Fig. I.7; Podlaska et al., 2012). The nitrite peaks in the OMZ coexist with

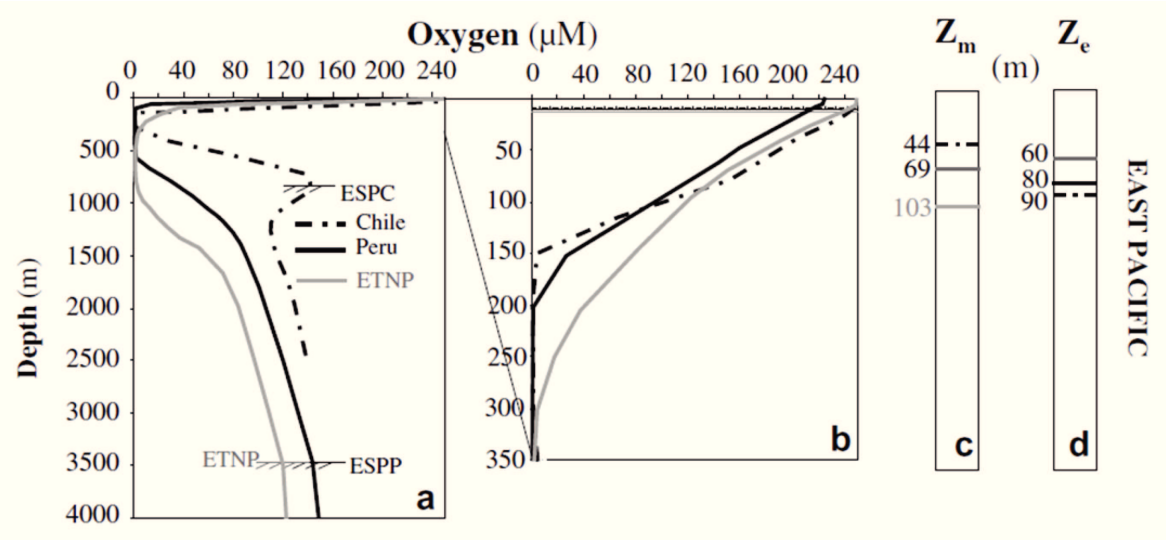

Fig. I.6. (a) O_2 profile for the main OMZs in the Pacific Ocean. Horizontal striped line: the lower boundary of OMZs. (b) Detailed oxygen profile from surface to 300 m. Horizontal lines: the upper OMZ boundary. (c) Z_m: mean maximal mixed-layer. (d) Z_e: euphotic layer. ESPC: Eastern South Pacific off Chile. ESPP: Eastern South Pacific off Peru. ETNP: Eastern Tropical North Pacific. Figure is taken from Paulmier and Ruiz-Pino (2009).

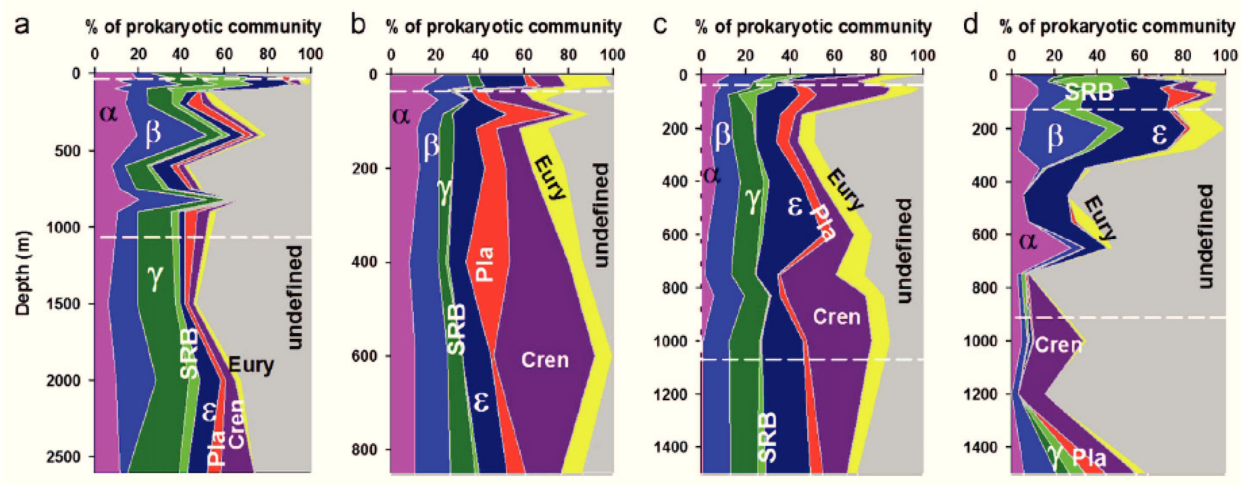

Fig. I.7. Relative abundance of microorganisms detected in the OMZ of the ETNP at Station 1 (a), 2 (b), 5 (c) and 8 (d), respectively. *α*: *α*-proteobacteria; *β*: *β*-proteobacteria; *γ*: *γ*-proteobacteria; SRB: sulfate-reducing bacteria; *ε*: *ε*-proteobacteria; Pla: *Planctomycetes*; Cren: Crenarchaeota; Eury: Euryarchaeota. Figure is taken from Podlaska et al. (2012).

nitrate deficits indicating nitrate reduction by denitrifying bacteria (denitrification) (Sambrotto and Swenson, 2007). Ladderanes, the lipid biomarker of Bacteria performing the anaerobic oxidation of ammonium (anammox), are abundant within the mid OMZ which indicates that anammox is an important process in the nitrogen cycle of the ETNP (Rush et al., 2012). Crenarchaeota and Euryarchaeota are most abundant in the euphotic zone and depths below the OMZ, with secondary abundance in the OMZ (Fig. I.7; Podlaska et al., 2012). Besides the identified organisms, a large fraction of cells are undefined (Fig. I.7).

I.1.4. Marine deep biosphere

I.1.4.1. Populations in marine deep biosphere

Deeply buried marine sediments, defined as marine sediments from several centimeters to thousand meters below sea floor, host 1% (Kallmeyer et al., 2012) to one third of total biomass on Earth (Whitman et al., 1998). Life in the deep subseafloor is reported mainly in the form of prokaryotic microorganisms which are invisible to the naked eyes (Whitman et al., 1998). So far, the microbial community inhabiting in the deep biosphere has not been fully understood. The topic about which domain of prokaryotes, Archaea or Bacteria, dominates the deep biosphere has been investigated for several years but conclusion is still ambiguous. Based on molecular approaches, Schippers et al. (2005) presented that all detectable living cells in the representative open ocean and ocean margin deep subsurface sediments (up to 400 mbsf) belong to Bacteria. Similar conclusion was drawn in the marine sediments (up to 350 mbsf) of Peru and Cascadia Margin, where prokaryotic communities (10^5~10^7 cells cm^{-3} sediment) was composed mostly of Bacteria (Inagaki et al., 2006). However, a contrary point of view arises simultaneously, which suggests Archaea as significant contributors to sedimentary subsurface ecosystems. Based on both cell counts data and intact polar lipids (IPLs) analysis, active portion of the microbial community was indicated to be dominated by Archaea in the subseafloor sediment (up to 120 mbsf) of Peru Margin (Mauclaire et al., 2004; Biddle et al., 2006). Archaeal IPLs which are considered as biomarkers for living Archaea biomass accounted for more than 90% of total IPLs in the top 1 km of the sediment, which suggests that Archaea could have a significant contribution to the biomass in marine subsurface sediments (Fig. I.8; Lipp et al., 2008). On the other hand, dormant bacterial endospores were recently reported as abundant as vegetative prokaryotes in the deep marine biosphere based on biomarker analysis, which sheds new light on the composition of microbial

community in the deep biosphere (Lomstein et al., 2012).

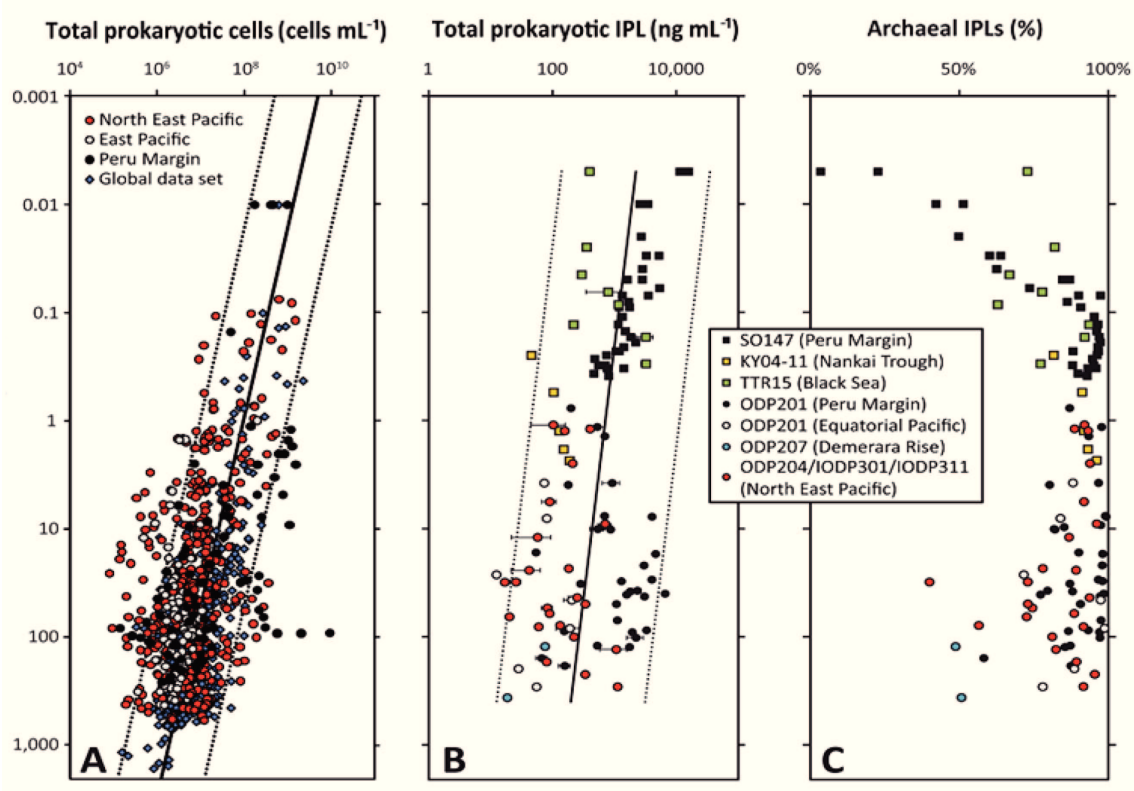

Fig. I.8. (A) Depth profile of total prokaryotic cell numbers. (B) Concentration of total IPLs versus Depth. (C) Relative contribution of archaeal IPLs to total microbial IPLs. Cell counts data are compiled from Parkes et al. (2000), D'Hondt et al. (2004), Engelen et al. (2008), Roussel et al. (2008), Webster et al. (2009). Figure A is provided by Dr. Julius S. Lipp. Figure B and C are taken from Lipp et al. (2008).

I.1.4.2. Turnover of microbial communities and biomolecules in the deep biosphere

Deep biosphere is buried and highly energy-limited ecosystem, where microorganisms utilize old and recalcitrant organic matter at a very slow rate (Parkes et al., 2000). The metabolic rates of deep biosphere life are by orders of magnitude lower than those of life on the Earth' surface (D'Hondt et al., 2002). Typical metabolic rate of microorganisms in the ecosystems on the surface of our planet, such as soil, lake water or seawater, is 10^{-3} to 10^{-1} g C per gram cell C per hour (g C g^{-1} cell C hour $^{-1}$), whereas for deep subsurface bacteria is by four orders of magnitude lower, ranging from 10^{-7} to 10^{-5} g C g^{-1} cell C hour $^{-1}$ (Fig. I.9; D'Hondt et al., 2002; Jørgensen and D'Hondt, 2006; Jørgensen 2011). Therefore, populations in the deep biosphere undergoing a very long turnover time varying by several orders of magnitude, in a range of hundred to hundreds of

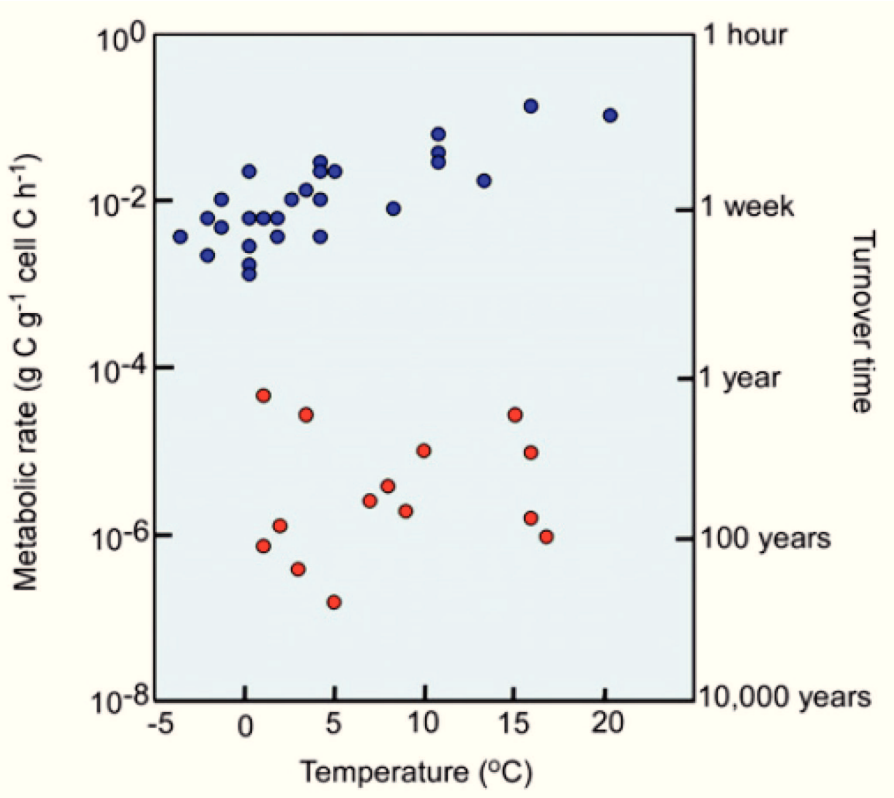

Fig. I.9. Turnover times and metabolic rates of microorganisms in different environments. Blue circles: nutrient-rich environments such as soil, lake water, or seawater. Red circles: nutrient-starved environments such as subsurface sediments. Figure is taken from Jørgensen (2011).

thousands years (Whitman et al., 1998; Biddle et al., 2006; Lomstein et al., 2012). Although calculated community turnover is dependent on choice of different datasets and parameters (e.g., size of the deep population and cell growth efficiency), overall deep biosphere microbes have much longer turnover time than microbes living on surface Earth.

In addition to molecular biological techniques, IPL analysis provides further insight into the active microbial communities under deep biosphere. Faster turnover of biomolecule relative to community turnover time is a prerequisite for these compounds acting as living biomarkers. To act as a proxy for living cells, turnover time of extracellular IPLs in the deep biosphere needs to be lower than the presumed cell population turnover (Biddle et al., 2006; Lipp et al., 2008). If the turnover of archaeal IPLs is far beyond the community turnover, archaeal IPLs detected in the subsurface sediments are mostly derived from extracellular components which representing fossil signals rather than active biomass, therefore contribution of Archaea to deeply buried sediments should be reconsidered. So far, the degradation kinetics of archaeal IPLs in the deep sediments has

not been fully understood.

I.1.5. Microbial formation of ethane and propane in anoxic marine sediment

Low molecular weight hydrocarbons, such as ethane, propane and their corresponding alkenes, ethylene and propylene, commonly occurred in various cold marine sediment settings, including anaerobic estuarine mudflat (Vogel et al., 1982; Oremland et al., 1988), shallow subseafloor from continental shelves and slopes (Bernard et al., 1978; Kvenvolden and Redden, 1980; Whelan et al., 1980; Kvenvolden 1988), Mediterranean sapropels (Egorov and Ivanov, 1998), gas hydrate nodules (Sassen and Curiale, 2006), and even deep subseafloor sediment at margins and the open ocean (Waseda and Didyk, 1995; Paull et al., 2000; Hinrichs et al., 2006; cf. Janus Web Database, http://www-odp.tamu.edu/database/). Because ethane and propane are usually coexist with ethylene and propylene in low temperature marine sediments and their concentration is more or less constant with increasing depths (Bernard et al., 1978; Kvenvolden and Redden, 1980; Kvenvolden 1988; Egorov and Ivanov, 1998), ethane and propane are suggested to be biogenic gases rather than thermogenic origin (Davis and Squires, 1954; Kvenvolden et al., 1979; Whelan et al., 1980).

Microbial formation of ethane and propane in the deep marine subsurface has been recently suggested to a pervasive process (Hinrichs et al., 2006). The proposed mechanism for ethano- and propanogenesis from acetate remains speculative but previous studies demonstrated that certain methanogenic archaea may be capable of ethane and propane production. An enrichment culture containing methanogens and homoacetogens performed reduction of ethylene to ethane (Koene-Cottaar et al., 1998). *Methanosarcina barkeri* has been known to be able to convert ethanol to ethane, very likely via a pathway that corresponds to the conversion from methanol to methane (Belay et al., 1988). Furthermore, in surface anoxic sediments, ethylated sulfur compounds can be transformed by microbe to ethane, while propanethiol only result in a minor enhancement of propane concentration (Oremland et al., 1988). Oremland et al. (1988) suggested that the inhibition of ethane formation from all these precursors by 2-bromoethanesulfonic acid indicated HS-CoM and the related enzyme system as the key reaction steps (Fig. I.10).

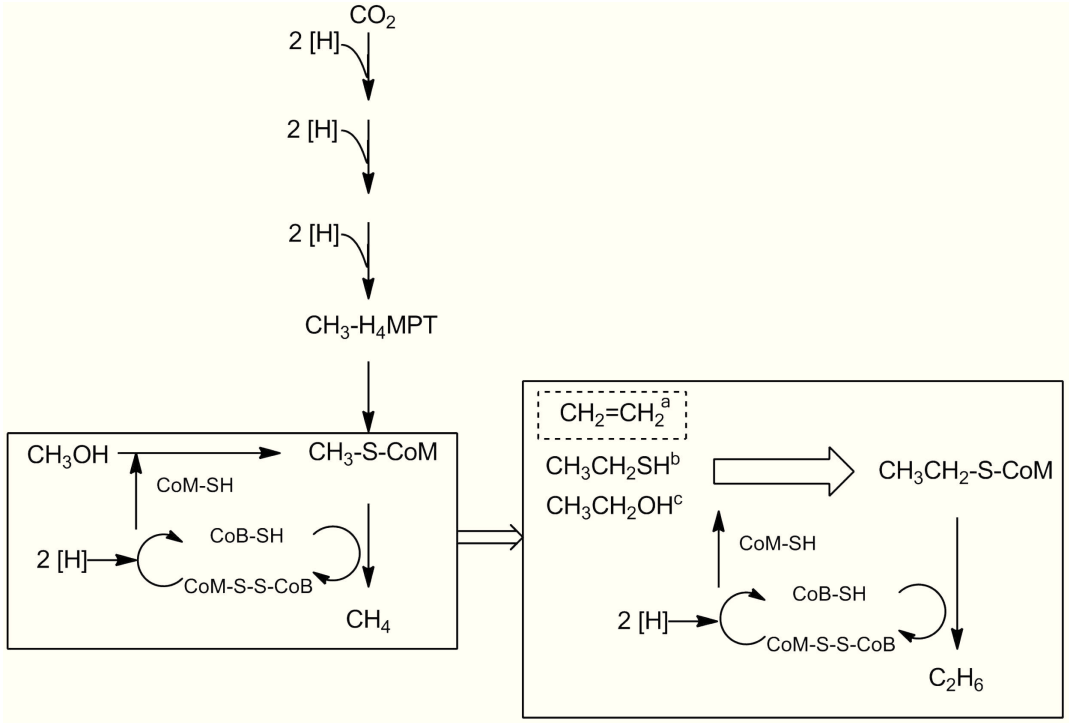

Fig. I.10. Simplified pathways of methanogenesis from CO_2 and methanol and the corresponding enzymatic steps in which ethanogenesis takes place according to studies on methanogen isolates or enrichments culture. Transformation of ethanol (c: Belay and Daniels, 1988) and ethanethiol (b: Oremland et al., 1988) to ethane have a similar pathway as methane formation from methanol. The exact mechanism of reducing ethylene to ethane (a: Koene-Cottaar, 1998) is still unclear but probably also related to CoM-SH. H_4MPT: tetrahydromethanopterin; CoM-SH: coenzyme M; CoB-SH: coenzyme B; CH_3-S-CoM: methyl-coenzyme M; CH_3CH_2-S-CoM: ethyl-coenyzme M; CoM-S-S-CoB: heterodisulfide of coenzyme M and coenzyme B.

I.2. METHODS

I.2.1. Lipid biomarker as tool to study microbial community in the natural environment

I.2.1.1. The structure and function of membrane lipids

As a complementary approach to the molecular biological techniques, lipid analysis provides further insight into the microbial communities under various environmental conditions. Lipids are building blocks of cell membranes. Membrane lipids usually contain a hydrophilic polar head group and a hydrophobic tail (Fig. I.11), which function as a permeability barrier to separate the inner of a cell from the outer environments (Fig. I.11). In addition to their function as physical barrier, membrane lipids are also used as energy storage, transmission of information in cells (signal transduction), transport of nutrients into the cell, providing stabilizing matrix for transmembrane proteins and maintenance of the proton-motive force (cf. Dowhan and Bogdanov, 2002; Eyster, 2007; Haucke and Di Paolo, 2007). Lipids have ability to regulate membrane fluidity by restructuring of the lipid composition in response to environmental changes, such as in pressure, temperature, pH, salinity or osmolarity (e.g., Cronan and Gelmann, 1975; Hazel and Wiliams, 1990; Russell et al., 1995).

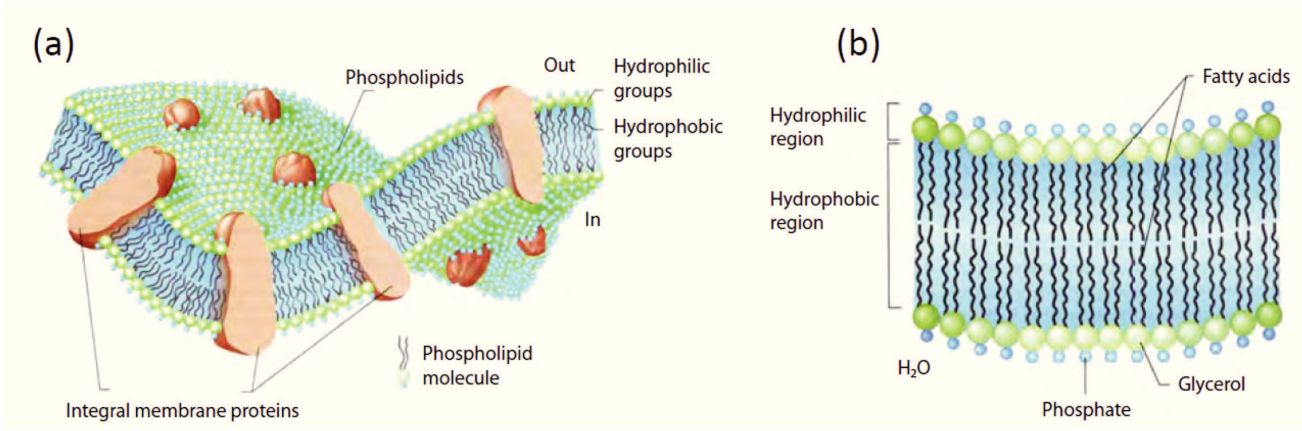

Fig. I.11. (a) Bacterial cytoplasmic membrane including a bilayer phospholipid and transmembrane proteins. (b) Detailed structure of the lipid bilayer. Figure is adopted from Madigan et al. (2003).

Lipid composition is impacted not only by the environmental parameters, but also by different groups of organisms, e.g., within the three domains of life, Eukarya, Bacteria and Archaea, therefore lipids could be used as chemotaxonomic markers for organisms. The majority of membrane lipids are glycerol-based with two hydrophobic chains connected to the glycerol backbone via ester or ether bonds and a polar head group. The synthesis of polar head groups is similar between the three domains, with typical head groups of phosphate-, glycosidic-, amino- or sulfate-based head groups (cf. Kates, 1989; Dembitsky, 1996; Hölzl and Dörmann, 2007). Significant differences are found in the compositions of their hydrophobic core membrane lipids, especially the chain architecture (isoprenoidal for Archaea versus n-alkyl for Eukarya and Bacteria; Langworthy and Pond, 1986; De Rosa and Gambacorta, 1988; Itoh et al., 2001) and the stereochemistry of the glycerol backbone (2,3-di-*O*-alkyl-*sn*-glycerol for Archaea versus 1,2-di-*O*-alkyl-*sn*-glycerol for Eukarya and Bacteria; Kates, 1978).

I.2.1.2. Intact polar membrane lipids (IPLs) as biomarkers for living biomass

In the natural environments, lipids can either exist in the form of intact polar membrane lipids (IPLs) or core lipids (Structures are shown in Fig. I.12) after hydrolysis of polar head groups from IPLs. IPLs, especially phospholipids, are found to be degraded quickly after cell lysis (White et al., 1979; Harvey et al., 1986) in the surface sediment. So far, IPLs have been successfully applied as biomarkers in a variety of ecosystems where microbial activity are high, such as water column of the ocean (Schubotz et al., 2009; Van Mooy et al., 2006, 2009; Van Mooy and Fredericks, 2010; Popendorf et al., 2011; Wakeham et al., 2012), surface marine sediments (e.g., Rütters et al., 2002a, 2002b), cold seeps and hydrothermal vents (Zink et al., 2003; Sturt et al., 2004; Rossel et al., 2008, 2011; Schubotz et al., 2011; Yoshinaga et al., 2011), peat bog (Liu et al., 2010) and a meromictic lake (Ertefai et al., 2008).

However, application of IPLs, especially archaeal IPLs, as biomarker for active biomass in low-activity deep biosphere (Biddle et al., 2006; Lipp et al., 2008) remains controversial (cf. Lipp and Hinrichs, 2009; Schouten et al., 2010). Hence, a better understanding of the degradation kinetics of archaeal IPLs under energy-limited deep sediments is essential for interpretation of lipid signals in the deep biosphere.

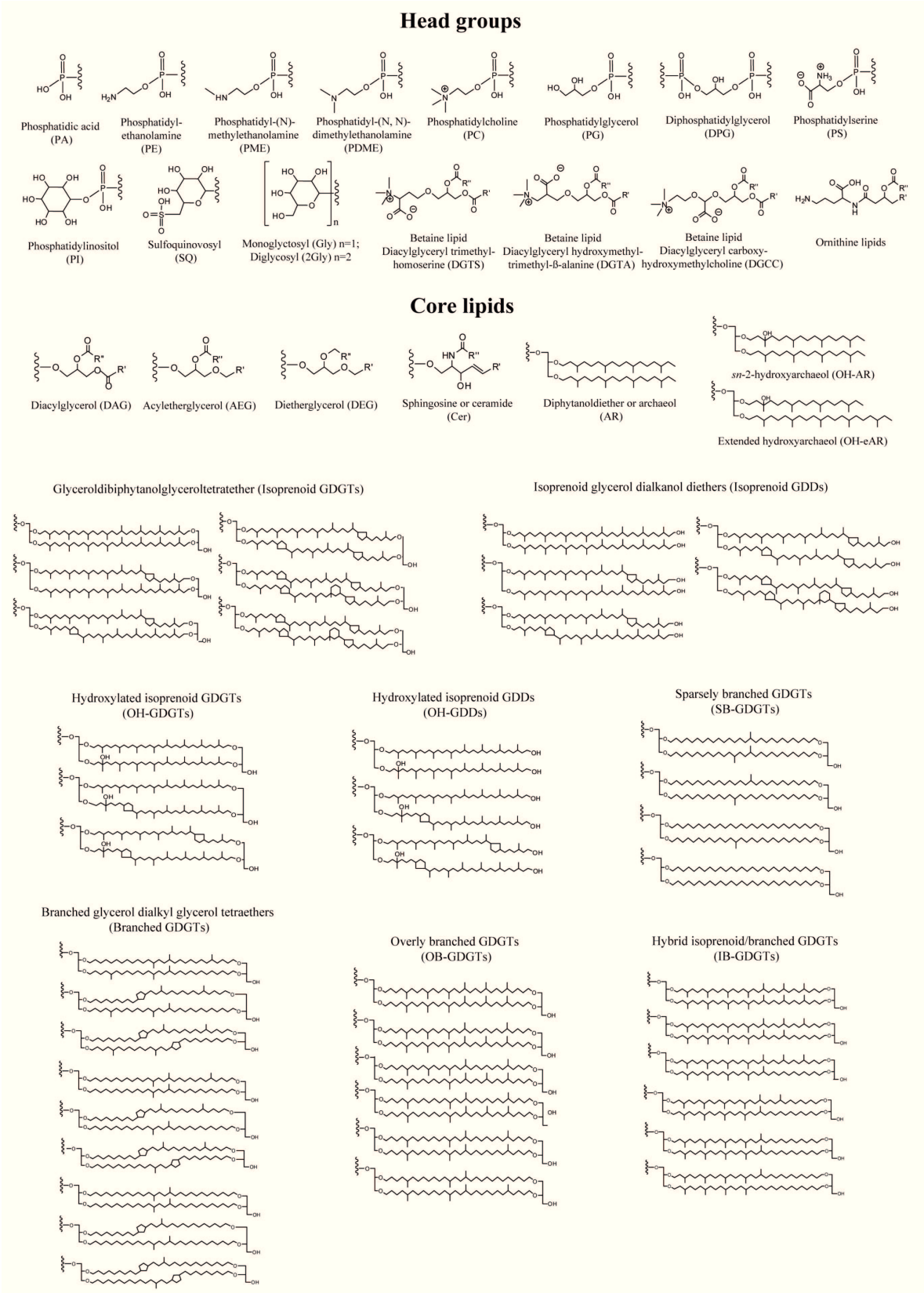

Fig. I.12. Structures of representative polar head groups and core lipids in the natural environments.

I.2.1.3. Studies of degradation kinetics of archaeal IPLs

In marine sediments, many of the reactions and processes, including degradation of IPLs, are related either directly or indirectly to the degradation of total organic matter (Middelburg, 1989), each of which undergoes first-order decomposition (Jørgensen, 1978). According to the first-order kinetics, concentration of IPLs and the rate of IPL decomposition both decrease exponentially with time. The reactivity of IPLs is gradually decreased with time in a series of experimental investigations (Fig. I.13; Harvey et al., 1986; Logemann et al., 2011). According to the data provided by Logemann et al. (2011), degradation of ester-bond IPLs is by one to two orders of magnitude faster than that of ether-bond IPLs, and the degradation rate of IPLs under anaerobic condition is faster than those under oxic condition (Fig. I.13).

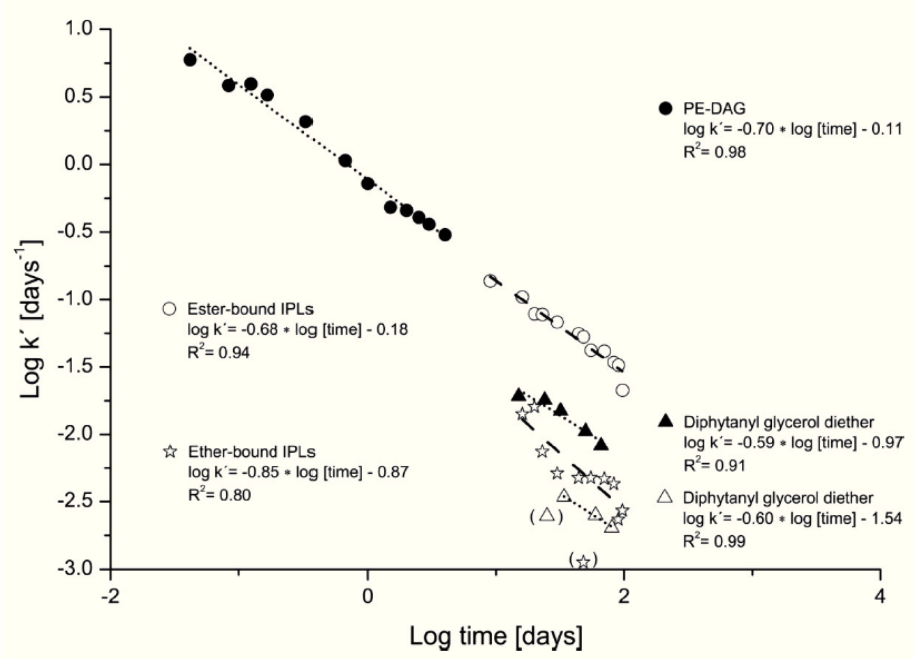

Fig. I.13. Log-log plot of degradation rate constants (*k'*) with time for different IPL groups. Degradation results of PE-DAG and diphytanyl glycerol diether are from Harvey et al. (1986). Degradation results of ester-bound and ether-bound IPLs are coming from Logemann et al. (2011). Closed symbols: aerobic degradation. Open symbols: anaerobic degradation. Figure is taken from Logemann et al. (2011).

In the deep sediments, if IPL input only occurs at surface, IPL concentration will tend to toward extreme low concentration at depth between 1 and 50 mbsf depending on different choice of IPL half-life (Fig. I.14A). Hence, in order to better simulate the observed IPL concentration in the deep biosphere, continuous input of IPL is required (Lipp and Hinrichs, 2009;

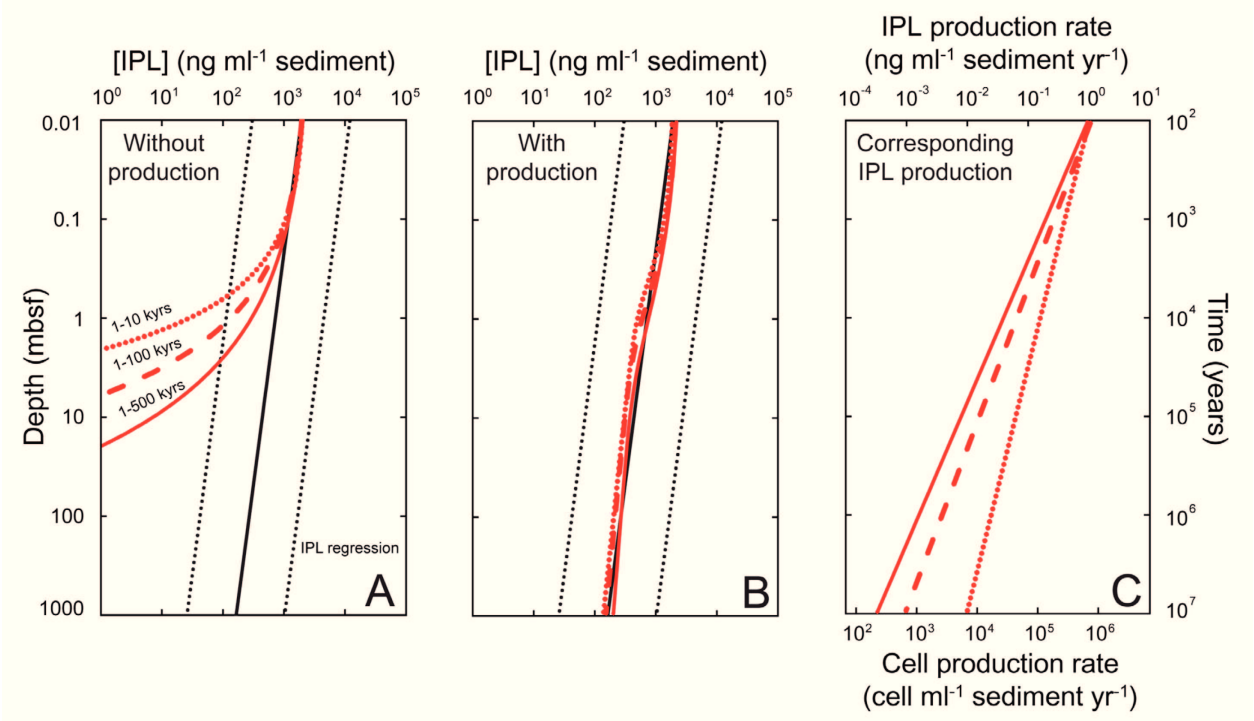

Fig. I.14. (A) Depth profile of IPL concentration with input of IPL at surface depth only. Red-dotted line: half-life of IPL is 1~10 kyrs. Red-dashed line: half-life of IPL is 1~100 kyrs. Red solid line: half-life of IPL is 1~500 kyrs. Black solid line represents regression line and 95% prediction interval (black-dotted line) of observed IPL concentration (Lipp et al., 2008) for comparison. (B) Model of IPL concentration allowing sedimentary input of archaeal IPL to better simulate of observed IPL profiles for the three scenarios from panel A. (C) Input of archaeal IPL which is selected so that the modeled concentration is in the range of observed extractable IPL. IPL production rate at surface sediment is set to be 1 ng ml^{-1} sediment, which has been determined in recent stable-isotope probing study for coastal sediments younger than 100 years old (Wegener et al., 2012).

Fig. I.14B and C), in a range of 1000 to 3.2~100 pg lipid g^{-1} sediment yr^{-1} from surface to 1000 mbsf.

However, the concentration of observed IPLs is by two orders of magnitude higher than the IPLs converted from cell abundance, which suggests that previous estimation of archaeal biomass is overestimated (Fig. I.15; Schouten et al., 2010). If degradation rate of IPLs is assumed to be similar as TOC (IPL half-life is in a range of 0.35~34 700 kyrs), IPL concentration (without in-situ production) fits quite well with observed IPLs in the deep subseafloor, which suggests that IPLs in the deep biosphere may contain a substantial fossil component potentially masking in-situ IPL production (Schouten et al., 2010). Based on this conclusion, observed archaeal IPLs below 1 mbsf are almost derived from fossil signal.

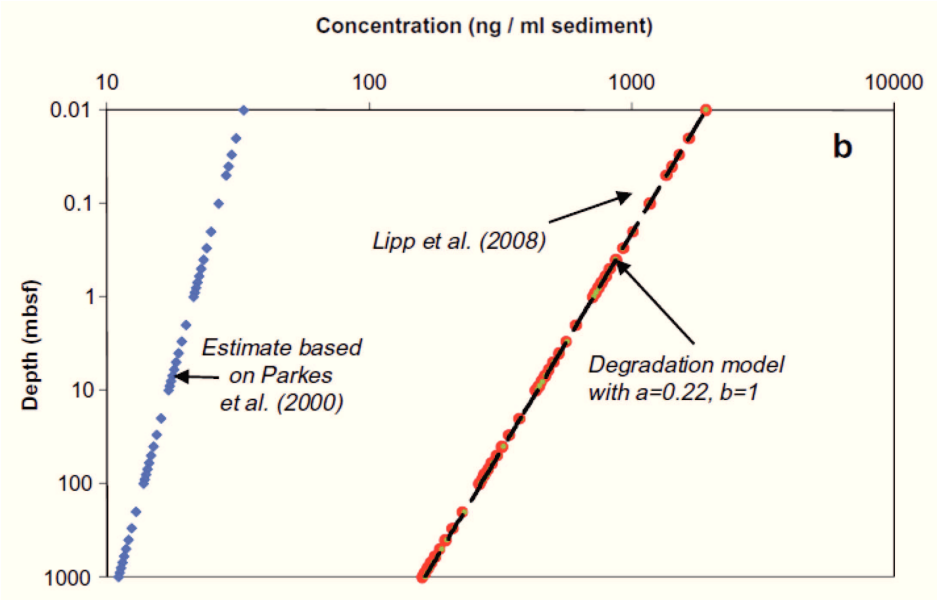

Fig. I.15. Log-log plot of IPL concentration with depth complied from previous studies. Black line: observed IPL concentration by Lipp et al. (2008). Blue line: IPL concentration converted from cell counts data by Parkes et al. (2000). IPL content in a single cell is assumed to be 1 fg. Red dots: modeled IPL concentration using typical degradation kinetics of TOC. Figure is taken from Schouten et al. (2010)

I.2.2. Lipids analysis

In this thesis, particulate organic matter samples from the oxygen minimum zones (OMZ) of the Eastern Tropical North Pacific Ocean (ETNP) were collected by in-situ filtration of seawater, and were immediately frozen at -20°C until extraction (see *Chapter II and III* for details). Lipids were Soxhlet-extracted (Wakeham et al., 2007) by DCM/MeOH (9:1, v/v) for 8 hrs. Total lipids extracts (TLEs) were performed on ThermoFinnigan Surveyor high-performance liquid chromatography system coupled to a ThermoFinnigan LCQ DecaXP Plus ion-trap mass spectrometer via electrospray interface (HPLC-ESI-IT-MS^n) under conditions described previously (Sturt et al., 2004). Lipids were dominated by eukaryotic and bacterial IPLs, and archaeal IPLs could not be observed. In order to reduce the ions suppression of complex compounds, total lipids extracts (TLEs) were separated into three fractions by preparative HPLC, e.g., fraction one (F1) containing glycerol ether core lipids (core lipids), archaeal IPLs (IP GDGTs) were in the second fraction (F2), and all the other eukaryotic and bacterial IPLs in the last fraction (F3) (Fig. I.16). Core lipid of IP GDGTs was acquired by acid hydrolysis that heating an aliquot of IP GDGTs in 500 µL of 6 M HCl/methanol/dichloromethane (1:9:1, v/v) at 70°C for 24 h. Core lipids in the first fraction and core lipids of IP GDGTs were analyzed by Bruker Maxis

Accurate-Mass Quadrupole Time-of-Flight (Q-TOF) mass spectrometer connected to a Dionex Ultimate 3000 RS HPLC (UHPLC) system, coupled via an atmospheric pressure chemical ionization (APCI) interface (Becker et al., in preparation). IP GDGTs in the second fraction was measured on the same UHPLC and Q-TOF system, but coupled via an electrospray ionization (ESI) ion source (Wörmer et al., in preparation).

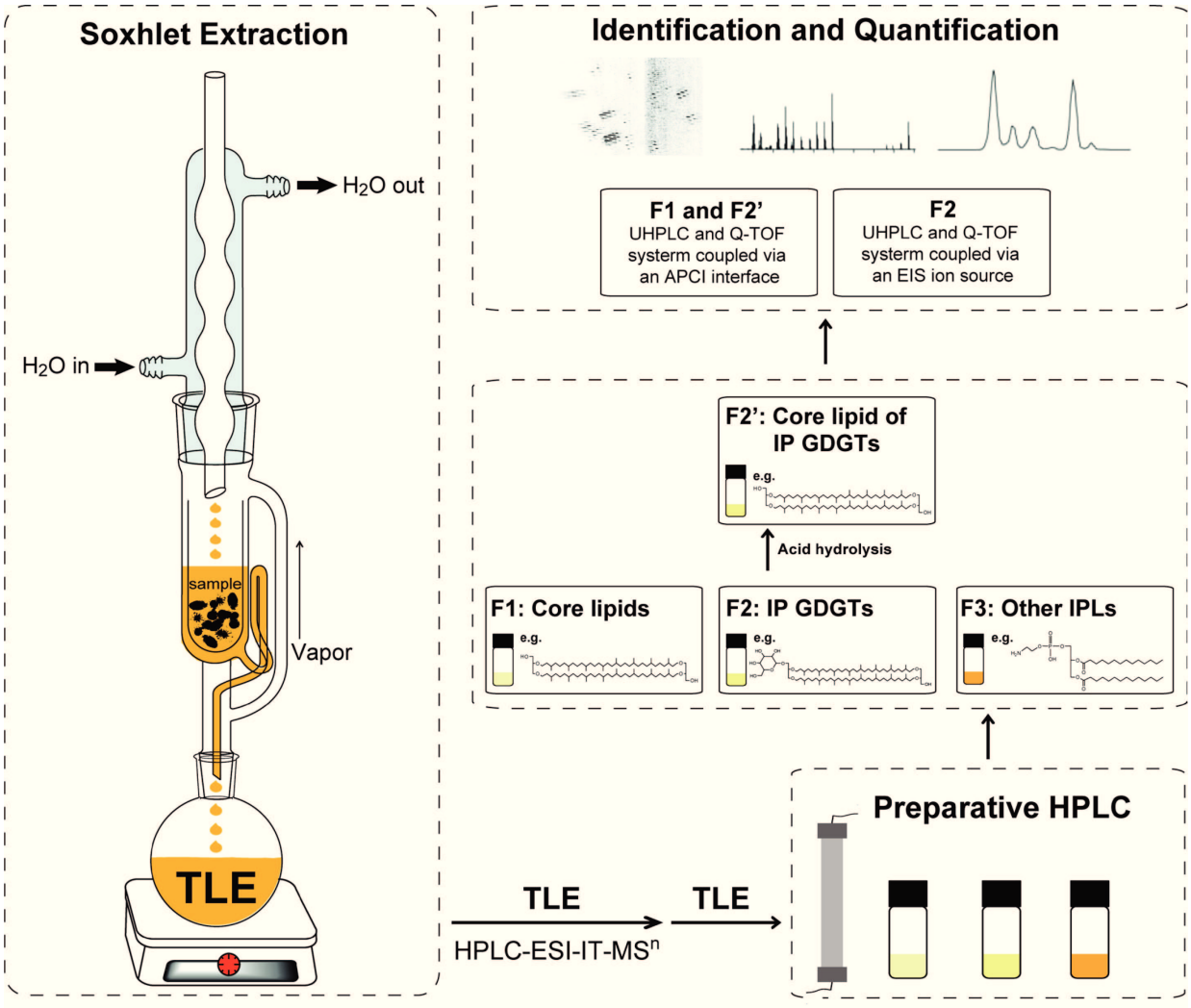

Fig. I.16. Flow scheme of lipid analysis.

I.2.3. Radioactive tracers

Due to the identical chemical properties as their nonradioactive counterparts and superior in sensitivity (e.g., stable isotope, fluorescence), radioactive isotopes of common elements are

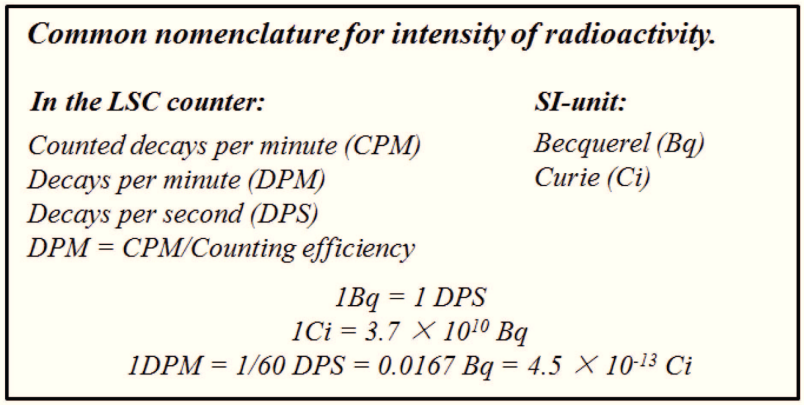

Fig. I.17. Common units that express intensity of radioactivity. Counting efficiency varies for different isotopes, sample compositions and scintillation counters, mostly it is around 95% for ^{14}C and ^{35}S, but only 50 ~ 60% for ^{3}H.

widely used in scientific research. Radioactivity includes the emission of alpha particles (α), beta particles (β) and gamma rays (γ) (Schimel, 1993). To be applied as a radiotracer, selected radioactive isotope must have a reasonable half-life so that it could continuously emit its radiation during the course of the experiment. For experiments in the lab, the half-life of commonly used isotopes is in a range of days (e.g., 14.3 days for ^{32}P) to thousands of years (5,730 years for ^{14}C) (Browne and Firestone, 1986). Quantification of the radiation, such as β-emitting, could be done by liquid scintillation counting (LSC) technique which is defined by incorporating of the radiolabeled analyte into a liquid chemical medium (cocktail) to get a homogenous solution, which is capable of converting the kinetic energy of nuclear emissions into light energy, and later to be recorded by the system (Horrocks, 1974; Measuring units see Fig. I.17).

In this thesis, we designed a sensitive radiotracer experiment to constrain the decay rate of a model archaeal IPL in the deep biosphere (see *Chapter IV* for details). A synthesized GlcDGD with head group ^{14}C-labeled was used in order to closely mimic the structural properties of the most abundant microbial group of IPLs in the subseafloor sediments. Radiolabeled IPLs were added to anaerobic slurries of sediments from the Wadden Sea surface (in-situ temperature 4°C) and Cascadia Margin subsurface (138.21 mbsf; in-situ temperature 20°C) sediments. The slurries were incubated at in-situ temperature, 4°C and 20°C, respectively. Independent of the chemical fate of the polar head groups after its hydrolysis from the glycerol backbone, ^{14}C enters into the aqueous or gas phase while the intact lipid is still insoluble and remains in the solid phase. Reaction progress was monitored by quantifying the increase of radioactivity in the aqueous

solution and gas phase with LSC (Fig. I.18).

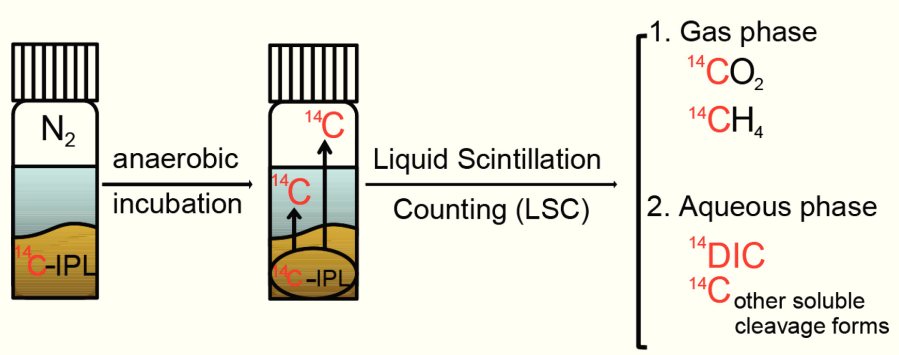

Fig. I.18. Flow sketch of the radiotracer experiment.

I.3. OBJECTIVES OF THIS THESIS

The objective of this thesis is to get a better understanding of the distribution, ecology and turnover of microorganisms in oxygen-deficient marine environments based on biomolecule analysis. Organic-geochemical studies targeting microbial lipids and carbon flow were performed in the water column of the oxygen minimum zone (OMZ) of the Eastern Tropical North Pacific Ocean (ETNP), subsurface sediment, and anoxic estuarine sediment.

In chapter II and III, the distribution of IPLs and glycerol ether core lipids in the oxygen minimum zone (OMZ) of the Eastern Tropical North Pacific Ocean (ETNP) and their potential sources are discussed. Our data will provide more insights into the ecology and distribution of Eukaryotes, Bacteria and Archaea in the open ocean.

Intact polar membrane lipids (IPLs) as biomarkers for living biomass have been analyzed in a variety of surface ecosystems. Recently, significant contribution of Archaea in the deep biosphere has been suggested with the observed dominant distribution of archaeal IPLs. However, the application of IPL analysis, especially using archaeal IPLs as biomarkers for active biomass, still remains controversial in low-activity deep biosphere. In Chapter IV, we performed a sensitive radiotracer experiment and a comprehensive modeling work to check whether IPLs can be used as biomarker for living organisms in deep subsurface sediments, and to understand turnover of microbial lipids and activity of archaeal populations in the deep biosphere.

Low-molecular weight hydrocarbons are widely detected as biogenic gases in the anoxic cold marine sediments. In chapter V, a series of substrates, including alkenes, alcohols, thiols, and

carboxyl acids with C-2 or C-3 skeleton, were tested for their alkane-producing potential in the anoxic sediment collected from the German Wadden Sea. Analysis of bacterial and archaeal 16S rRNA gene as well as archaeal *mcrA* gene were carried out in an ethane-producing enrichment with ethylene as substrate to characterize the composition of the microbial community that have a potential to produce ethane from ethylene.

I.4. CONTRIBUTIONS TO PUBLICATIONS

This thesis includes the complete versions of four first-author manuscripts for submission in international journals (*Chapters II-V*)

Chapter II – full manuscript

Distribution of eukaryotic and bacterial intact polar lipids in the oxygen minimum zone of the Eastern Tropical North Pacific Ocean

Sitan Xie, Florence Schubotz, Stuart G. Wakeham, Kai-Uwe Hinrichs

S.X. and F.S. designed the project under supervision of S.G.W. and K.-U.H. S.G.W. collected samples, extracted, and performed sample clean-up on TLE of filters of particulate organic matter. S.X. measured and identified IPLs. LC-MS interpretation was supervised by F.S. S.X. wrote the paper with input from all coauthors. In preparation for *Organic Geochemistry*.

Chapter III – full manuscript

Distribution of glycerol ether lipids in the oxygen minimum zone of the Eastern Tropical North Pacific Ocean

Sitan Xie, Xiao-Lei Liu, Florence Schubotz, Stuart G. Wakeham, Kai-Uwe Hinrichs

S.X. and F.S. designed the project under supervision of S.G.W. and K.-U.H. S.G.W. collected samples, extracted, and performed sample clean-up on TLE of filters of particulate organic matter. S.X. performed fractionation of distinct lipids classes with the help of F.S. S.X. measured and identified glycerol ether core lipids with the help of X.-L.L. S.X. wrote the paper with input from all coauthors. In preparation for *Organic Geochemistry*.

Chapter IV – full manuscript

Turnover of microbial lipids in the deep biosphere and activity of benthic archaeal populations

Sitan Xie, Julius S. Lipp, Gunter Wegener, Timothy G. Ferdelman, Kai-Uwe Hinrichs

J.S.L., T.G.F. and K.-U.H. designed the project. S.X. and J.S.L. collected surface sediment sample. S.X. performed lab work and data analysis with the help of G.W. J.S.L. provided technical suggestions for modeling work. S.X., J.S.L., and K.-U.H designed the models, S.X. carried out the modeling work, S.X. and K.-U.H wrote the paper. In preparation for *Proceedings of the National Academy of Sciences of the United States of America.*

Chapter V – full manuscript

Ethane- and propane-producing potential and molecular characterization of an ethanogenic enrichment in anoxic estuarine sediment

Sitan Xie, Cassandre Sara Lazar, Yu-Shih Lin, Andreas Teske, Kai-Uwe Hinrichs

S.X. and Y.-S.L. designed the project under supervision of K.-U.H. Y.-S.L. collected sediment samples. S.X. performed incubation experiment and corresponding data analysis. C.S.L. performed molecular characterization of an ethanogenic enrichment. S.X., Y.-S.L and C.S.L wrote the paper jointly with input from all coauthors. Revised version prepared for submission to *Organic Geochemistry*.

I.5. REFERENCES

Alldredge AL, Cohen Y (1987) Can microscale chemical patches persist in the sea? Microelectrode study of marine snow, fecal pellets. *Science* **235**: 689-691.

Alldredge AL, Silver MW (1988) Characteristics, dynamics and significance of marine snow. *Prog Oceanog* **20**: 41-82.

Arthur MA (2000) Volcanic contributions to the carbon and sulfur geochemical cycles and global change. *In* Encyclopedia of Volcanoes (ed. Houghton BF, McNutt SR, Rymer H, Stix J.), 1045-1056. Academic Press, San Diego.

Azam F, Ammerman JW (1984) Cycling of organic matter by bacterioplankton in pelagic marine ecosystems: microenvironmental considerations. *In* Flow of energy and materials in marine ecosystems (ed. Fasham MJR.), 345-360. Plenum Press, New York.

Azam F (1998) Microbial control of oceanic carbon flux: The plot thickens. *Science* **280**: 694-696.

Azam F, Malfatti F (2007) Microbial structuring of marine ecosystems. *Nat Rev Microbiol* **5**: 782-791.

Becker KW, Lipp JS, Zhu C, Liu X-L, Hinrichs K-U (In preparation) An improved chromatographic method for the analysis of archaeal and bacterial ether lipids.

Belay N, Daniels L (1988) Ethane production by *Methanosarcina barkeri* during growth in ethanol supplemented medium. *Antonie Van Leeuwenhoek* **54**:113-125.

Berner RA (1999) A new look at the long-term carbon cycle. *GSA Today* **9**: 1-6.

Bernard BB, Brooks JM, Sackett WM (1978) Light hydrocarbons in recent Texas continental shelf and slope. *J Geophys Res* **83**: 4053-4061.

Biddle JF, Lipp JS, Lever MA, LIoyd KG, Sørensen KB, Anderson R, Fredricks HF, Elvert M, Kelly TJ, Schrag DP, Sogin ML, Brenchley JE, Teske A, House CH, Hinrichs K-U (2006) Heterotrophic Archaea dominant sedimentary subsurface ecosystems off Peru. *Proc Natl Acad Sci USA* **103**: 3846-3851.

Bolin B, Degens ET, Duvigneaud P, Kempe S (1979) The global biogeochemical carbon cycle. *In The Global Carbon Cycle* (ed. Bolin B, Degens ET, Kempe S, Ketner P.), *SCOPE Rep.No.13*, 1-56. Wiley, Chichester.

Bolin B, Rosswall T, Richey JE, Freney JR, Ivanov MV, Rodhe H (1983) C, N, P, and S cycles: major reservoirs and fluxes. *In The Global Carbon Cycle* (ed. Bolin B, Degens ET, Kempe S, Ketner P.), *SCOPE Rep.No.21*, 41-65. Wiley, Chichester.

Browne E, Firestone RB (1986) Table of radioactive isotopes. Wiley, New York.

Canfield DE, Stewart FJ, Thamdrup B, Brabandere LD, Dalsgaard T, Delong EF, Revsbech NP, Ulloa O (2010) A cryptic sulfur cycle in oxygen-minimum-zone waters off the Chilean Coast. *Science* **330**: 1375-1378.

Codispoti LA, Brandes JA, Christensen JP, Devol AH, Naqvi SWA, Paerl HW, Yoshinari T (2001) The oceanic fixed nitrogen and nitrous oxide budgets: Moving targets as we enter the anthropocene? *Sci Mar* **65**: 85-105.

Cronan JE, Gelmann EP (1975) Physical properties of membrane lipids: Biological relevance and regulation. *Bacteriol Rev* **39**: 232-256.

Davis JB, Squires RM (1954) Detection of microbially produced gaseous hydrocarbons other than methane. *Science* **119**: 381-382.

Dembitsky VM (1996) Betaine ether-linked glycerolipids: chemistry and biology. *Prog Lipid Res* **35**: 1-51.

De Rosa M, Gambacorta A (1988) The lipids of Archaebacteria. *Prog Lipid Res* **27**: 153-175.

Des Marais DJ (1997) Isotopic evolution of the biogeochemical carbon cycle during the

Proterozoic Eon. *Org Geochem* **27**: 185-193.

De Vooys CGN (1979) Primary production in aquatic environments. In *The Global carbon Cycle* (ed. Bolin B, Degens ET, Kempe S, Ketner P.) *SCOPE Rep. No. 13*, 259-292. Wiley, Chichester.

D'Hondt S, Rutherford S, Spivack AJ (2002) Metabolic activity of subsurface life in deep-sea sediments. *Science* **295**: 2067-2070.

D'Hondt SL, Jørgensen BB, Miller DJ and scientists from ODP Expedition 201 (2003) Leg 201 summary. *Proc ODP Init Repts* **201**: 1-81.

D'Hondt S, Jørgensen BB, Miller DJ, Batzke A, Blake R, Cragg BA, Cypionka H, Dickens GR, Ferdelman T, Hinrichs K-U, Holm NG, Mitterer R, Spivack A, Wang G, Bekins B, Engelen B, Ford K, Gettemy G, Rutherford SD, Sass H, Skilbeck CG, Aiello IW, Guèrin G, House CH, Inagaki F, Meister P, Naehr T, Niitsuma S, Parkes RJ, Schippers A, Smith DC, Teske A, Wiegel J, Padilla CN, Acosta JLS (2004) Distributions of microbial activities in deep subseafloor sediments. *Science* **306**: 2216-2220.

Diaz RJ, Rosenberg R (2008) Spreading dead zones and consequences for marine ecosystems. *Science* **321**: 926-929.

Dowhan H, Bogdanov M (2002) Functional roles of lipids in membranes. *In* Biochemistry of Lipids, Lipoproteins and Membranes, 4th Ed. (ed. Vance DE, Vance JE.), 1-35. Elsevier Science.

Ducklow HW, Carlson CA (1992) Oceanic bacterial production. *Adv Microb Ecol* **12**: 113-181.

Egorov AV, Ivanov MK (1998) Hydrocarbon gases in sediments and mud breccia from the central and eastern part of the Mediterranean Ridge. *Geo-Mar Lett* **18**:127-138.

Engelen B, Ziegelmüller K, Wolf L, Köpke B, Gittel A, Cypionka H, Treude T, Nakagawa S, Inagaki F, Lever MA, Steinsbu BO (2008) Fluids from the oceanic crust support microbial activities within the deep biosphere. *Geomicrobiol J* **25**: 56-66.

Ertefai TF, Fisher MC, Fredricks HF, Lipp JS, Pearson A, Birgel D, Udert KM, Cavanaugh CM, Gschwend PM, Hinrichs K-U (2008) Vertical distribution of microbial lipids and functional genes in chemically distinct laysers of a highly polluted meromictic lake. *Org Geochem* **39**: 1572-1588.

Eyster K (2007) The membrane and lipids as integral participants in signal transduction: lipid signal transduction for the non-lipid biochemist. *Adv Physiol Educ* **31**: 5-16.

Falkowski PG, Barber RT, Smetacek V (1998) Biogeochemical controls and feedbacks on ocean

primary production. *Science* **281**: 200-206

Falkowski P, Scholes RJ, Boyle E, Canadell J, Canfield D, Elser J, Gruber N, Hibbard K, Högberg P, Linder S, Mackenzie FT, Moore III B, Pedersen T, Rosenthal Y, Seitzinger S, Smetacek V, Steffen W (2000) The global carbon cycle: A test of our knowledge of Earth as a system. *Science* **290**: 291-296.

Fiedler PC, Talley LD (2006) Hydrography of the eastern tropical Pacific: A review. *Prog Oceanogr* **69**: 143-180.

Field CB, Behrenfeld MJ, Randerson JT, Falkowski P (1998) Primary production of the biosphere: Integrating terrestrial and oceanic components. *Science* **281**: 237-240.

Gruber N (2008) The marine nitrogen cycle: Overview and challenges. *In* Nitrogen in the Marine Environment (ed. Capone DG, Bronk DA, Mulholland MR, Carpenter EJ.), 1-50. Elsevier Science.

Harvey HR, Fallon RD, Patton JS (1986) The effect of organic matter and oxygen on the degradation of bacterial membrane lipids in marine sediments. *Geochim Cosmochim Acta* **50**: 795-804.

Haucke V, Di Paolo G (2007) Lipids and lipid modifications in the regulation of membrane traffic. *Curr Opin Cell Biol* **19**: 426-435.

Hazel JR, Williams EE (1990) The role of alterations in membrane lipid composition in enabling physiological adaptation of organisms to their physical environment. *Prog Lipid Res* **29**: 167-227.

Hinrichs K-U, Hayes JM, Bach W, Spivack AJ, Hmelo LR, Holm NG, Johnson CG, Sylva SP (2006) Biological formation of ethane and propane in the deep marine subsurface. *Proc Natl Acad Sci USA* **103**:14684-14689.

Horrocks DL (1974) Applications of liquid scintillation counting. Academic Press, New York and London

Hölzl G, Dörmann P (2007) Structure and function of glycoglycerolipids in plants and bacteria. *Prog Lipid Res* **46**: 225-243.

Inagaki F, Nunoura T, Nakagawa S, Teske A, Lever M, Lauer A, Suzuki M, Takai K, Delwiche M, Colwell FS, Nealson KH, Horikoshi K, D'Hondt S, Jørgensen BB (2006) Biogeographical distribution and diversity of microbes in methane hydrate-bearing deep marine sediments on the Pacific Ocean Margin. *Proc Natl Acad Sci USA* **103**: 2815-2820.

Itoh YH, Sugai A, Uda I, Itoh T (2001) The evolution of lipids. *Adv Space Res* **28**: 719-724.

Jørgensen BB (1978) A comparison of methods for the quantification of bacterial sulfate reduction in coastal marine sediments. *Geomicrobiol J* **1**: 29-47.

Jørgensen BB, D'Hondt S (2006) A starving majority deep beneath the seafloor. *Science* **314**: 932-934.

Jørgensen BB (2011) Deep subseafloor microbial cells on physiological standby. *Proc Natl Acad Sci USA* **108**: 18193-18194.

Kallmeyer J, Pockalny R, Adhikari RR, Smith DC, D'Hondt S (2012) Global distribution of microbial abundance and biomass in subseafloor sediment. *Proc Natl Acad Sci USA*: doi/10.1073/pnas.1203849109

Karl DM, Knauer GA, Martin JH, Ward BB (1984) Bacterial chemolithotrophy in the ocean is associated with sinking particles. *Nature* **309**: 54-56.

Karstensen J, Stramma L, Visbeck M (2008) Oxygen minimum zones in the eastern tropical Atlantic and Pacific oceans. *Prog Oceanogr* **77**: 331-350.

Kates M (1978) The phytanyl ether-linked polar lipids and isoprenoid neutral lipids of extremely halophilic bacteria. *Prog Chem Fats other Lipids* **15**: 301-342.

Kates M (1989) The sulfolipids of diatoms. *In* Ackman RG (ed), Marine biogenic lipids, fats, and oils, volume 1. CRC Press, Inc., Florida.

Keeling RF, Körtzinger A, Gruber N (2010) Ocean deoxygenation in a warming world. *Annu Rev Mar Sci* **2**: 199-229.

Kempe S (1979) Carbon in the rock cycle, p 343-377. In *The Global carbon Cycle* (ed. Bolin B, Degens ET, Kempe S, Ketner P.) *SCOPE Rep. No. 13*, 343-377. Wiley, Chichester.

Killops SD, Killops VJ (2005) Introduction to Organic Geochemistry, 2nd ed., Blackwell Publishing, Malden, Mass.

Koene-Cottaar FHM, Schraa G (1998) Anaerobic reduction of ethane to ethane in an enrichment culture. *FEMS Microbiol Ecol* **25:** 251-256.

Kuypers MMM, Sliekers AO, Lavik G, Schmid M, Jørgensen BB, Kuenen JG, Sinninghe Damsté JS, Strous M, Jetten MSM (2003) Anaerobic ammonium oxidation by anammox bacteria in the Black Sea. *Nature* **422**: 608-611.

Kvenvolden KA, Weliky K, Nelson H, Des Marais DJ (1979) Submarine seep of carbon dioxide in Norton Sound, Alaska. *Science* **205**: 1264-1266.

Kvenvolden KA, Redden GD (1980) Hydrocarbon gas in sediment from the shelf, slope, and basin of the Bering Sea. *Geochim Cosmochim Acta* **44**: 1145-1150.

Kvenvolden KA (1988) Hydrocarbon gas in sediment of the Southern Pacific Ocean. *Geo-Mar Lett* **8**: 179-187.

Lam P, Kuypers MMM (2011) Microbial nitrogen cycling processes in oxygen minimum zones. *Annu Rev Mar Sci* **3**: 317-345.

Langworthy TA, Pond JL (1986) Archaebacterial ether lipids and chemotaxonomy. *Syst Appl Microbiol* **7**: 253-257.

Laws EA, Falkowski PG, Smith WO, Ducklow H, McCarthy JJ (2000) Temperature effects on export production in the open ocean. *Global Biogeochem Cycles* **14**: 1231-1246.

Lipp JS, Morono Y, Inagaki F, Hinrichs K-U (2008) Significant contribution of Archaea to extant biomass in marine subsurface sediments. *Nature* **454**: 991-994.

Lipp JS, Hinrichs K-U (2009) Structural diversity and fate of intact polar lipids in marine sediments. *Geochim Cosmochim Acta* **73**: 6816-6833.

Liu X-L, Leider A, Gillespie A, Gröger J, Versteegh GJM, Hinrichs K-U (2010) Identification of polar lipid precursors of the ubiquitous branched GDGT orphan lipids in a peat bog in Northern Germany. *Org Geochem* **41**: 653-660.

Logemann J, Graue J, Köster J, Engelen B, Rullkötter J, Cypionka H (2011) A laboratory experiment of intact polar lipid degradation in sandy sediments. *Biogeosciences* **8**: 2547-2560.

Lomstein BA, Langerhuus AT, D'Hondt S, Jørgensen BB, Spivack AJ (2012) Endospore abundance, microbial growth and necromass turnover in deep sub-seafloor sediment. *Nature* **484**: 101-104.

Madigan MT, Martinko JM, Parker J (2003) Brock-Biology of Microorganisms. Prentice Hall, Upper Saddle River, New Jersey.

Marinov I, Sarmiento JL (2004) The role of the oceans in the global carbon cycle: An overview. *In* The Ocean Cycle and Climate (ed. Follows M, Oguz T) *NATO Sci. Ser., Ser. IV,* 251-295.

Mauclaire L, Zepp K, Meister P, Mckenzie J (2004) Direct *in situ* detection of cells in deep-sea sediment cores from the Peru Margin (ODP Leg 201, Site 1229). *Geobiology* **2**: 217-223.

Middelburg JJ (1989) A simple rate model for organic matter decomposition in marine sediments. *Geochim Cosmochim Acta* **53**: 1577-1581.

Milliman JD (1993) Production and accumulation of calcium carbonate in the ocean: Budget of a nonsteady state. *Global Biogeochem Cycles* **7**: 927-957.

Mopper K, Degens ET (1979) Organic carbon in the ocean: nature and cycling. *In The Global*

Carbon Cycle (ed. Bolin B, Degens ET, Kempe S, Ketner P.), *SCOPE Rep.No.13*, 293-316. Wiley, Chichester.

Oremland RS, Whiticar MJ, Strohmaier FE, Kiene RP (1988) Bacterial ethane formation from reduced, ethylated sulfur compounds in anoxic sediments. *Geochim Cosmochim Acta* **52:** 1895-1904.

Parkes RJ, Cragg BA, Wellsbury P (2000) Recent studies on bacterial populations and processes in subseafloor sediments: A review. *Hydrogeol J* **8**: 11-28.

Paull CK, Lorenson TD, Borowski WS, Ussler III W, Olsen K, Rodriguez NM (2000) Isotopic composition of CH_4, CO_2 species, and sedimentary organic matter within samples from the black ridge: Gas source implications. *Proc Ocean Drill Prog Sci Results* **164**:67-78.

Paulmier A, Ruiz-Pino D, Garçon, Farias L (2006) Maintaining of the Eastern South Pacific oxygen minimum zone (OMZ) off Chile. *Geophys Res Lett* **33**: L20601, doi:10.1029/2006GL026801.

Paulmier A, Ruiz-Pino D (2009) Oxygen minimum zones (OMZs) in the modern ocean. *Prog Oceanogr* **80**: 113-128.

Podlaska A, Wakeham SG, Fanning KA, Taylor GT (2012) Microbial community structure and productivity in the oxygen minimum zone of the eastern tropical North Pacific. *Deep Sea Res I* **66**: 77-89.

Popendorf KJ, Lomas MW, Van Mooy BAS (2011) Microbial sources of intact polar diacylglycerolipids in the Western North Atlantic Ocean. *Org Geochem* **42**: 803-811.

Prentice IC, Farquhar, GD, Fasham MJR, Goulden ML, Heimann M, Jaramillo VJ, Kheshgi HS, Le Quéré C, Scholes RJ, Wallace DWR, Archer D, Ashmore MR, Aumont O, Baker D, Battle M, Bender M, Bopp LP, Bousquet P, Caldeira K, Ciais P, Cox PM, Cramer W, Dentener F, Enting IG, Field CB, Friedlingstein P, Holland EA, Houghton RA, House JI, Ishida A, Jain AK, Janssens IA, Joos F, Kaminski T, Keeling CD, Keeling RF, Kicklighter DW, Kohfeld KE, Knorr, W, Law R, Lenton T, Lindsay K, Maier-Reimer E, Manning AC, Matear RJ, McGuire AD, Melillo JM, Meyer R, Mund M, Orr JC, Piper S, Plattner K, Rayner PJ, Sitch S, Slater R, Taguchi S, Tans PP, Tian HQ, Weirig MF, Whorf T, Yool A (2001) The carbon cycle and atmospheric carbon dioxide. *In* Climate change 2001: the scientific basis (ed. Houghton JT), 183-237. Cambridge University Press, Cambridge.

Rossel PE, Lipp JS, Fredricks HF, Arnds J, Boetius A, Elvert M, Hinrichs K-U (2008) Intact polar lipids of anaerobic methanotrophic archaea and associated bacteria. *Org Geochem* **39**:

992-999.

Rossel PE, Elvert M, Ramette A, Boetius A, Hinrichs K-U (2011) Factors controlling the distribution of anaerobic methanotrophic communities in marine environments: Evidence from intact polar membrane lipids. *Geochim Cosmochim Acta* **75**: 164-184.

Roussel EG, Bonavita M-AC, Querellou J, Cragg BA, Webster G, Prieur D, Parkes RJ (2008) Extending the sub-sea-floor biosphere. *Science* **320**: 1046.

Rush D, Wakeham SG, Hopmans EC, Schouten S, Sinninghe Damsté JS (2012) Biomarker evidence for anammox in the oxygen minimum zone of the Eastern Tropical North pacific. *Org Geochem*, doi: 10.1016/j.orggeochem.2012.02.005.

Russell NJ, Evans RI, Ter Steeg PF, Hellemons J, Verheul A, Abee T (1995) Membranes as a target for stress adaptation. *Int J Food Microbiol* **28**: 255-261.

Rütters H, Sass H, Cypionka H, Rullkötter JJ (2002a) Phospholipid analysis as a tool to study complex microbial communities in marine sediments. *J Microbiol Methods* **48**: 149-160.

Rütters H, Sass H, Cypionka H, Rullkötter J (2002b) Microbial communities in a Wadden Sea sediment core-clues from analyses of intact glyceride lipids, and released fatty acids. *Org Geochem* **33**: 803-816.

Saltzman J, Wishner KF (1997) Zooplankton ecology in the eastern tropical Pacific oxygen minimum zone above a seamout: 1. General trends. *Deep-Sea Res I* **44**: 907-930.

Sambrotto R, Swenson K (2007) Biogeochemical flows of nitrogen in a tropical upwelling system-a cariaco time series project: PI. *In* Cruise report-Eastern Tropical Pacific Cruise, R/V *Seward Johnson* 18 October – 17 November 2007, 28-31.

Sassen R, Curiale JA (2006) Microbial methane and ethane from gas hydrate nodules of the Makassar Strait, Indonesia. *Org Geochem* **37**: 977-980.

Schimel DS (1993) Theory and application of tracers. Academic Press, Inc., San Diego.

Schippers A, Neretin LN, Kallmeyer J, Ferdelman TG, Cragg BA, Parkes RJ, Jørgensen BB (2005) Prokaryotic cells of the deep sub-seafloor biosphere identified as living bacteria. *Nature* **433**: 861-864.

Schouten S, Middelburg JJ, Hopmans EC, Sinninghe Damsté JS (2010) Fossilization and degradation of intact polar lipids in deep subsurface sediments: A theoretical approach. *Geochim Cosmochim Acta* **74**: 3806-3814.

Schubotz F, Wakeham SG, Lipp JS, Fredricks HF, Hinrichs K-U (2009) Detection of microbial biomass by intact polar membrane lipid analysis in the water column and surface sediments

of the Black Sea. *Environ Microbiol* **11**: 2720-2734.

Schubotz F, Lipp JS, Elvert M, Hinrichs K-U (2011) Stable carbon isotopic compositions of intact polar lipids reveal complex carbon flow patterns among hydrocarbon degrading microbial communities at the Chapopote asphalt volcano. *Geochim Cosmochim Acta* **75**: 4399-4415.

Siegenthaler U, Sarmiento JL (1993) Atmospheric carbon dioxide and the ocean. *Nature* **365**: 119-125.

Stramma L, Johnson GC, Sprintall J, Mohrholz V (2008) Expanding oxygen-minimum zones in the tropical oceans. *Science* **320**: 655-658.

Sturt HF, Summons RE, Smith K, Elvert M, Hinrichs, K-U (2004) Intact polar membrane lipids in prokaryotes and sediments deciphered by high-performance liquid chromatography/electrospray ionization multistage mass spectrometry-new biomarkers for biogeochemistry and microbial ecology. *Rapid Commun Mass Spectrom* **18**: 617-628.

Suess E (1980) Particulate organic carbon flux in the oceans-surface productivity and oxygen utilization. *Nature* **288**: 260-263.

Sundquist ET (1993) The global carbon dioxide budget. *Science* **259**: 934-941.

Taylor G, Flagg C and scientists from ETNP 2007 Expedition (2007) Cruise report-Eastern Tropical Pacific Cruise, R/V *Seward Johnson* 18 October – 17 November 2007.

Van Mooy BAS, Rocap G, Fredricks HF, Evans CT, Devol AH (2006) Sulfolipids dramatically decrease phosphorus demand by picocyanobacteria in oligotrophic marine environments. *Proc Natl Acad Sci USA* **103**: 8607-8612.

Van Mooy BAS, Fredricks HF, Pedler BE, Dyhrman ST, Karl DM, Koblížek M, Lomas MW, Mincer TJ, Moore LR, Moutin T, Rappé MS, Webb EA (2009) Phytoplankton in the ocean use non-phosphorus lipids in response to phosphorus scarcity. *Nature* **458**: 69-72.

Van Mooy BAS, Fredricks HF (2010) Bacterial and eukaryotic intact polar lipids in the eastern subtropical South Pacific: Water-column distribution, planktonic sources, and fatty acid composition. *Geochim Cosmochim Acta* **74**: 6499-6516.

Vogel TM, Oremland RS, Kvenvolden KA (1982) Low-temperature formation of hydrocarbon gases in San Francisco Bay sediment (California, U.S.A.). *Chem Geol* **37**: 289-298.

Volk T, Hoffert MI (1985) Ocean carbon pumps: Analysis of relative strengths and efficiencies in ocean driven atmospheric CO_2 changes. *In* Natural variations in carbon dioxide and the carbon cycle (ed. Sundquist ET, Broecker WS.), Am. Geophys, Union Mon 32, 99-110.

Wakeham SG, Amann R, Freeman KH, Hopmans EC, Jørgensen BB, Putnam IF, Schouten S,

Sinninghe Damsté JS, Talbot HM, Woebken D (2007) Microbial ecology of the stratified water column of the Black Sea as revealed by a comprehensive biomarker study. *Org Geochem* **38**: 2070-2097.

Wakeham SG, Turich C, Schubotz F, Podlaska A, Li XN, Varela R, Astor Y, Sáenz JP, Rush D, Sinninghe Damsté JS, Summons RE, Scranton MI, Taylor GT, Hinrichs K-U (2012) Biomarkers, chemistry and microbiology show chemoautotrophy in a multilayer chemocline in the Cariaco Basin. *Deep-Sea Res* I **63**: 133-156.

Walsh DA, Zaikova E, Howes CG, Song YC, Wright JJ, Tringe SG, Tortell PD, Hallam SJ (2009) Metagenome of a versatile chemolithoautotroph from expanding oceanic dead zones. *Science* **326**: 578-582.

Waseda A, Didyk BM (1995) Isotope compositions of gases in sediments from the Chile continental margin. *Proc Ocean Drill Prog Sci Results* **141**: 307-312.

Webster G, Blazejak A, Cragg BA, Schippers A, Sass H, Rinna J, Tang X, Mathes F, Ferdelman TG, Fry JC, Weightman AJ, Parkes RJ (2009) Subsurface microbiology and biogeochemistry of a deep, cold-water carbonate mound from the Porcupine Seabight (IODP Expedition 307). *Environ Microbiol* **11**: 239-257.

Wegener G, Bausch M, Holler T, Thang NM, Mollar XP, Kellermann MY, Hinrichs K-U, Boetius A (2012) Assessing sub-seafloor microbial activity by combined stable isotope probing with deuterated water and ^{13}C-bicarbonate. *Environ Microbiol,* doi:10.1111/j.1462-2920.2012.02739.x

Whelan JK, Hunt JM, Berman J (1980) Volatile C_1-C_7 organic compounds in surface sediments from Walvis Bay. *Geochim Cosmochim Acta* **44**: 1767-1785.

White DC, Davis WM, Nickels JS, King JD, Bobbie RJ (1979) Determination of the sedimentary microbial biomass by extractible lipid phosphate. *Oecologia* **40**: 51-62.

Whitman WB, Coleman DC, Wiebe WJ (1998) Prokaryotes: The unseen majority. *Proc Natl Acad Sci USA* **95**: 6578-6583.

Williams PJL (1981) Microbial contribution to overall marine plankton metabolism: Direct measurements of respiration. *Oceanol Acta* **4**: 359-364.

Williams PJLB (1998) The balance of plankton respiration and photosynthesis in the open oceans. *Nature* **394**: 55-57.

Woebken D, Fuchs BM, Kuypers MMM, Amann R (2007) Potential interactions of particle-associated anammox bacteria with bacterial and archaeal partners in the Namibian

upwelling system. *Appl Environ Microbiol* **73**: 4648-4657.

Wörmer L-P, Lipp JS, Schröder JM, Hinrichs K-U (In preparation) Application of two new LC-ESI-MS methods for improved detection of intact polar lipids (IPLs) in environmental samples.

Wright JJ, Konwar KM, Hallam SJ (2012) Microbial ecology of expanding oxygen minimum zones. *Nat Rev Microbiol* **10**: 381-394.

Yoshinaga MY, Kellermann MY, Rossel PE, Schubotz F, Lipp JS, Hinrichs K-U (2011) Systematic fragmentation patterns of archaeal intact polar lipids by high-performance liquid chromatography/electrospray ionization ion-trap mass spectrometry. *Rapid Commun Mass Spectrom* **25**: 3563-3574.

Zink K-G, Wilkes H, Disko U, Elvert M, Horsfield B (2003) Intact phospholipids-microbial "life markers" in marine deep subsurface sediments. *Org Geochem* **34**: 755-769.

Chapter II

Distribution of eukaryotic and bacterial intact polar lipids in the oxygen minimum zone of the Eastern Tropical North Pacific Ocean

Sitan Xie [a*], Florence Schubotz [a,¶], Stuart G. Wakeham [b,§], Kai-Uwe Hinrichs [a]

In preparation for *Organic Geochemistry*

[a]*Organic Geochemistry Group, MARUM Center for Marine Environmental Sciences and Department of Geosciences, University of Bremen, Leobener Straße, 28359 Bremen, Germany*

[b]*Skidaway Institute of Oceanography, Savannah, GA 31411, USA*

[¶]*Current address: Department of Earth, Atmospheric, and Planetary Sciences, Massachusetts Institute of Technology, Cambridge, MA, 02139 USA*

[§]*Current address: Department of Oceanography, University of Washington, Seattle, WA 98195-7940 USA*

**Corresponding author. Organic Geochemistry Group, MARUM Center for Marine Environmental Science and Department of Geosciences, University of Bremen, Leobener Straße, 28359Bremen, Germany. Tel: +49-421-21865744. Fax: +49-421-21865715. E-mail: sitan.xie@uni-bremen.de*

II.1. ABSTRACT

The distribution of intact polar lipids (IPLs) from eukaryotic and bacterial sources was investigated in the oxygen minimum zone (OMZ) of the Eastern Tropical North Pacific Ocean (ETNP). Ten major IPL classes were identified in the water column of the ETNP: monoglycosyldiacylglycerol (MGDG), diglycosyldiacylglycerol (DGDG), sulfoquinovosyldiacylglycerol (SQDG), glycosylceramides (Gly-Cer), phosphatidylethanolamine (PE) and its methylated derivatives (phosphatidyl-(N)-methylethanolamine (PME) and phosphatidyl-(N,N)-dimethylethanolamine) (PDME), phosphatidylglycerol (PG), phosphatidylcholine (PC), and betaine lipids (BL). Highest concentrations of IPLs (300~1400 ng/L) were observed in the euphotic zone where eukaryotes are abundant, and increased abundances (15~40 ng/L) were found within the OMZ where prokaryotes have elevated concentration. In the euphotic zone and upper layers of OMZ (< 100 m), glycolipids, including MGDG, DGDG and SQDG, account for more than 50% of total IPLs, whereas phospholipids (PE, PME, PDME, PG and PC) and BL were dominant (60%~100%) in the OMZ and deep oxycline layers. Ratios between phosphate-based lipids and their corresponding non-phosphorous-bearing substitute lipids, e.g., SQDG/PG and BL/PC, were studied in a continuous water column profile down to 1 km water depth. High values of SQDG/PG and BL/PC were observed at depths where phosphate is abundant, which suggests that enrichment of substitute lipids is not only impacted by phosphate limitation but also the microbial community that inhabits the oceanic water. Our study extends our understanding on the distribution and ecology of eukaryotes and bacteria in oxygen-deficient oceanic water column.

II.2. INTRODUCTION

In the modern ocean, oxygen minimum zones (OMZs) characterized by dissolved oxygen concentration less than 20 μM account for ~8% of the total oceanic area (Paulmier and Ruiz-Pino, 2009). The Eastern Tropical North Pacific Ocean (ETNP) off Mexico and Central America hosts one of the largest oxygen minimum zones (OMZs) in the open ocean, at depths between ~100 and ~800 m (Paulmier and Ruiz-Pino, 2009, and observations from the present sampling expedition). Rapid oxygen consumption via respiration of organic matter exported from the highly productive upper water column, together with a sharp permanent pycnocline that prevents ventilation of more oxygenated deep waters result in the occurrence of the strong OMZ in the ETNP (Fiedler and

Talley, 2006). Expansion of OMZs occurred during the past 50 years due to global warming (Stramma et al., 2008; Keeling et al., 2010) and has a profound effect on global carbon and nitrogen cycles. As oxygen concentrations decline, organisms that are unable to survive under oxygen limitation wane. OMZs are therefore good targets for studying the effect of low-O_2 on the marine biogeochemistry and, in particular, the microbial communities (Karstensen et al., 2008; Wright et al., 2012). In this study, the OMZ of the ETNP could be roughly compartmentalized into four horizons based on O_2 concentrations: a euphotic and upper oxycline zone (200 μM > O_2 > 20 μM), the upper OMZ (20 μM > O_2 > 2 μM), the mid or core OMZ (O_2 < 2 μM), and the deep oxycline layer below mid OMZ (O_2 > 2 μM) where O_2 levels begin to rise again (see *Experiments II.3.3* for details). Highest concentrations of Chlorophyll *α* fluorescence were observed in the top 100 m and decreased to absence in deeper water indicating abundance of phytoplankton (Podlaska et al., 2012). Cell numbers of total prokaryotes (dominated by bacteria) were most abundant in the euphotic layers, decreased with depth, but rose again within mid OMZs (Podlaska et al., 2012), which is consistent with the former observations in other oxygen-deficient regions such as the upwelling area off the coast of Namibia (Woebken et al., 2007) and anoxic basins, e.g., the Black Sea and Cariaco Basin (Lin et al., 2006; Lam et al., 2007; Wakeham et al., 2007, 2012).

As a complementary approach to molecular biological techniques, intact polar membrane lipids (IPLs) analysis provide further insight into the microbial communities under varying environmental conditions. IPLs are ubiquitous in a wide range of geological settings as membrane constituents of every living organism, although applicability of archaeal IPLs to low-activity subseafloor sediment remains controversial (cf. Lipp and Hinrichs, 2009; Schouten et al., 2010, Logemann et al., 2011). Due to rapid degradation after cell lysis (White et al., 1979; Harvey et al., 1986), IPLs are used as biomarkers for living microbes (Sturt et al., 2004; Schubotz et al., 2009; Van Mooy and Fredricks, 2010). Among all the IPL groups, diacylglycerolipids are likely the most abundant group in the oceanic waters (Christie, 2003; Van Mooy and Fredricks, 2010). Glycolipids, such as MGDG, DGDG and SQDG, are well known as thylakoid membrane lipids of chloroplasts (Kates, 1990; Wada and Murata, 1998), whereas bacterial membranes are dominated by phospholipids, e.g., PG, PC, PE and its methyl derivatives (Barridge and Shively, 1968; Imhoff and Bias-Imhoff, 1995). Betaine lipids are widely distributed in lower plants and green algae (Volkman et al., 1989; Dembitsky, 1996; Kato et al, 1996). So far, distributions of IPLs in oceanic water have been presented in several regions, such as in anoxic basins (Black Sea: Schubotz et al., 2009; Cariaco Basin: Wakeham et al., 2012), in the Eastern Subtropical South Pacific (Van Mooy

and Fredricks, 2010) and in the Western North Atlantic Ocean (Popendorf et al., 2011a). Here, we provide the first report of distributions of eukaryotic and bacterial IPLs in the OMZ of the ETNP. The distribution patterns provide unique insights on the ecology and distribution of microbial communities as well as the cycling of nitrogen and phosphorous in relation to lipid biosynthesis.

II.3. EXPERIMENTS

II.3.1. Samples

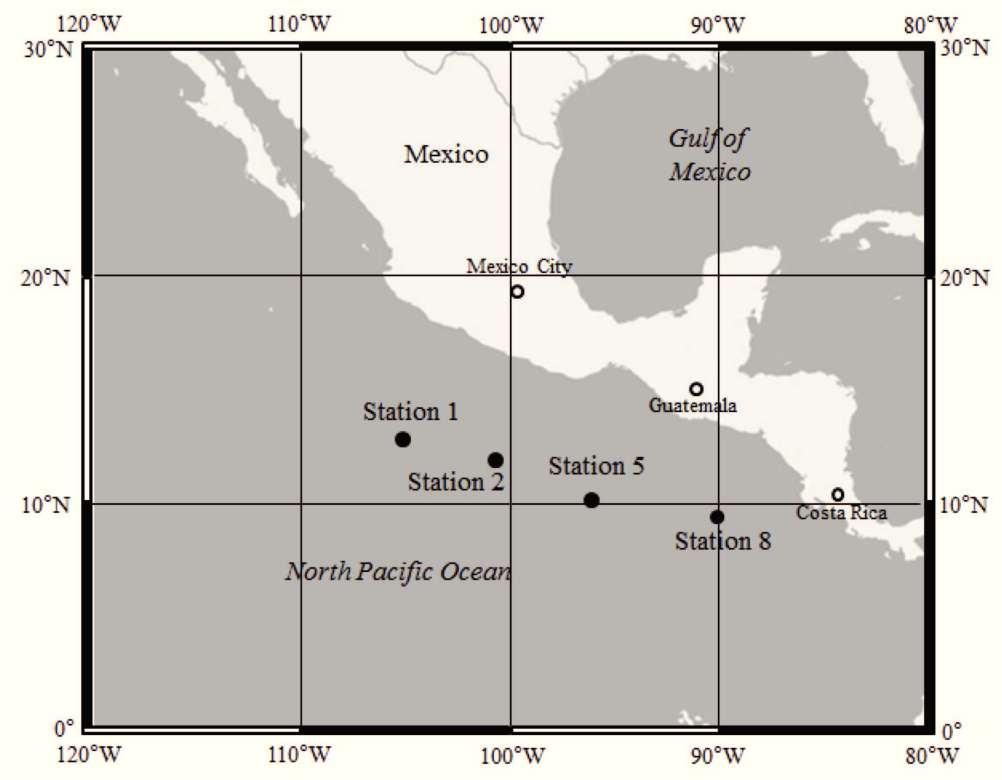

Fig. II.1. Map of the ETNP with sampling stations.

Particulate matter (PM) samples were collected by in-situ filtration of seawater using McLane Research filtration systems (WTS-142) deployed on the conducting cable of the CTD/rosette in the OMZ of the ETNP during the R/V *Seward Johnson* cruise in November 2007. Temperature, conductivity, fluorescence and dissolved oxygen were measured during pump deployments and again during recovery; pump depths (four pumps per cast) were monitored from the CTD depth during pumping. The locations of Station 1 (13°N，105°W), Station 2 (12° 14’ N，101° 13.74’ W), Station 5 (10° 41.41’ N，96° 56.6’ W) and Station 8 (9°N，90°W) followed a

south-east transect, where Station 1 was located in the Tehuantepec Bowl off southern Mexico and Station 8 was in Costa Rica Dome, a year-round upwelling area (Fig. II.1). PM was collected on ashed glass fiber filters (142 mm, Gelman type A/E) after "prefiltration" through a 53 µm screen to remove most eukaryotes. Double type A/E filters (nominal pore size 0.7 µm) were used to maximize the collection of small particles that might contain microbial biomarkers. After filtration samples were stored frozen at -20°C until extraction.

II.3.2. Elemental analysis and total lipids extraction

Particulate organic carbon (POC) and total nitrogen (TN) were measured on 14 mm-diameter subsamples of each filter prior to lipid extraction. The plugs were acidified in HCl vapor in a dessicator for 12 hours to remove inorganic carbon and analyzed with a ThermoFinnigan Flash EA Series 1112 interfaced to a ThermoFinnigan Delta V isotope ratio mass spectrometer. Organic carbon and nitrogen content were calibrated against internal laboratory chitin powder standards which in turn had previously been cross-calibrated against USGS 40 and 41 international standards.

Lipids were extracted by soxhlet at Skidaway Institute of Oceanography from GFFs using dichloromethane:methanol (DCM/MeOH; 9:1 v/v) for 8 hr (Wakeham et al., 2007). Extracted lipids were partitioned into DCM against 5% NaCl solution and dried over Na_2SO_4. Total lipid extracts (TLEs) were stored at -20°C.

II.3.3. Analysis of IPLs

An aliquot of the TLE was dissolved in DCM/methanol (5:1 v/v) for analysis on a ThermoFinnigan Surveyor high-performance liquid chromatography system coupled to a ThermoFinnigan LCQ DecaXP Plus ion-trap mass spectrometer via electrospray interface (HPLC-ESI-IT-MS^n) using conditions described previously (Sturt et al., 2004). 10 µL of an aliquot spiked with C_{19}-PC as internal standard was injected onto a LiChrosphere Diol-100 column (150×2.1 mm, 5 µm, Alltech, Germany) equipped with a guard column of the same packing material. Individual samples were measured in positive and negative ionization modes with automated data-dependent fragmentation of base peak ions up to MS^2. Details of mass spectral interpretation, IPL quantification, and identification of fatty acids moieties were described in Schubotz et al. (2009). The Betaine lipids diacylglyceryl trimethylhomoserine (DGTS) and

diacylglyceryl hydroxymethyl-trimethyl-ß-alanine (DGTA) were summarized as one group because the structural similarity of their polar head groups did not allow identification on fragmentation patterns alone. PE, PME and PDME could not be quantified separately due to co-elution and overlapping *m/z* values in the MS^1 (Schubotz et al., 2009). The detection limit (0.01~0.04 ng/L) is determined for each individual run using the same approach as shown in Lipp et al. (2008).

For the subsequent interpretation of IPL distributions, the OMZ of the ETNP for each station is roughly compartmentalized into four horizons based on O_2 concentrations: a euphotic and upper oxycline zone (0~50 m), the upper OMZ (Station 1 and 8: 50~300 m; Station 2 and 5: 50~200 m), the mid or core OMZ (Station 1 and 8: 300~800 m; Station 2 and 5: 200~600 m), and the deep oxycline layer below mid OMZ (Station 1 and 8 ≥ 800 m; Station 2 and 5 ≥ 600 m).

II.4. RESULTS AND DISCUSSION

II.4.1. Water column chemistry in the OMZ of the ETNP

The water depths for all stations were deeper than 2500 m. Samples for lipid analysis were collected within the upper 1300 m. Sea water temperature was around 26°C at the surface, and decreased with increasing water depth. Temperature was about 4°C at 1200 m (Fig. II.2B, F, J, N). The oxygen content of surface waters was around 200 µM and dropped rapidly to < 30 µM within the euphotic zone due to biological respiration (Fig. II.2B, F, J, N). Although a secondary peak of O_2 occurred at 200 m depth at Station 1 and 5, the O_2 was lower than 20 µM in the main body of the OMZ. Significant nitrite (NO_2^-) maxima was observed in the mid OMZ at all stations except in the upper OMZ at Station 2 (Fig. II.2A, E, I, M). The nitrite peaks coexisted with nitrate deficits indicating nitrate reduction in the OMZ was a source for nitrite (Sambrotto and Swenson, 2007). Ammonium (NH_4^+) concentrations were rather constant through the water column at all stations (Fig. II.2A, E, I, M). The sources of ammonium include nitrate reduction, mineralized organic matter from surface waters and excretion by macrozooplankton during their vertical migrations. Similar depth profiles could be observed for POC and TN concentrations (Fig. II.2C, G, K, O), which were highest in the euphotic zone, mainly due to planktonic sources (POC: 40~80 µg/L; TN: 5~15 µg/L), rapidly dropped to 5 µg/L and 1 µg/L, respectively, below the upper OMZ, increased slightly in the mid OMZ (POC: 10 µg/L; TN: 2 µg/L), and finally were below 3 µg/L and 0.5 µg/L in the deeper oxycline layer.

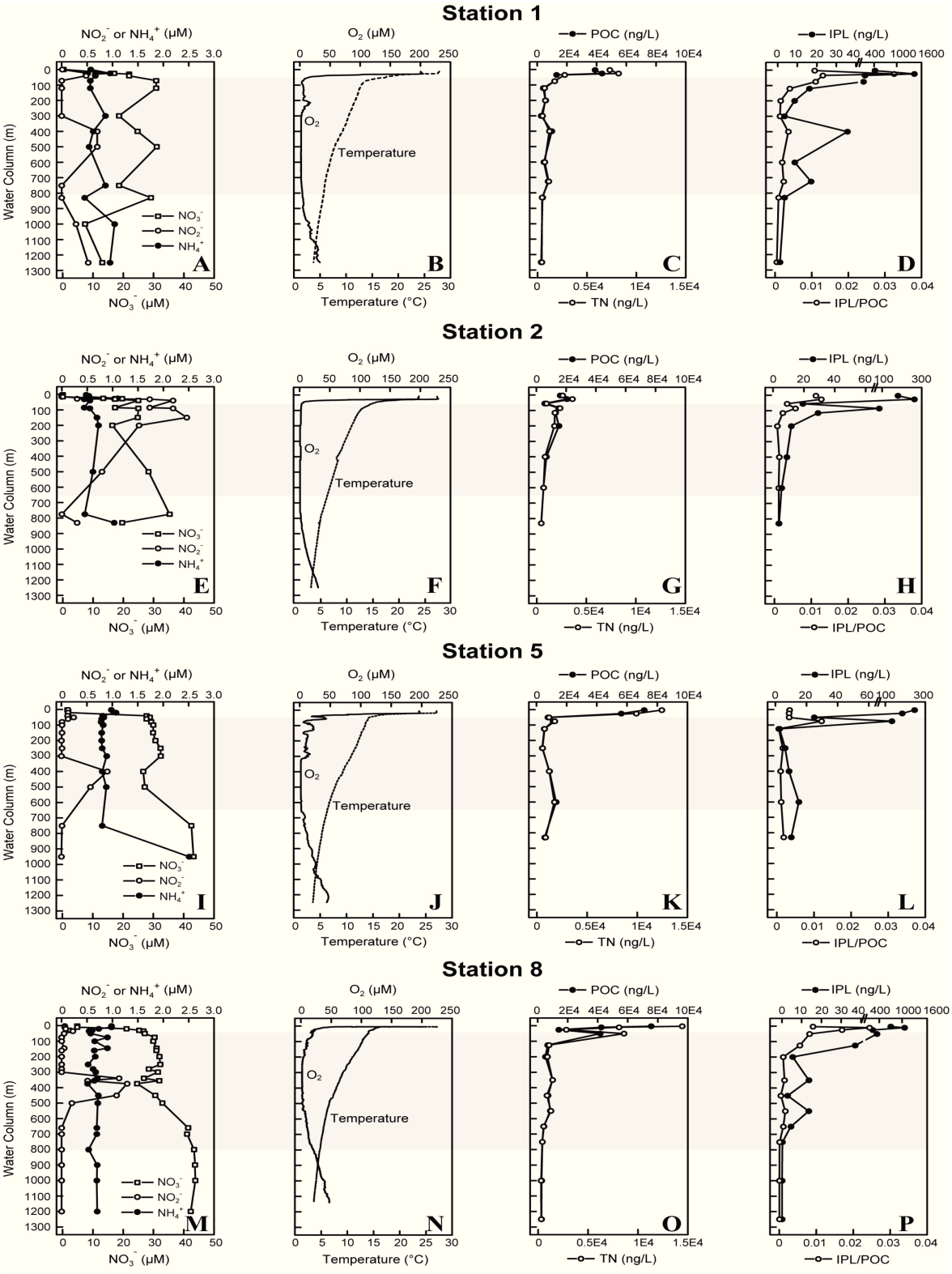

Fig. II.2. Depth profiles of A, E, I, M) nitrate, nitrite and ammonia; B, F, J, N) oxygen and temperature; C, G, K, O) POC and TN; D, H, L, P) IPL concentration and IPL/POC at Station 1, 2, 5 and 8 in the ETNP, respectively. Grey bars designate the OMZ.

II.4.2. Overview of IPL distribution in the OMZ of the ETNP

Lipids were dominated by eukaryotic and bacterial IPLs in the water column of the ETNP. After purification of the total lipid extract (TLE) using preparative HPLC, archaeal IPLs could be observed as well, but will be discussed in a separate work. Highest concentrations of IPLs (300~1400 ng/L) were observed in the euphotic zone, and abruptly decreased (< 20 ng/L) more than 10-fold in the upper OMZ as O_2 levels declined (Fig. II.2D, H, L, P). At surface depths, IPL concentrations were by one order of magnitude higher at Station 1 and 8 than those at Station 2 and 5, which was consistent with higher chlorophyll *α* fluorescence found at Station 1 and 8 (Podlaska et al., 2012). Small peaks in IPL concentrations (15~40 ng/L) were present within the OMZ at all stations where prokaryotes had elevated amounts (Podlaska et al., 2012). IPL/POC ratios decreased with increasing depth (Fig. II.2 D, H, L, P) indicating preferential degradation of lipids relative to total organic carbon (Wakeham and Canuel, 1988). IPL concentrations and IPL/POC ratios track trends of POC and TN (Fig. II.2) suggesting significant contribution of lipids to total organic carbon and total nitrogen pools in the OMZ of the ETNP.

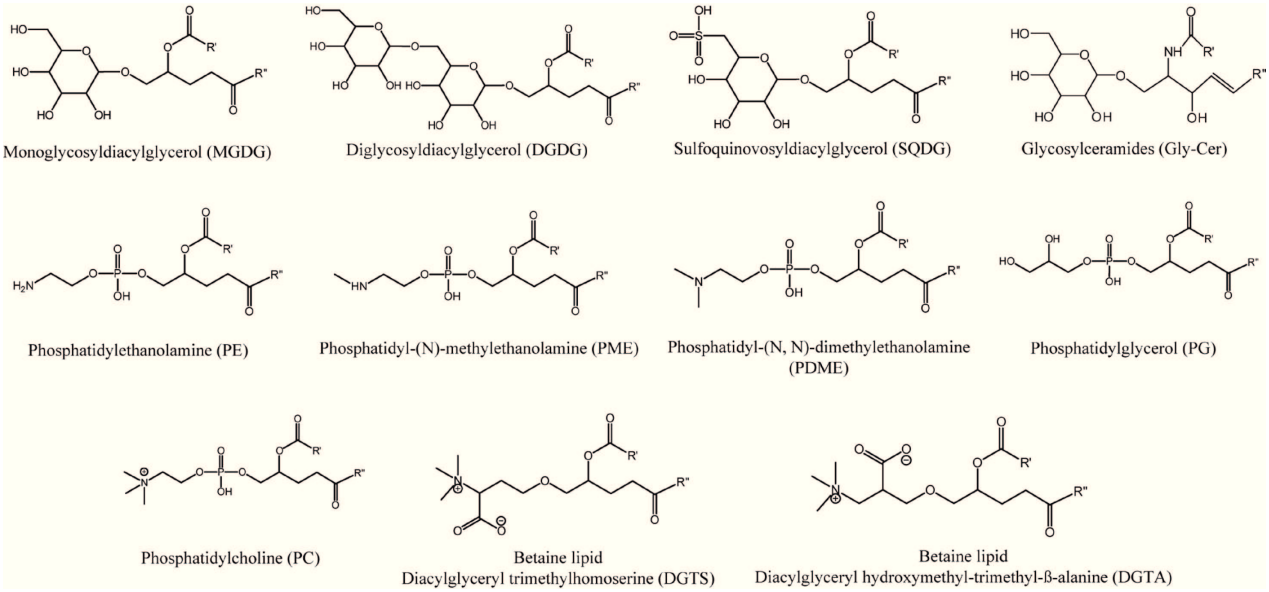

Fig. II.3. Structures of IPLs observed in the ETNP. R' and R'' represent acyl groups.

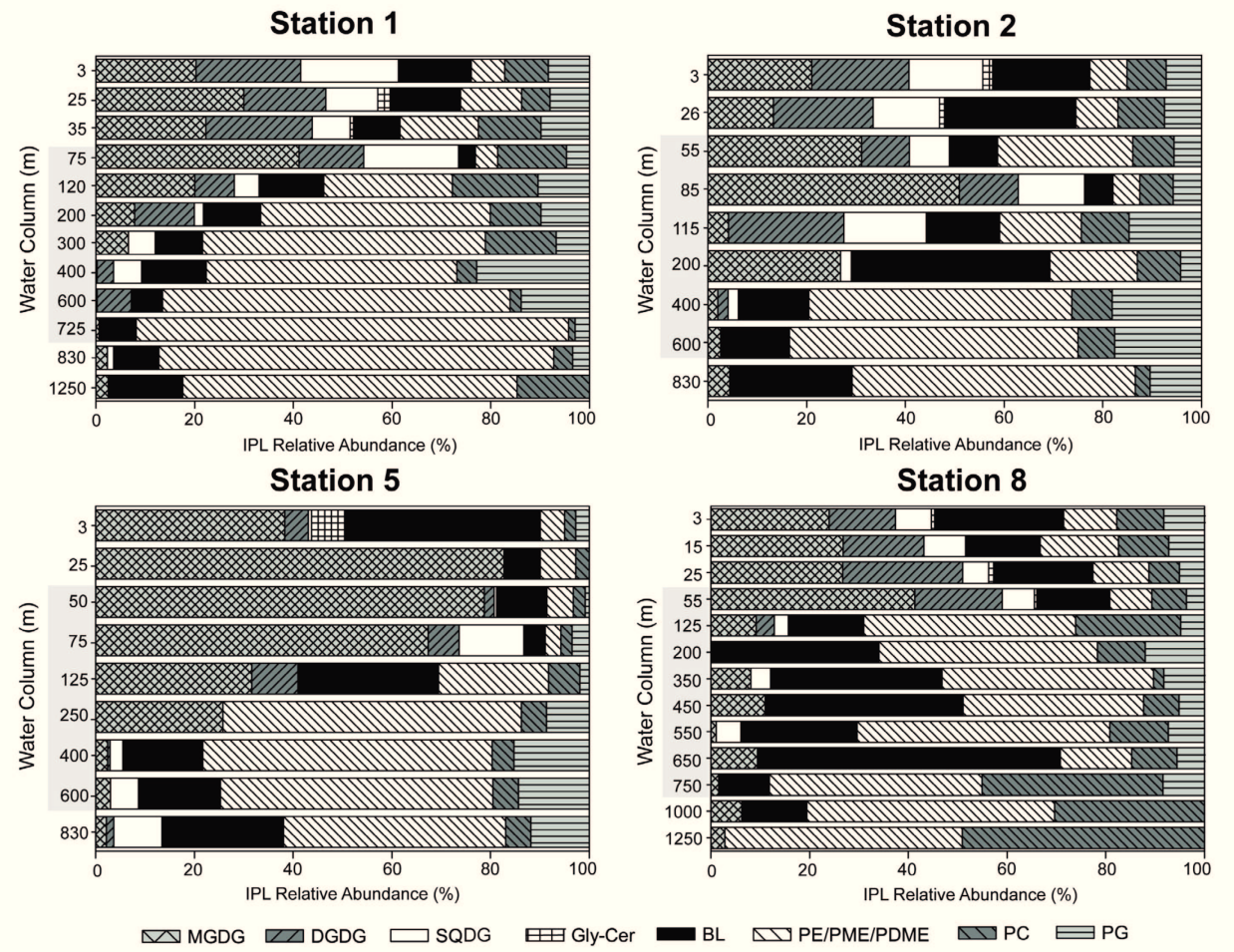

Fig. II.4. Relative abundance of IPLs at Station 1, 2, 5, and 8 in the water column of the ETNP, respectively. Grey bars refer to the OMZ.

Ten major IPL classes were at the four stations in the ETNP: MGDG, DGDG, SQDG, Gly-Cer, BL, PE, PME, PDME, PG and PC (structures are shown in Fig. II.3). In the water column above 100 m, glycolipids, including MGDG, DGDG and SQDG, accounted for more than 50% of total IPLs, whereas phospholipids (PE, PME, PDME, PG and PC) and BL dominated (60%~100%) after 120 m and in deeper depths (Fig. II.4). This zonation pattern of IPLs in the surface waters is similar to what was observed in the Eastern Subtropical South Pacific where glycolipids dominated the total IPL composition in surface waters (Van Mooy and Fredricks, 2010). However, in this study glycolipids composed 50 ± 15% of total IPLs up to 250 m, which might be due to high oxygen concentration throughout the water column (150~200 μM in the top 800 m). At depths where glycolipids dominated IPLs, MGDG was the most abundant (10%~80%) glycolipid, followed by DGDG (5%~20%), and SQDG (3%~17%). Gly-Cer was only detected in

the euphotic zone as a minor component (≤ 5%), and recent results highlight their potential role in viral lysis of phytoplankton (Vardi et al., 2009). Phospholipids were abundant at depths below 100 meters. Concentration of PE, PME and PDME (14%~87%) was higher compared to other phospholipids, e.g., PC (2%~50%) and PG (5%~23%). Individual abundances of IPLs in the OMZ of the ETNP were different from the Eastern Subtropical South Pacific where SQDG and PC were the most abundant compounds within the glycolipids and phospholipids, respectively (Van Mooy and Fredricks, 2010). The difference might be induced by varying response factors for each IPL group by different analytical protocols. BL is a common compound with fluctuation in relative abundance throughout the water column at all stations, ranging from 3%~40% (Fig. II.4).

II.4.3. Potential biological sources for each IPL group in the OMZ of the ETNP

II.4.3.1. Glycolipids: MGDG, DGDG, SQDG and Gly-Cer

Three classes of glycoglycerides with diacyl core lipids were identified in the OMZ of the ETNP: MGDG, DGDG and sulfur-containing SQDG. They are common glycolipids in oceanic waters (Schubotz et al., 2009; Van Mooy and Fredricks, 2010; Wakeham et al., 2012). Glycolipids were major components of IPLs in surface waters up to 100 m (with relative abundance of up to 83%), and became a minor fraction in the mid OMZ and deep oxycline layers (relative abundance less than 10%) (Fig. II.4). MGDG, DGDG and SQDG are the main constituents of photosynthetic membranes, such as chloroplast lipids of plants (Poincelot 1973, 1976; Mackender and Leech, 1974; Nishihara et al., 1980), eukaryotic algae (Araki et al., 1991; Thompson, 1996) and cyanobacteria (Wada and Murata, 1998; Siegenthaler, 1998; Hölzl and Dörmann, 2007; Popendorf et al., 2011a). Photosynthetic algae are possible the primary biological source of glycolipids in the euphotic zone. Cyanobacteria are abundant from the surface to 200 m (Wishner et al., 2007) which could also be considered as an additional origin in the euphotic zone and upper OMZ. Another potential source for MGDG in the OMZ could be heterotrophic bacteria as their growth was correlated with an increase in the concentration of MGDG in the Western North Atlantic Ocean (Popendorf et al., 2011a). Besides heterotrophic bacteria, anoxygenic phototrophic bacteria could also be origin for MGDG in the OMZ (Hölzl and Dörmann, 2007). Below 100 m, MGDG decreased quickly to less than 10%, which is likely due to remineralization of this compound (Harvey et al., 1986; Matos and Pham-Thi, 2009). A similar situation was found in the Cariaco Basin, where MGDG disappeared quickly with depth (Wakeham et al., 2012).

The dominant fatty acid combination of MGDG was $C_{14:0}/C_{16:1}$ throughout the water column (Table II.1). $C_{16:0}/ C_{16:1}$ was predominant in the suboxic layer of the Black sea (Schubotz et al., 2009), but was not detectable in the OMZ of the ETNP. $C_{14:0}/C_{16:2}$ was a significant component in the euphotic zone and upper OMZ, but became undetectable in the deeper depth. Combination of polyunsaturated fatty acids (PUFA), such as $C_{16:4}/C_{18:3}$, $C_{16:4}/C_{18:4}$, $C_{18:4}/C_{18:4}$, $C_{18:4}/C_{18:5}$ and $C_{18:5}/C_{18:5}$, which are widespread in marine plankton (Brett and Müller-Navarra, 1997; Okuyama et al., 1993) were detected in the euphotic zone, but disappeared in the deeper depths due to rapid degradation of the most-labile highly unsaturated compounds (De Baar et al., 1983; Prahl et al., 1984; Neal et al., 1986). The pattern of fatty acid combinations of MGDG suggest that 1) MGDG in the deeper depths represents residual material from surficial algal material where rapid degradation of PUFAs has occurred or, the more likely scenario, 2) a distinct microbial community inhabiting the OMZ and deep oxycline which does not produce PUFAs. Major fatty acids moieties for DGDG were $C_{14:0}/C_{16:0}$ and $C_{14:0}/C_{16:1}$ in the euphotic zone and OMZ, $C_{14:0}/C_{16:1}$ could not be observed in the mid OMZ and deep oxycline (Table II.1). Similar to MGDG, DGDG also contained planktonic PUFA ($C_{16:3}$, $C_{16:4}$, $C_{18:3}$, $C_{18:4}$, $C_{18:5}$, $C_{20:5}$) in significant amounts in the euphotic zone, which then gradually disappeared in the OMZ and deep oxycline layer. $C_{14:0}$, $C_{16:0}$, and $C_{16:1}$ were the major fatty acids moieties for SQDG, although dominant combinations change throughout the water column: $C_{14:0}/C_{14:0}$, $C_{14:0}/C_{16:0}$ and $C_{14:0}/C_{16:1}$ were dominant in the euphotic zone and mid OMZ, $C_{14:0}/C_{16:0}$, $C_{14:0}/C_{16:1}$ and $C_{16:1}/C_{16:1}$ in the upper OMZ, and $C_{14:0}/C_{14:0}$, $C_{14:0}/C_{16:0}$ and $C_{16:0}/C_{16:0}$ in the deep oxycline layer, probably due to different biological sources (Table II.1). Notably, SQDG in the deep oxycline layers was only detected at Station 5, and therefore fatty acids moieties for SQDG at this horizon may not be representative. Combinations of fatty acids with odd numbers of carbon atoms, e.g., $C_{15:0}/C_{16:0}$ and $C_{14:0}/C_{15:0}$, were also found for SQDG indicating bacterial contribution.

Gly-Cer belongs to the class of sphingolipids consisting of a sphingosine linked to a fatty acid via an amide bond. Gly-Cer was detected only in the euphotic zone with relative abundance less than 5% at all stations (Fig. II.4). The presence of Gly-Cer in natural environment was initially reported in the anoxic zone (100 m) of the Black sea (Schubotz et al., 2009); the compound type is also found in coccolithophore populations in the North Atlantic, where they have been identified to be involved in viral attacks (Vardi et al., 2009). Gly-Cer was also observed in the deep chemocline and anoxic layers of the Cariaco Basin as minor component, constituting ~3% of IPLs (Wakeham et al., 2012). The occurrence of Gly-Cer in the euphotic zone might

suggest eukaryotic cells or viral infection as potential sources (Lynch and Dunn et al., 2004; Vardi et al., 2009). Gly-Cer was only detected in the euphotic zone with trace amount, and therefore it is not included for comparison of diacylglyceride moieties for each IPL group.

Table II.1. Acyl carbon numbers and fatty acid combinations for each IPL group observed in the ETNP. Relative abundance is presented as medians and standard deviation.

	Euphotic Zone	Upper OMZ	Mid OMZ	Deep Oxycline
MGDG	**28:0**(14:0/14:0, 4±2%); **30:0**(14:0/16:0; 6±2%); **30:1**(14:0/16:1; 44±10%); **30:2**(14:0/16:2;20±8%); **30:3**(14:1/16:2; 2±2%); **32:1**(14:0/18:1; 2±2%); **34:1**(16:0/18:1; 3±1%); **34:7**(16:4/18:3; 4±3%); **34:8**(16:4/18:4; 2±2%); **36:8**(18:4/18:4; 3±2%); **36:9**(18:4/18:5; 4±2%); **36:10**(18:5/18:5; 1±2%);	**30:0**(14:0/16:0; 9±8%); **30:1**(14:0/16:1;56±18%); **30:2**(14:0/16:2; 17±15%); **30:3**(14:1/16:2; 3±7%); **32:1**(14:0/18:1; 3±6%); **36:8**(18:4/18:4; 4±9%);	**30:0**(14:0/16:0; 11±16%);**30:1**(14:0/16:1; 80±20%); **30:3**(14:1/16:2; 3±7%);**32:1**(14:0/18:1; 3±8%);	**30:0**(14:0/16:0; 10±17%); **30:1**(14:0/16:1; 86±27%); **32:1**(14:0/18:1; 4±10%);
DGDG	**28:0**(14:0/14:0, 3±2%); **30:0**(14:0/16:0; 12±8%); **30:1**(14:0/16:1; 11±8%); **32:2**(16:1/16:1; 3±3%); **32:2**(14:1/18:1; 3±3%); **32:4**(14:0/18:4; 8±6%); **32:5**(14:0/18:5; 5±4%); **34:1**(16:0/18:1; 6±3%); **34:2**(16:0/18:2; 8±5%); **34:3**(16:0/18:3; 6±3%); **34:4**(16:0/18:4; 5±2%); **34:6**(16:3/18:3; 5±3%); **34:7**(16:4/18:3; 8±4%); **34:8**(16:4/18:4; 5±8%); **34:9**(18:4/18:5; 4±3%); **36:10**(18:5/18:5; 5±6%); **38:9**(18:4/20:5; 3±5%);	**28:0**(14:0/14:0, 6±7%); **30:0**(14:0/16:0; 11±9%); **30:1**(14:0/16:1; 22±18%); **32:2**(16:1/16:1; 9±10%); **32:2**(14:1/18:1; 8±7%); **32:4**(14:0/18:4; 5±5%); **32:5**(14:0/18:5; 4±3%); **34:1**(16:0/18:1; 2±4%); **34:2**(16:0/18:2; 2±4%); **34:3**(16:0/18:3; 3±4%);; **34:7**(16:4/18:3; 3±3%); **34:8**(16:4/18:4; 7±13%); **34:9**(18:4/18:5; 5±6%); **36:10**(18:5/18:5; 6±12%); **38:9**(18:4/20:5; 3±5%);	**28:0**(14:0/14:0, 3±6%); **30:0**(14:0/16:0; 28±48%); **30:1**(14:0/16:1; 9±11%); **32:2**(14:1/18:1; 7±8%); **32:4**(14:0/18:4; 10±15%); **34:1**(16:0/18:1; 3±6%); **34:2**(16:0/18:2; 3±6%); **34:7**(16:4/18:3; 7±7%); **34:8**(16:4/18:4; 6±7%); **34:9**(18:4/18:5; 6±12%); **36:10**(18:5/18:5; 13±18%); **38:9**(18:4/20:5; 4±8%);	**30:0**(14:0/16:0; 41%); **34:1**(16:0/18:1; 28%); **34:2**(16:0/18:2; 31%);
SQDG	**28:0**(14:0/14:0, 15±16%); **30:0**(14:0/16:0; 27±10%); **30:1**(14:0/16:1; 25±27%); **31:0**(15:0/16:0; 5±6%); **32:0**(16:0/16:0; 7±5%); **32:1**(16:0/16:1; 7±5%); **32:2**(16:1/16:1; 5±4%); **34:2**(16:0/18:2; 4±4%);	**28:0**(14:0/14:0, 3±4%); **29:0**(14:0/15:0; 3±6%); **30:0**(14:0/16:0; 21±21%); **30:1**(14:0/16:1; 22±18%); **31:0**(15:0/16:0; 5±14%);**32:0**(16:0/16:0; 4±5%); **32:1**(16:0/16:1; 15±13%); **32:2**(16:1/16:1; 25±35%);	**28:0**(14:0/14:0, 19±17%); **29:0**(14:0/15:0; 15±11%);**30:0**(14:0/16:0; 26±11%); **30:1**(14:0/16:1; 7±9%); **31:0**(15:0/16:0; 6±7%); **32:0**(16:0/16:0; 5±10%); **32:1**(16:0/16:1; 10±21%); **32:2**(16:1/16:1; 3±6%); **34:1**(16:0/18:1; 8±11%);	**28:0**(14:0/14:0, 19%); **29:0**(14:0/15:0; 18%); **30:0**(14:0/16:0; 24%); **30:1**(14:0/16:1; 13%); **32:0**(16:0/16:0; 18%); **34:1**(16:0/18:1; 8%);
PE/ PME/ PDME	**28:0**(14:0/14:0, 5±3%); **30:0**(14:0/16:0; 5±5%); **30:1**(14:0/16:1; 8±5%); **32:0**(16:0/16:0; 5±7%); **32:1**(16:0/16:1; 12±11%);**32:1**(15:1/17:0; 5±4%); **33:1**(16:0/17:1; 11±6%); **33:2**(15:1/18:1; 5±5%); **34:1**(16:0/18:1; 3±3%); **34:1**(15:1/19:0; 4±9%); **34:2**(16:1/18:1; 8±5%); **34:2**(17:1/17:1; 4±3%); **35:2**(15:1/20:1; 3±4%); **36:2**(18:1/18:1; 3±3%); **38:6**(16:0/22:6; 6±6%);	**28:0**(14:0/14:0, 3±9%); **30:1**(14:0/16:1; 7±4%); **32:0**(16:0/16:0; 5±6%); **32:1**(16:0/16:1; 5±6%); **32:1**(15:1/17:0; 7±5%); **32:2**(15:0/17:2; 4±6%); **33:1**(16:0/17:1; 10±6%); **33:2**(15:1/18:1; 7±9%); **34:2**(16:1/18:1; 7±8%); **34:2**(17:1/17:1; 3±3%); **35:2**(15:1/20:1; 4±4%); **38:6**(16:0/22:6; 9±16%); **38:9**(18:5/20:4; 6±8%); **39:9**(18:5/21:4; 6±12%);	**30:1**(14:0/16:1; 5±3%); **32:0**(16:0/16:0; 9±16%); **32:1**(16:0/16:1; 5±3%); **32:1**(15:0/17:1; 8±18%); **32:1**(15:1/17:0; 5±3%); **32:2**(16:1/16:1; 4±3%); **32:2**(15:0/17:2; 4±5%); **33:1**(16:0/17:1; 9±5%); **34:1**(16:0/18:1; 6±8%); **34:2**(16:1/18:1; 9±5%); **34:2**(17:1/17:1; 3±2%); **35:2**(15:1/20:1; 4±2%); **38:6**(16:0/22:6; 8±12%); **38:9**(18:5/20:4; 6±4%); **39:9**(18:5/21:4; 4±4%)	**30:1**(14:0/16:1; 5±1%); **32:1**(16:0/16:1; 6±2%); **32:1**(15:1/17:0; 5±1%); **32:2**(16:1/16:1; 6±3%); **32:2**(15:0/17:2; 7±6%); **33:1**(16:0/17:1; 9±2%); **33:2**(15:1/18:1; 7±4%); **34:1**(15:1/19:0; 3±3%); **34:2**(16:1/18:1; 11±4%); **34:2**(17:1/17:1; 7±4%); **35:2**(15:1/20:1; 8±5%);

Table II.1. (continued).

	Euphotic Zone	Upper OMZ	Mid OMZ	Deep Oxycline
PG	**28:0**(14:0/14:0, 9±9%); **30:0**(14:0/16:0; 3±2%); **32:1**(16:0/16:1; 11±15%);**32:2**(16:1/16:1; 10±7%); **33:2**(16:1/17:1; 14±18%); **34:1**(16:0/18:1; 15±7%); **34:2**(16:1/18:1; 10±7%); **34:3**(16:0/18:3; 7±7%); **34:4**(16:0/18:4; 6±5%); **35:2**(17:1/18:1; 3±2%); **36:1**(18:0/18:1; 6±8%); **36:2**(18:1/18:1; 6±4%);	**28:0**(14:0/14:0, 8±13%); **30:0**(14:0/16:0; 3±4%); **32:1**(16:0/16:1; 17±15%); **32:2**(16:1/16:1; 17±16%); **33:2**(16:1/17:1; 18±14%); **34:1**(16:0/18:1; 8±9%); **34:2**(16:1/18:1; 11±7%); **35:2**(17:1/18:1; 5±7%); **36:1**(18:0/18:1; 5±14%); **36:2**(18:1/18:1; 6±8%);	**28:0**(14:0/14:0, 7±20%); **30:0**(14:0/16:0; 2±3%); **32:1**(16:0/16:1; 8±8%); **32:2**(16:1/16:1; 5±6%); **33:2**(16:1/17:1; 14±10%); **34:1**(16:0/18:1; 19±24%);**34:2**(16:1/18:1; 11±7%); **35:2**(17:1/18:1; 21±29%); **36:2**(18:1/18:1; 8±8%);	**28:0**(14:0/14:0, 7±7%); **30:0**(14:0/16:0; 5±6%); **32:1**(16:0/16:1; 7±12%); **33:2**(16:1/17:1; 20±4%); **34:1**(16:0/18:1; 11±11%); **34:2**(16:1/18:1; 22±6%); **35:2**(17:1/18:1; 20±11%); **36:2**(18:1/18:1; 5±9%);
PC	**28:0**(14:0/14:0, 6±4%); **28:2**(14:1/14:1, 6±14%); **30:0**(14:0/16:0; 5±3%); **32:0**(16:0/16:0; 5±3%); **32:1**(16:0/16:1; 3±3%); **32:3**(16:0/16:3; 3±2%); **32:5**(14:0/18:5; 5±4%); **35:5**(15:0/20:5; 3±3%); **35:7**(15:2/20:5; 4±4%); **36:5**(16:0/20:5; 6±5%); **36:6**(14:0/22:6; 5±4%); **37:6**(15:0/22:6; 3±3%); **38:0**(18:0/20:0; 19±27%); **38:6**(16:0/22:6; 17±9%); **38:9**(16:3/22:6; 6±7%);	**28:2**(14:1/14:1, 3±4%);**32:0**(16:0/16:0; 9±27%); **32:3**(16:0/16:3; 5±5%); **35:5**(15:0/20:5; 4±4%); **36:5**(16:0/20:5; 4±5%); **36:6**(14:0/22:6; 5±4%); **37:6**(15:0/22:6; 3±6%); **38:0**(18:0/20:0; 28±30%); **38:6**(16:0/22:6; 16±21%); **38:9**(16:3/22:6; 7±11%); **40:16**(20:8/20:8; 3±8%);	**28:0**(14:0/14:0, 3±6%); **30:0**(14:0/16:0; 5±7%); **32:1**(16:0/16:1; 13±13%); **32:3**(16:0/16:3; 4±8%); **35:5**(15:0/20:5; 3±4%); **36:6**(14:0/22:6; 4±4%);**38:0**(18:0/20:0; 42±29%); **38:6**(16:0/22:6; 3±7%); **38:9**(16:3/22:6; 6±14%); **40:16**(20:8/20:8; 7±14%);	**37:6**(15:0/22:6; 3±7%); **38:0**(18:0/20:0; 65±36%); **38:3**(16:1/22:2; 6±14%); **38:6**(16:0/22:6; 14±16%); **38:9**(16:3/22:6; 5±13%);
BL	**28:0**(14:0/14:0, 8±4%); **30:1**(14:0/16:1; 5±6%); **32:1**(14:1/18:0; 4±3%); **34:1**(16:0/18:1; 4±3%); **34:2**(16:0/18:2; 6±4%); **34:3**(16:0/18:3; 6±3%); **34:4**(16:2/18:2; 6±3%); **34:5**(16:2/18:3; 4±3%); **34:6**(16:2/18:4; 3±2%); **34:7**(16:4/18:3; 3±2%); **35:0**(15:0/20:0; 3±2%); **36:1**(16:1/20:0; 4±2%); **36:2**(16:2/20:0; 8±4%); **36:3**(16:3/20:0; 4±1%); **36:4**(16:4/20:0; 7±2%); **36:5**(18:2/18:3; 6±3%); **36:6**(18:3/18:3; 4±1%);	**28:0**(14:0/14:0, 6±4%); **30:1**(14:0/16:1; 10±7%); **32:1**(14:1/18:0; 8±5%); **32:7**(16:3/16:4; 3±4%); **32:8**(16:4/16:4; 3±4%); **34:1**(16:0/18:1; 15±13%); **34:2**(16:0/18:2; 9±5%); **34:3**(16:0/18:3; 4±3%); **36:1**(16:1/20:0; 7±5%); **36:2**(16:2/20:0; 9±4%); **36:3**(16:3/20:0; 4±3%); **36:4**(16:4/20:0; 6±5%); **36:5**(18:2/18:3; 3±3%);	**28:0**(14:0/14:0, 4±3%); **32:1**(14:1/18:0; 10±7%); **32:8**(16:4/16:4; 3±4%);**34:1**(16:0/18:1; 23±12%); **34:2**(16:0/18:2; 8±3%); **34:5**(16:2/18:3; 6±14%); **34:8**(16:4/18:4; 3±4%); **36:1**(16:1/20:0; 5±3%); **36:2**(16:2/20:0; 9±5%); **36:4**(16:4/20:0; 4±3%); **38:1**(18:1/20:0; 8±16%);	**26:0**(12:0/14:0, 5±9%); **28:0**(14:0/14:0, 6±4%); **28:1**(14:0/14:1; 3±5%); **30:1**(14:0/16:1; 5±5%); **32:1**(14:1/18:0; 6±6%); **32:8**(16:4/16:4; 13±22%); **34:1**(16:0/18:1; 12±8%); **34:2**(16:0/18:2; 8±5%); **34:3**(16:0/18:3; 13±20%); **36:1**(16:1/20:0; 4±3%); **36:2**(16:2/20:0; 7±5%); **36:4**(16:4/20:0; 3±4%); **36:5**(18:2/18:3; 3±3%);

II.4.3.2. Phospholipids: PE, PME, PDME, PG, PC

Five groups of phosphoglycerides with diacyl core lipids were identified in the OMZ of the ETNP: PE, PME, PDME**,** PG and PC. PE, PME and PDME were the most abundant lipids in the mid OMZ and deep oxycline layer of the ETNP (Fig. II.4). In eukaryotic algae, PE has been

sometimes found, but only in very low abundances, but it is a common phospholipid in membranes of bacteria. Reported sources for PE are diverse, e.g., nitrifying bacteria (Goldfine and Hagen, 1968), sulfur-oxidizing bacteria (Barridge and Shively, 1968), metal-oxidizing bacteria (Short et al., 1969), marine heterotrophic bacteria (Oliver and Colwell, 1973; Van Mooy et al., 2009; Popendorf et al., 2011a), fermentative bacteria (De Siervo and Reynolds, 1975), methanotrophic bacteria (Makula, 1978; Fang et al., 2000), sulfate-reducing bacteria (Rütters et al., 2001; Sturt et al., 2004), and methylotrophic bacteria (Fang and Barcelona, 1998). PME and PDME are intermediates in the *N*-methylation pathway for PC biosynthesis from PE (Bremer and Greenberg, 1959; Vance and Ridgway, 1988; Sohlenkamp et al., 2003). Sources for PME and PDME are similar as PE but more specific, such as absence of PME in the fermentative bacteria (De Siervo and Reynolds, 1975) and less than 1% abundance of PDME in the gram-negative marine bacteria (Oliver and Colwell, 1973). In the ETNP, heterotrophic bacteria, such as *α*-proteobacteria and *ß*-proteobacteria which were significant proportions of total prokaryotic population (Podlaska et al., 2012) are potential biological sources for PE, PME and PDME. Recent studies have shown that in the upper water column PE is produced by both heterotrophic bacteria and by autotrophs (Popendorf et al., 2011a). Nitrifying bacteria presenting throughout the water column of the ETNP with higher abundance at Station 2 and 5 than Station 1 and 8 (Podlaska et al., 2012) could also be considered as source for these three IPLs. Sulfate-reducing bacteria and sulfur-oxidizing bacteria were found prevalent in the OMZ of the ETNP (Podlaska et al., 2012), which are additional contributors for PE. The dominant combinations of fatty acids for PE, PME, PDME were variable throughout the water column indicating distinct sources in different horizons, for example $C_{16:0}/C_{16:1}$ and $C_{16:0}/C_{17:1}$ were major fractions in the euphotic zone, $C_{16:0}/C_{17:1}$ and $C_{16:0}/C_{22:6}$ were abundant in the upper OMZ, $C_{16:0}/C_{16:0}$, $C_{16:0}/C_{17:1}$, $C_{16:1}/C_{18:1}$ and $C_{16:0}/C_{22:6}$ became major combinations in the mid OMZ, and $C_{16:0}/C_{17:1}$, $C_{16:1}/C_{18:1}$ and $C_{15:1}/C_{20:1}$ were the dominant combinations in the deep oxycline. Presence of $C_{15:1}$ and $C_{17:1}$ indicated bacteria as biological source (Table II.1).

PC is the only phospholipid that contains the long-chain PUFA which are typically observed in the eukaryotic algae (Brett and Müller-Navarra, 1997). In our water column sample, PC has a high unsaturation degree (Table II.1) which indicates that eukaryotic phytoplankton is likely the major source for PC in the ETNP. Besides eukaryotic phytoplankton, PC is also found in some bacteria, such as some gram-negative bacteria (Goldfine 1984; Dowhan 1997), purple sulfur bacteria (Imhoff and Bias-Imhoff, 1995), nitrifying bacteria (Goldfine and Hagen, 1968),

methanotrophic bacteria (Makula, 1978), sulfate reducing bacteria (Rütters et al., 2001), picocyanobacteria (Van Mooy et al., 2006) and metal oxidizing bacteria (Short et al., 1969), which could be considered as minor contributors for PC in the OMZ of the ETNP. ^{13}C labeling studies in the North Atlantic have confirmed that in surface waters the predominant source for PC are autotrophic organisms, indicating a planktonic source (Popendorf et al., 2011a). In the euphotic zone and upper OMZ, dominant fatty acids for PC were $C_{16:0}$, $C_{18:0}$, $C_{20:0}$ and long-chain PUFA $C_{20:5}$ and $C_{22:6}$ indicating eukaryotic origin (Table II.1). $C_{18:0}$ and $C_{20:0}$ became major fractions in the mid OMZ and deep oxycline suggesting a different source of PC.

PG is a major phospholipid in eukaryotic cells and bacterial organisms (Goldfine, 1984; Dowhan, 1997). Eukaryotic phytoplankton and picocyanobacteria could be major sources for PG in the euphotic zone and upper layers of the OMZ. However, Popendorf et al. (2011a) have shown that in surface waters of the Atlantic, heterotrophic bacteria seem to be dominating source for PG. There are some other plausible sources for PG in the OMZ and deeper depths, such as anoxygenic phototrophic bacteria (Imhoff and Bias-Imhoff, 1995), methanotrophic bacteria (Makula, 1978; Fang et al., 2000), fermentative marine bacteria (De Siervo and Reynolds, 1975), metal-oxidizing bacteria (Short et al., 1969) and methylotrophic bacteria (Fang and Barcelona, 1998). Major fatty acids for PG were $C_{14:0}$, $C_{16:0}$, $C_{16:1}$, $C_{18:1}$ plus $C_{17:1}$ (Table II.1). Saturated fatty acids, e.g., $C_{14:0}$ and $C_{16:0}$, became less abundant in the deeper depths (mid OMZ and deeper oxycline). Combinations of fatty acids with odd numbers of carbon atoms, e.g., $C_{16:1}/C_{17:1}$ and $C_{17:1}/C_{18:1}$, indicating bacterial origin.

II.4.3.3. BL

BL are diacylglycerol lipids containing an amino acid as head group. BL presented significant components at most depths in the OMZ of the ETNP (relative abundance from 5% to 40%) with the exception of 1250 m at Station 8 (Fig. II.4), where they were not detected. BL are widely distributed in lower plants and green algae (e.g., Kato et al., 1994; 1996; Dembitsky, 1996), which are major sources for BL in the euphotic zone (cf. Popendorf et al., 2011a). Besides eukaryotes, two photoheterotrophic bacteria have the ability to produce the BL DGTS under phosphate limiting conditions: *Rhodobacter sphaeroides* (Benning et al., 1995) and *Rhizobium meliloti* (Geiger et al., 1999). Elevated heterotrophic activities were observed within the OMZ and deep oxycline layers in our study area (Podlaska et al., 2012), however, no phosphate limiting

conditions were prevalent. Genes which are responsible for synthesis of BL DGTS are only found in some orders of *α*-proteobacteria (López-Lara et al., 2003). In the water column of the Black sea, *α*-proteobacteria and some unknown anaerobic bacteria were suggested to be possible producers of BL in the anoxic zone (Schubotz et al., 2009). In the OMZ of the ETNP, *α*-proteobacteria was present throughout water column, with elevated relative abundance in the mid OMZ at Station 1 and Station 8 (Podlaska et al., 2012). Although heterotrophic bacteria and cyanobacteria were not considered as sources of BL in the surface waters of the Eastern Subtrophic South Pacific (Van Mooy and Fredricks, 2010), we could not exclude them as possible biological input of BLs in the OMZ of the ETNP. BL contained significant amount of C_{14}, C_{16}, C_{18} and C_{20} in the euphotic zone (Table II.1). $C_{14:0}/C_{16:1}$ and $C_{16:0}/C_{18:1}$ were major combinations in the upper OMZ, whereas $C_{14:0}/C_{16:1}$ became undetectable in the mid OMZ. In the deep oxycline layer, $C_{16:4}/C_{16:4}$, $C_{16:0}/C_{18:1}$ and $C_{16:0}/C_{18:3}$ were the dominant fatty acids combinations for BL. Minor amount of $C_{15:0}$ (3%) was only found in euphotic zone.

II.4.4. Correlation between distribution of IPLs and environmental parameters

In order to get a better understanding on the influence of environmental parameters on IPL distributions in the water column of the ETNP, a principal component analysis (PCA) was performed including all the lipids data and selected biogeochemical parameters, such as oxygen, temperature, fluorescence, depth and nutrient concentrations (e.g., NO_3^-, NH_4^+, PO_4^{3-}, POC and TN). All of the glycolipids MGDG, DGDG, SQDG and Gly-Cer were loaded positively on the first principal component as was O_2, temperature, fluorescence, NH_4^+, POC and TN, explaining 43% of the total variance (Fig. II.5). In contrast, PE, PME, PDME as well as depth, NO_3^- and PO_4^{3-}, were all negatively loaded on the first principal component, while BL, PC, PG and NO_2^- did not show a significant loading on either the first or second principal component. None of the compounds was significantly loaded on the second principal component, which explained 12% of the variance. These results reflect the vertical distribution of IPLs in the water column of the ETNP: glycolipids were most prevalent in surface waters where oxygen contents were high accompanied with elevated primary productivity (high POC and TN). Phospholipids, in particular PE, PME and PDME become more prevalent with deeper depths where bacterial picoplankton dominated the microbial communities, at deeper depths also nutrient concentrations (NO_3^- and

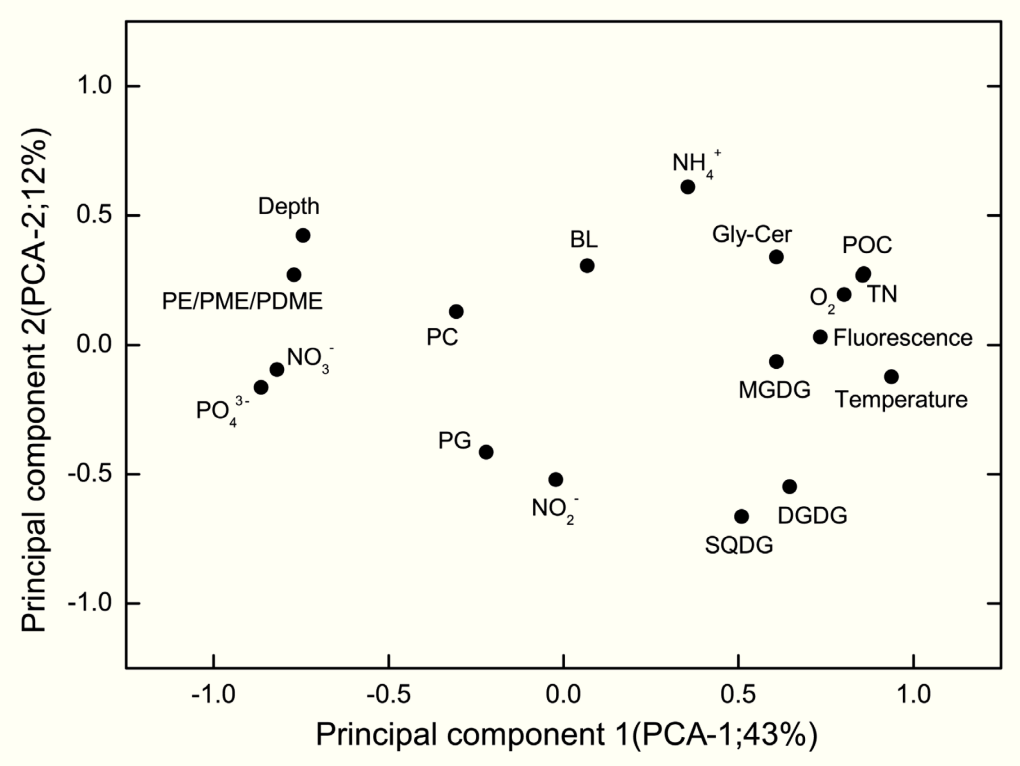

Fig. II.5. Results of PCA. The concentrations of ten lipid groups and selected biogeochemical parameters from all sites were included in this PCA analysis. Percentages indicate the amount of variability accounted for by each principle component.

PO_4^{3-}) were elevated. IPLs that did not show a loading on either PCA1 or PCA2 were found throughout the water column, such as BL and PG.

II.4.5 Substitute IPLs

Because of similar biochemical functions and same ionic charge under same ionic charge at physiological pH, SQDG and BL are known as substitute lipids for PG and PC, respectively. Substitution of these phospholipids with their respective non-phosphorous containing counterparts has been shown for eukaryotic phytoplankton, cyanobacteria and anoxygenic phototrophs both in the lab and in the environment, when phosphorus is limiting (Benning et al., 1993; 1995; Van Mooy et al., 2009; Popendorf et al., 2011b). Substitution can be tracked by calculating the molar ratios of the respective lipids. The ratios SQDG/PG and BL/PC ratios have been observed to be lower (both around 3.6) in the phosphate-replete (PO_4^{3-} >100 nmol L^{-1}) surface waters of South Pacific Ocean (< 60 m), but they were high (4.5 and 13.1, respectively) in the phosphate-limited (PO_4^{3-} <10 nmol L^{-1}) top waters in Sargasso Sea (< 60 m) (Van Mooy et al., 2009). More recently

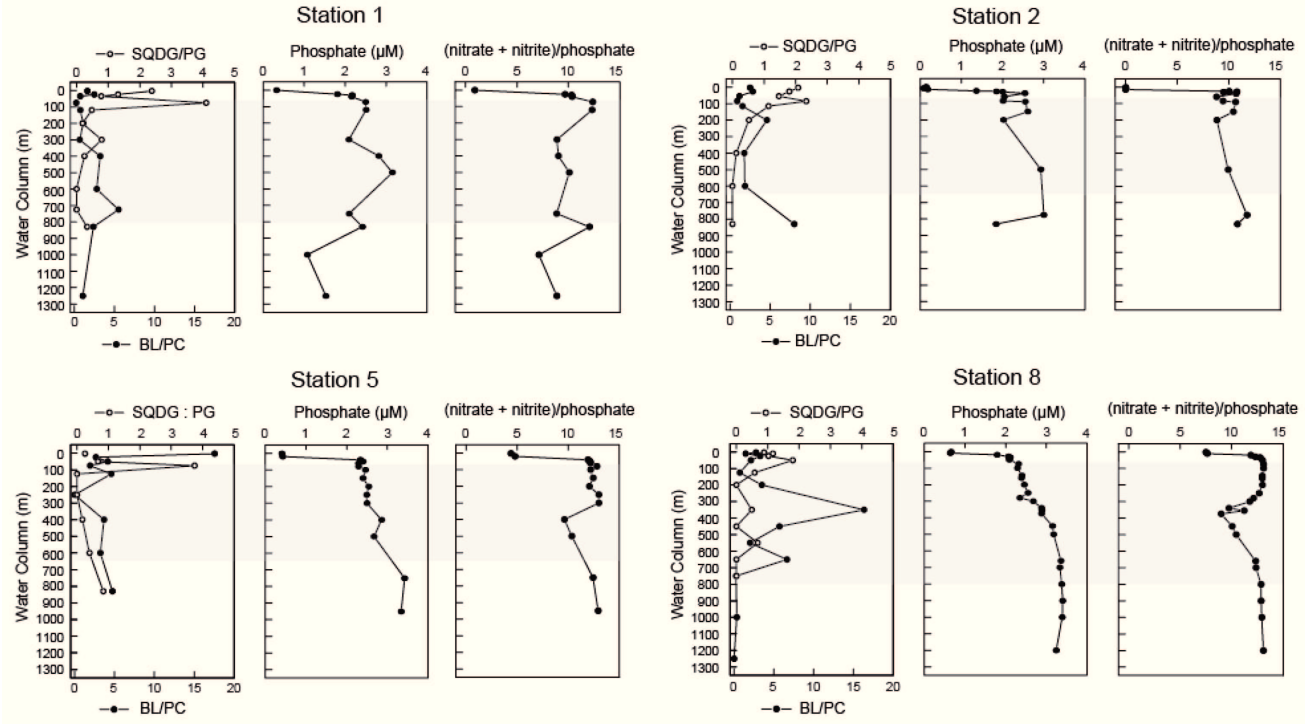

Fig. II.6. Depth profiles of molar ratio of SQDG/PG, BL/PC, phosphate concentration, and N/P ratio at Stations 1, 2, 5 and 8 in the ETNP. Grey bars designate the OMZ.

it was shown that the relative abundance of phospholipids is positively correlated with phosphate concentration across the Mediterranean Sea, which was explained as either a consequence of the microbial community composition as well as physiological response of organisms in the face of phosphorus-deficient (Popendorf et al., 2011b). Microcosm incubations amended with ammonium resulting in the increase of SQDG/PG and BL/PC suggested that changes in substitute lipid ratios are mainly caused by a strong physiological response to increased phosphorus stress (Popendorf et al., 2011b). In the water column of the Eastern Subtropical South Pacific (less than 250 m), increasing SQDG/PG ratios were observed with increasing depth and phosphate concentration, but neither SQDG nor BL concentrations was correlated with phosphate concentration indicating that not only phosphate concentrations but also community structure influences the presence or absence of phospholipids (Van Mooy and Fredericks, 2010). In this study, SQDG/PG and BL/PC ratios were calculated in water samples up to 1000 m. SQDG/PG were relatively low in the surface waters where phosphate concentrations were less than 0.5 µM (Fig. II.6) but peaked in the upper OMZ where phosphate levels were around 2 µM. High values of BL/PC were also observed in the mid OMZ where phosphate was abundant (with the exception of Station 5), and tend to

increase again below the OMZ at Station 2 and 5. Overall, the depth profiles of SQDG/PG and BL/PC are contrasting the hypothesis that lipid substitution occurs only when phosphorous is scarce. Additionally, our results show an anti-correlation of substitute lipid ratios with N/P in which suggesting that in the OMZ of the ETNP rather the microbial community composition controls the IPL composition than phosphorus stress. Similar to the Eastern Subtropical South Pacific, SQDG/PG and BL/PC in the OMZ of the ETNP does not seem to be impacted by both phosphate limitation, instead the indigenous microbial communities seem to dictate the shifts in these ratios. In surface waters cyanobacteria and phytoplankton, who abundantly synthesize SQDG and BL, are the likely reason of high substitute lipid ratios. However, in the deeper water depths the microbial biological sources for non-phosphorous containing lipids still need to be elucidated.

II.5. CONCLUSIONS

Four glycolipids, MGDG, DGDG, SQDG and Gly-Cer, five phospholipids, PE, PME, PDME, PG and PC, together with BL were observed eukaryotic and bacterial IPLs in the OMZ of the ETNP. Highest concentrations of IPLs (300~1400 ng/L) were observed in the euphotic zone, and secondary peaks in concentration (15~40 ng/L) were found within the OMZ, mimicking the zones of phototrophic and chemoautotrophic production in surface waters and the OMZ, respectively. Glycolipids accounted for more than 50% of total IPLs in the surface waters (< 100 m), while phospholipids and BL were predominant (60% - 100%) in the OMZ and deep oxycline layers. The biological sources for each IPL group were distinct in each horizon, reflected in the dominant fatty acid compositions for each IPL class, which was variable throughout the water column. High values of SQDG/PG and BL/PC were observed at depths where phosphate concentrations were high, suggesting that not only phosphate limitation but possibly also microbial community composition influences the distribution of substitute lipids in the oceanic water column.

II.6. ACKNOELEDGEMENTS

We are grateful to the captain and the crew of R/V *Seward Johnson* and to K. Daly and K. Wishner as co-chief scientists. We would like to thank H. Albrecht, B. Olsen and S. Habtes who helped with PM sampling. We thank Kent Fanning and Rob Masserini at University of South

Florida for providing their nutrient results. Lab supplies and analytical infrastructure is funded by the Deutsche Forschungsgemeinschaft through the Cluster of Excellence/Research Center MARUM. S. Xie was funded by the China Scholarship Council, and U.S. National Science Foundation grant OCE-0550654 to S. G. Wakeham supported this project. SGW also acknowledges a Fellowship from the Hanse-Wissenschaftskolleg (Hanse Institute for Advanced Studies) in Delmenhorst, Germany.

II.7. REFERENCES

Araki S, Eichenberger W, Sakurai T, Sato N (1991) Distribution of diacylglycerylhydroxymethyltrimethyl-*ß*-alanine (DGTA) and phosphatidylcholine in brown algae. *Plant and Cell Physiol* **32**: 623-628.

Barridge JK, Shively JM (1968) Phospholipids of the Thiobacilli. *J Bacteriol* **95**: 2182-2185.

Benning C, Beatty JT, Prince RC, Somerville CR (1993) The sulfolipid sulfoquinovosyldiacylglycerol is not required for photosynthetic electron transport in *Rhodobacter sphaeroides* but enhances growth under phosphate limitation. *Proc Natl Acad Sci USA* **90**: 1561-1565.

Benning C, Huang Z-H, Gage DA (1995) Accumulation of a novel glycolipid and a betaine lipid in cells of *Rhodobacter sphaeroides* grown under phosphate limitation. *Arch Biochem Biophys* **317**: 103-111.

Bremer J, Greenberg DM (1959) Mono- and dimethylethanolamine isolated from rat-liver phospholipids. *Biochim Biophys Acta* **35**: 287-288.

Brett MT, Müller-Navarra DC (1997) The role of highly unsaturated fatty acids in aquatic foodweb processes. *Freshw Biol* **38**: 483-499.

Christie WW (2003) Lipid Analysis, 3rd Edition. Oily Press, Bridgewater, UK.

De Baar HJW, Farrington JW, Wakeham SG (1983) Vertical flux of fatty acids in the North Atlantic Ocean. *J Mar Res* **41**: 19-41.

Dembitsky VM (1996) Betaine ether-linked glycerolipids: chemistry and biology. *Prog Lipid Res* **35**: 1-51.

De Siervo AJ, Reynolds JW (1975) Phospholipid composition and cardiolipin synthesis in fermentative and nonfermentative marine bacteria. *J Bacteriol* **123**: 294-301.

Dowhan W (1997) Molecular basis for membrane phospholipid diversity: Why are there so many lipids? *Annu Rev Biochem* **66**: 199-232.

Fiedler PC, Talley LD (2006) Hydrography of the eastern tropical Pacific: A review. *Prog Oceanogr* **69**: 143-180.

Fang J, Barcelona MJ (1998) Structural determination and quantitative analysis of bacterial phospholipids using liquid chromatography/electrospray ionization/mass spectrometry. *J Microbiol Methods* **33**: 23-35.

Fang J, Barcelona MJ, Semrau JD (2000) Characterization of methanotrophic bacteria on the basis of intact phospholipid profiles. *FEMS Microbiol Lett* **189**: 67-72.

Geiger O, Röhrs V, Weissenmayer B, Finan TM, Thomas-Oates JE (1999) The regulator gene *phoB* mediates phosphate stress-controlled synthesis of the membrane lipid diacylglyceryl-*N,N,N*-trimethylhomoserine in *Rhizobium* (*Sinorhizobium*) *meliloti*. *Mol Microbiol* **32**: 63-73.

Goldfine H, Hagen P-O (1968) *N*-methyl groups in bacterial lipids III. Phospholipids of hyphomicrobia. *J Bacteriol* **95**: 367-375.

Goldfine H (1984) Bacterial membranes and lipid packing theory. *J Lipid Res* **25**: 1501-1507.

Harvey HR, Fallon RD, Patton JS (1986) The effect of organic matter and oxygen on the degradation of bacterial membrane lipids in marine sediments. *Geochim Cosmochim Acta* **50**: 795-804.

Hölzl G, Dörmann P (2007) Structure and function of glycoglycerolipids in plants and bacteria. *Prog Lipid Res* **46**: 225-243.

Imhoff JF, Bias-Imhoff U (1995) Lipids, quinones and fatty acids of anoxygenic phototrophic bacteria. *In* Anoxygenic Photosynthetic Bacteria (ed. Blankenship RE, Madigan MT, Bauer CE.), 179-205. Kluwer Academic Publishers, Netherlands.

Karstensen J, Stramma L, Visbeck M (2008) Oxygen minimum zones in the eastern tropical Atlantic and Pacific oceans. *Prog Oceanogr* **77**: 331-350.

Keeling RF, Körtzinger A, Gruber N (2010) Ocean deoxygenation in a warming world. *Annu Rev Mar Sci* **2**: 199-229.

Kates M (1990) Handbook of lipid research: glycolipids, phosphoglycolipids and sulfoglycolipids. Plenum Press, New York.

Kato M, Adachi K, Hajiro-Nakanishi K, Ishigaki E, Sano H, Miyachi S (1994) A betaine lipid from *Pavlova Lutheri*. *Phytochemistry* **37**: 279-280.

Kato M, Sakai M, Adachi K, Ikemoto H, Sano H (1996) Distribution of betaine lipids in marine algae. *Phytochemistry* **42**: 1341-1345.

Lam P, Jensen MM, Lavik G, McGinnis DF, Müller B, Schubert CJ, Amann R, Thamdrup B, Kuypers MMM (2007) Linking crenarchaeal and bacterial nitrification to anammox in the Black Sea. *Proc Natl Acad Sci USA* **104**: 7104-7109.

Lin X, Wakeham SG, Putnam IF, Astor YM, Scranton MI, Chistoserdov AY, Taylor GT (2006) Comparison of vertical distributions of prokaryotic assemblages in the anoxic Cariaco Basin and Black Sea by use of fluorescence in situ hybridization. *Appl Environ Microbiol* **72**: 2679-2690.

Lipp JS, Hinrichs K-U (2009) Structural diversity and fate of intact polar lipids in marine sediments. *Geochim Cosmochim Acta* **73**: 6816-6833.

Logemann J, Graue J, Köster J, Engelen B, Rullkötter J, Cypionka H (2011) A laboratory experiment of intact polar lipid degradation in sandy sediments. *Biogeosciences* **8**: 2547-2560.

López-Lara IM, Sohlenkamp C, Geiger O (2003) Membrane lipids in plant-associated bacteria: Their biosynthesis and possible functions. *Mol Plant Microbe Interact* **16**: 567-579.

Lynch DV, Dunn TM (2004) An introduction to plant sphingolipids and a review of recent advances in understanding their metabolism and function. *New Phytol* **161**: 677-702.

Mackender RO, Leech RM (1974) The galactolipid, phospholipid, and fatty acid composition of the chloroplast envelope membranes of *Vicia faba* L. *Plant Physiol* **53**: 496-502.

Makula RA (1978) Phospholipid composition of methane-utilizing bacteria. *J Bacteriol* 134: 771-777.

Matos AR, Pham-Thi A-T (2009) Lipid deacylating enzymes in plants: Old activities, new genes. *Plant Physiol Biochem* **47**: 491-503.

Nishihara M, Yokota K, Kito M (1980) Lipid molecular species composition of thylakoid membranes. *Biochimi Biophys Acta* **617**: 12-19.

Neal AC, Prahl FG, Eglinton G, O'Hara SCM, Corner EDS (1986) Lipid changes during a planktonic feeding sequence involving unicellular algae, *Elminius Nauplii* and adult *Calanus*. *J Mar Biol Assoc U.K.* **66**: 1-13.

Okuyama H, Kogame K, Takeda S (1993) Phylogenetic significance of the limited distribution of octadecapentaenoic acid in prymnesiophytes and photosynthetic dinoflagellates. *Proc NIPR Symp Polar Biol* **6**: 21-26.

Oliver JD, Colwell RR (1973) Extractable lipids of gram-negative marine bacteria: Phospholipid composition. *J Bacteriol* **114**: 897-908.

Paulmier A, Ruiz-Pino D (2009) Oxygen minimum zones (OMZs) in the modern ocean. *Prog Oceanogr* **80**: 113-128.

Podlaska A, Wakeham SG, Fanning KA, Taylor GT (2012) Microbial community structure and productivity in the oxygen minimum zone of the eastern tropical North Pacific. *Deep Sea Res I* **66**: 77-89.

Poincelot RP (1973) Isolation and lipid composition of spinach chloroplast envelope membranes. *Arch Biochem Biophys* **159**:134-142.

Poincelot RP (1976) Lipid and fatty acid composition of chloroplast envelope membranes from species with differing net photosynthesis. *Plant Physiol* **58**: 595-598.

Popendorf KJ, Lomas MW, Van Mooy BAS (2011a) Microbial sources of intact polar diacylglycerolipids in the Western North Atlantic Ocean. *Org Geochem* **42**: 803-811.

Popendorf KJ, Tanaka T, Pujo-Pay M, Lagaria A, Courties C, Conan P, Oriol L, Sofen LE, Moutin T, Van Mooy BAS (2011b) Gradients in intact polar diacylglycerolipids across the Mediterranean Sea are related to phosphate availability. *Biogeosciences* **8**: 3733-3745.

Prahl FG, Eglinton G, Corner EDS, O'Hara SCM, Forsberg TEV (1984) Changes in plant lipids during passage through the gut of *Calanus*. *J Mar Biol Assoc U.K.* **64**: 317-334.

Rütters H, Sass H, Cypionka H, Rullkötter J (2001) Monoalkylether phospholipids in the sulfate-reducing bacteria *Desulfosarcina variabilis* and *Desulforhabdus amnigenus*. *Arch Microbiol* **176**: 435-442.

Sambrotto R, Swenson K (2007) Biogeochemical flows of nitrogen in a tropical upwelling system-a cariaco time series project: PI. *In* Cruise report-Eastern Tropical Pacific Cruise, R/V *Seward Johnson* 18 October – 17 November 2007, 28-31.

Schouten S, Middelburg JJ, Hopmans EC, Sinninghe Damsté JS (2010) Fossilization and degradation of intact polar lipids in deep subsurface sediments: A theoretical approach. *Geochim Cosmochim Acta* **74**: 3806-3814.

Schubotz F, Wakeham SG, Lipp JS, Fredricks HF, Hinrichs K-U (2009) Detection of microbial biomass by intact polar membrane lipid analysis in the water column and surface sediments of the Black Sea. *Environ Microbiol* **11**: 2720-2734.

Short SA, White DC, Aleem MIH (1969) Phospholipid metabolism in *Ferrobacillus ferrooxidans*. *J Bacteriol* **99**: 142-150.

Siegenthaler P-A (1998) Molecular organization of acyl lipids in photosynthetic membranes of higher plants. *In* Lipids in Photosynthesis: Structure, Function and Genetics (ed. Siegenthaler P-A, Murata N.), 119-144. Kluwer Academic Pbulishers, Netherlands.

Sohlenkamp C, López-Lara IM, Geiger O (2003) Biosynthesis of phosphatidylcholine in bacteria. *Prog Lipid Res* **42**: 115-162.

Stramma L, Johnson GC, Sprintall J, Mohrholz V (2008) Expanding oxygen-minimum zones in the tropical oceans. *Science* **320**: 655-658.

Sturt HF, Summons RE, Smith K, Elvert M, Hinrichs, K-U (2004) Intact polar membrane lipids in prokaryotes and sediments deciphered by high-performance liquid chromatography/electrospray ionization multistage mass spectrometry-new biomarkers for biogeochemistry and microbial ecology. *Rapid Commun Mass Spectrom* **18**: 617-628.

Thompson GA (1996) Review: lipids and membrane function in green algae. *Biochim Biophys Acta* **1302**: 17-45.

Vance DE, Ridgway ND (1988) The methylation of phosphatidylethanolamine. *Prog Lipid Res* **27**: 61-79.

Van Mooy BAS, Rocap G, Fredricks HF, Evans CT, Devol AH (2006) Sulfolipids dramatically decrease phosphorus demand by picocyanobacteria in oligotrophic marine environments. *Proc Natl Acad Sci USA* **103**: 8607-8612.

Van Mooy BAS, Fredricks HF, Pedler BE, Dyhrman ST, Karl DM, Koblížek M, Lomas MW, Mincer TJ, Moore LR, Moutin T, Rappé MS, Webb EA (2009) Phytoplankton in the ocean use non-phosphorus lipids in response to phosphorus scarcity. *Nature* **458**: 69-72.

Van Mooy BAS, Fredricks HF (2010) Bacterial and eukaryotic intact polar lipids in the eastern subtropical South Pacific: Water-column distribution, planktonic sources, and fatty acid composition. *Geochim Cosmochim Acta* **74**: 6499-6516.

Vardi A, Van Mooy BAS, Fredricks HF, Popendorf KJ, Ossolinski JE, Haramaty L, Bidle KD (2009) Viral glycosphingolipids induce lytic infection and cell death in marine phytoplankton. *Science* **326**: 861-865.

Volkman JK, Jeffrey SW, Nichols PD, Rogers GI, Garland CD (1989) Fatty acid and lipid composition of 10 species of microalgae used in mariculture. *J Exp Mar Biol Ecol* **128**: 219-240.

Wada H, Murata N (1998) Membrane lipids in cyanobacteria. *In* Lipids in Photosynthesis: Structure, Function and Genetics (ed. Siegenthaler P-A, Murata N.), 65-81. Kluwer

Academic Publishers, Netherlands.

Wakeham SG, Canuel EA (1988) Organic geochemistry of particulate matter in the eastern tropical North Pacific Ocean: Implications for particle dynamics. *J Mar Res* **46**: 183-213.

Wakeham SG, Amann R, Freeman KH, Hopmans EC, Jørgensen BB, Putnam IF, Schouten S, Sinninghe Damsté JS, Talbot HM, Woebken D (2007) Microbial ecology of the stratified water column of the Black Sea as revealed by a comprehensive biomarker study. *Org Geochem* **38**: 2070-2097.

Wakeham SG, Turich C, Schubotz F, Podlaska A, Li XN, Varela R, Astor Y, Sáenz JP, Rush D, Sinninghe Damsté JS, Summons RE, Scranton MI, Taylor GT, Hinrichs K-U (2012) Biomarkers, chemistry and microbiology show chemoautotrophy in a multilayer chemocline in the Cariaco Basin. *Deep-Sea Res* I **63**: 133-156.

White DC, Davis WM, Nickels JS, King JD, Bobbie RJ (1979) Determination of the sedimentary microbial biomass by extractible lipid phosphate. *Oecologia* **40**: 51-62.

Wishner K, Graff J, McNamara M, Outram D, Phillips B, Williams R (2007) Collaborative research: zooplankton in the redoxcline of the Cariaco Basin: impact on biogeochemical cycling. *In* Cruise report-Eastern Tropical Pacific Cruise, R/V *Seward Johnson* 18 October – 17 November 2007, 16-20.

Woebken D, Fuchs BM, Kuypers MMM, Amann R (2007) Potential interactions of particle-associated anammox bacteria with bacterial and archaeal partners in the Namibian upwelling system. *Appl Environ Microbiol* **73**: 4648-4657.

Wright JJ, Konwar KM, Hallam SJ (2012) Microbial ecology of expanding oxygen minimum zones. *Nat Rev Microbiol* **10**: 381-394.

Chapter III

Distribution of glycerol ether lipids in the oxygen minimum zone of the Eastern Tropical North Pacific Ocean

Sitan Xie [a*], Xiao-Lei Liu [a], Florence Schubotz [a,¶], Stuart G. Wakeham [b,§], Kai-Uwe Hinrichs [a]

In preparation for *Organic Geochemistry*

[a]*Organic Geochemistry Group, MARUM Center for Marine Environmental Sciences and Department of Geosciences, University of Bremen, Leobener Straße, 28359 Bremen, Germany*

[b]*Skidaway Institute of Oceanography, Savannah, GA 31411, USA*

[¶]*Current address: Department of Earth, Atmospheric, and Planetary Sciences, Massachusetts Institute of Technology, Cambridge, MA, 02139 USA*

[§]*Current address: Department of Oceanography, University of Washington, Seattle, WA 98195-7940 USA*

**Corresponding author. Organic Geochemistry Group, MARUM Center for Marine Environmental Science and Department of Geosciences, University of Bremen, Leobener Straße, 28359Bremen, Germany. Tel: +49-421-21865744. Fax: +49-421-21865715. E-mail: sitan.xie@uni-bremen.de*

III.1. ABSTRACT

The distribution of archaeal and bacterial glycerol ether lipids was investigated in the oxygen minimum zone (OMZ) of the Eastern Tropical North Pacific Ocean (ETNP). Archaeal intact polar lipids (IPLs) including both mono- and diglycosidic isoprenoid glycerol dialkyl glycerol tetraethers (GDGTs) were detected after extract purification. Nine groups of glycerol ether core lipids occurred in analyzed samples, namely, isoprenoid GDGTs (iso-GDGTs), isoprenoid glycerol dialkanol diethers (iso-GDDs), branched glycerol dialkyl glycerol tetraethers (branched GDGTs), hydroxylated isoprenoid GDGTs and GDDs (OH-GDGTs and OH-GDDs), overly branched GDGTs (OB-GDGTs), sparsely branched GDGTs (SB-GDGTs), hybrid isoprenoid/branched GDGTs (IB-GDGTs) and a tentatively identified H-shaped GDGT (H-1020). iso-GDGTs were the most abundant component of detected core lipids, an average of 89% of total core glycerol ethers, followed by iso-GDDs (4%), branched GDGTs (2%) and OH-GDGTs (1%). Other newly identified lipids in sediments such as OH-GDDs, OB-GDGTs, SB-GDGTs, IB-GDGTs and H-1020 were all observed as minor components in the OMZ of the ETNP. Intact polar GDGTs (IP GDGTs) and OH-GDGTs showed a similar down core profile with the maximum concentrations in the upper OMZ and a second spike in the euphotic zone, while the core lipids of iso-GDGTs and other glycerol ethers were more abundant in the deeper water column, mid OMZ. Therefore, it is suggest that IP GDGTs and OH-GDGTs may represent an in-situ contribution of planktonic archaeal community whereas the other core lipids are fossil molecules exported downward and accumulated in the mid OMZ due to the presence of a permanent pycnocline, together with deep low-salinity intermediate waters.

III.2. INTRODUCTION

The Eastern Tropical North Pacific Ocean (ETNP) off Mexico and Central America hosts one of the largest oxygen minimum zones (OMZs) in the open ocean, characterized by dissolved oxygen concentrations of less than 20 μM at depths between ~100 and ~800 m (Paulmier and Ruiz-Pino, 2009, and observations from the present sampling expedition). The strong OMZ in the ETNP is attributed to three factors (Fiedler and Talley, 2006): 1) oxygen consumption via respiration of organic matter exported from the highly productive upper water column; 2) a sharp permanent pycnocline that prevents local ventilation of subsurface waters; and 3) sluggish and convoluted deep-water circulation coupled with the absence of a source of oxygen saturated, high

density surface water in the North Pacific. Expansion of OMZs due to global warming (Stramma et al., 2008; Keeling et al., 2010) would have a profound effect on global carbon and nitrogen cycles. OMZs are therefore good targets for studying the marine biogeochemistry and, in particular, the microbial communities of low-O_2 environments (Karstensen et al., 2008). Here we present organic geochemical results from an expedition to the ETNP in November, 2007.

The OMZ of the ETNP at the time of our cruise could be roughly compartmentalized into four horizons based on O_2 concentrations: a euphotic and upper oxycline zone (0~50 m; 200 μM > O_2 > 20 μM), the upper OMZ (50~300 m; 20 μM > O_2 > 2 μM), the mid or core OMZ (300~800 m; O_2 < 2 μM), and the deep oxycline layer below mid OMZ (≥ 800 m) where O_2 levels begin to rise. Total prokaryotic cells were most abundant in the euphotic layers, decreased with depth, but rose again within mid OMZ (Podlaska et al., 2012). In general, Bacteria were more abundant compared to Archaea throughout the water column (Podlaska et al., 2012), which is consistent with the former observations in other oxygen deficient regions such as the upwelling area off the coast of Namibia (Woebken et al., 2007) and anoxic basins such as the Black Sea and Cariaco Basin (Lin et al., 2006; Lam et al., 2007; Wakeham et al., 2007, 2012).

As a complementary approach to molecular biological techniques, lipid analysis provides further insight into the microbial communities under various environmental conditions. As membrane constituents of Archaea, glycerol ether lipids are ubiquitous in a wide range of geological settings and are present in two forms. Intact polar isoprenoid GDGTs (IP GDGTs) are comprised of glycosidic and/or phosphate head groups linked to isoprenoid GDGTs and are assumed to be degraded quickly after cell lysis (White et al., 1979; Harvey et al., 1986). Thus they are used as biomarkers of living microbes (Sturt et al., 2004; Lipp et al., 2008; Schubotz et al., 2009), although their applicability to low-activity subseafloor sediment remains controversial (cf. Lipp and Hinrichs, 2009; Schouten et al., 2010). Different from their intact analogues, glycerol ether core lipids that remain after loss of polar head groups persist over tens of millions of years in sediments (Kuypers et al., 2001) and can be used as fossil biomarkers of their source organisms. Since their identification about a decade ago (e.g., Schouten et al., 2000), distributions of glycerol ether core lipids have been intensively studied over the last decade and a wide range of molecular structures have been identified. For instance, isoprenoid GDGTs with varying numbers of cyclopentane rings are common archaeal lipids in soils and sediments (e.g., Schouten et al., 2000, 2002; Powers et al., 2004; Turich et al., 2007; Lipp et al., 2008). Methyl-branched GDGTs of mainly terrestrial origin are relatively less abundant in marine sediments compared to their

isoprenoid counterparts (Hopmans et al., 2004; Weijers et al., 2006). A series of glycerol diethers, iso-GDDs, were recently found in marine sediments as potential biosynthetic intermediates or degradation products of their corresponding GDGTs (Liu et al., 2012a). Moreover, other novel glycerol ethers including, OH-GDGTs (Liu et al., 2012b), OB-GDGTs, SB-GDGTs, IB-GDGTs and H-1020 (Liu et al., 2012c), have also been reported to be widespread in various marine sediments (tentative structures are shown in Fig. III.1). However, previous surveys of glycerol ether lipids were mostly focused on marine sediments and soils. In this study, the complexity of intact and core glycerol ether lipids in the open ocean is presented for the first time, providing a better understanding of the potential origins and biological precursors of these lipids in suboxic oceanic settings.

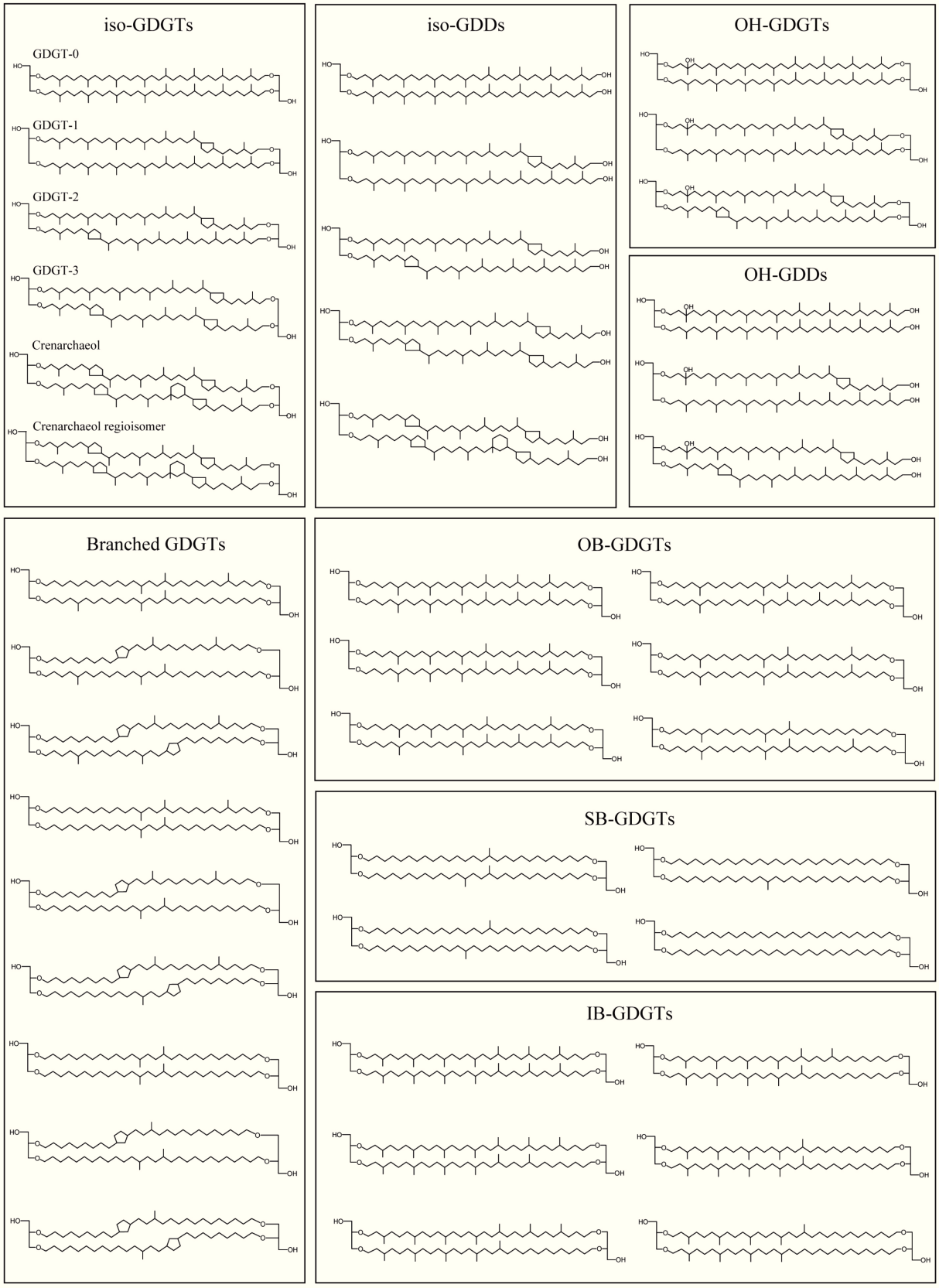

Fig. III.1. Molecular structures of observed glycerol ether core lipids in the ETNP.

III.3. EXPERIMENTS

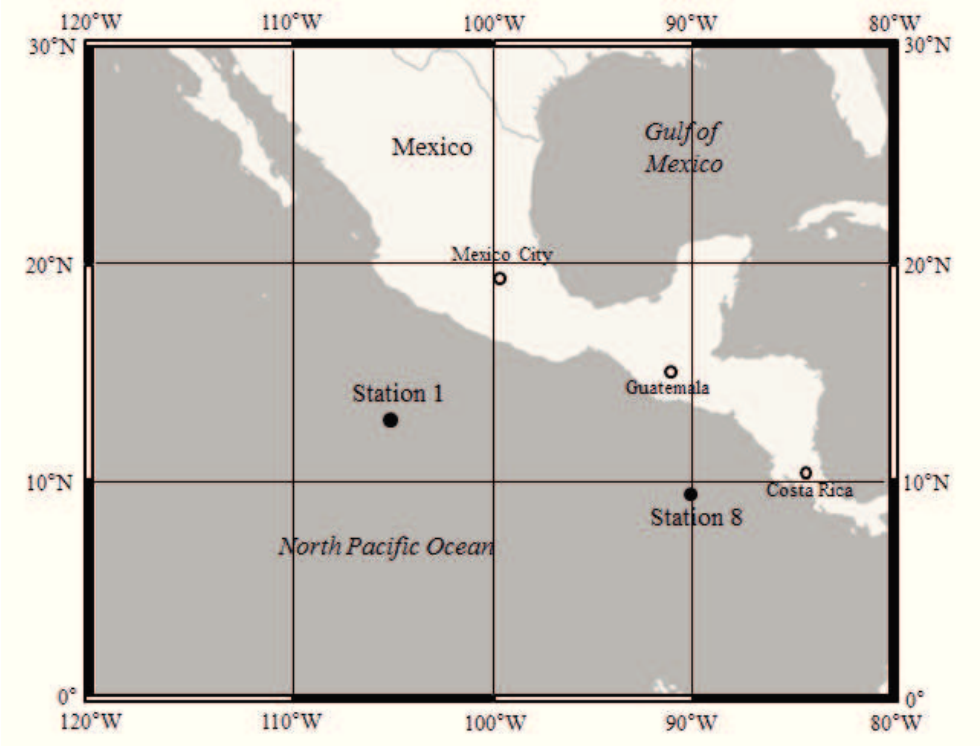

Fig. III.2. Map of the ETNP with sampling stations.

III.3.1. Samples

Particulate matter (PM) samples were collected by in-situ filtration of seawater using McLane Research filtration systems (WTS-142) deployed on the conducting cable of the CTD/rosette in the OMZ of the ETNP during the R/V *Seward Johnson* cruise in November 2007. Temperature, conductivity, fluorescence and dissolved oxygen were measured during pump deployments and again during recovery; pump depths (4 pumps per cast) were monitored from the CTD depth during pumping. Station 1 (13°N，105°W) was located in the Tehuantepec Bowl off southern Mexico, whereas Station 8 (9°N，90°W) was in Costa Rica Dome, a year-round upwelling area (Fig. III.2). PM was collected on ashed glass fiber filters (142 mm, Gelman type A/E) after "prefiltration" through a 53 µm screen to remove most eukaryotes. Double type A/E filters (nominal pore size 0.7 µm) were used to maximize the collection of small particles that might contain microbial biomarkers. After filtration samples were stored frozen at -20°C until extraction.

III.3.2. Elemental analysis and total lipids extraction

Particulate organic carbon (POC) was measured on 14 mm-diameter subsamples of each filter prior to lipid extraction. The plugs were acidified in HCl vapor in a dessicator for 12 hours to remove inorganic carbon and analyzed with a ThermoFinnigan Flash EA Series 1112 interfaced to a ThermoFinnigan Delta V isotope ratio mass spectrometer. OC content was calibrated against internal laboratory chitin powder standards which in turn had previously been cross-calibrated against USGS 40 and 41 international standards.

Lipids were Soxhlet-extracted at Skidaway Institute of Oceanography from GFFs using dichloromethane:methanol (DCM/MeOH; 9:1 v/v) for 8 hr. Extracted lipids were partitioned into DCM against 5% NaCl solution and dried over Na_2SO_4. Total lipid extracts (TLEs) were stored at -20°C.

III.3.3. Fractionation of distinct lipid classes with preparative HPLC

TLEs were separated into three fractions at the University of Bremen with a semi-preparative LiChrosphere Diol column (250×10 mm, 5 μm, Alltech, Germany) connected to a ThermoFinnigan Surveyor HPLC system. Fractions were collected with a Gilson FC204 fraction collector. With a flow rate of 1.5 mL min^{-1} the eluent gradient program was set to a linear gradient from 100% A to 88.4% A and 11.6% B in 16 min, and then to 35% A and 65% B in 44 min, and then changed to 100% A to re-equilibrate the column for another 20 min, where eluent A was composed of *n*-hexane/2-propanol (79:20, v:v) and eluent B was 2-propanol/MilliQ water (88:10, v:v). The first fraction collected in the first 16 minutes contained only glycerol ether core lipids, while the second fraction, 16~42 min, contained glycosidic IP GDGTs, e.g., 1Gly-GDGT and 2Gly-GDGT. The later eluting IPLs, included mostly bacterial and eukaryotic lipids, were collected in the third fraction, 42~60 min, and a separate repost will discuss their distributions.

III.3.4. Analysis of IPLs

Fraction of IP GDGTs were spiked with C_{19} PC (phosphatidylcholine) and dissolved in dichloromethane/methanol (5:1, v/v) for direct injection. The analyses were carried out on Bruker Maxis Accurate-Mass Quadrupole Time-of-Flight (Q-TOF) mass spectrometer connected to a Dionex Ultimate 3000 RS HPLC (UHPLC) system via an electrospray ionization (ESI) ion source. A recently developed separation protocol using An ACQUITY UPLC® BEH Amide column

(2.1×150 mm, 1.7μm, Waters.) was used for the separation of IPLs (Wörmer et al., in preparation). The mobile phase gradient was set to a flow rate of 0.4 mL min^{-1} and 100% A for the first 3 min, and a linear gradient to 80% A: 20% B at 23 min, and then to 60% A: 40% B at 26.5 min, held for 1 min, and returned to 100% A for 10 min to re-equilibrate the column, where A was acetonitrile/2-propanol/hexane/formic acid/14.8 M NH_{3aq} (50:25:25:0.065:0.065) and B was methanol/water/formic acid/14.8 M NH_{3aq} (25:75:0.065:0.065). Column temperature was set to 40°C. ESI settings were set to a dry gas flow rate of 4 L min^{-1}, dry gas temperature of 150°C, nebulizer pressure 1 bar, end plate offset -500 V, scan rate 2 scans $second^{-1}$, and capillary voltage 4 kV. We did not account for response factor of each lipid class we detected, due to the lack of commercially available standards for some of the IPL classes. The detection limit (0.02~0.04 ng/L) was determined for each individual run using the same approach as shown in Lipp et al. (2008).

III.3.5. Analysis of glycerol ether core lipids

In order to analyze the core lipid composition of IP GDGTs, polar head groups of IP GDGTs were cleaved with acid hydrolysis by heating an aliquot of IP GDGTs in 500 μL of 6 M HCl/methanol/dichloromethane (1:9:1, v/v) at 70°C for 24 h. An aliquot of each core lipid fraction were spiked with C_{46} GTGT (glycerol trialkyl glycerol triethers), a commercial standard (Huguet et al, 2006), and dissolved in n-hexane/2-propanol (99:1 v/v) for analysis, respectively. Measurements were made on the same UHPLC and Q/TOF system, but coupled via an atmospheric pressure chemical ionization (APCI) interface. Separation of compounds was achieved with ACQUITY UPLC® BEH Hilic Amide column (2.1×150 mm, 1.7 μm, Waters.) maintained at 50°C (Becker et al., in preparation). The solvent gradient program was at a constant flow rate of 0.5 mL $min^{-1}$and a linear gradient from 3% B to 20% B in 20 minutes, and then increased linearly to 50% B at 35 minutes, and to 100% B at 45 minutes, held for 6 minutes, and switched back to 3% B for 9 minutes to re-equilibrate the column, where A was n-hexane and B was n-hexane/2-propanol (90:10). Detection of GDGTs was achieved using the positive ion mode APCI. APCI-source parameters were as follows: corona current 3500 nA, nebulizer gas pressure 5 bar, drying gas flow 8 L min^{-1}, drying gas temperature 160°C, vaporizer temperature 400°C. The scan rate for the analysis was 2 Hz (Becker et al., in preparation).

III.3.6. Calculations of TEX_{86}, sea surface temperature (SST) and ring index

TEX_{86} (Eq. III.1) was calculated according to Schouten et al. (2002), and TEX_{86} derived SST (Eq. III.2) was based on the calibration of Kim et al. (2010) for subtropical ocean. The ring index, which represents the ring composition of iso-GDGTs, was calculated with Eq. III.3 (cf. Uda et al., 2001; Pearson et al., 2004). TEX_{86} and ring index were calculated for both core and intact lipids of iso-GDGTs in this study.

[Eq. III.1] $$TEX_{86} = \frac{[GDGT-2]+[GDGT-3]+[\text{Crenarchaeol isomer}]}{[GDGT-1]+[GDGT-2]+[GDGT-3]+[\text{Crenarchaeo lisomer}]}$$

[Eq. III.2] $$SST = 68.4 \times \log TEX_{86} + 38.6$$

[Eq. III.3] $$\text{Ring Index} = \frac{[GDGT-1]+2\times[GDGT-2]+3\times[GDGT-3]+5\times[\text{Crenarchaeol isomer}]}{[\text{Total isoprenoid GDGTs}]}$$

III.4. RESULTS AND DISCUSSION

III.4.1. Water column chemistry in the OMZ of the ETNP

The water depths for both stations were deeper than 2500 m. Samples for lipid analysis were collected within the upper 1300 m. The oxygen content of water was around 200 μM at the surface and dropped rapidly to < 30 μM within the euphotic zone due to biological respiration (Fig. III.3 B, F). Although a secondary peak of O_2 occurred at 200 m depth at Station 1, the O_2 was lower than 20 μM in the main body of the OMZ. At both stations, nitrite (NO_2^-) was elevated in the surface layer compared to the upper OMZ, but there were significant NO_2^- maxima in the core OMZ at both stations (Fig. III.3A, E). The nitrite peaks coexisted with nitrate deficits indicating nitrate reduction in the core OMZ was a source for nitrite (Sambrotto and Swenson, 2007). Ammonium (NH_4^+) concentrations are rather constant through the water column in both stations (Fig. III.3A, E). The sources of ammonium were complex, including nitrate reduction, mineralized organic matter from surface waters and excretion by macrozooplankton during their vertical migrations. POC concentrations (Fig. III.3C, G) were highest in the euphotic zone (40~80 μg/L), mainly from plankton, rapidly dropped to 5 μg/L below the upper OMZ, increased slightly in the mid OMZ (10 μg/L), and finally were below 3 μg/L in the deeper oxycline layer.

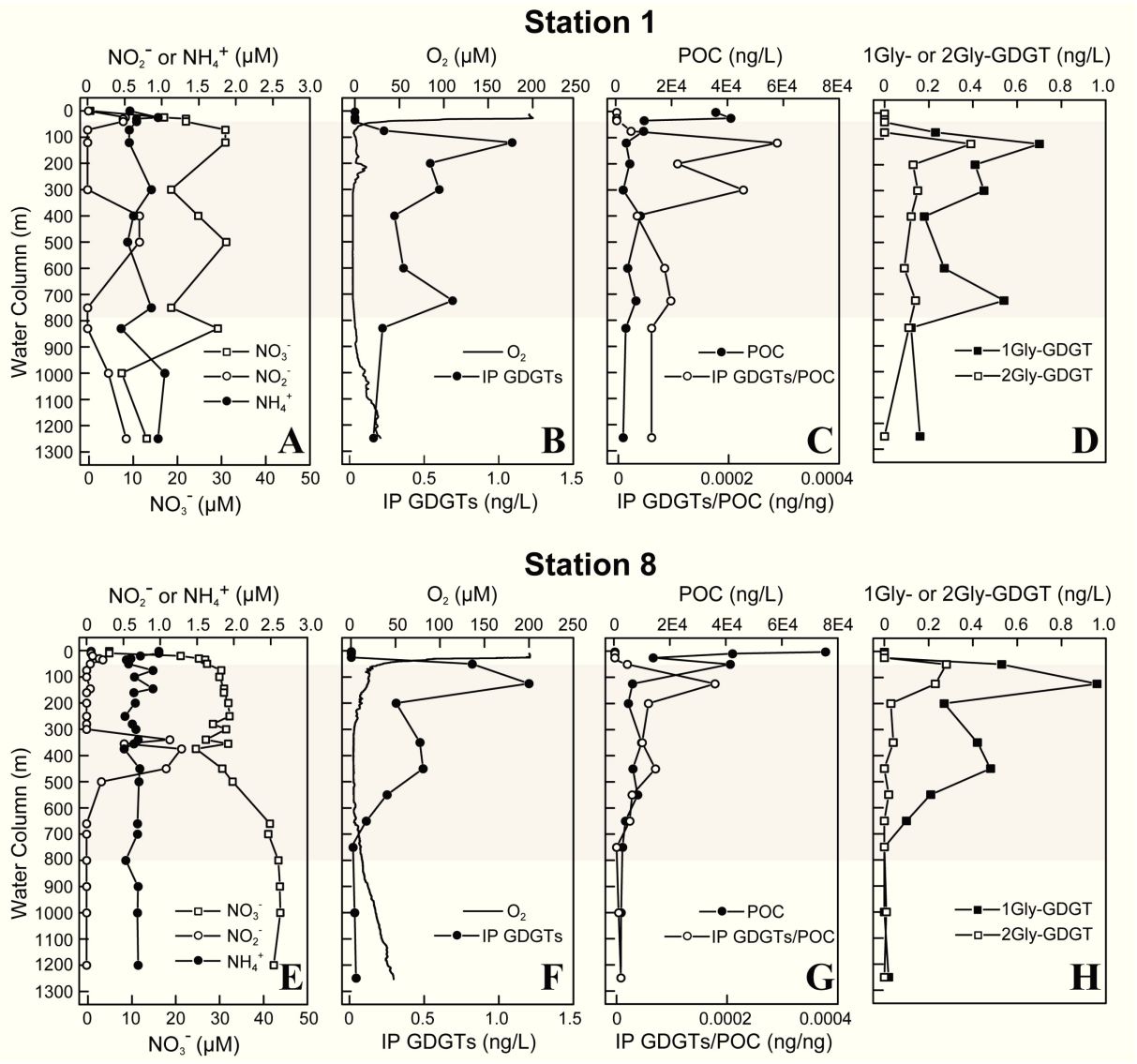

Fig. III.3. Depth profiles of A, E) nitrate, nitrite and ammonia; B, F) oxygen and IP GDGTs; C, G) POC and IP GDGTs/POC; D, H) 1Gly- and 2Gly-GDGT at Station 1 and Station 8 in the water column of the ETNP, respectively. Grey bars refer to the OMZ.

III.4.2. IP GDGTs distribution in the OMZ of the ETNP

In this study, we focused on the distributions of archaeal glycerol ether core lipids and IP GDGTs in the OMZ of the ETNP. Further discussion of intact bacterial polar lipids will be reported separately. In all samples, glycosidic isoprenoid GDGTs, 1Gly-GDGT and 2Gly-GDGT, were only detected after extract purification via preparative HPLC. IPLs of branched GDGTs and other glycerol ethers were not detected (detection limit 0.02~0.04 ng/L). IP GDGTs were first detected in the upper OMZ, between 50~75 m, at both stations (Fig. III.3B, F). In spite of

concentration fluctuations in the deeper water column, there were secondary peaks of IP GDGTs within the core OMZ at both stations, below which concentrations of IP GDGTs decreased (Fig. III.3B, F). IP GDGT/POC ratios peaked in the upper and mid OMZ where POC concentrations were low, indicating that particles were preferentially enriched in archaeal IPLs at these depths (Fig. III.3C, G), probably because these were the depths where Archaea were thriving.

In the OMZ of the ETNP where IP GDGTs occurred with high concentration (Fig. III.3B, F) the cell abundance of Crenarchaeota and Euryarchaeota was reported to be relatively low (Podlaska et al., 2012). Similar mismatch between glycosidic GDGTs and archaeal gene abundance were also observed in the surface water and deeper waters of the Cariaco Basin (Wakeham et al., 2012) and in the OMZ of the Arabian Sea (Schouten et al., 2012). Discrepancy between depth profile of IP GDGTs and microbial results could possibly result from different things, such as sampling heterogeneity (time and space) and analytical biases of lipids extraction and the genetic probing techniques. Alternatively, it is also possible that the Archaea inhabiting in the euphotic zone and deep oxycline produced lower amount of glycosidic GDGTs compared with those in the OMZs. However, this is the first open ocean site where lipids concentration is compared to cells abundance. Lipids concentration converted from euryarchaeotal and crenarchaeotal cell counts data is by one to two orders of magnitude higher than measured IP GDGTs (0~0.5 ng/L versus 2.5~10 ng/L) (ratio of IPL/cell is in a range of 0.25~1.0 fg ; Lipp et al., 2008; Schouten et al., 2012). Sampling for lipid and genetic analysis were performed by seawater filtering with different pore size filters, 0.7 μm and 0.2 μm, respectively. It should be noticed that the small sized archaeal cells could not be quantitatively captured by 0.7 μm filters (Ingalls et al., 2012; Pitcher et al., 2011a; Schouten et al., 2012; Wakeham et al., 2012) which could result in low abundance of IP GDGTs compared to the estimated values from microbial data. Therefore, more research needs to be done to overcome these differences in methods, and smaller size filters is recommend to be used during SPM sampling for lipid analysis in the future.

1Gly-GDGT was two to five times more abundant than 2Gly-GDGT throughout the water column (Fig. III.3D, H). Core lipids of 1Gly-GDGT were dominated by crenarchaeol and GDGT-0, but 2Gly-GDGTs were composed of isoprenoid GDGTs with 1 and 2 rings. However, since the depth profiles of 1Gly- and 2Gly-GDGTs are in general quite similar, we suspect related biological sources for both. Recent studies have proposed that planktonic Crenarchaea were

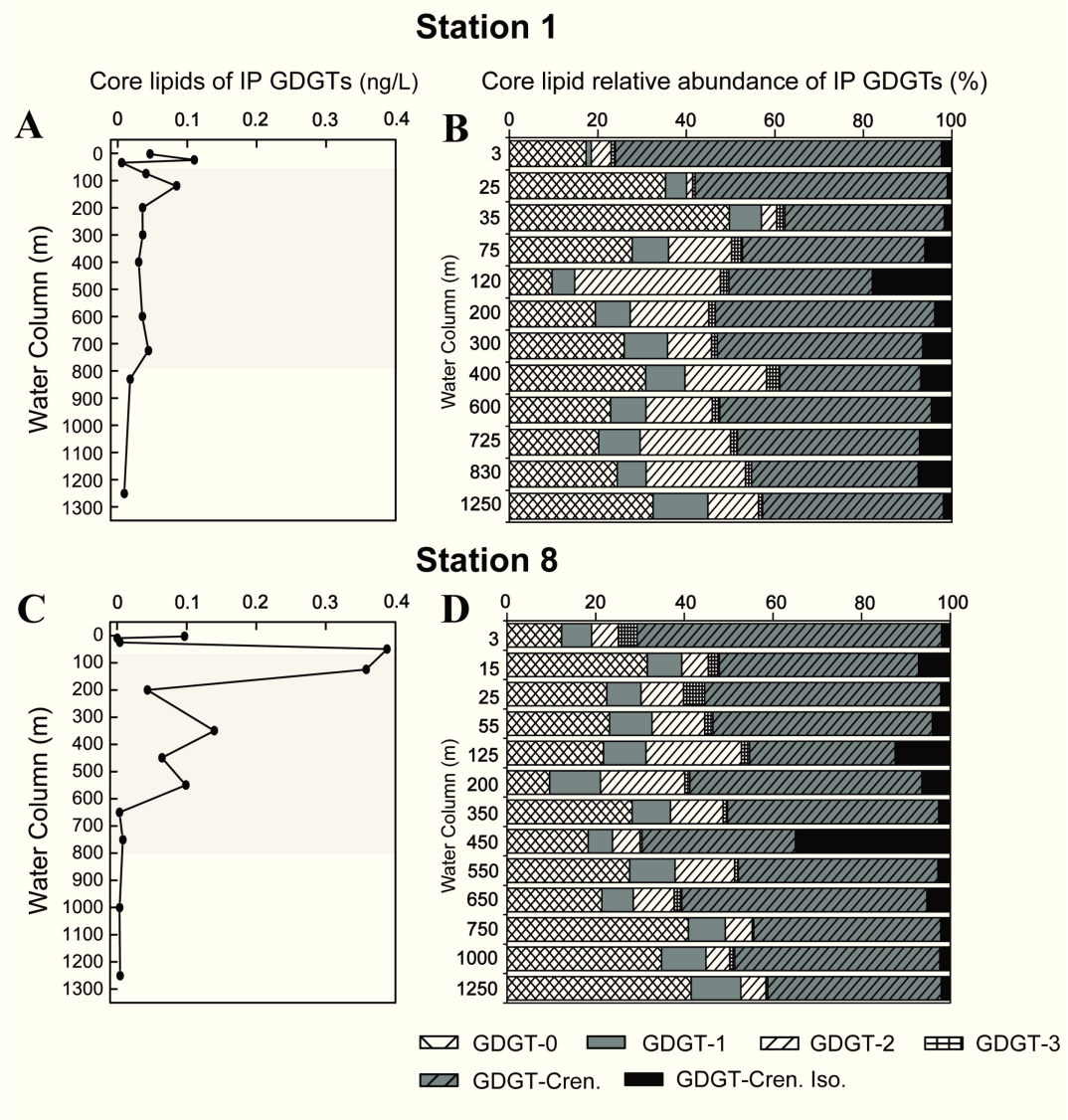

Fig. III.4. A, C) Concentration of core lipids released from IP GDGTs; B, D) relative abundance of core lipids of IP GDGTs at Station 1 and Station 8, respectively. Grey bars refer to the OMZ.

actively involved in the marine nitrogen cycle, in particular ammonium oxidation (Francis et al., 2005, 2007; Könneke et al., 2005; Wuchter et al., 2006; Lam et al., 2007; Lam and Kuypers, 2011) (the term Thaumarchaeota has recently been proposed for these ammonium oxidizing Marine Group I Crenarchaea, Brochier-Armanet et al., 2008). GDGT abundances in the OMZs often occur at depths characterized by nitrite concentration maxima (Coolen et al., 2007; Pitcher et al., 2011b; Wakeham et al., 2012). At Station 8 in the ETNP, the peak of IP GDGTs in the core OMZ corresponded with high nitrite abundance, but this relationship was less clear at Station 1 (Fig. III.3). The autotrophic ammonia-oxidizing Thaumarchaeon, *Candidatus* Nitrosopumilus

maritimus, synthesizes both 1Gly- and 2Gly-GDGTs (Schouten et al., 2008; Könneke et al., 2012). Additionally, ladderane lipids, the molecular tracers of Bacteria performing the anaerobic oxidation of ammonium (anammox), were also found in the mid OMZ of the ETNP (Rush et al., 2012), further pointing to the coexistence of active nitrogen cycling by both Archaea and Bacteria.

After acid hydrolysis, the core lipids released from IP GDGTs was analyzed. The vertical distribution of core lipids released from IP GDGTs was similar as the direct analyzed IP GDGTs (Fig. III.3B, F and Fig. III.4A, C). In the euphotic zone the IP GDGTs, 1Gly- and 2Gly-GDGT, were not detected, but after acid hydrolysis we got high abundant of core iso-GDGT which could be released from other types of IP GDGTs. The core lipids of IP GDGTs were dominated by GDGT-0, GDGT-2, crenarchaeol (GDGT-Cren.) (Fig. III.4B, D).

III.4.3. Glycerol ether core lipid distributions in the OMZ of the ETNP

III.4.3.1. Core iso-GDGTs and iso-GDDs

All analyzed glycerol ether core lipids had relative high concentrations throughout the water column of the OMZ. iso-GDGTs comprised up to 89% of the total core lipids. The highest concentrations of core iso-GDGTs (Fig. III.1 for structures) were detected within the upper and mid OMZ at both stations. In general, core iso-GDGTs were dominated by GDGT-0 and crenarchaeol (GDGT-Cren.) (Fig. III.5B, E). Considering that 1Gly-GDGTs were also dominated by GDGT-0 and crenarchaeol, it was suspected that 1Gly-GDGTs, rather than 2Gly-GDGTs, contributed substantially to the isoprenoid core GDGT pool. The IP GDGTs ratio, IP-GDGTs/(IP-GDGTs+core iso-GDGTs), spiked in the upper OMZ (0.6~0.8 above 150 m), and subsequently decreased in the mid and lower OMZ (less than 0.4 in 200 m~750 m) indicating increased proportion of core iso-GDGTs (Fig. III.6 A, E). It was shown that maximum core iso-GDGTs occurred below the peak of corresponding IP GDGTs. This typical lipids distribution may be caused by the degradation of archaeal biomass and downward export of fossil lipids within the OMZ. It was assumed that IP GDGTs, which represents in-situ living biomass, were degraded in the upper OMZ, and the fossil core iso-GDGTs were then transported downward and accumulated in the deeper OMZ because of the presence of a permanent pycnocline, as well as deep low-salinity intermediate water between 100 and 400 m (Fiedler and Tally, 2006). At Station 8 the IP GDGTs ratio in the mid OMZ decreased more rapidly than Station 1 (Fig. III.6A, E). The Ring index of core iso-GDGTs at Station 8 was generally higher compared to Station 1 in the mid

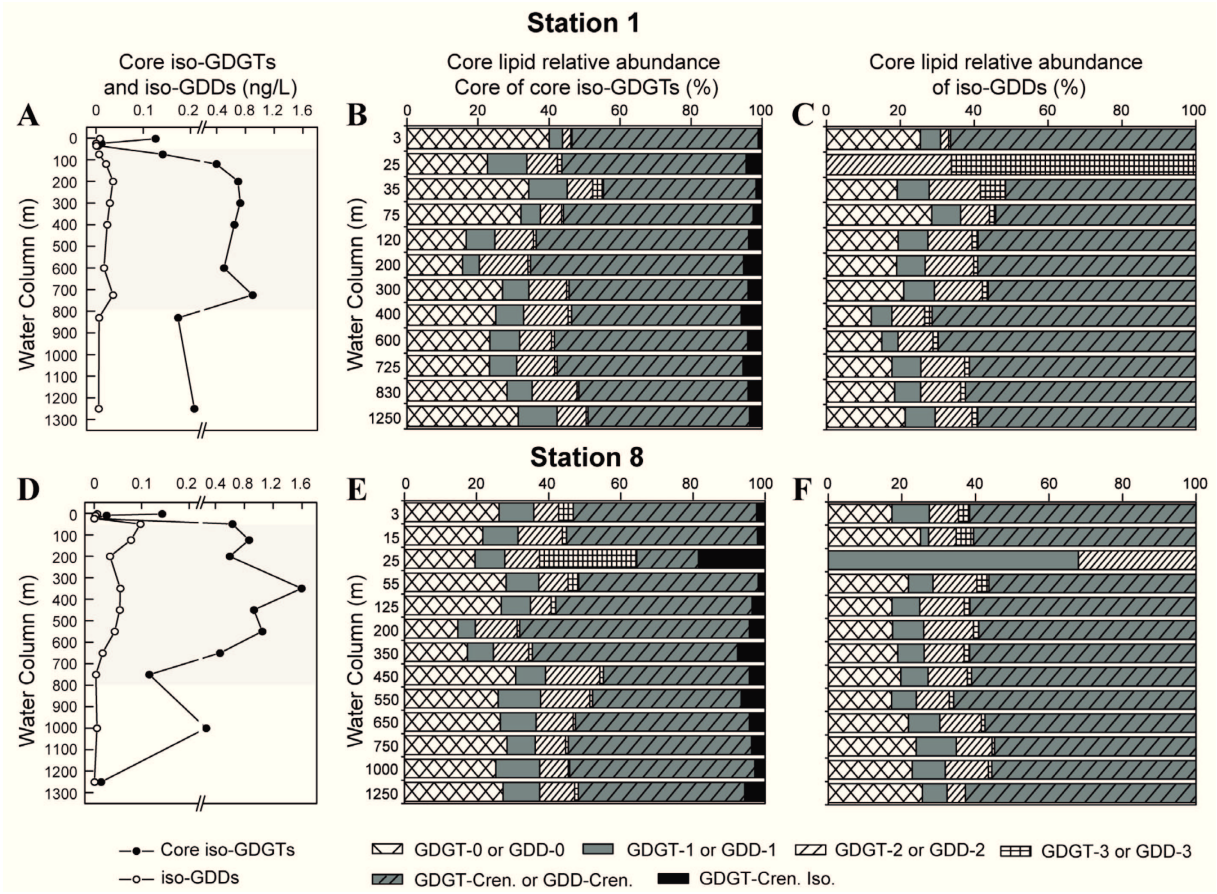

Fig. III.5. A, D) Concentration of core iso-GDGTs and iso-GDDs; B, E) core lipid relative abundance of core iso-GDGTs; C, F) core lipid relative distribution of iso-GDDs at Station 1 and Station 8, respectively. Grey bars refer to the OMZ.

OMZ, which might cause different degradation rate of core iso-GDGTs at both stations, and further result in different relative abundance of IP GDGTs in the OMZ (Fig. III.6B, F).

iso-GDDs are glycerol diethers with the structures of one glycerol moiety less than core iso-GDGTs (Liu et al., 2012a). Both core iso-GDGTs and iso-GDDs were abundant in the first near-surface sample at both stations, but dropped abruptly in the strongly expressed oxycline, and then rose again in the upper OMZ (Fig. III.5A, D). In general, the vertical distribution patterns of iso-GDDs resembled those of core iso-GDGTs, but with almost one order of magnitude lower abundance (Fig. 5A, D). The compositions of core iso-GDGTs and iso-GDDs at 25 m at both stations were quite different from other depths (Fig. III.5B, C, E, F), which is probably due to the quantification bias caused by very low concentrations (less than 0.0001 ng/L). The ring distributions of iso-GDDs resembled that of core iso-GDGTs, dominated by GDD-0 and

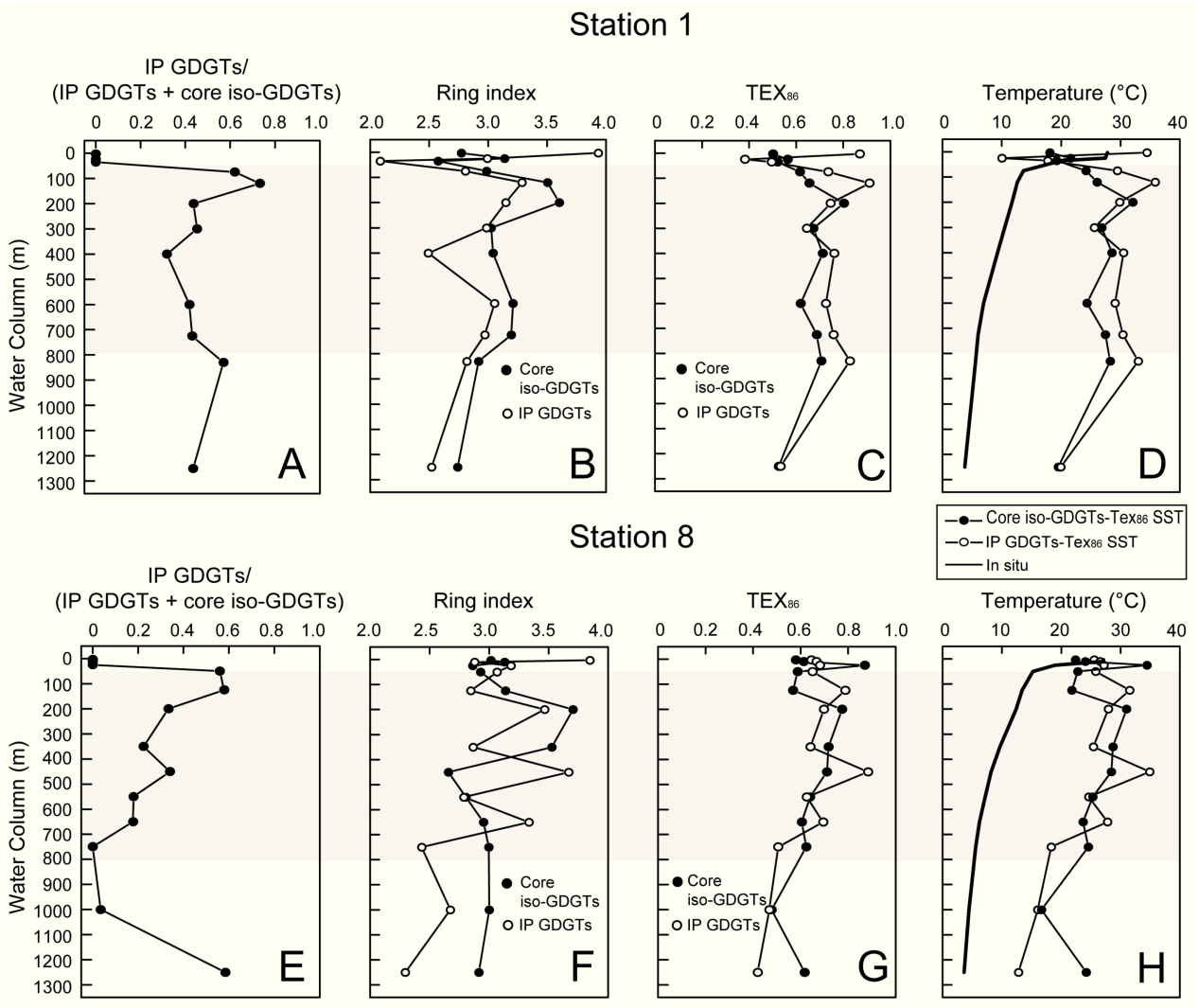

Fig. III.6. A, E) Ratios of IP GDGTs versus IP GDGTs and core iso-GDGTs; B, F) Ring index of core iso-GDGTs and IP GDGTs; C, G) TEX_{86} values of core iso-GDGTs and IP GDGTs; D, H) SST estimated from core iso-GDGTs and IP GDGTs, and in-situ temperature at Station 1 and Station 8, respectively. Grey bars refer to the OMZ.

GDD-Cren. (Fig. III.5C, F), which is consistent with our previous observations in subsurface sediments (Liu et al., 2012a). The correspondence between depth profiles and ring distributions for both GDGTs and GDDs suggest highly related source of these two classes of lipids.

III.4.3.2. Tex_{86} of core iso-GDGTs and IP GDGTs

Overall, the TEX_{86} values of core iso-GDGTs and IP GDGTs were quite similar throughout the water column (Fig. III.6C, G). At Station 1, TEX_{86} values were low in the euphotic zone

(0.6~0.8) but high within the OMZ (> 0.6), and then dropped again in the deeper water under the OMZ (Fig. III.6C). At Station 8, TEX_{86} fluctuated throughout the water column, but in general decreased with increasing depths (Fig. III.6G). When TEX_{86} was converted to temperature, it shows that only SST estimated from core iso-GDGTs at surface waters reflect in-situ temperature (Fig. III.6D, H). TEX_{86} of IP GDGTs might not be as reliable as core iso-GDGTs due to their relative low concentration. Similar observation was found in the OMZ of the Arabian Sea (Schouten et al., 2012). In the OMZ of the Arabian Sea, a potential explanation for similar SST in the surface and deep depth is that temperature adaption of microbial lipids are blurred by variable composition of marine Thaumarchaeota throughout the water column (Schouten et al., 2012). Additionally, transporting of lipids material from other warm surface waters could also be possible (Schouten et al., 2012). However, phylogenetic distribution of the marine Archaea is not available in this study area. Additionally, because 1Gly-GDGT was dominated by crenarchaeol and GDGT-0, but 2Gly-GDGT by iso-GDGTs with 1 and 2 rings (see *section III.4.2* for detailed discussion), relative high concentration of 2Gly-GDGT below euphotic zone could also influence TEX_{86} value by contributing higher amount of iso-GDGTs with 1 and 2 rings to GDGTs pool.

Previous studies reported that temperature estimated from TEX_{86} values of IP GDGTs were generally higher than those of core iso-GDGTs in the OMZ of water column and sediments in the Arabian Sea (Lengger et al., 2012; Schouten et al., 2012), and also in other deep subsurface marine sediments (Lipp and Hinrichs, 2009; Liu et al., 2011). Schouten et al. (2012) and Lengger et al. (2012) suggested that 2Gly-GDGTs were less labile than 1Gly-GDGTs, and iso-GDGTs with 2 and 3 rings were generally more abundant in 2Gly-GDGTs, therefore, preferentially preservation of 2Gly-GDGTs in IP GDGTs pool will lead to consistently higher TEX_{86} value of IP GDGTs than those of core iso-GDGTs. In this work, IP GDGTs derived TEX_{86} and temperature at Station 1 were generally higher than those of core iso-GDGTs (Fig. III.6C, D), but this trend was not very obvious at Station 8 (Fig. III.6G, H). Station 8 was in a year-round upwelling area, and therefore vertical disturbance of the water mass might be an explanation for the fluctuation of TEX_{86} values of both IP GDGTs and core iso-GDGTs.

III.4.3.3. Minor glycerol ether components in the OMZ of the ETNP

In addition to core iso-GDGTs and iso-GDDs, branched GDGTs and six other groups of tentatively identified glycerol ether lipids, e.g., OH-GDGTs (an hydroxyl group located at C-3 in

one of the biphytanyl chains of isoprenoid GDGTs; Liu et al., 2012b) and OH-GDDs (hydroxylated analogues of GDDs; Liu et al., 2012c), OB-GDGTs (branched GDGTs with more numbers of methyl groups; Liu et al., 2012c), SB-GDGTs (branched GDGTs with less numbers of methyl groups; Liu et al., 2012c), IB-GDGTs (tentatively designated as hybrid lipid with both archaeal and bacterial properties: fused phytanyl and tetradecyl moiety with between 1 – 3 methylations; Liu et al., 2012c) and H-1020 (contains a general carbon skeleton of H-shaped GDGT; Liu et al., 2012c) (structures in Fig. III.1) occurred as minor components in the OMZ of the ETNP, at concentrations one to three orders of magnitude lower than core iso-GDGTs. These compounds were first identified in marine sediments and now appear to be widespread in a variety of marine settings (Liu et al., 2012c). This study strongly suggests that these compounds are also products of planktonic microbes; their distribution patterns provide first clues regarding their producer's affinities to certain biogeochemical conditions.

The branched GDGTs were the most abundant non-isoprenoid components in the ETNP. At the two stations we investigated, the vertical distribution of branched GDGTs showed highest concentrations in the mid OMZ (Fig. III.7C, J). One major source of branched GDGTs is presumably soil bacteria; these compounds are thus used to reconstruct terrestrial inputs into coastal sediments (Hopmans et al., 2004; Weijers et al., 2006). Recently, *Acidobacteria* were revealed as a potential source for branched GDGTs in the soil and peat bogs (Sinninghe Damsté et al., 2011). However soils may not be the only sources of branched GDGTs, since in-situ production in fjord sediments has also been proposed (Peterse et al., 2009). In terrestrial environments, the dominant branched GDGT is usually branched GDGT containing two dimethyl octacosanyl moieties ($[M+H]^+$, m/z 1022; e.g., Schouten et al., 2000; Hopmans et al., 2004). By contrast, branched GDGTs in the mid OMZ of the ETNP are dominated by branched GDGT containing two trimethyl octacosanyl moieties ($[M+H]^+$, m/z 1050). Given the 400~600 km distance of the study area from the coast (Fig. III.2), the enrichment of branched GDGTs in the OMZ is unlikely to originate from terrestrial input but rather from in-situ production by microorganisms inhabiting the OMZ. However, lateral transport of continental margin sediments (e.g., North Pacific Intermediate Water (NPIW) north of 12°N along 110°W; Fiedler and Talley, 2006) to our study site cannot be completely ruled out.

The structural relatives of branched GDGDs, OB-GDGTs, SB-GDGTs, IB-GDGTs and H-1020, were observed in the OMZ (Fig. III.7D, E, F, G, K, L, M, N). The biological source(s) of compounds are still unknown, but in general they all showed similar depth profiles characterized

by concentration maxima in the mid OMZ of both stations (Fig. III.7). Regarding the correspondence between vertical distributions and the observation that proposed molecular structures of OB-GDGTs and SB-GDGTs differ from branched GDGTs by different degrees of methylation, we suggest that these three groups of ether lipids derive from related biological sources. The proposed structures of IB-GDGTs and H-1020 are distinct from the branched GDGTs, but again their distribution in the water column points to in-situ production and possibly a common origin with the various branched GDGTs. The ecological significance of these diverse GDGTs in the marine environment remains uncertain but may eventually serve as biomarkers of yet unknown microbial communities in the ocean.

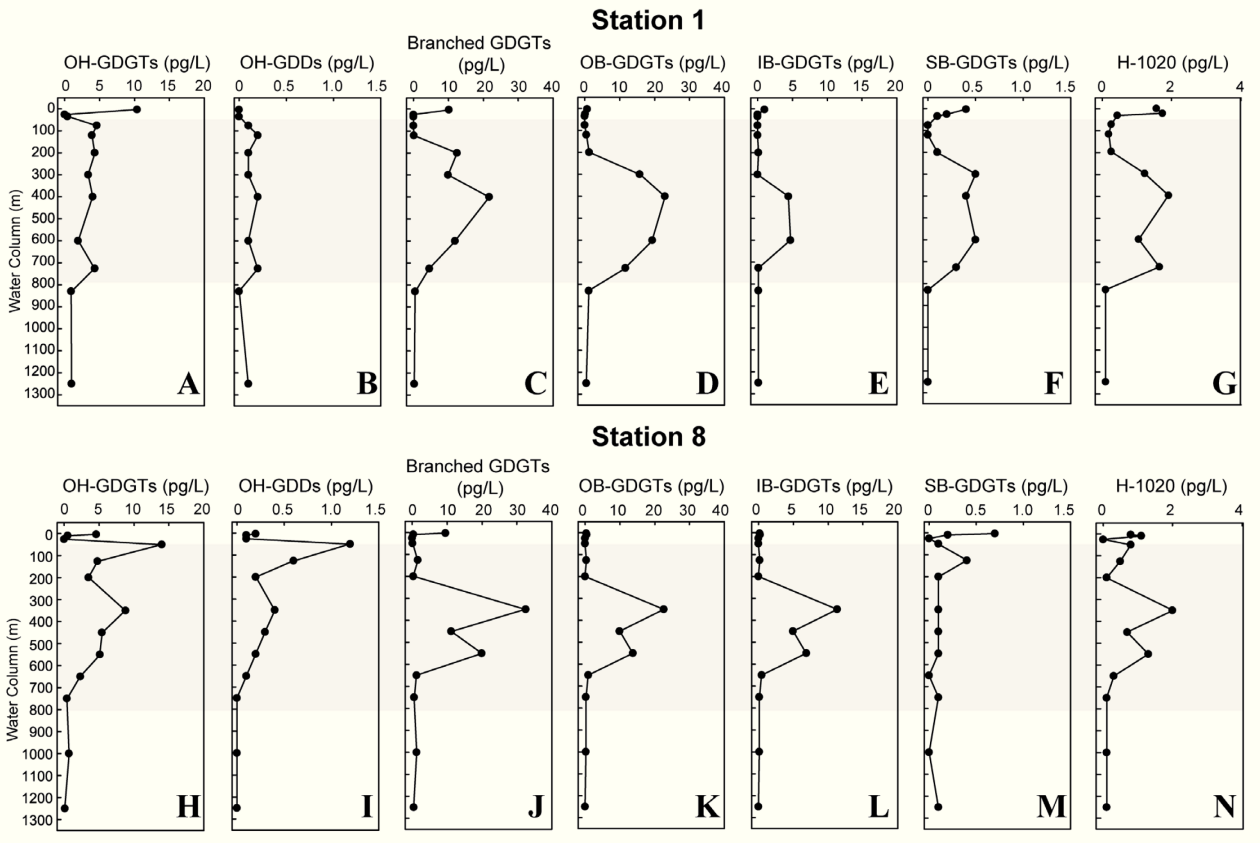

Fig. III.7. Depth profiles of A, H) OH-GDGTs; B, I) OH-GDDs; C, J) branched GDGTs; D, K) OB-GDGTs; E, L) IB-GDGTs; F, M) SB-GDGTs; G, N) H-1020 at Station 1 and Station 8, respectively. Grey bars refer to the OMZ. Grey bars refer to the OMZ.

OH-GDGTs are hydroxylated analogues of iso-GDGTs that are widely distributed in marine sediments (Liu et al., 2012b). In contrast to the other minor glycerol ether core lipids discussed

above, OH-GDGTs and OH-GDD showed the highest abundances in the euphotic zone, along with a secondary peak in the mid OMZ (Fig. III.7A, B, H, I), similar to the depth profiles of IP GDGTs. Different depth profiles of OH-GDGTs and OH-GDDs comparing to other glycerol ether core lipids suggests that OH-GDGTs and OH-GDDs are probably derived from distinct sources. Due to the labile nature of tertiary hydroxyl group, as has been discussed for hydroxy-archaeol (Aquilina et al., 2010), OH-GDGTs and OH-GDDs could probably represent fresher signals than the other core lipids. OH-GDDs may be more likely biosynthetic intermediates rather than degradation products of OH-GDGTs, as diagenesis may not be able to preserve the labile tertiary hydroxyl group but only cleave the ether bonds of OH-GDGTs to generate OH-GDDs. Species of both Euryarchaeota and Crenarchaeota are both proposed to be capable of synthesizing OH-GDGTs, such as, the methane oxidizing *Methanothermococcus thermolithotrophicus* (Liu et al., 2012b) and the ammonium-oxidizing *Candidatus* Nitrosopumilus maritimus (Schouten et al., 2008; as suggested by Liu et al., 2012b). But the biological sources of OH-GDGTs in the OMZ of ETNP still need to be further constrained.

III.4.4. Export and preservation of glycerol ether lipids in the OMZ of the ETNP

As discussed above, IP GDGTs, OH-GDGTs and OH-GDDs exhibited distinct vertical profiles relative to other classes of ether lipids (Fig. III.3B, F; Fig. III.7). The highest concentrations of IP GDGTs (as well as OH-GDGTs and OH-GDDs) were observed in the upper OMZ (Station 1 at 120 m; Station 8 at 125 m), while OH-GDGTs and OH-GDDs were most abundant in the euphotic zone (Station 1 at 3m; Station 8 at 50 m). In contrast, the other glycerol ether core lipids occurred with relatively high abundance in deeper OMZ (Fig. III.7).

Our observation of distinct depth profiles of IP GDGTs and core iso-GDGTs in the OMZ of the ETNP is different to previously reported works. Such as in Hood Canal, a shallow, highly productive and seasonally hypoxic fjord in Puget Sound, Washington, USA (Huguet et al., 2010; Ingalls et al., 2012), IP GDGTs and core iso-GDGTs followed similar trends throughout the water column suggesting that removal of core iso-GDGTs occurs at a similar rate as production of IP GDGTs by microorganisms. In the Hood Canal study, based on the absence of core iso-GDGTs in the deep oxycline layer, core iso-GDGTs were thought not to be exported to the seafloor but rather to remain suspended and to accumulate at the same depth in the water column as their precursor IP GDGTs (Huguet et al., 2010; Ingalls et al., 2012). Similar observation was reported in the OMZ

of the Arabian Sea, that the intact polar lipids of crenarchaeol also showed a similar depth profile as core iso-GDGTs (Schouten et al., 2012). It is possible that the difference between IP GDGTs and core iso-GDGTs distributions in the ETNP comparing to Hood Canal and the OMZ of the Arabian Sea is related to different chemical and biological conditions of the OMZs in different areas.

Distinct depth profiles of IP GDGTs, OH-GDGTs and OH-GDDs comparing to other glycerol ether core lipids suggest that these groups of lipids are probably derived from biological sources. Additionally, the highest abundance of IP GDGTs and OH-GDGTs were observed in the upper OMZ and euphotic zone, respectively, but the core iso-GDGTs and other glycerol ethers were more abundant in the mid OMZ. Therefore, we suggest that IP GDGTs, OH-GDGTs and OH-GDDs might represent an in-situ contribution of planktonic archaeal community, whereas the other core glycerol ether lipids were more likely fossil lipids exported downward and accumulated in the mid OMZ due to the presence of a permanent pycnocline, together with deep low-salinity intermediate waters.

III.5. CONCLUSIONS

A diverse range of glycerol ether lipids exhibit unique distributions in the OMZ of the ETNP. IP GDGTs were majorly composed of 1Gly- and 2Gly-isoprenoid GDGTs. Among all the glycerol ether core lipids, core iso-GDGTs were the most abundant component, with an average relative abundance of 89%. Overall, depth profiles of TEX_{86} values of core iso-GDGTs and IP GDGTs were similar, and only at surface water column the temperature estimated from core iso-GDGTs and IP GDGTs reflect in-situ temperature. Eight other groups of glycerol ether lipids including iso-GDDs, branched GDGTs, OH-GDGTs, OH-GDDs, OB-GDGTs, IB-GDGTs, SB-GDGTs and H-1020 were also detected in the analyzed samples, Considering the hydrology and geochemistry of study area and the vertical distribution of lipids, the enrichment of branched GDGTs in the OMZ is likely due to in-situ production rather than terrestrial input. IP GDGTs, OH-GDGTs and OH-GDDs exhibited higher abundances in the upper OMZ while other glycerol ether core lipids were more enriched in mid OMZ, which suggests that IP GDGTs, OH-GDGTs and OH-GDDs might represent the living signal. Degradation of IP GDGTs results in the accumulation of core iso-GDGTs in the mid OMZ. Since the biological sources for glycerol ether lipids have not been fully understood further investigation is required to gain a better understanding of their origin and

fate in the open ocean.

III.6. ACKNOELEDGEMENTS

We are grateful to the captain and the crew of R/V *Seward Johnson* and to K. Daly and K. Wishner as co-chief scientists. H. Albrecht, B. Olsen and S. Habtes helped with PM sampling. We would like to thank Kent Fanning and Rob Masserini at University of South Florida for providing their nutrient results. We thank J. S. Lipp and L. Wörmer for help with IP GDGTs measurements in the lab. Lab supplies and analytical infrastructure is funded by the Deutsche Forschungsgemeinschaft through the Cluster of Excellence/Research Center MARUM. Instrument (UHPLC-QTOF) is granted by Deutsche Forschungsgemeinschaft (DFG-GZ: NIST 144/300-1). S. Xie was funded by China Scholarship Council, and U.S. National Science Foundation grant OCE-0550654 to S. G. Wakeham supported this project. SGW also acknowledges a Fellowship from the Hanse-Wissenschaftskolleg (Hanse Institute for Advanced Studies) in Delmenhorst, Germany.

III.7. REFERENCES

Aquilina A, Knab NJ, Knittel K, Kaur G, Geissler A, Kelly SP, Fossing H, Boot CS, Parkes RJ, Mills, RA, Boetius A, Lloyd JR, Pancost RD (2010) Biomarker indicators for anaerobic oxidizers of methane in brackish–marine sediments with diffusive methane fluxes. *Org Geochem* **41**: 414–426.

Becker KW, Lipp JS, Zhu C, Liu X-L, Hinrichs K-U (In preparation) An improved chromatographic method for the analysis of archaeal and bacterial ether lipids.

Brochier-Armanet C, Boussau B, Gribaldo S, Forterre P (2008) Mesophilic crenarchaeota: proposal for a third archaeal phylum, the Thaumarchaeota. *Nat Rev Microbiol* **6**: 245-252.

Coolen MJL, Abbas B, Van Bleijswijk J, Hopmans EC, Kuypers MMM, Wakeham SG, Sinninghe Damsté JS (2007) Putative ammonia-oxidizing Crenarchaeota thrive in suboxic waters of the Black Sea: A basin-wide ecological study using 16S ribosomal and functional genes and membrane lipids. *Environ Microbiol* **9**: 1001-1016.

Fiedler PC, Talley LD (2006) Hydrography of the eastern tropical Pacific: A review. *Prog Oceanogr* **69**: 143-180.

Francis CA, Roberts KJ, Beman JM, Santoro AE, Oakley BB (2005) Ubiquity and diversity of

ammonia-oxidizing archaea in water columns and sediments of the ocean. *Proc Natl Acad Sci USA* **102**: 14683-14688.

Francis CA, Beman JM, Kuypers MMM (2007) New processes and players in the nitrogen cycle: the microbial ecology of anaerobic and archaeal ammonia oxidation. *ISME J* **1**: 19-27.

Harvey HR, Fallon RD, Patton JS (1986) The effect of organic matter and oxygen on the degradation of bacterial membrane lipids in marine sediments. *Geochim Cosmochim Acta* **50**: 795-804.

Hopmans EC, Weijers JWH, Schefuß E, Herfort L, Sinninghe Damsté JS, Schouten S (2004) A novel proxy for terrestrial organic matter in sediments based on branched and isoprenoid tetraether lipids. *Earth Planet Sci Lett* **224**: 107-116.

Huguet C, Cartes JE, Sinninghe Damsté JS, Schouten S (2006) Marine crenarchaeotal membrane lipids in decapods: Implications for the TEX_{86} paleothermometer. *Geochem Geophys Geosyst* **7**: Q11010, doi:10.1029/2006GC001305.

Huguet C, Urakawa H, Martens-Habbena W, Truxal L, Stahl DA, Ingalls AE (2010) Changes in intact membrane lipid content of archaeal cells as an indication of metabolic status. *Org Geochem* **41**: 930-934.

Ingalls AE, Huguet C, Truxal LT (2012) Distribution of intact and core membrane lipids of archaeal glycerol dialkyl glycerol tetraethers among size-fractionated particulate organic matter in Hood Canal, Puget Sound. *Appl Environ Microbiol* **78**: 1480-1490.

Karstensen J, Stramma L, Visbeck M (2008) Oxygen minimum zones in the eastern tropical Atlantic and Pacific oceans. *Prog Oceanogr* **77**: 331-350.

Keeling RF, Körtzinger A, Gruber N (2010) Ocean deoxygenation in a warming world. *Annu Rev Mar Sci* **2**: 199-229.

Kim J-H, van der Meer J, Schouten S, Helmke P, Willmott V, Sangiorgi F, Koç N, Hopmans EC, Sinninghe Damsté JS (2010) New indices and calibrations derived from the distribution of crenarchaeol isoprenoid tetraether lipids: Implications for past sea surface temperature reconstructions. *Geochim Cosmochim Acta* **74**: 4639-4654.

Könneke M, Bernhard AE, de la Torre JR, Walker CB, Waterbury JB, Stahl DA (2005) Isolation of an autotrophic ammonia-oxidizing marine archaeon. *Nature* **437**: 543-546.

Könneke M, Lipp JS, Hinrichs K-U (2012) Carbon isotope fractionation by the marine ammonia-oxidizing archaeon *Nitrosopumilus maritimus*. *Org Geochem* **48**: 21-24.

Kuypers MMM, Blokker P, Erbacher J, Kinkel H, Pancost RD, Schouten S, Sinninghe Damsté JS

(2001) Massive expansion of marine archaea during a mid-Cretaceous oceanic anoxic event. *Science* **293**: 92-94.

Lam P, Jensen MM, Lavik G, McGinnis DF, Müller B, Schubert CJ, Amann R, Thamdrup B, Kuypers MMM (2007) Linking crenarchaeal and bacterial nitrification to anammox in the Black Sea. *Proc Natl Acad Sci USA* **104**: 7104-7109.

Lam P, Kuypers MMM (2011) Microbial nitrogen cycling processes in oxygen minimum zones. *Annu Rev Mar Sci* **3**: 317-345.

Lengger SK, Hopmans EC, Reichart G-J, Nierop KGJ, Sinninghe Damsté JS, Schouten S (2012) Intact polar and core glycerol dibiphytanyl glycerol tetraether lipids in the Arabian Sea oxygen minimum zone: II. Selective preservation and degradation in sediments and consequences for the TEX_{86}. *Geochim Cosmochim Acta*, doi: http://dx.doi.org/10.1016/j.gca.2012.05.003

Lin X, Wakeham SG, Putnam IF, Astor YM, Scranton MI, Chistoserdov AY, Taylor GT (2006) Comparison of vertical distributions of prokaryotic assemblages in the anoxic Cariaco Basin and Black Sea by use of fluorescence in situ hybridization. *Appl Environ Microbiol* **72**: 2679-2690.

Lipp JS, Morono Y, Inagaki F, Hinrichs K-U (2008) Significant contribution of Archaea to extant biomass in marine subsurface sediments. *Nature* **454**: 991-994.

Lipp JS, Hinrichs K-U (2009) Structural diversity and fate of intact polar lipids in marine sediments. *Geochim Cosmochim Acta* **73**: 6816-6833.

Liu X-L, Lipp JS, Hinrichs K-U (2011) Distribution of intact and core GDGTs in marine sediments. *Org Geochem* **42**: 368-375.

Liu X-L, Lipp JS, Schröder JM, Summons RE, Hinrichs K-U (2012a) Isoprenoid glycerol dialkanol diethers: A series of novel archaeal lipids in marine sediments. *Org Geochem* **43**: 50-55.

Liu X-L, Lipp JS, Simpson JH, Lin YS, Summons RE, Hinrichs K-U (2012b) Mono- and dihydroxyl glycerol dibiphytanyl glycerol tetraethers in marine sediments: identification of both core and intact polar lipid forms. *Geochim Cosmochim Acta* **89**: 102-115.

Liu X-L, Summons RE, Hinrichs K-U (2012c) Extending the known range of glycerol ether lipids in the environment: structural assignments based on tandem mass spectral fragmentation patterns. *Rapid Commun Mass Spectrom* **26**: 1-8.

Paulmier A, Ruiz-Pino D (2009) Oxygen minimum zones (OMZs) in the modern ocean. *Prog*

Oceanogr **80**: 113-128.

Pearson A, Huang Z, Ingalls AE, Romanek CS, Wiegel J, Freeman KH, Smittenberg RH, Zhang CL (2004) Nonmarine crenarchaeol in Nevada hot springs. *Appl Environ Microbiol* **70**: 5229-5237.

Peterse F, Kim J-H, Schouten S, Kristensen DK, Koç N, Sinninghe Damsté JS (2009) Constraints on the application of the MBT/CBT palaeothermometer at high latitude environments (Svalbard, Norway). *Org Geochem* **40**: 692-699.

Pitcher A, Hopmans EC, Mosier AC, Park S-J, Rhee S-K, Francis CA, Schouten S, Sinninghe Damsté JS (2011a) Core and intact polar glycerol dibiphytanyl glycerol tetraether lipids of ammonia-oxidizing Archaea enriched from marine and estuarine sediments. *Appl Environ Microbiol* **77**: 3468-3477.

Pitcher A, Villanueva L, Hopmans EC, Schouten S, Reichart G-J, Sinninghe Damsté JS (2011b) Niche segregation of ammonia-oxidizing archaea and anammox bacteria in the Arabian Sea oxygen minimum zone. *Microb Ecol* **5**: 1896-1904.

Podlaska A, Wakeham SG, Fanning KA, Taylor GT (2012) Microbial community structure and productivity in the oxygen minimum zone of the eastern tropical North Pacific. *Deep Sea Res I* **66**: 77-89.

Powers LA, Werne JP, Johnson TC, Hopmans EC, Sinninghe Damsté JS, Schouten S (2004) Crenarchaeotal membrane lipids in lake sediments: A new paleotemperature proxy for continental paleoclimate reconstruction? *Geology* **32**: 613-616.

Rush D, Wakeham SG, Hopmans EC, Schouten S, Sinninghe Damsté JS (2012) Biomarker evidence for anammox in the oxygen minimum zone of the Eastern Tropical North pacific. *Org Geochem*, doi: 10.1016/j.orggeochem.2012.02.005.

Sambrotto R, Swenson K (2007) Biogeochemical flows of nitrogen in a tropical upwelling system-a cariaco time series project: PI. *In* Cruise report-Eastern Tropical Pacific Cruise, R/V *Seward Johnson* 18 October – 17 November 2007, 28-31.

Schouten S, Hopmans EC, Pancost RD, Sinninghe Damsté JS (2000) Widespread occurrence of structurally diverse tetraether membrane lipids: evidence for the ubiquitous presence of low-temperature relatives of hyperthermophiles. *Proc Natl Acad Sci USA* **97**: 14421-14426.

Schouten S, Hopmans EC, Schefuß E, Sinninghe Damsté JS (2002) Distributional variations in marine crenarchaeotal membrane lipids: A new tool for reconstructing ancient sea water temperatures? *Earth Planet Sci Lett* **204**: 265-274.

Schouten S, Hopmans EC, Baas M, Boumann H, Standfest S, Könneke M, Stahl DA, Sinninghe Damsté JS (2008) Intact membrane lipids of "*Candidatus* Nitrosopumilus maritimus," a cultivated representative of the cosmopolitan mesophilic group I crenarchaeota. *Appl Environ Microbiol* **74**: 2433-2440.

Schouten S, Middelburg JJ, Hopmans EC, Sinninghe Damsté JS (2010) Fossilization and degradation of intact polar lipids in deep subsurface sediments: A theoretical approach. *Geochim Cosmochim Acta* **74**: 3806-3814.

Schouten S, Pitcher A, Hopmans EC, Villanueva L, van Bleijswijk J, Sinninghe Damsté JS (2012) Intact polar and core glycerol dibiphytanyl glycerol tetraether lipids in the Arabian Sea oxygen minimum zone: I. Selective preservation and degradation in the water column and its consequences for the TEX_{86}. *Geochim Cosmochim Acta*, doi: http://dx.doi.org/10.1016/j.gca.2012.05.002

Schubotz F, Wakeham SG, Lipp JS, Fredricks HF, Hinrichs K-U (2009) Detection of microbial biomass by intact polar membrane lipid analysis in the water column and surface sediments of the Black Sea. *Environ Microbiol* **11**: 2720-2734.

Sinninghe Damsté JS, Rijpstra WIC, Hopmans EC, Weijers JWH, Foesel BU, Overmann J, Dedysh SN (2011) 13, 16-dimethyl octacosanedioic acid (*iso*-diabolic acid), a common membrane-spanning lipid of *acidobacteria* subdivisions 1 and 3. *Appl Environ Microbiol* **77**: 4147-4154.

Stramma L, Johnson GC, Sprintall J, Mohrholz V (2008) Expanding oxygen-minimum zones in the tropical oceans. *Science* **320**: 655-658.

Sturt HF, Summons RE, Smith K, Elvert M, Hinrichs, K-U (2004) Intact polar membrane lipids in prokaryotes and sediments deciphered by high-performance liquid chromatography/electrospray ionization multistage mass spectrometry-new biomarkers for biogeochemistry and microbial ecology. *Rapid Commun Mass Spectrom* **18**: 617-628.

Turich C, Freeman KH, Bruns MA, Conte M, Jones AD, Wakeham SG (2007) Lipids of marine archaea: patterns and provenance in the water-column and sediments. *Geochim Cosmochim Acta* **71**: 3272-3291.

Uda I, Sugai A, Itoh YH, Itoh T (2001) Variation in molecular species of polar lipids from *Thermoplasma acidophilum* depends on growth temperature. *Lipids* **36**: 103-105.

Wakeham SG, Amann R, Freeman KH, Hopmans EC, Jørgensen BB, Putnam IF, Schouten S, Sinninghe Damsté JS, Talbot HM, Woebken D (2007) Microbial ecology of the stratified

water column of the Black Sea as revealed by a comprehensive biomarker study. *Org Geochem* **38**: 2070-2097.

Wakeham SG, Turich C, Schubotz F, Podlaska A, Li XN, Varela R, Astor Y, Sáenz JP, Rush D, Sinninghe Damsté JS, Summons RE, Scranton MI, Taylor GT, Hinrichs K-U (2012) Biomarkers, chemistry and microbiology show chemoautotrophy in a multilayer chemocline in the Cariaco Basin. *Deep-Sea Res* I **63**: 133-156.

Weijers JWH, Schouten S, Spaargaren OC, Sinninghe Damsté JS (2006) Occurrence and distribution of tetraether membrane lipids in soils: Implications for the use of the TEX_{86} proxy and the BIT index. *Org Geochem* **37**: 1680-1693.

White DC, Davis WM, Nickels JS, King JD, Bobbie RJ (1979) Determination of the sedimentary microbial biomass by extractible lipid phosphate. *Oecologia* **40**: 51-62.

Woebken D, Fuchs BM, Kuypers MMM, Amann R (2007) Potential interactions of particle-associated anammox bacteria with bacterial and archaeal partners in the Namibian upwelling system. *Appl Environ Microbiol* **73**: 4648-4657.

Wörmer L-P, Lipp JS, Schröder JM, Hinrichs K-U (In preparation) Application of two new LC-ESI-MS methods for improved detection of intact polar lipids (IPLs) in environmental samples.

Wuchte C, Abbas B, Coolen MJC, Herfort L, van Bleijswijk J, Timmers P, Strous M, Teira E, Herndl GJ, Middelburg JJ, Schouten S, Sinninghe Damsté JS (2006) Archaeal nitrification in the ocean. *Proc Natl Acad Sci USA* **103**: 12317-12322.

Chapter IV

Turnover of microbial lipids in the deep biosphere and activity of benthic archaeal populations

Sitan Xie[a], Julius S. Lipp[a], Gunter Wegener[b,c], Timothy G. Ferdelman[c], Kai-Uwe Hinrichs[a*]

In preparation for
Proceedings of the National Academy of Sciences of the United States of America

[a]*Organic Geochemistry Group, MARUM Center for Marine Environmental Sciences and Department of Geosciences, University of Bremen, Leobener Straße, 28359 Bremen, Germany*
[b]*HGF-MPG Group for Deep Sea Ecology and Technology, Alfred Wegener Institute for Polar and marine Research in the Helmholtz Association*
[c]*Max Planck Institute for Marine Microbiology, Celsiusstr. 1, 28359 Bremen, Germany*
**Corresponding author. Organic Geochemistry Group, MARUM Center for Marine Environmental Sciences and Department of Geosciences, University of Bremen, Leobener Straße, 28359 Bremen, Germany. Tel: +49-421-21865700. Fax: +49-421-21865715. E-mail: khinrichs@uni-bremen.de.*

IV.1. ABSTRACT

Deeply buried marine sediments host a vast microbial biosphere with unknown impact on global biogeochemical cycles. The size and taxonomic composition of this biosphere has been studied extensively with molecular techniques but no conclusive picture exists yet. This study seeks to test previous evidence that suggested a marine sedimentary biosphere dominated by Archaea (Lipp et al., Nature 454, 991-994, 2008); this interpretation was based on distributions of intact polar membrane lipids (IPLs) as proxies of live biomass. We devised a sensitive radiotracer assay to measure the decay rate of a model archaeal IPL in marine subseafloor sediment. Using model simulations incorporating the resulting degradation kinetics, we estimated the fossil, non-cellular fraction in existing data of subseafloor IPL distributions and constrained rates of archaeal growth. The IPL was the partially ^{14}C-labeled compound ^{14}C-glucosyl-diphytanylglyceroldiether (GlcDGD) that closely mimics structural properties of the most abundant microbial group of IPLs in subseafloor sediments, i.e., archaeal glycoetherlipids. In a model that simulates the top 1 km of sediment at a generic continental margin site, degradation rate constants of GlcDGD are estimated to be one to two orders of magnitude lower than those of typical bacterial IPLs with half-lives of GlcDGD increasing with depth from 20 to 310 kyrs. Given estimated microbial community turnover times of 1.6 to 73 kyrs in the modeled 1-km sediment column, a substantial fraction (50%-84%) of the archaeal IPLs in marine sediments thus represents fossil signals of past microbial populations. Using the new constraints on the degradation kinetics of archaeal IPLs, examination of concentration profiles of subseafloor archaeal IPLs yields clues to the rates of archaeal lipid production and thus growth in marine sediments. Concentration profiles require archaeal IPL production to balance decay with IPL synthesis rates of around 1000 pg ml^{-1} yr^{-1} at the surface to 0.2 pg ml^{-1} yr^{-1} at 1 km depth, equivalent to production of 7×10^5 to 140 archaeal cells ml^{-1} sediment yr^{-1}, respectively. These constraints on microbial growth in the deep biosphere are an important step towards understanding the relationship of this ecosystem and the carbon cycle. Due to the inferred high fossil proportion of archaeal IPLs of 80% and more, previous lipid-based estimates of global microbial subseafloor biomass were probably too high. Finally, the widely observed dominance of archaeal IPLs does not rule out an ecosystem dominated by bacterial biomass.

IV.2. INTRODUCTION

Deep marine sediments host a large microbial population (Parkes et al., 2000). Estimates of its size range from around 1% (Kallmeyer et al., 2012) to one third (Whitman et al., 1998) of total biomass on Earth. Estimates of cellular carbon in subseafloor sediments range from ~4 to 303 Pg C (Parkes et al., 1994; Whitman et al., 1998; Lipp et al., 2008; Kallmeyer et al., 2012). This deep biosphere inhabits an important interface in global element cycles, that is, the transition of short-lived oceanic cycles and geologic cycles that sequester matter on million-year time scales. Yet, the actual quantitative impact of this biosphere on global biogeochemical cycles is poorly constrained. This is partly due to the lack of robust information regarding the activity and growth of subseafloor microbial communities. The deep sedimentary biosphere is highly energy-limited; recalcitrant organic matter constitutes the major source of metabolic energy (Parkes et al., 2000). Metabolic rates of deep biosphere life are orders of magnitude lower than those surface communities (D' Hondt et al., 2002). Consequently, turnover times of microbial populations in the subseafloor are estimated to range from hundreds to thousands of years (Whitman et al., 1998; Biddle et al., 2006; Lomstein et al., 2012). DNA-based molecular techniques have provided controversial results regarding relative abundance of microbial communities, with some studies suggesting communities strongly dominated by Bacteria (Schippers et al., 2005; Inagaki et al., 2006), and others suggesting archaeal predominance (Biddle et al., 2006).

Lipid analysis provides complementary information on the microbial communities and the processes they are mediating (e.g., Biddle et al., 2006; Lipp et al., 2008). Intact polar lipids (IPLs) of both Archaea and Bacteria have been proposed as life markers of microbes in sediments and soils (Zink et al., 2003; Sturt et al., 2004). Because of the reactivity of the bond linking the polar head group to the glycerol backbone of IPLs, these are assumed to be unstable after cellular decay (White et al., 1979; Harvey et al., 1986; Logemann et al., 2011) and have therefore been applied as proxies for live microbial cells in a variety of ecosystems (e.g., Sturt et al., 2004; Lipp et al., 2008; Schubotz et al., 2009; Van Mooy et al., 2009). The value of an IPL as life marker depends directly on the fate of extracellular IPLs, i.e., compounds no longer associated with intact cells that could be preserved as molecular fossils.

In marine subseafloor sediments, archaeal IPLs are generally more abundant than their bacterial counterparts (Lipp et al., 2008; Lipp and Hinrichs, 2009). This observation led to the suggestion that Archaea are the dominant microbial domain in this habitat (Biddle et al., 2006;

Lipp et al., 2008). The predominant archaeal IPL type consists of glycosidic ether lipids (Lipp et al., 2008), while phosphate ester-based IPLs commonly found in Bacteria, so-called phospholipids, are rarely detected in deeply buried subseafloor sediments (e.g., Lipp et al., 2008). This dominance of one structurally distinct IPL type raised questions regarding the suitability of these glycosidic IPLs as proxies for live biomass in the deep biosphere (Lipp and Hinrichs, 2009; Schouten et al., 2010). Preservation of glycolipids from planktonic cyanobacteria in Mediterranean sapropels is suggestive of the potential for slow turnover of glycolipids in sediments (Bauersachs et al., 2010).

Previous experiments that enabled direct comparison between archaeal and bacterial IPL stabilities were all conducted as relatively short incubations of active surface sediments. Degradation rate constants of bacterial phospholipids were two to three orders of magnitude higher than those of archaeal glycolipids (Harvey et al., 1986; Logemann et al., 2011); these differences in reactivity were attributed to greater water solubility of phospholipids and the higher susceptibility of ester bonds towards enzymatic attack. A recent experiment with extended duration examined the degradation kinetics of ester-bound IPLs typically found in Bacteria and Eukarya (Logemann et al., 2011). Independent of whether attached to glycosidic or phosphate ester-based headgroups, these displayed 50% degradation within two weeks (Logemann et al., 2011). Comparable data for ether-bound glycolipids representative of archaeal membranes is lacking.

A more quantitative understanding of the fate of IPLs in sediments on geologic time scales is required. In order to serve as useful proxy for live cells in the deep biosphere, the turnover times of IPLs after cellular decay have to be lower than biomass turnover times (Biddle et al., 2006; Lipp and Hinrichs, 2009). Conversely, if the IPLs' turnover time greatly exceeds biomass turnover, IPLs in subseafloor sediments would constitute extracellular, fossil components (Lipp and Hinrichs, 2009; Schouten et al., 2010). Independent of the presence of fossil contribution to sedimentary IPLs, the implementation of the IPLs' degradation kinetics in geochemical models will provide unique constraints regarding cellular growth and turnover in the deep biosphere (cf. ref. Lipp and Hinrichs, 2009).

In this study, we first determined the degradation kinetics of a model archaeal lipid (^{14}C-glucosyl-diphytanylglyceroldiether, GlcDGD) in a 300-day incubation of both microbially active surface sediment and deeply buried low-activity sediment. GlcDGD mimics the structural properties of the most abundant polar lipids in marine sediments. We designed a highly sensitive radiotracer assay that enabled detection of small incremental decreases in concentration of the partially ^{14}C-labeled compound GlcDGD. In a next step, we modeled archaeal and bacterial lipid

concentrations profiles in a hypothetical generic continental margin subseafloor sediment column in order to assess the validity of microbial lipid profiles as proxies of amount and taxonomic composition of subseafloor biomass. For this purpose, we used a model that links the production rate of microbial lipids to the decay rate of total organic carbon (TOC). Degradation rates of lipids were computed utilizing the basis of the experimentally derived degradation rate constant; resulting were the simulated profiles of archaeal and bacterial lipid concentration. In an independent model, we determined the sedimentary production rates of archaeal lipids required to balance the experimentally determined decay rates in order to account for observed subseafloor lipid profiles (Lipp et al., 2008). Collectively, this study provides novel quantitative information regarding the significance of microbial lipid distributions in subseafloor sediments and constrains the growth of subseafloor microbial populations.

IV.3. METHODS

IV.3.1. Marine Sediment Samples

Microbially active surface sediments were sampled in February of 2010 from the upper tidal flat of the German Wadden Sea near Wremen (53° 38' 60N, 8° 31' 0E) . The sediment was oxic at surface and anoxic below about 2 cm with a dark color suggesting high levels of reduced compounds. Deep subsurface sediments were recovered from northern Cascadia Margin during IODP Expedition 311 (Site U1325, 138.21 mbsf, in-situ temperature 20°C; Expedition 311 Scientists, 2005). Until preparation of sediment slurries both sediment types were stored at +4°C in 0.5-L Schott bottles without headspace sealed with a black rubber stopper.

IV.3.2. Preparation of Sediment Slurry

Anoxic sediment slurries were prepared in a glove box (Coy Laboratory Products Inc., atmosphere 3% H_2 in N_2) by mixing 0.5 L sediment with approximately the same volume of sterilized, sulfate-free artificial seawater (in g L^{-1} of deionized water KCl, 0.68; $CaCl_2 \cdot 2H_2O$, 1.5; $MgCl_2 \cdot 6H_2O$, 11.3; NaCl, 26.4; KBr, 0.10; $NaHCO_3$, 0.84). Sediment slurries were stored in a series of 1-L Schott bottles with ca. 500 mL headspace, the headspace was exchanged with pure N_2 (1 bar). Sterilized slurries (by threefold heating for 25 minutes to 120°C were produced as control for non-biological degradation of the IPLs. Afterwards, water was removed and replaced by freshly autoclaved artificial seawater. Estuarine surface sediment contained substantial levels of sulfate. In order to deplete sulfate, we pre-incubated the slurries at room temperature in the dark. After one month, a sub-sample was taken out and filtered through a 0.45-µM filter for

sulfate measurement. Sulfate was measured in 1:50 diluted samples via suppressed ion chromatography with conductivity detection on a 761 Compact IC (Metrohm AG, Herisau, Switzerland) equipped with a Metrosep A Supp 5-100 column with a carbonate eluent (3.2 mmol L^{-1} Na_2CO_3/1 mmol L^{-1} $NaHCO_3$ in deionized water) at a flow rate of 0.7 mL min^{-1}. Sulfate was below detection limit (detection limit: 100 µM) after one month of incubation. The sediment slurry was stored at +4°C for subsequent experiments.

IV.3.3. Synthesized model compound GlcDGD

The represented archaeal IPL, 1,2-di-*O*-phytanyl-*sn*-glycerol-3-glucosyl [glucose-^{14}C(U)] (^{14}C-glucosyl-diphytanylglyceroldiether, GlcDGD, ARC Inc.), was synthesized by ARC Inc. (Saint Louis, USA) from commercially available 1,2-di-*O*-phytanyl-*sn*-glycerol (Avanti Polar Lipids, Inc.), which is present in the "bacterial" sn-1,2 stereoconfiguration. Based on the assumption that enzymes are involved in the hydrolysis of the glycosidic bond, a potential effect of stereoselectivity on the activity of hydrolytic glycosidases is conceivable. However, this selectivity is in the case of this molecule probably more sensitive to the stereochemistry of the sugar's alpha C-atom rather than to the stereogenic center of the glycerol C-atom in beta position.

VI.3.4. Setup of degradation experiment

Aliquots of 4 mL slurry were dispensed into a series of 5.9 mL Exetainer® Vials (Labco Limited) in the glove box. The headspace was replaced with N_2 and pressurized to atmospheric pressure. 3.4 µCi GlcDGD (equivalent to 45 ng/mL sediment slurry) was injected into the sediment slurry through the stopper in 30 µL dimethyl sulfoxide (≥ 99.8%, ROTIPURAN®). After mixing by Vortex, vials of surface and subsurface sediment slurry were incubated in the dark at in-situ temperature, 4°C and 20°C for 300-days, respectively. The sterilized slurry was stored at 20°C. The sampling frequency was high during the first half month, i.e., after 1, 2 and 7 and 14 days; thereafter the sediment slurry was sampled every two months. At each time point, samples were taken in triplicate for radioactivity measurements. At sampling, the headspace was flushed using synthetic air at 10 mL/min for 20 minutes. The gases were first passed through a 20-mL scintillation vial containing 10 mL Carbo-Sorb E (Perkin Elmer) to trap ^{14}C-CO_2 and then through a heated CuO column (850°C) where ^{14}C-CH_4 was combusted into ^{14}C-CO_2, and finally the ^{14}C-CO_2 converted from ^{14}C-CH_4 was trapped in the second Carbo-Sorb E container. 10 mL

Permafluor® E^+ (Perkin Elmer) was added to the scintillation vial before measurement. The radioactivity was quantified by liquid scintillation counting (LSC) (TR-2900; Caberra-Packard). To determine the non-degraded lipid fraction, aliquots of 100 μL homogenous slurry were taken out after flushing the headspace and transferred into a 20-mL scintillation vial containing 10 mL Filter Count (Perkin Elmer) for LSC measurements. Afterwards, the remaining slurry was centrifuged at 2000 rpm for 10 minutes (5810 R, Eppendorf). The aqueous phase was removed and combined with 10 mL Lumasafe Plus (Perkin Elmer) for radioactivity analysis. The degradation of organic matter or IPLs can be hampered by adsorption to the sediment matrix (Harvey et al., 1986; Hedges et al., 2001; Rossel, 2009; Seidel, 2009). In order to exclude the adsorption of degraded lipids to sediment matrix or the glass wall, sediment was rinsed three times with 2 mL Milli-Q water, and then combined with 10 mL Lumasafe Plus (Perkin Elmer) for LSC measurements. After measuring total radioactivity in the aqueous phase, all the liquid (from direct removal after centrifugation and collecting from washing step) was combined together for analyzing ^{14}C-dissolved inorganic carbon (^{14}C-DIC) in the water phase produced from degradation of IPLs. The aqueous phase was acidified to release carbon dioxide which was trapped in scintillation vials with Permafluor® E^+ (Perkin Elmer), and the radioactivity was counted (Treude et al., 2003).

IV.4. CALCULATIONS FRO MODELING WORK

IV.4.1. Determination of IPL degradation rate constant (k')

The degradation rate of IPLs can be described by first-order kinetics (Eq. IV.1). In a previous study, Schouten et al. (2010) assumed that *k'* is a constant during each sampling interval Δt, and therefore the *k'* value was calculated for each sampling interval by Eq. IV.2 from published data (Harvey et al., 1986) for short time experiments with short sampling intervals. In the next step, these authors applied linear fitting between log *k'* and log *t* (midpoint of each interval) according to Eq. IV.3 to derive log *a* and *b* (intercept and slope). Given the length of our experiment, we refined the approach adopted by Schouten et al. (2010) in order to account for the relatively long time intervals between sampling intervals, in which *k'* cannot be considered constant. Using reverse fitting of experimental results, we derived refined values for *a'* and *b'* by Eq. IV.4 which results from integration of Eq. IV.1 after substitution of *k'* with Eq. IV.3. Values of *a'* and *b'* differ slightly from values derived by simple linear interpolation (Table IV.1).

[Eq. IV.1] **First-order kinetics for IPL degradation**:

$$\frac{d[IPL_t]}{dt} = k' \times [IPL_t]$$

k' is degradation rate constant of IPL, IPL_t is IPL concentration at time *t*.

[Eq. IV.2] **Expression of *k'* during short time interval Δ*t*** (Fig. IV.1C):

$$k' = \frac{1}{\Delta t} \times \ln \frac{[IPL_t]}{[IPL_{(t+\Delta t)}]}$$

Assuming that *k'* is a constant during short time sampling interval Δ*t*.

[Eq. IV.3] **Linear fitting between log *k'* and log *t*** (Fig. IV.1C):

$$\log k' = -b \times \log t + \log a$$

k' is degradation rate constant of IPL, log *a* is intercept, *b* is slope.

[Eq. IV.4] **IPL concentration at time *t*** (Figs. IV.1C, IV.S1A and S1B, S2A and S2B, S3A and S3B): $[IPL_t] = [IPL_0] \times e^{\frac{a'}{b'-1} \times (t^{1-b'} - t_0^{1-b'})}$

Integration form of Eq. IV.1 after substituting with Eq. IV.3. $[IPL_t]$ is IPL concentration at time *t*, $[IPL_0]$ is IPL concentration at time zero. *a'* and *b'* could be obtained by reverse fitting of experimental results.

Table IV.1. Comparison of slopes (*b* and *b'*) and intercepts (log *a* and log *a'*) (Eq. IV.2 and IV.4) derived from two different approaches to calculate of degradation rate constant (*k'*) (see *IV.4.1* for details); CM = Cascadia Margin, WS = Wadden Sea.

Variable	*a*	*b*	*a'*	*b'*
$IPL_{ester\text{-}bond}$, WS (Logemann et al., 2011)	1.428	0.776	1.101	0.704
GlcDGD, CM	0.0008	0.401	0.0009	0.371
GlcDGD, WS	0.004	0.356	0.0033	0.382

IV.4.2. Error propagation for degradation kinetics of IPLs

In order to evaluate the effect of propagated errors introduced by the extrapolation of *k'* to geologic time scales, we performed parallel modeling for each IPL group with *a'* and *b'* and their standard errors generated from reverse fitting of experimental results (Eq. IV.4). We applied all

possible combinations of *a'* and *b'* and their standard errors for the subsequent modeling works, but only those cases resulting in the most extreme deviations of *k'* are shown (Fig. IV.S1-S3). The effects on *k'* values of bacterial IPLs were comparatively small (Fig. IV.S1B), but values for GlcDGD are associated with larger errors (Fig. IV.S2B; Fig. IV.S3B). Hence, the modeled bacterial IPL concentration are only slightly affected, whereas the modeled archaeal IPL concentration can differ by up to two orders of magnitude from values indicated in Fig. IV.3C (Fig. IV.S2D; Fig. IV.S3D). Consequently, in deeper sections of the 1-km model, when applying the faster Wadden Sea degradation kinetics for GlcDGD, in the extreme combinations of errors, the bacterial and IPL profiles could converge and become indistinguishable. However, even with maximum errors, the majority of predictions are for both the Wadden Sea and Cascadia Margin kinetics consistent with actual observations from samples in that they predict higher archaeal IPL concentrations.

IV.4.3. Modeling TOC degradation as source of carbon for microbial growth

Our simulation uses the fraction of organic carbon that is degraded over time in each given sediment interval as source of carbon and energy for microbial growth. Degradation of TOC is derived according to the first-order kinetics (Eq. IV.5), where $[TOC_t]$ is the concentration of TOC at time t and k is the first-order rate constant (Jørgensen, 1978). We assumed the sedimentation rate to be 10 cm kyr^{-1}; this corresponds to sediment ages of the sediment interval from 0.01 m to 1000 m illustrated in our simulations from 10^2 yr to 10^7 yr. For a short time interval Δt, k can be presented using Eq. IV.6 (Middelburg, 1989). If Δt is defined as sampling intervals and t as the midpoint of each interval, k is found to be exponentially decreasing with time (Eq. IV.7), where log a_{TOC} and $-b_{TOC}$ represent the intercept and the slope from a linear fit between log t and log k (Middelburg, 1989). Previous research has documented generally consistent decrease of the reactivity of TOC with time (b_{TOC}), but the initial reactivities (log a_{TOC}) are quite different and depend on the choice of apparent initial age ($t_{initial}$), which is an expression of the initial reactivity of TOC at the sediment-water interface (Middelburg, 1989). In our model, $t_{initial}$ is set to 10 kyrs (Lipp et al., 2008). The sensitivity of the model to the choice of this parameter has been tested within a reasonable range of 1 to 100 kyr. The relative differences of TOC and lipid turnover and concentration induced by this factor are typically substantially lower than a factor of two and are thus considered insignificant compared to potential errors induced by errors propagated though

extrapolation of *k'*. The least-square fit between the reactivity of organic carbon (*k*) and time (*t*) is shown in Eq. IV.8, which is based on TOC concentration versus depth under different conditions, such as sediment cores and laboratory experiments (Middelburg, 1989), and the water column (Suess, 1980). If Eq. IV.5 is substituted with Eq. IV.8, TOC degradation rate can be modeled. After integration of the degradation rate of TOC (integration of Eq. IV.4 after substitution of *k* with Eq. IV.8), a depth profile of TOC concentration was obtained (Fig. IV.3A). If we set the average TOC content in surface sediments to 1% (Lipp et al., 2008), the TOC depth profile in Fig. IV.3A is obtained, with the value of 0.2% at 1000 m depth.

[Eq. IV.5] TOC degradation (Fig. IV.3A):

$$\frac{d[TOC_t]}{dt} = k \times [TOC_t]$$

k is degradation rate constant of TOC.

[Eq. IV.6] Expression of *k* during short time interval Δ*t*:

$$k = \frac{1}{\Delta t} \times \ln \frac{[TOC_t]}{[TOC_{(t+\Delta t)}]}$$

Assuming that *k* is a constant during short time sampling interval Δ*t*.

[Eq. IV.7] Linear fitting between log *k* and log *t*:

$$k = a_{TOC} \times t^{-b_{TOC}} \quad or \quad \log k = -b_{TOC} \times \log t + \log a_{TOC}$$

k is degradation rate constant of TOC, log a_{TOC} is intercept, b_{TOC} is slope.

[Eq. IV.8] Least-square fit between the reactivity of organic carbon (*k*) and time (*t*) (Middelburg, 1989) (Fig. IV.3A):

$$k = -0.21 \times (t_{initial} + t)^{-0.985}$$

$t_{initial}$ is apparent initial age (10000 yrs, chosen according to ref. Lipp et al., 2008) which is an expression of the initial reactivity of TOC at the sediment-water interface.

IV.4.4. Modeling $IPL_{pro\text{-}TOC}$, IPL_{deg}, and concentration of archaeal and bacterial IPLs

It has been demonstrated that carbon conversion efficiency of microbes is scaled with the free energy of their metabolism (Heijnen and Van Dijken, 1992). The free energy yield of the net metabolism in the deep biosphere cannot be constrained but there is general consensus that microbially mediated biogeochemical reactions in sediments are close to thermodynamic equilibrium. We therefore chose the growth efficiency of one of the best-studied groups of anaerobic sedimentary microbes for our model, i.e., anaerobic methanotrophic archaea, which represent microbes living close to the biological energy quantum (Hoehler et al., 1994). For these, the carbon assimilation efficiency is 1% (Hinrichs, 2002; Nauhaus et al., 2007; Wegener et al., 2008). We assume a sediment dry mass of 1 g ml^{-1} sediment. For a cell diameter of 500 nm, the conversion factor cellular carbon/cellular IPL is 13 (Lipp et al., 2008). In order to examine the effects of different degradation kinetics of archaeal and bacterial IPLs, we simply divide the flow of carbon from TOC to microbially lipids equally between Archaea and Bacteria, that is, IPL production rates for Archaea and Bacteria are identical (Eq. IV.9). The effect of this factor on degradation model was also examined for ratios of carbon flowing into Archaea vs. Bacteria of 10:90 and 90:10, respectively. The resulting trends of simulated concentrations of archaeal and bacterial IPLs are generally consistent with those from the 50:50 ratio (Fig. IV.3C) in that archaeal IPLs dominate, except for the 10:90 (Archaea:Bacteria) scenario in which concentrations of both IPL types begin to converge; however, in this scenario archaeal IPLs in these deeper interval were substantially lower than the actual observations. Degradation kinetics of ester-bound IPLs (Logemann et al., 2011) and GlcDGD are described by Eq. IV.4. By combining production and degradation of IPLs, IPL concentration can be modeled through a simple box-model (Lipp and Hinrichs, 2009) (Eq. IV.10). After integration of Eq. IV.10, depth profiles of archaeal and bacterial IPL concentrations are calculated by using the respective *k'* values for these two IPL groups. Total IPL concentration is assumed to be 1860 ng ml^{-1} sediment at surface depth based on the intercept defined by the regression line (Lipp et al., 2008); we assume that the IPL pool consists of equal fractions of archaeal and bacterial IPLs.

[Eq. IV.9] IPL production rate estimated from TOC decay (Fig. IV.3B):

$$IPL_{pro-TOC} = 0.21 \times (t + 10000)^{-0.985} \times [TOC_t] \times 1\% \times \frac{1}{2} \times \frac{1}{13}$$

10000 is apparent initial age (chosen according to ref. Logemann et al., 2011); $[TOC_t]$ is TOC concentration at time *t*, set to 1%; the carbon assimilation efficiency is assumed as 1% (Hinrichs, 2002; Nauhaus et al., 2007; Wegener et al., 2008), $\frac{1}{2}$ is carbon flow split ratio between Archaea and Bacteria, $\frac{1}{13}$ is the ratio for cellular IPL versus cellular carbon for a cell diameter of 500 nm (Lipp et al., 2008).

[Eq. IV.10] Box-model for modeling IPL concentration from input ($IPL_{pro\text{-}TOC}$) flux (Eq. IV.9) and an output (IPL_{deg}) flux (Fig. IV.3C):

$$\frac{d[IPL_t]}{dt} = dIPL_{pro-TOC} - dIPL_{deg} =$$

$$(0.21 \times (t + 10000)^{-0.985} \times [TOC_t] \times 1\% \times \frac{1}{2} \times \frac{1}{13}) - (k' \times IPL_t)$$

Variables as in Eq. IV.9, *k'* is degradation rate constant of IPL.

VI.4.5. Half-life of IPL, generation time of cellular population and percentage of cellular IPL

We define the period of time required for IPLs at any given depth to decrease to 50% of the original concentration without considering potential input fluxes by in-situ production as half-life ($t_{1/2}$) (Eq. IV.11). Biomass turnover times are the time period required to accumulate the cellular concentration represented by the global regression line of directly counted microbial cells (Parkes et al., 2000) with $IPL_{prod\text{-}TOC}$ (after conversion of IPL concentration into cell concentration using IPL cell^{-1} of 1.4 fg (Lipp et al., 2008); Eq. IV.12). If we assume that the cellular populations depicted by the regression line (Parkes et al., 2000) consist of equal portions Archaea and Bacteria (cf. ref. Parkes et al., 2000 for DNA-based evidence), biomass turnover times are in the range of 1.6 to 73 kyrs from surface to 1000 mbsf (Fig. IV.4A). Half-life of bacterial IPLs (0.017 to 53.4 kyrs) is much shorter than turnover of biomass above 100 mbsf indicating that all bacterial IPL should be associated with cells. Below 100 m, half-life of bacterial IPL is approaching cell turnover times, resulting in a small portion of bacterial IPL (less than 5%) as fossil (non-cellular) components below 300 mbsf. Conversely, the half-life of archaeal IPL ranges from 20 to 312 kyrs from the top to the bottom of the 1-km sediment column, i.e., substantially longer than the

biomass turnover times. Consequently, a substantial fraction of archaeal IPLs is non-cellular (=fossil). Percentage cellular (=live) IPLs is derived from conversion of microbial cell concentrations derived from regression line (Parkes et al., 2000) into IPL concentrations; this pool is defined to consist of 50% each of archaeal and bacterial IPLs, division of the archaeal or bacterial concentration through the respective IPL concentration derived from simulated TOC degradation yields the percentage of cellular IPLs; values higher than 100%, derived for bacterial IPLs in some intervals, are not meaningful solution and were therefore depicted as 100%.

[Eq. IV.11] Half-life of IPL (Fig. IV.4A):

$$t_{1/2} = (t^{1-b'} + \ln 2 \times \frac{1-b'}{a'})^{\frac{1}{1-b'}} - t$$

a' and *b'* were obtained by reverse fitting of experimental results by Eq. IV.4

[Eq. IV.12] Cellular production rate converted from $IPL_{pro\text{-}TOC}$ (Fig. IV.3C and 4A):

$$Cell_{pro-TOC} = 0.21 \times (t + 10000)^{-0.985} \times [TOC_t] \times 1\% \times \frac{1}{13} \times \frac{1}{1.4 \times 10^{-6}}$$

10000 is apparent initial ages for continental margin sediments (Lipp et al., 2008), $[TOC_t]$ is TOC concentration at time *t*, 1% is carbon assimilation efficiencies of deep biosphere microbes (Hinrichs, 2002; Nauhaus et al., 2007; Wegener et al., 2008), $\frac{1}{13}$ is the ratio for cellular IPL versus cellular carbon and the amount of IPL versus cell is 1.4 fg for a cell diameter of 500 nm (Lipp et al., 2008), cellular production rate is given in ng (10^{-9}g)

IV.4.6. IPL decay and production in relation to IPL regression line (Fig. IV.5).

The down core profile of archaeal IPL concentration without in-situ production was modeled by Eq. IV.4 (Fig. IV.5A). IPL concentration at surface depth is set to 1860 ng mL^{-1} sediment, i.e., the intercept defined by the regression line (Lipp et al., 2008). The production rate of archaeal IPL (IPL_{input}) is assumed to follow power function (Eq. IV.13). If IPL_{input} is set to 1 ng ml^{-1} sediment yr^{-1} at the 100-yr old surface of our model sediment column (according to stable isotope probing results, ref. Wegener et al., 2012, that quantify archaeal lipid production rates in coastal sediment of similar age), the depth profile of archaeal IPL_{input} is described by Eq. IV.14. Based on the

box-model (Lipp and Hinrichs, 2009), archaeal IPL_{input} was selected by adjustment of slope (*d'*) to best match observed IPL concentration (Eq. IV.15; Fig. IV.5B and IV.5C). For converting input rate of archaeal IPL to cell production rate, the amount of IPL cell^{-1} is 1.4 fg (Lipp et al., 2008).

[Eq. IV.13] The input rate of archaeal IPL production rate (IPL_{input}) are assumed to follow power function: $IPL_{input} = c' \times t^{-d'}$ or $\log IPL_{input} = -d' \times \log t + \log c'$

d' and log *c'* are the slope and intercept of log IPL_{input} and log *t*.

[Eq. IV.14] The expression of production rate of archaeal IPL (Fig. IV.5B and C):

$$IPL_{input} = 1 \times (\frac{100}{t})^{d'}$$

If IPL_{input} rate is set to be 1 ng ml^{-1} sediment yr^{-1} at surface sediment (Wegener et al., 2012), Eq. IV.13 will become $1 = c' \times 100^{-d'}$ (0.01 mbsf equals 100 yrs) and therefore $c' = (\frac{1}{100})^{-d'}$. If Eq. IV.13 is substituted by *c'*, production rate of archaeal IPL could be expressed by Eq. IV.14. According to Eq. IV.14, IPL_{input} rate is only influenced by *d'* (slope) and *t*.

[Eq. IV.15] Box-model to determine IPL concentration by assuming that it is only related to an input (IPL_{pro}) and an output (IPL_{deg}) flux (Fig. IV.5B):

$$\frac{d[IPL_t]}{dt} = dIPL_{pro-TOC} - dIPL_{deg} = (1 \times (\frac{100}{t})^{d'}) - (k' \times IPL_t)$$

IPL_{pro} follows power function according to Eq. IV14, while IPL_{deg} is according to Eq. IV.1 with degradation rate constant *k'* of GlcDGD in different sediments (Table IV.1).

IV.5. RESULTS AND DISCUSSION

IV.5.1. Degradation kinetics of IPLs in the deep biosphere

To assess the degradation kinetics of IPL**s** in both surface and subsurface marine sediment, the partially labeled compound GlcDGD enabled us to monitor hydrolysis of the glycosidic bond during the 300-day long anaerobic incubation experiment using sediment from the German Wadden Sea and the deep subseafloor at Hydrate Ridge, Cascadia Margin. The premise of the experiment is that the IPL GlcDGD is largely insoluble in water, while all products of reactions

resulting in cleavage of the polar headgroup are either highly water-soluble (^{14}C-DIC, ^{14}C-glucose and organic degradation products of glucose) or detectable in the gas phase (^{14}C-CO_2, ^{14}C-CH_4) (see Fig. IV.1 for a sketch of the experimental design). However, due to the slight solubility (equivalent to 2% of initial radioactivity) of GlcDGD in water and the lack of significant change of this radioactivity level during the course of the experiment, the potential release of miniscule fractions of radioactive, water-soluble organic compounds by hydrolysis of the glycosidic bond could not be detected accurately (Fig. IV.2). Consequently, degraded products were only detected as radioactive DIC, CH_4, and CO_2. Therefore reported degradation rates are minimum estimates; actual rates may be slightly higher. After 300-day incubation, 0.5% GlcDGD was degraded in Wadden sea surface sediment, while only 0.15% was degraded in Cascadia Margin subsurface sediment (Fig. IV.2).

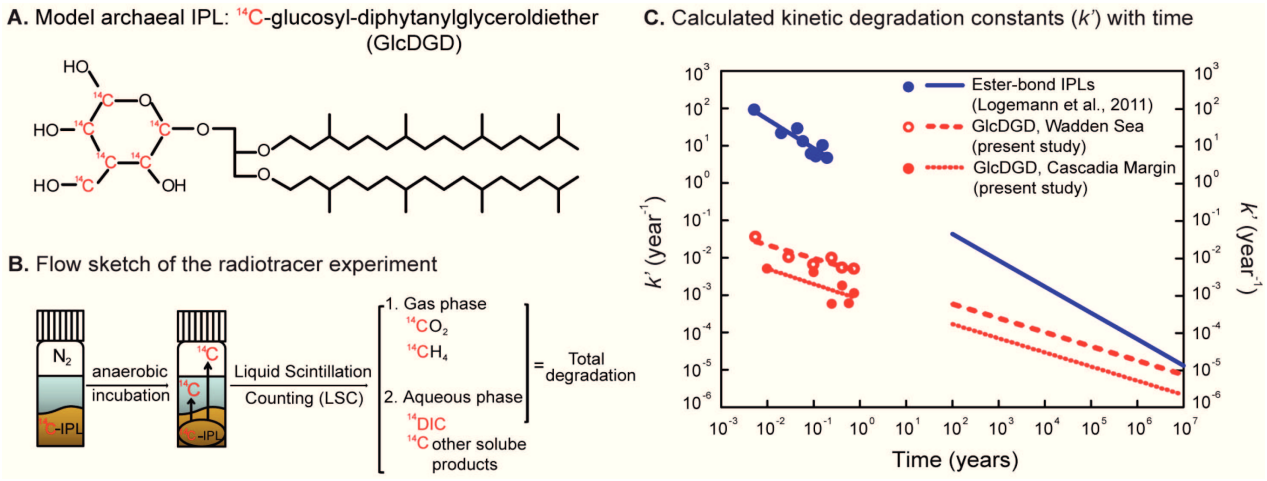

Fig. IV.1. Schematic view of the experiment for the determination the degradation kinetics of GlcDGD and resulting degradation constants as a function of time. (A) Molecular structure of partially radiolabeled GlcDGD that serves as model compound for prominent sedimentary archaeal IPLs. (B) Flow sketch of the anaerobic incubation experiment. (C) Relationship of degradation constants (*k'*) of GlcDGD (this study) and ester-bound IPLs (Logemann et al., 2011; representative of typical bacterial IPLs). Open and closed circles: *k'* values determined from experimental results; lines for $t < 1$ year were derived via linear fitting between calculated *k'* and *t* (Eq. IV.2); lines for $t > 100$ year represent modeling results based on reverse fitting of experimental results (Eq. IV.4; see IV.4.1 for details); gap is not covered due to minimum age of modeled sediment column (Fig. IV.3) of 100 years.

A large majority of the diagenetic reactions and processes in marine sediments are related either directly or indirectly to the degradation of TOC (Middelburg, 1989), which follows first-order kinetics (Jørgensen, 1978). The degradation rate of IPLs (IPL_{deg}) in sediments can also

be described by first-order kinetics (Eq. IV.1), where [IPL_t] is the IPL concentration at time-point t, and k' is degradation rate constant that decreases with time (Scouten et al., 2010; Logemann et al., 2011). For a short time interval Δt, k' can be expressed using Eq. IV.2 (Middelburg, 1989), where Δt represents the sampling interval. Accordingly, k' decreases exponentially with time (Eq. IV.3; an overview of all calculations is provided in supporting online material). Through linear fitting between log k' and log t (midpoint of each interval) (Eq. IV.3), log a and b (intercept and slope) can be derived. Given the length of our incubation experiment, we refined the approach adopted by Schouten et al. (2010) in order to account for the relatively long time intervals between sampling intervals in our experiment, during which k' cannot be considered constant. Using reverse fitting of experimental results, we derived refined values for a' and b' by Eq. IV.4, which was derived by integrating Eq. IV.1 after substituting k' with Eq. IV.3. The obtained values of a' and b' differ slightly from corresponding values of a and b derived by simple linear interpolation (Table IV.1).

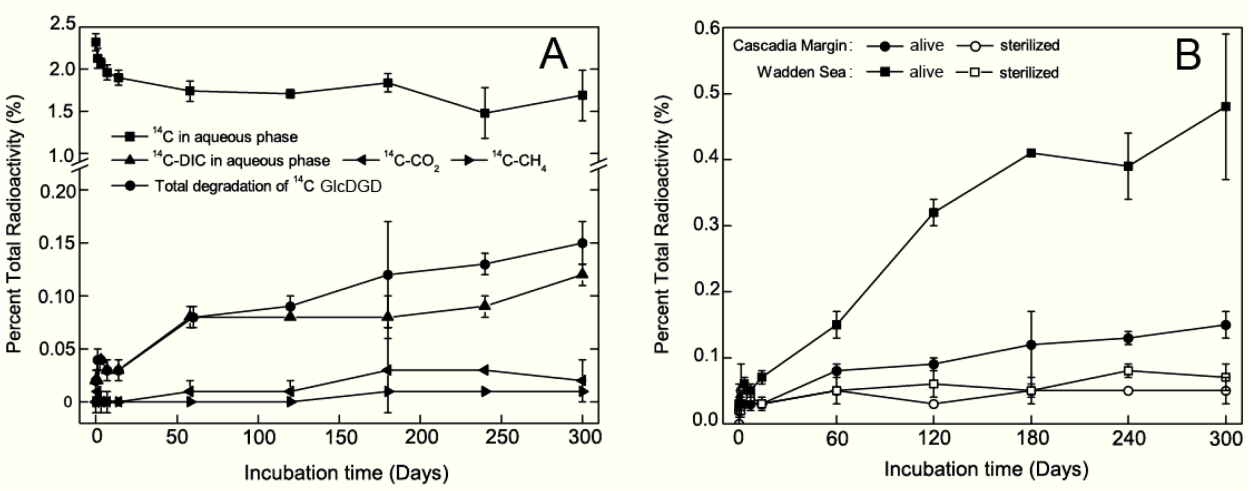

Fig. IV.2. (A) Degradation of ^{14}C-GlcDGD in Cascadia Margin sediment. Radioactivity was detected in gas phase (^{14}C-CH$_4$, ^{14}C-CO$_2$) and aqueous phase (^{14}C-DIC). (B) Radioactivity release from ^{14}C-GlcDGD detected in four different experiments, detected as the sum of ^{14}C-CH$_4$, ^{14}C-CO$_2$, and ^{14}C-DIC. Results are presented as the average and standard deviation of triplicate tubes.

The slope b' (Eq. IV.3) for ester-bond IPLs (Logemann et al., 2011), plotted as representative of typical bacterial IPLs (Fig. IV.1C), is larger than b' for GlcDGD, which suggests that k' for ester-bond IPLs decreases at a faster rate compared with GlcDGD. However, large differences

between the intercepts (log *a'*) of ester-bound IPLs and GlcDGD are consistent with the degradation rate constant of ester-bond IPLs being two to four orders of magnitude higher than those of GlcDGD. The slopes *b'* for degradation of GlcDGD are similar for both sediments, but the higher *a'* values of GlcDGD in active surface sediment relative to subsurface sediment result in an order of magnitude higher k' values in the surface sediment.

Simulation of the fate of IPLs in the deep biosphere requires extrapolation of *k'* to a geological time scale (Fig. IV.1C; IV.4.1; Fig. IV.S1-S3). Extrapolated values of *k'* for both ester-bond IPLs and GlcDGD decline with depth; values of *k'* for GlcDGD and ester-bound IPLs converge due to the different slopes *b'* but *k'* values for GlcDGD in both surface and subsurface sediment remain lower than those of ester-bound IPLs for more than 10^7 years (Fig. IV.1C). The effect of the higher microbial activity in the Wadden Sea surface sediment is reflected in around four to five times higher *k'* values of GlcDGD relative to Cascadia Margin subsurface sediment in the projected time interval.

Potential uncertainties induced by the extrapolation to geologic time scales are considerable and require careful examination of propagated errors caused by reverse fitting of experimental results for the determination of *a'* and *b'*. The methodology and consequences for subsequent models are discussed in the supporting online text and illustrated in Figures IV.S1-3. The uncertainties are generally larger for extrapolations of *k'* for GlcDGD compared to ester-bound IPLs, with the consequence that we can confidently predict *k'* within less than two orders of magnitude for 10 Myr old sediments (Fig. IV.S2, S3).

IV.5.2. Simulation of IPL profiles in the deep biosphere and implications for subseafloor life

In order to simulate the effect of different values of *k'* on sedimentary profiles of both bacterial and archaeal IPLs, realistic estimates of their production rates in subseafloor sediments are required. Calculation of IPL production rates on the basis of estimates of turnover times of microbial biomass in subseafloor sediment appears impracticable, since these estimates vary from hundreds to hundred thousands of years (Whitman et al., 1998; Biddle et al., 2006; Lomstein et al., 2012). We therefore simulated the production of IPLs in a generic model sequence of continental margin sediment under the assumption that microbial growth, and thus production of lipids, is tightly linked to the degradation kinetics of TOC. For this purpose, we used a diagenetic model of TOC decay (Middelburg et al., 1993) that has been independently validated as widely applicable

(Rothman and Formey, 2007). Detailed parameters used in the model are presented in the supporting information. In brief, sedimentation rates are set to 10 cm kyr^{-1}, TOC concentration at the sediment surface is set to 1% and decreases through simulated degradation to 0.2% at 1 km subseafloor depth (Fig. IV.3A). The biomass of microbial populations is scaled with the free energy yield of the utilized metabolic reaction (Heijnen and Van Dijken, 1992), which is considered to be minimal in the deep biosphere (D'Hondt et al., 2002). We converted the rate of degraded TOC into microbial biomass using carbon assimilation efficiencies of 1%; such low values have been established for anaerobic methanotrophic archaea (Hinrichs, 2002; Nauhaus et al., 2007; Wegener et al., 2008) that are considered to live close to the biological energy quantum (Hoehler et al., 1994); 1/13 of the assimilated carbon is then flowing into biosynthesis of IPLs (Simon and Azam, 1989; Lipp et al., 2008; IV.4.4). For the sake of illustrating the fate of both bacterial and archaeal IPLs, represented by ester-bond IPLs (Logemann et al., 2011) and GlcDGD, respectively, we divided the flow of carbon from microbial cells equally between Bacteria and Archaea; other ratios resulted in qualitatively similar results. Consequently, the resulting microbial biomass should comprise equal portions of both domains if the respective cellular populations turn over at equal rates.

The simulated rate of IPL production, $IPL_{pro\text{-}TOC}$, decreases with depth from 90 to 0.02 pg ml^{-1} sed. yr^{-1} in the top 1 km sediment (Fig. IV.3B). IPL concentration was then modeled using a simple box model that assumes that IPL concentration at each depth is represented by an input ($IPL_{pro\text{-}TOC}$) and an output (IPL_{deg}) flux into each sediment interval (ref. Lipp and Hinrichs, 2009; Eq. IV.10; Fig. IV.3B and C). The resulting profiles exhibit some of the general features also found in a compilation of widely distributed IPL profiles (Fig. IV.3C; ref. Lipp et al., 2008). For example, the concentrations of archaeal IPLs exceed those of their bacterial counterparts by up to two orders of magnitude in sediments below 1 mbsf. The minimum of simulated bacterial IPL concentration in the top 5 cm results from a higher rate of degradation relative to production due to the input of large quantities of water column-derived material at the sediment-water interface and is presumed to be a model artifact. The predicted concentration profiles of archaeal and bacterial IPLs fall in the general concentration ranges also observed in nature. These general trends remain largely unchanged when we consider the error propagation related to our extrapolation of *k'* (Fig. IV.S1-S3). This simulation thus demonstrates that, even though archaeal and bacterial populations are of equal size, the use of glycosidic etherlipid IPLs as proxy of microbial biomass concentration and its taxonomic composition would overestimate both total

biomass and the proportion of Archaea. This simulation shows that the distribution of archaeal and bacterial IPLs does not reflect the relative distribution of Archaea and Bacteria in this environment. We therefore suggest that the currently most realistic estimates of archaeal vs. bacterial biomass are derived from refined DNA-based techniques (Lipp et al., 2008;

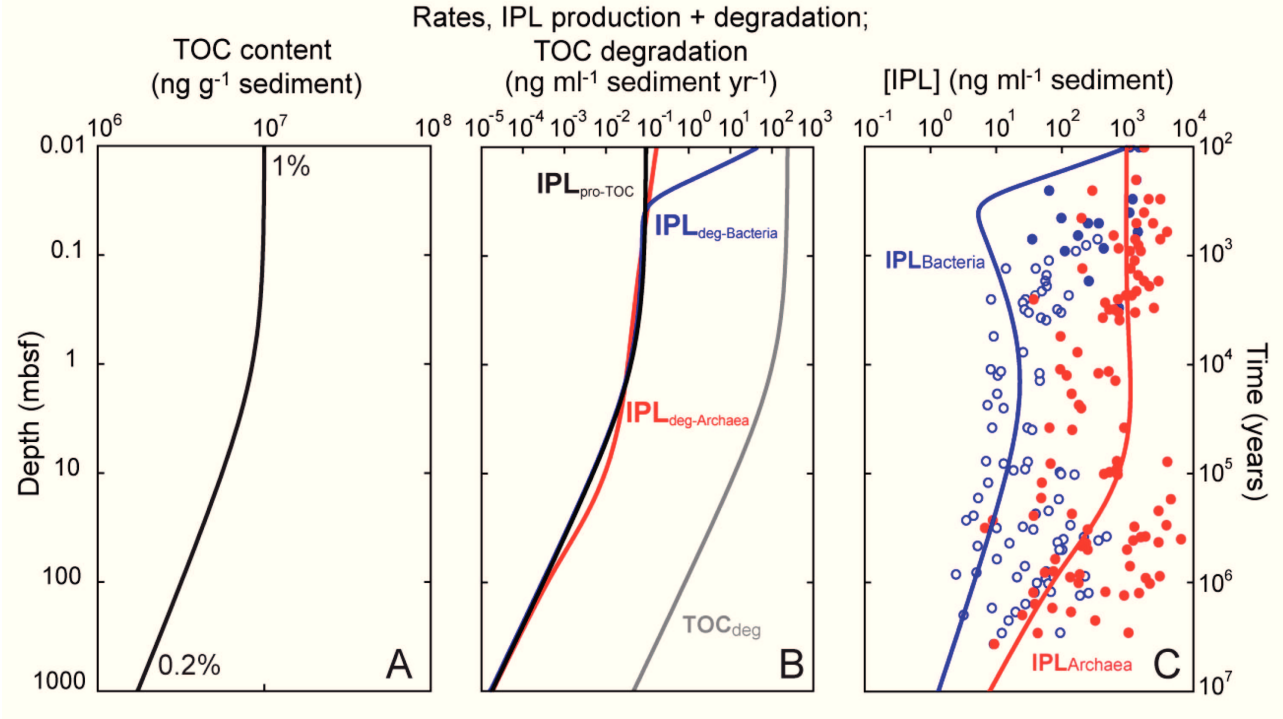

Fig. IV.3. Production, decay and concentrations of IPLs in a model that simulates microbial growth linked to the degradation of organic carbon in a generic continental margin sediment column. (A) Depth (age) profile of TOC concentration derived from diagenetic modeling of TOC decay using first-order kinetics (Middelburg et al., 1993). (B) Depth profile of corresponding rates of TOC degradation, modeled production of bacterial and archaeal IPLs energetically linked to TOC decay, and degradation rates of bacterial IPL (based on extrapolation of experimental data from ref. Logemann et al., 2011), and degradation rates of archaeal IPL assuming the degradation kinetics of Cascadia Margin sediment (see Fig. IV.S3 for simulation with Wadden Sea kinetics). (C) Modeled concentration of archaeal and bacterial IPLs; blue and red filled circles: observed concentrations of bacterial and archaeal IPLs (Lipp et al., 2008); open blue circle: estimated maximum concentration of bacterial IPLs considering the analytical limit of detection (Lipp et al., 2008). See text for model assumptions and methodology.

Schippers et al., 2010; 2012); accordingly, Bacteria are similarly abundant to Archaea, while deviations towards a higher fraction of one domain may occur in specific environments.

The comparison of our simulated microbial biomass production with the global regression of cellular counts (Parkes et al., 2000) constrains the turnover of pools of IPLs and cells as well as the fossil fractions of the different IPL types (Fig. IV.4), keeping in mind the limitation that the

samples included in the global data set of subseafloor cells (Parkes et al., 2000) may not be ideally represented by our model continental margin section. Biomass turnover times generally ranges from 1600 to 73000 years. The steep decrease of cell concentrations in the top meter (Parkes et al., 2000) combined with the relatively low decrease of $IPL_{pro\text{-}TOC}$ (derived from TOC degradation;

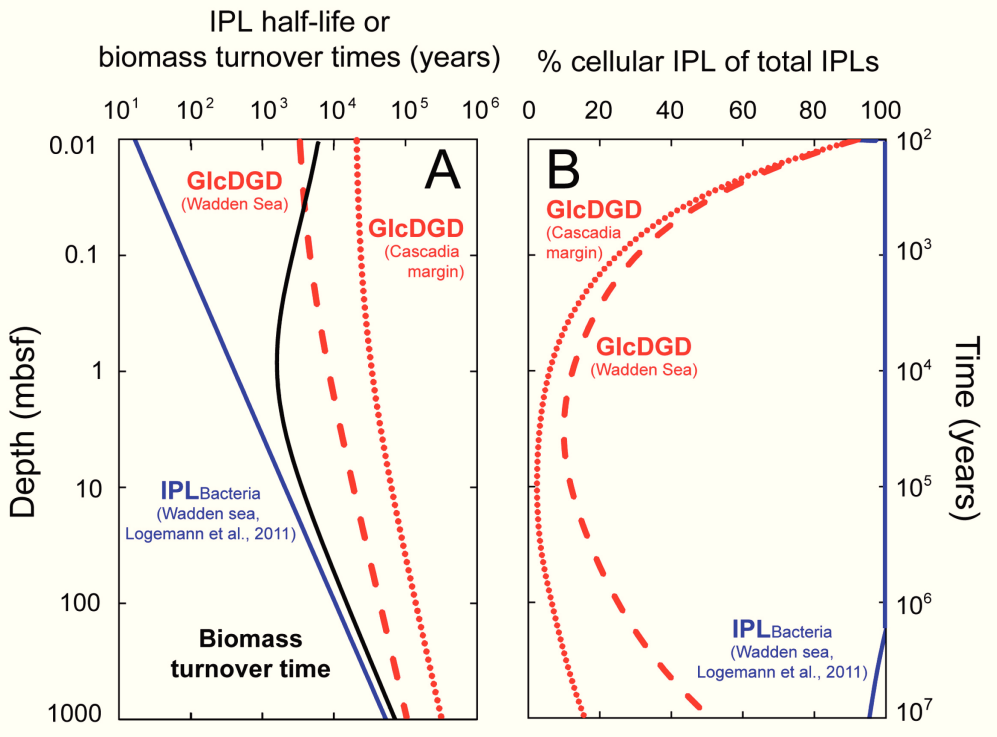

Fig. IV.4. Biomass turnover times, turnover times of IPLs and relative fractions of cellular IPLs based on simulated IPL concentrations (Fig. IV.3) and cellular concentrations in globally distributed sediments (Parkes et al., 2000). (A) Modeled half-life of archaeal and bacterial IPLs (Eq. IV.11) based on degradation kinetics obtained from degradation experiment and literature data (bacterial IPLs; ref. Logemann et al., 2011). Biomass turnover time (black curve) is the time required to accumulate the cellular concentrations derived from the global regression line of direct cell counts (Parkes et al., 2000), when converting $IPL_{pro\text{-}TOC}$ into number of cells (Eq. IV.12). (B) Percentage of cellular IPLs in subseafloor sediment, derived from dividing cell concentrations from the global cell concentration-vs.-depth regression line for each depth (Parkes et al., 2000; converted to IPL concentration) by modeled IPL concentration (Eq. IV.10; see IV.4.5 for details).

Middelburg, 1989) result in the minimum of biomass turnover at 1 mbsf. Because the turnover times of archaeal IPL pools exceed biomass turnover times for sediments below 0.1 mbsf (Fig. IV.4A), fossil, non-cellular archaeal IPLs accumulate to the effect that only a fraction of 5 to 40% below a depth of 1 mbsf represent intact cells (Fig. IV.4B), while the low turnover times of bacterial ester-bound IPLs relative to biomass turnover times qualify them as useful markers for

live bacterial cells in the deep biosphere. The size of fractions of cellular and non-cellular archaeal IPLs is controlled by IPL turnover. Therefore the shape of the curve of cellular IPLs (Fig. IV.4B) is related to the relationship between production rate and degradation rate (Fig. IV.4B). For example, maximum non-cellular IPLs are expected in intervals in which production exceeds degradation; this is the case in sediment around 5 to 10 mbsf in our simulation where the cellular component may be as low as a few percent. In both shallower and more deeply buried sediment, archaeal IPL production is lower than degradation (Fig. IV.3B), which results in high proportion of cellular archaeal IPLs (Fig. IV.4B). Accordingly, in sediment deeper than 100 mbsf, the fossil fraction of archaeal IPLs is projected to be lower than 70 to 90%, dependent on the kinetics used (Fig. IV.4B).

IV.5.3. Constraints on growth rates of archaeal populations in subseafloor sediments

Independent of the above-described limitations of IPLs for determining the abundance of archaeal cells in deep subseafloor sediments, the measured degradation kinetics provide new constraints regarding the growth of archaeal populations. The experimentally determined kinetics of GlcDGD now enable us to extend a previous model (Lipp and Hinrichs, 2009) and demonstrate that in-situ production of archaeal IPLs in subseafloor sediments is required to balance degradation. Mathematically it is possible to generate a solution that does not require in-situ production (Schouten et al., 2010) but that this leads to unrealistically high half-lives (in a range of 350 years to 35 million years in the top 1 km of sediment). Therefore we consider the more realistic experimentally derived degradation parameters. Without in-situ production, the pool of archaeal IPLs would tend towards extremely low concentration at depths between 10 and 100 mbsf, dependent on whether the degradation kinetics from the Wadden Sea (faster) or the Cascadia subseafloor sample (slower) are assumed (Fig. IV.5A). Consequently, the continuous production of archaeal IPLs is required to produce the general trends observed in subseafloor sediments (Lipp et al., 2008). Estimates of the production rates were derived by reverse fitting (IV.4.6; Eq. IV.15). The rates required to fit the concentration profile of archaeal IPLs closely to the IPL regression line (Lipp et al., 2008) (Fig. IV.5B; IV.4.6 for details) decrease from 1 ng IPL ml^{-1} sediment yr^{-1} at the sediment surface to ~0.2 pg IPL ml^{-1} sediment yr^{-1} at 1,000 mbsf. Experimental evidence from a stable isotope probing experiment using a 8-m-deep subseafloor sediment from Hydrate Ridge, Cascadia Margin (Lin et al., 2012), provides independent support

for the modeled growth rates (Fig. IV.5C). Conversion of IPLs to archaeal cells yields corresponding population growth rates, e.g., at 100 mbsf an annual growth of ~1000 archaeal cells ml^{-1} is consistent with the IPL concentrations represented by the regression line at that depth. While the uncertainties induced by the extrapolation of the degradation rate constant to geologic

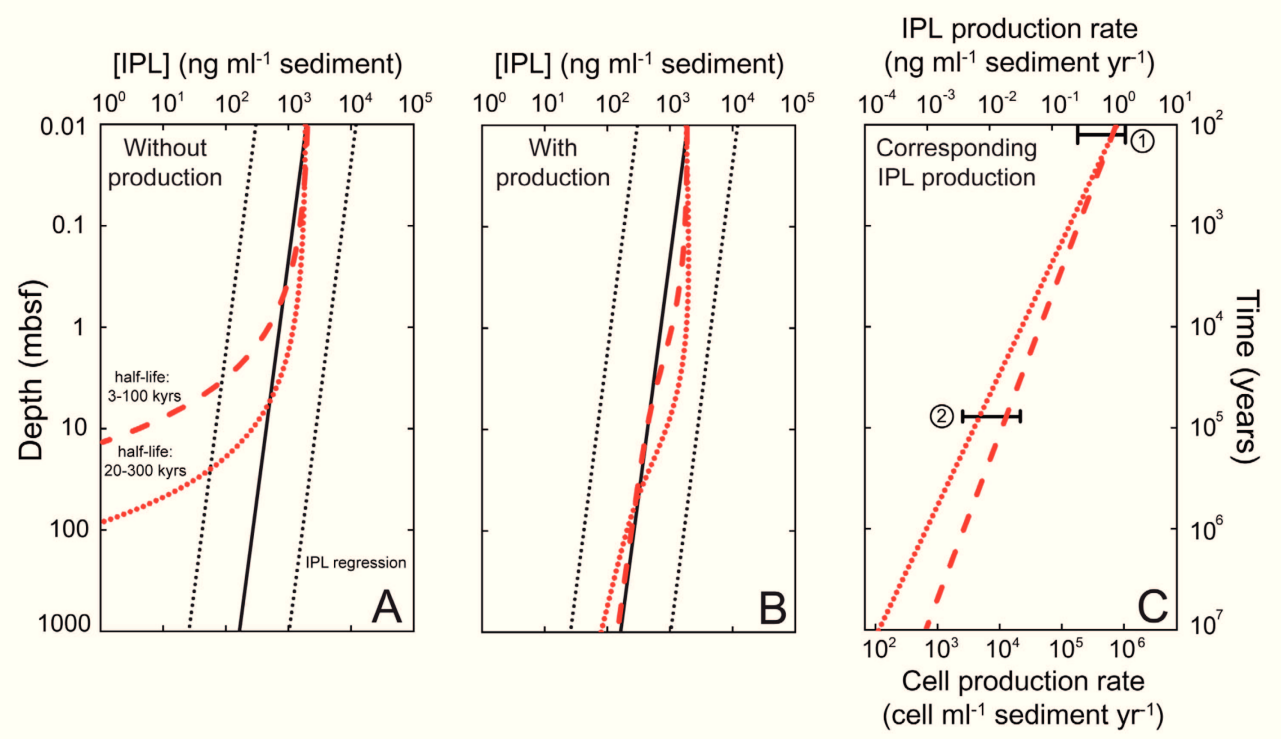

Fig. IV.5. Simulation of archaeal IPL production rates and corresponding populations growth rates required to balance IPL degradation in order to explain IPL concentration profiles. (A) IPL concentration profile of a generic continental margin sediment column with input of IPLs limited to surface sediment (red-dotted curve: degradation kinetics of GlcDGD in Cascadia Margin sediment, red-dashed curve: degradation kinetics of GlcDGD in Wadden Sea sediment, black solid line is regression line and black-dotted lines are 95% prediction interval of observed IPL concentration (Lipp et al., 2008). (B) Simulated of IPL concentration as in A but with sedimentary production of archaeal IPLs to counter balance degradation for the two scenarios from panel A. (C) Corresponding IPL production rates required to obtain concentration profile in panel B; IPL production rate at surface sediment is set to be 1 ng ml^{-1} sediment, which has been determined in recent stable-isotope probing study for coastal sediments younger than 100 years old (Wegener et al., 2012), range of observation in that study is indicated by bar ①; bar ② designates range of IPL production rate (0.006-0.031 ng g^{-1}sediment yr^{-1}) determined in stable-isotope probing study using subseafloor sample at 8 mbsf from Cascadia Margin (Lin et al., 2012). See text for model assumptions and methodology.

time scales need to be considered, the resulting biomass turnover times of microbial populations

are broadly consistent with estimates based on other methods. For example, using the model based on TOC degradation (Fig. IV.3), we obtain a biomass turnover time of 15,500 years for sediments at 100 mbsf. If we assume that 50% of the cellular population consists of Archaea (cf. Lipp et al., 2008; Schippers et al., 2010; 2012) and use the reverse model that matches lipid production to the cell-versus-depth regression line (Parkes et al., 2000), we obtain a range of 1,200 to 4,800 years of biomass turnover for the archaeal community. For comparison, Lomstein et al. (Lomstein et al., 2012) estimated a few hundred to 12,000 years for high-TOC sediments at the Peru Margin. When comparing our two model simulations, the higher biomass turnover times in the TOC-based model directly result from its lower lipid production rates compared to the reverse model (cf. Figs. IV.4B and 5C). A plausible explanation for this difference is the bias of our IPL data set (Lipp et al., 2008) towards high-TOC sediment off the Peru Margin, which is associated with higher microbial activity, growth and lipid production.

On the basis of newly determined experimental data on the degradation kinetics of a glycosidic glyceroldiether lipid resembling the properties of typical archaeal membrane lipids found ubiquitously in marine sediments, we conclude that a substantial portion of the archaeal IPLs found in subseafloor sediments are probably fossil products of past cell generations. Consequently, previous estimates of subseafloor biomass based largely on archaeal IPLs (Lipp et al., 2008) were probably too high. Two independent model simulations of decay and production of microbial IPLs in subseafloor established a quantitative framework that (i) demonstrates the effects of different degradation kinetics on concentration profiles of typical microbial lipids and (ii) provides constraints on the activity of the subseafloor biosphere. Our study highlights the challenges of distinguishing between bio- and geomolecules in the deep sedimentary biosphere; these factors should be taken into consideration in the microbial ecological studies based on molecular techniques and may equally complicate assays based on other types of biomolecules such as DNA (e.g. Dell'Anno and Danovaro, 2005; Corinaldesi et al., 2011) and cell wall components (Lomstein et al., 2012).

IV.6. ACKNOWLEDGEMENTS

The sediment sample from the Cascadia Margin was provided by the Integrated Ocean Drilling Program (IODP Expedition 311). We thank the participating crews and scientists for sample recovery and Verena Heuer for sample donation; Gabriele Schüßler, Marc Lamshöft and

Nguyen Manh Thang for their technical support. This work was supported by the Deutsche Forschungsgemeinschaft through projects Hi 616/11 and Li 1901/1; Sitan Xie was funded by the China Scholarship Council.

IV.7. REFERENCES

Bauersachs T, Speelman EN, Hopmans EC, Reichart G-J, Schouten S, Sinninghe Damsté (2010) Fossilized glycolipids reveal post oceanic N_2 fixation by heterocystous cyanobacteria. *Proc Natl Acad Sci USA* **107**: 19190-19194.

Biddle JF, Lipp JS, Lever MA, LIoyd KG, Sørensen KB, Anderson R, Fredricks HF, Elvert M, Kelly TJ, Schrag DP, Sogin ML, Brenchley JE, Teske A, House CH, Hinrichs K-U (2006) Heterotrophic Archaea dominant sedimentary subsurface ecosystems off Peru. *Proc Natl Acad Sci USA* **103**: 3846-3851.

Corinaldesi C, Barucca M, Luna GM, Dell'Anno A (2011) Preservation, origin and genetic imprint of extracellular DNA in permanently anoxic deep-sea sediments. *Mol Ecol* **20**: 642-654.

Dell'Anno A, Danovaro R (2005) Extracellular DNA plays a key role in deep-sea ecosystem functioning. *Science* **309**: 2179.

D'Hondt S, Rutherford S, Spivack AJ (2002) Metabolic activity of subsurface life in deep-sea sediments. *Science* **295**: 2067-2070.

Expedition 311 Scientists (2005) Integrated ocean drilling program expedition 311 preliminary report-Cascadia margin gas hydrates. doi:10.2204/iodp.pr.311.2005.

Harvey HR, Fallon RD, Patton JS (1986) The effect of organic matter and oxygen on the degradation of bacterial membrane lipids in marine sediments. *Geochim Cosmochim Acta* **50**: 795-804.

Hedges JI, Baldock JA, Gélinas Y, Lee C, Peterson M, Wakeham SG (2001) Evidence for non-selective preservation of organic matter in sinking marine particles. *Nature* **409**: 801-804.

Heijnen JJ, Van Dijken JP (1992) In search of a thermodynamic description of biomass yields for the chemotrophic growth of microorganisms. *Biotechnol Bioeng* **39**: 833-858.

Hinrichs, K.-U. (2002) Microbial fixation of methane-carbon at 2.7 Ga: Was an anaerobic mechanism possible? *Geochemi Geophys Geosyst* 3: doi:10.1029/2001GC000286.

Hoehler TM, Alperin MJ, Albert DB, Martens CS (1994) Field and laboratory studies of methane oxidation in an anoxic marine sediment: Evidence for a methanogen-sulfate reducer consortium. *Global Biogeochem Cycles* **8**: 451-463.

Inagaki F, Nunoura T, Nakagawa S, Teske A, Lever M, Lauer A, Suzuki M, Takai K, Delwiche M, Colwell FS, Nealson KH, Horikoshi K, D'Hondt S, Jørgensen BB (2006) Biogeographical distribution and diversity of microbes in methane hydrate-bearing deep marine sediments on the Pacific Ocean Margin. *Proc Natl Acad Sci USA* **103**: 2815-2820.

Jørgensen BB (1978) A comparison of methods for the quantification of bacterial sulfate reduction in coastal marine sediments. *Geomicrobiol* J **1**: 29-47.

Kallmeyer J, Pockalny R, Adhikari RR, Smith DC, D'Hondt S (2012) Global distribution of microbial abundance and biomass in subseafloor sediment. *Proc Natl Acad Sci USA*: doi/10.1073/pnas.1203849109.

Lin Y-S, Lipp JS, Elvert M, Holler T, Hinrichs K-U (2012). Assessing production of the ubiquitous archaeal diglycosyl tetraether lipids in marine subsurface sediment using intramolecular stable isotope probing. *Environ Microbiol*: doi: 10.1111/j.1462-2920.2012.02888.x.

Lipp JS, Morono Y, Inagaki F, Hinrichs K-U (2008) Significant contribution of Archaea to extant biomass in marine subsurface sediments. *Nature* **454**: 991-994.

Lipp JS, Hinrichs K-U (2009) Structural diversity and fate of intact polar lipids in marine sediments. *Geochim Cosmochim Acta* **73**: 6816-6833.

Logemann J, Graue J, Köster J, Engelen B, Rullkötter J, Cypionka H (2011) A laboratory experiment of intact polar lipid degradation in sandy sediments. *Biogeosciences* **8**: 2547-2560.

Lomstein BA, Langerhuus AT, D'Hondt S, Jørgensen BB, Spivack AJ (2012) Endospore abundance, microbial growth and necromass turnover in deep sub-seafloor sediment. *Nature* **484**: 101-104.

Middelburg JJ (1989) A simple rate model for organic matter decomposition in marine sediments. *Geochim Cosmochim Acta* **53**: 1577-1581.

Middelburg JJ, Vlug T, Van Der Nat FJWA (1993) Organic matter mineralization in marine systems. *Glob Planet Change* **8**: 47-58.

Nauhaus K, Albrecht M, Elvert M, Boetius A, Widdel F (2007) In vitro cell growth of marine archaeal-bacterial consortia during anaerobic oxidation of methane with sulfate. *Environ*

Microbiol **9**: 187-196.

Parkes RJ, Cragg BA, Wellsbury P (1994) Deep bacterial biosphere in Pacific Ocean sediments. *Nature* **371**: 410-413.

Parkes RJ, Cragg BA, Wellsbury P (2000) Recent studies on bacterial populations and processes in subseafloor sediments: A review. *Hydrogeol J* **8**: 11-28.

Rossel PE (2009) Ph.D. thesis (University of Bremen, Bremen, Germany)

Rothman DH, Forney DC (2007) Physical model for the decay and preservation of marine organic carbon. *Science* **316**: 1325-1328.

Schippers A, Neretin LN, Kallmeyer J, Ferdelman TG, Cragg BA, Parkes RJ, Jørgensen BB (2005) Prokaryotic cells of the deep sub-seafloor biosphere identified as living bacteria. *Nature* **433**: 861-864.

Schippers A, Köweker G, Höft C, Teichert BMA (2010) Quantification of microbial communities in forearc sediment basins off Sumatra. *Geomicrobiol J* **27**: 170-182.

Schippers A, Kock D, Höft C, Köweker G, Siegert M (2012) Quantification of microbial communities in subsurface marine sediments of the Black Sea and off Namibia. *Front Microbiol* **3**: 16. doi: 10.3389/fmicb.2012.00016.

Schouten S, Middelburg JJ, Hopmans EC, Sinninghe Damsté (2010) Fossilization and degradation of intact polar lipids in deep subsurface sediments: A theoretical approach. *Geochim Cosmochim Acta* **74**: 3806-3814.

Schubotz F, Wakeham SG, Lipp JS, Fredricks HF, Hinrichs K-U (2009) Detection of microbial biomass by intact polar membrane lipid analysis in the water column and surface sediments of the Black Sea. *Environ Microbiol* **11**: 2720-2734.

Seidel M (2009) Ph.D. thesis (University of Oldenburg, Oldenburg, Germany)

Simon M, Azam F (1989) Protein content and protein synthesis rates of planktonic marine bacteria. *Mar Ecol Progr Ser* **51**: 201-213.

Sturt HF, Summons RE, Smith K, Elvert M, Hinrichs, K-U (2004) Intact polar membrane lipids in prokaryotes and sediments deciphered by high-performance liquid chromatography/electrospray ionization multistage mass spectrometry-new biomarkers for biogeochemistry and microbial ecology. *Rapid Commun Mass Spectrom* **18**: 617-628.

Suess E (1980) Particulate organic carbon flux in the oceans-surface productivity and oxygen utilization. Nature 288: 260-263.

Treude T, Boetius A, Knittel K, Wallmann K, Jørgensen BB (2003) Anaerobic oxidation of

methane above gas hydrates at Hydrate Ridge, NE Pacific Ocean. *Mar Ecol Prog Ser* **264**: 1-14.

Van Mooy BAS, Fredricks HF, Pedler BE, Dyhrman ST, Karl DM, Koblížek M, Lomas MW, Mincer TJ, Moore LR, Moutin T, Rappé MS, Webb EA (2009) Phytoplankton in the ocean use non-phosphorus lipids in response to phosphorus scarcity. *Nature* **458**: 69-72.

Wegener G, Niemann H, Elvert M, Hinrichs K-U, Boetius A (2008) Assimilation of methane and inorganic carbon by microbial communities mediating the anaerobic oxidation of methane. *Environ Microbiol* **10**: 2287-2298.

Wegener G, Bausch M, Holler T, Thang NM, Mollar XP, Kellermann MY, Hinrichs K-U, Boetius A (2012) Assessing sub-seafloor microbial activity by combined stable isotope probing with deuterated water and ^{13}C-bicarbonate. *Environ Microbiol* **14**: 1517-1527.

White DC, Davis WM, Nickels JS, King JD, Bobbie RJ (1979) Determination of the sedimentary microbial biomass by extractible lipid phosphate. *Oecologia* **40**: 51-62.

Whitman WB, Coleman DC, Wiebe WJ (1998) Prokaryotes: The unseen majority. *Proc Natl Acad Sci USA* **95**: 6578-6583.

Zink K-G, Wilkes H, Disko U, Elvert M, Horsfield B (2003) Intact phospholipids-microbial "life markers" in marine deep subsurface sediments. *Org Geochem* **34**: 755-769.

IV.S1. SUPPORTING FIGURES

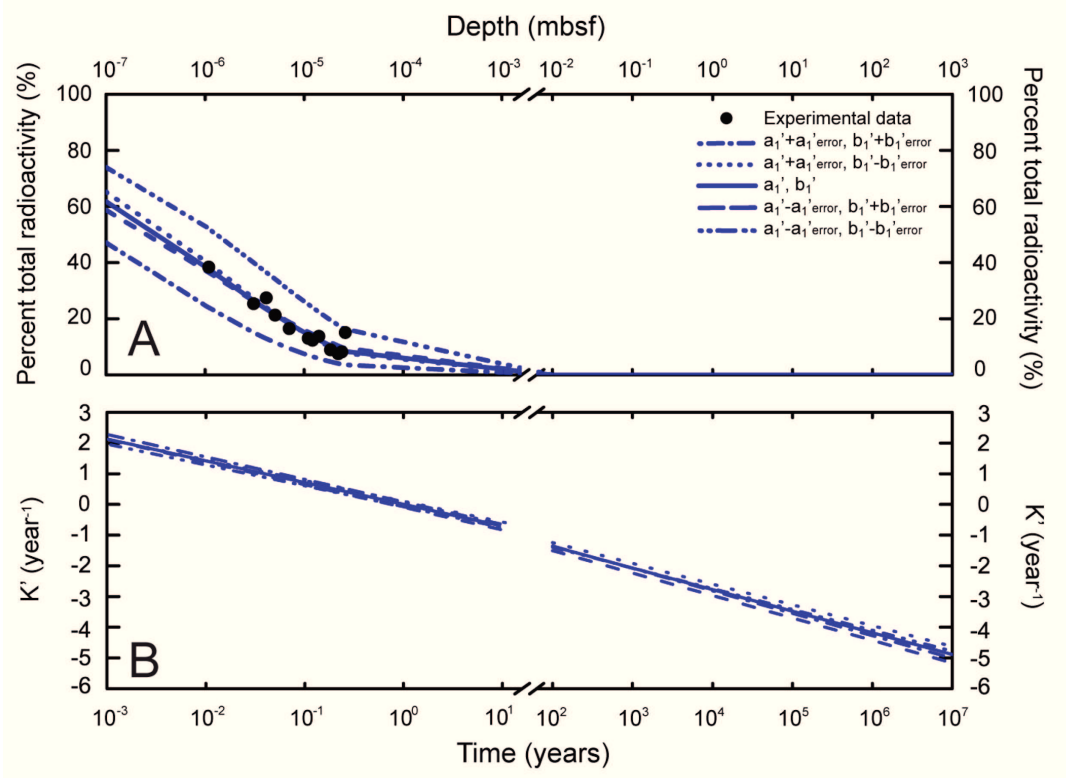

Fig. IV.S1. (A) Reverse fitting of experimental results of ester-bond IPLs (Logemann et al., 2011). The different lines represent the extreme cases of the degradation rate of lipids influenced by standard error of *a'* and *b'*. (B) The effect of standard error of *a'* and *b'* on k' of ester-bond IPLs.

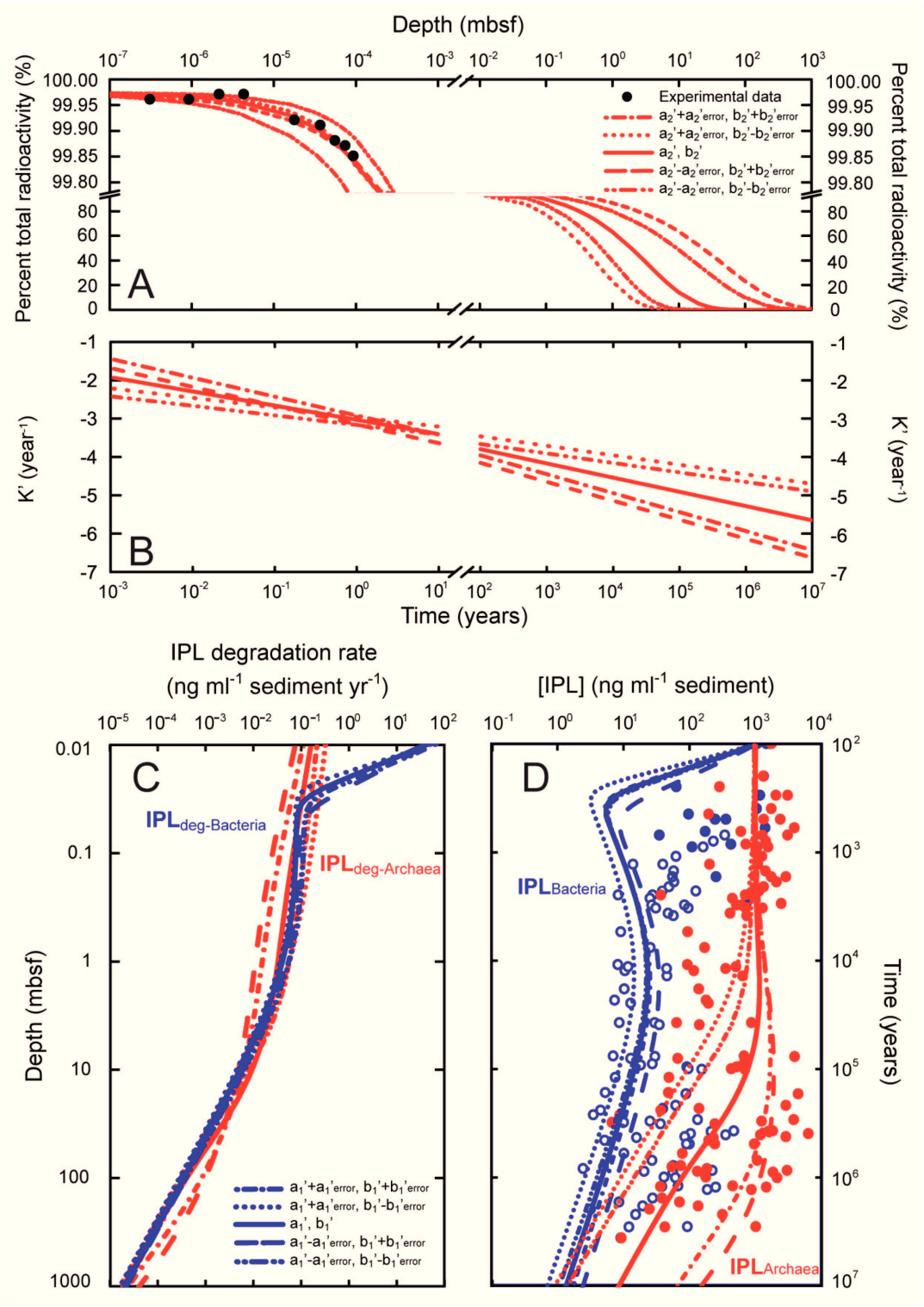

Fig. IV.S2. (A) Reverse fitting of experimental results of GlcDGD in Cascadia Margin sediment. The different lines represent extreme cases of the degradation rate of lipids influenced by standard error of *a'* and *b'*. (B) The effect of standard error of *a'* and *b'* on degradation rate constant of GlcDGD. (C) The effect of standard error of *a'* and *b'* on degradation rate of archaeal IPLs and bacterial IPLs, the latter is identical to Fig. IV.S3. (D) The effect of standard error of *a'* and *b'* on concentration of archaeal IPLs and bacterial IPLs.

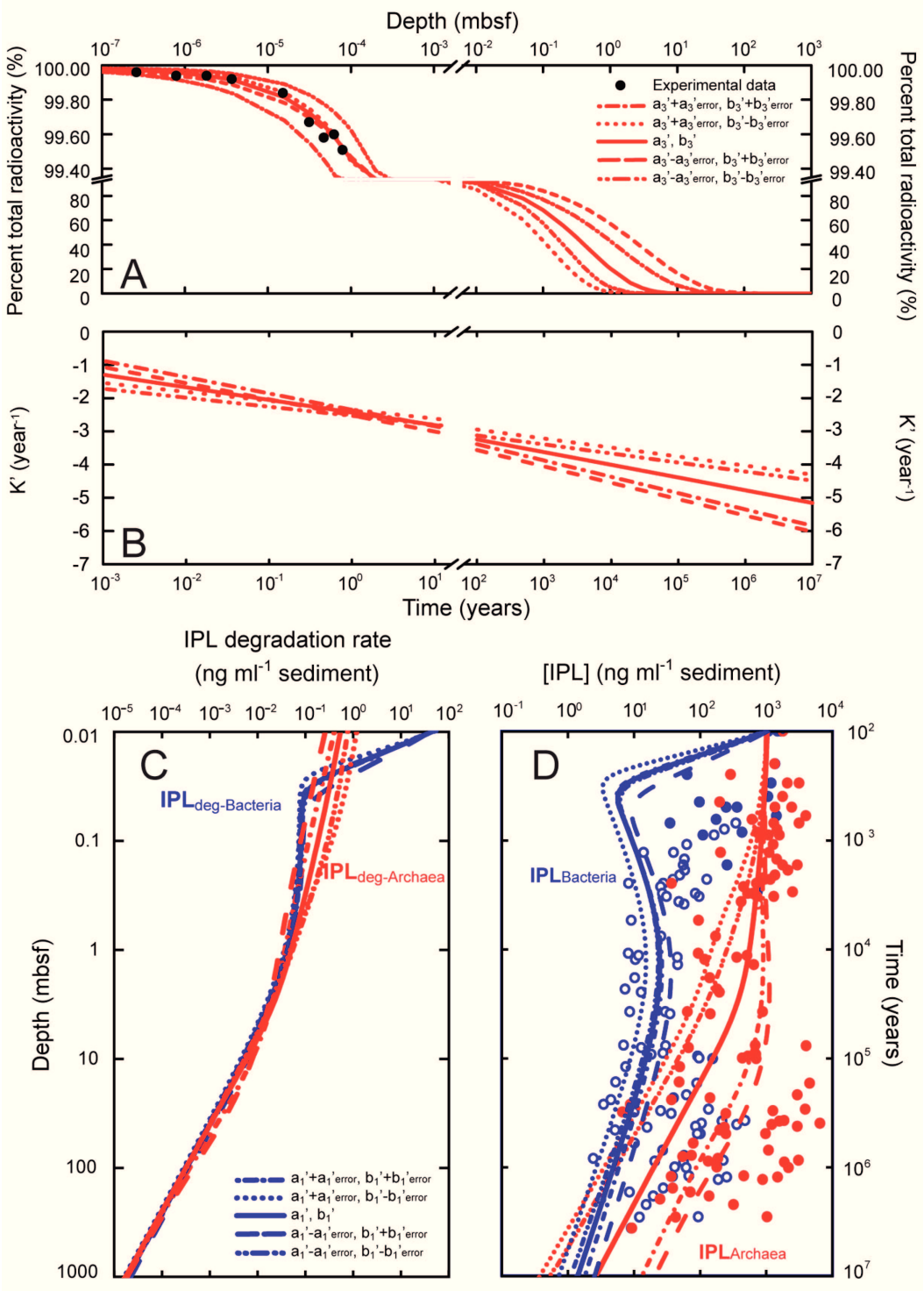

Fig. IV.S3 (A) Reverse fitting of experimental results of GlcDGD in Wadden Sea sediment. The different lines represent extreme cases of the degradation rate of lipids influenced by standard error of *a'* and *b'*. (B) The effect of standard error of *a'* and *b'* on degradation rate constant of GlcDGD. (C) The effect of standard error of *a'* and *b'* on degradation rate of archaeal IPLs and bacterial IPLs, the latter is identical to Fig. IV.S2. (D) The effect of standard error of *a'* and *b'* on concentration of archaeal IPLs and bacterial IPLs.

Chapter V

Ethane- and propane-producing potential and molecular characterization of an ethanogenic enrichment in anoxic estuarine sediment

Sitan Xie,[a] Cassandre Sara Lazar,[a,b] Yu-Shih Lin,[a*] Andreas Teske,[b] Kai-Uwe Hinrichs[a]

Revised version prepared for submission to *Organic Geochemistry*.

[a]*Organic Geochemistry Group, MARUM Center for Marine Environmental Sciences and Department of Geosciences, University of Bremen, Leobener Straße, 28359 Bremen, Germany*

[b]*Department of Marine Sciences, University of North Carolina at Chapel Hill, Chapel Hill, NC, USA*

[*]*Corresponding author. Organic Geochemistry Group, MARUM Center for Marine Environmental Science and Department of Geosciences, University of Bremen, Leobener Straße, 28359 Bremen, Germany. Tel: +49-421-21865744. Fax: +49-421-21865715. E-mail: yushih@uni-bremen.de*

V.1. ABSTRACT

Ethane and propane are low-molecular-weight hydrocarbons observed widely at trace levels in cold marine sediments; thermogenic sources are inconceivable in many settings. Several C-2 and C-3 compounds have been tested in separate studies for their alkane-producing potential, but their relative potential and environmental relevance have not been evaluated. In this study, a series of substrates, including alkenes, alcohols, thiols, and carboxyl acids with C-2 or C-3 skeleton, were tested for their alkane-producing potential in anoxic sediment from the German Wadden Sea. Alkane production was only observed in the sediment supplemented with ethylene, ethanethiol and propanethiol, with ethylene showing maximum conversion efficiency (up to 38%). Experiments with sterilized sediment or chemicals inhibitory to methanogenesis were negative for alkane production, suggesting that methanogens were involved in the processes of alkane generation. Further biogeochemical characterization focusing on ethylene showed that the H_2 concentration required for ethanogenesis from ethylene was lower than 0.01% H_2 (equivalent to 120 nmol dissolved H_2 L^{-1} slurry). The apparent stable carbon isotope fractionations from ethylene to ethane ($\varepsilon_{ethane/ethylene}$) averaged -8.6±2.4‰. Further molecular characterization was carried out in an ethane-producing enrichment with ethylene as the substrate. The homoacetogens *Acetobacterium* and *Clostridium* were the most abundant in the bacterial 16S rRNA gene library, whereas *Methanocalculus* and sequences belonging to the *Methanomicrobiales* were the dominant groups in the archaeal 16S gene library and the *mcrA* gene library, respectively. *Methanocalculus* is a candidate responsible for ethanogenesis from ethylene, but other methanogens detected in the gene libraries cannot be ruled out.

V.2. INTRODUCTION

Ethane and propane have been reported as commonly occurring light hydrocarbons in many cold marine environments where the contributions from thermogenic gases are considered insignificant. Both gases were detected in oxic (Swinnerton and Lamontagne, 1974) and anoxic (Hunt, 1974) seawater. They were also found in sedimentary materials collected from different settings, including intertidal mudflats (Vogel et al., 1982; Oremland et al., 1988), shallow subseafloor depths from continental shelves and slopes (Bernard et al., 1978; Kvenvolden and Redden, 1980; Whelan et al., 1980; Kvenvolden, 1988), Mediterranean sapropels (Egorov and Ivanov, 1998), gas hydrate nodules (Sassen and Curiale, 2006), and even deep subseafloor

sediment at continental margins and the open ocean (Waseda and Didyk, 1995; Paull et al., 2000; Hinrichs et al., 2006). In general, the concentrations of dissolved ethane and propane in recent sediments are one to three orders of magnitude lower than that of dissolved methane. These concentrations are relatively constant with subseafloor depth but tend to decrease with distance from shore (Bernard et al., 1978; Kvenvolden and Redden, 1980). In subseafloor sediment off Peru, the concentrations of sorbed ethane and propane are 10- to 100-fold higher than the reported range for dissolved C-2 and C-3 alkanes in other cold, near-surface sediments (Hinrichs et al., 2006). These earlier studies posited that the observed ethane and propane are of microbial origin because these compounds were prominent at sites of low in situ temperatures with no apparent increase of ethane or propane concentration with depth. Moreover, some studies (Bernard et al., 1978; Kvenvolden and Redden, 1980; Kvenvolden, 1988; Egorov and Ivanov, 1998) also reported substantial amount of coexisting C-2 and C-3 alkenes, both of which are not typical constituents of thermogenic gas but can be generated during microbial decomposition of organic matter (Davis and Squires, 1954; Fukuda et al., 1993).

The stable carbon isotopic ($\delta^{13}C$, reported relative to the standard Vienna-PeeDee Belemnite and defined by the equation $\delta^{13}C$ (‰) = ($R_{sample}/R_{standard} - 1$) × 1000 with $R = {}^{13}C/{}^{12}C$ and $R_{standard}$ = 0.0112372) values of ethane and propane provide deeper insights into the potential precursors and pathways for microbial ethano- and propanogenesis. ^{13}C-Depleted ethane is present in several anoxic marine sediments ($\delta^{13}C$ values of -44‰ to -70‰; Waseda and Didyk, 1995; Seifert et al., 1999; Paull et al., 2000). Claypool (1999) proposed that biogenic ethane can be formed from reduction of two-carbon carboxylic acids (acetic and oxalic) in a process analogous to reductive methanogenesis. This hypothesis was supported by geochemical evidence provided in Hinrichs et al. (2006), who further suggested that condensation of dissolved inorganic carbon (DIC) to C-2 compounds (acetate or related intermediates) leads to biogenic propane. Such a scenario would explain the ^{13}C enrichment of propane relative to ethane in biogenic gas, as DIC in sedimentary pore waters is usually isotopically heavy (Hinrichs et al., 2006).

Here, we outline some shared features of previous studies that focused on substrates and mechanisms for anaerobic ethano- and propanogenesis and summarize the remaining open questions. First, the precursors for ethane and propane evaluated in previous studies already possess C-2 and C-3 skeletons, respectively. The ethane-producing potential of the following substrates has been confirmed in separate studies: ethylene (Koene-Cottaar and Schraa, 1998), ethanol (Belay and Daniels, 1988; Oremland et al., 1988), and ethylated sulfur compounds

(Oremland, 1981; Oremland et al., 1988). For propane, the only tested precursor to date is propanethiol, which resulted in only minor enhancement of propane formation (Oremland et al., 1988). The precursors and routes proposed in geochemical studies (Claypool, 1999; Hinrichs et al., 2006) for production of biogenic ethane and propane have not been experimentally evaluated. Second, because of the requirement for reducing power to convert precursors to ethane and propane, these studies employed high H_2 partial pressure (100-200 kPa) in the incubations. It is unclear whether biological formation of C-2 and C-3 alkanes can proceed at the lower H_2 concentrations typical of sedimentary environments (Hoehler et al., 1998; Lin et al., 2012). Third, methanogens were believed to be involved in the production of ethane or propane. Therefore, these studies were performed using isolated methanogens (Belay and Daniels, 1988; Oremland et al., 1988) or methanogenic sediment (Oremland et al., 1988; Vogel et al., 1982). Two studies have succeeded in enriching microbes that can convert specific precursors: Oremland (1981) obtained a methanogenic enrichment from estuary sediment supplemented with ethylthioethanesulfonic acid, while Koene-Cottaar and Schraa (1998) acquired a freshwater methanogenic enrichment capable of reducing ethylene to ethane. However, no phylogenetic analysis has been carried out to further characterize the microbial community composition of either enrichment. Described methanogens have been divided into three categories based on methanogenic substrate: hydrogenotrophs oxidize H_2 and reduce CO_2, acetoclastic methanogens utilize acetate, and methylotrophs use methyl compounds (Garcia et al., 2000). Since all described methanogens need the methyl co-enzyme M reductase for methane production, the *mcrA* gene is a functional gene that targets methanogenic communities in the environment (Friedrich, 2005; Hallam et al., 2003).

The goal of this study is to identify the compound that possesses the highest alkane-producing potential and the microorganisms that are responsible for this reaction. First, a series of C-2 and C-3 precursors with different functional groups, including alkenes, alcohols and thiols, were tested using one sediment sample under comparable experimental conditions to assess the alkane-generating potential of different classes of compounds. In addition, we included acetate in our substrate assay to test the hypothesis put forward by Claypool (1999) and Hinrichs et al. (2006). For substrates that gave a positive response, inhibition tests were conducted to obtain a first indication of whether methanogens were involved in the conversion. Based on the results of the substrate assays, we focused on the compound that gave the highest yield of ethane or propane and performed additional experiments, including isotopic analysis of substrates and products, evaluation of H_2 requirement, and microbial enrichment. We then characterized the microbial

composition of the enrichment using molecular approaches.

V.3. MATERIAL AND METHODS

V.3.1. Study sites and sampling

The anoxic estuary sediment was collected from the upper tidal flat area near Wremen (53° 38' 60N，8° 31' 0E) in the German Wadden Sea in 2008. The sediment was oxic at its surface and became anoxic below about 2 cm with a dark color suggesting high levels of reduced sulfur minerals. The anoxic sediment was collected in a 1 L Schott bottle without headspace and sealed with a black rubber stopper. The sediment was stored at 4°C for one year until incubation.

V.3.2. Preparation of sediment slurries

The estuary sediment contained a substantial amount of sulfate. To obtain a methanogenic sediment, we pre-incubated a batch of sediment slurry prepared by mixing 250 mL of sediment with approximately the same volume of sterilized, sulfate-free artificial seawater. The composition of the artificial seawater was as follows (in g L^{-1} of deionized water): KCl, 0.68; $CaCl_2 \cdot 2H_2O$, 1.5; $MgCl_2 \cdot 6H_2O$, 11.3; NaCl, 26.4; KBr, 0.10; $NaHCO_3$, 0.84; Resazurin, 0.001. Before mixed with the sediment, the artificial seawater was reduced slowly with a freshly prepared sodium dithionite solution until the pink color of the liquid indicative for oxic conditions had cleared out completely. The slurry was stored in a 1 L Schott bottle with ca. 500 mL headspace filled with H_2:CO_2 (90:10, v/v) at 200 kPa, sealed with a black butyl rubber stopper, and incubated at room temperature in the dark. Gas samples were taken regularly from the headspace to monitor the progress of the methanogenesis that usually follows depletion of sulfate. After about one month of pre-incubation, methanogenic conditions were established, and the resulting mixture served as the stock slurry for the subsequent experiments.

Incubation experiments were carried out using 1:10 diluted sediment slurries prepared by mixing one volume of the stock slurry with nine volumes of sulfate-free artificial seawater, which contained salts identical to those described above plus NH_4Cl (final concentration = 0.25 g L^{-1}), KH_2PO_4 (0.20 g L^{-1}), and trace metals and vitamins required for microbial growth (Widdel and Bak, 1992). All the incubations were performed at room temperature in the dark.

V.3.3. Slurry amendments

The experiments were set up in a glove box filled with 3% H_2 in N_2. Aliquots of 10 mL 1:10 sediment slurry were dispensed into a series of 16 mL Hungate tubes. The tubes were sealed with butyl stoppers that had previously been treated with boiling 0.1 M NaOH to remove trace organic contaminants. The headspace of the tubes was later replaced with H_2:CO_2 (90:10, v/v) and pressurized to 200 kPa. The following C-2 and C-3 compounds (reported in final concentrations after amendment) were added as individual substrates: ethylene (0.025% in the headspace, equivalent to 12.4 µmol dissolved ethylene L^{-1} slurry when the added amount was divided by the volume of slurry), ethanol (1 mmol L^{-1} slurry), ethanethiol (1 mmol L^{-1} slurry), acetate (1 mmol L^{-1} slurry as sodium salt), propylene (0.025% in the headspace, equivalent to 12.4 µmol propylene L^{-1} slurry), propanol (1 mmol L^{-1} slurry), and propanethiol (1 mmol L^{-1} slurry). These concentrations were chosen based on the results of Koene-Cottaar and Schraa (1998) and Oremland et al. (1988), who demonstrated ethane formation in the presence of 0.025% ethylene or 1 mmol L^{-1} slurry ethanethiol. Consumption of H_2 in the headspace resulted in loss of headspace pressure. Therefore, we monitored the headspace pressure over the course of the incubation and brought the pressure back to 200 kPa with H_2:CO_2 = 90:10 (v/v) when the pressure dropped below 100 kPa. Autoclaved slurries (120 °C, 25 min) were used as controls to account for non-biological processes.

We used two different chemicals to suppress the activity of methanogens. One is 2-bromoethanesulfonic acid (BES, 20 mmol L^{-1} slurry), a chemical best known for its inhibitory effect on methanogenesis. However, long-term incubation of sediment with BES in the presence of H_2 can lead to formation of ethylene (Belay and Daniels, 1987; Oremland et al., 1988), which would complicate data interpretation. Therefore, in separate experiments, we added nitrate (1.2 mmol L^{-1} slurry as $NaNO_3$, under a headspace of H_2:CO_2 = 90:10) to make methanogenesis a less favorable H_2-consuming reaction (Akunna et al., 1998). The slurries turned pink once nitrate was added and became colorless when nitrate was exhausted. Because of its rapid consumption as indicated by color changes, we replenished the slurry with nitrate every three days. The concentrations of substrates in sterilized sediment or sediment supplemented with chemical inhibitors were the same as those in the active sediment.

The effect of H_2 partial pressure on alkane formation was only evaluated with the substrate ethylene, which gave the highest yield of ethane in our substrate assay (see below). Ethylene was

added to yield an initial concentration of 0.025% in the headspace. We used a gas mixture of H_2 and CO_2 (90:10 v/v) to adjust the initial headspace H_2 partial pressure to the following levels: 0.01%, 0.1%, 1%, and 90% (total pressure = 200 kPa), with the balance gas for the first three treatments being N_2. These values correspond to 0.12, 1.2, 12.1 and 1088 µmol dissolved H_2 L^{-1} slurry at the beginning of the incubation when calculated using the Bunsen constant published by Crozier and Yamamoto (1974). In addition, a pair of test tubes containing 0.5 mmol glucose L^{-1} slurry under a N_2 headspace was used to simulate the natural conditions under which H_2 is produced by fermentation of organic matter (Hoehler et al., 1998). Over the course of the incubation, the pressure was adjusted to 200 kPa with H_2 in the tubes containing 90% H_2 and with N_2 in the others.

V.3.4. Incubations for stable carbon isotopic analysis

The carbon isotopic fractionation from precursor compounds to hydrocarbon gases was evaluated for the conversion of ethylene to ethane. To reduce competing microbial processes and microbes, the initial ethylene-supplemented slurries (1:10 dilution) were diluted by a factor of 1.5, 6 or 10 and incubated with ethylene in the presence of H_2/CO_2. Ethane-producing activities were maintained in all the transfers. Gas samples were taken after 74-220 days of incubation for quantification and isotopic analysis of gaseous compounds in these higher dilutions. We also determined the $\delta^{13}C$ of ethylene from the stock gas container supplied to the microcosms.

In addition to gaseous products, we analyzed the concentrations of acetate in the 1:100 dilutions. After 84 days of incubation, the slurries were centrifuged and a 2-mL aliquot of the supernatant was taken and stored at -20°C until analysis.

V.3.5. Enrichment of ethanogenic microorganisms

To acquire sufficient biomass for molecular characterization, we prepared a large batch of sediment slurries containing 500 mL of 1:10 slurries under a 500 mL headspace of ethylene (0.025%) balanced by H_2/CO_2 (90:10 v/v). After ethanogenesis was detected, the slurry was diluted by a factor of 10 with fresh medium and further incubated under a similar headspace composition. Ethane production continued in the diluted enrichments and leveled off after 80 days of incubation. Particles in the 1:100 dilutions were then harvested by centrifugation (9000 rpm, 30 min) for analysis of 16S rRNA gene and the *mcrA* functional gene.

V.3.6. Chemical analysis

Identification of hydrocarbons was achieved by either comparison with authentic standards or by injecting selected samples into a gas chromatograph-mass spectrometer. For quantification, we first determined the headspace pressure using a digital pressure probe (constructed at the Max Planck Institute for Marine Microbiology, Bremen). An aliquot of 100 µL gas was then taken from the headspace using a Hamilton SampleLock syringe for on-column injection via a programmable temperature vaporizing inlet. A gas chromatograph (Trace GC Ultra, ThermoFinnigan GmbH, Bremen, Germany) equipped with a CP-PoraBOND Q column (Agilent Technologies Deutschland GmbH, Böblingen, Germany) and a flame ionization detector was used to quantify the compounds. The column temperature was programmed from 60°C (1 min isothermal) to 240°C (2 min isothermal) at a rate of 40°C min^{-1}. Calibration was made with the commercially available 100 ppm C_1-C_6 standards (Scotty Gases). The detection limits for methane, ethane and propane (µmol L^{-1} slurry) were 0.078, 0.032 and 0.008, respectively, under the analytical conditions described for the slurries in Hungate tubes.

For stable carbon isotope analysis, the same model of gas chromatograph was coupled to a Delta Plus XP isotope ratio mass spectrometer via a combustion interface-III (all from ThermoFinnigan GmbH). Five hundred microliters of gas was injected into the split/splitless inlet. A column and a temperature program identical to those described above were used. The internal precision of $\delta^{13}C$ was better than ± 0.1‰ (one standard deviation).

Concentrations of acetate were analyzed by liquid chromatography-isotope ratio mass spectrometry as described in Heuer et al (2006). Briefly, analysis was achieved by separation of water soluble organic compounds by a Surveyor high performance liquid chromatograph, chemical oxidation of the effluents in an LC IsoLink interface, and subsequent online transfer of the resulting CO_2 into a Delta Plus XP isotope ratio mass spectrometer (all from ThermoFinnigan GmbH) via routine open split (Krummen et al., 2004).

V.3.7. Analysis of archaeal and bacterial 16S rRNA and methyl-coenzyme M reductase A (mcrA) genes

DNA was extracted using the UltraClean® Mega Soil DNA Isolation Kit (MO BIO, CA), using 6g of sediment precipitated from the 1:100 dilutions. Archaeal 16S rRNA genes amplification was carried out using the primer combination A8F

(5'-CGGTTGATCCTGCCGGA-3'; Casamayor et al., 2000) and A915R (5'-GTGCTCCCCCGCCAATTCCT; Casamayor et al., 2002), and Flexi GoTaq DNA polymerase (Promega, WI). Conditions for the PCR amplification were as follows: 1 min denaturation at 94°C, 1 min annealing at 58°C, and 2 min elongation at 72°C, repeated for 30 cycles in a BIO-RAD iCycler (Hercules, CA). Bacterial 16S rRNA gene amplification was carried out using the E8F (5'-AGAGGTTGATCATGGCTCAG-3') and U1492R (5'-GTTACCTTGTTACGACTT-3') primers (Lane, 1991). Conditions for the PCR amplification were as follows: 1 min denaturation at 94°C, 1 min annealing at 55°C, and 2 min elongation at 72°C, repeated for 30 cycles. Methyl co-enzyme M reductase (*mcrA*) genes amplification was carried out using the ME1 (5'-GCMATGCARATHGGWATGTC-3') and ME2 (5'-TCATKGCRTAGTTDGGRTAGT-3') primers (Hales et al., 1996). Conditions for the PCR amplification were as follows: 40 s denaturation at 94°C, 1 min 30 s annealing at 50°C, and 3 min elongation at 72°C, repeated for 30 cycles. PCR products were cloned using the TOPO XL cloning kit (Invitrogen, CA), and chemically transformed into *Escherichia coli* TOPO10 One Shot cells.

Sequences were obtained by Genewiz (South Plainfield, NJ) on an ABI Prism 3730xl sequencer. Chimeras were identified with Green Genes (http://greengenes.lbl.gov) and removed. Sequences were analyzed by using the NCBI BLASTN search program within GenBank (http://blast.ncbi.nlm.nih.gov/Blast) (Altschul et al., 1990). The sequences were then edited in the BioEdit v7.0.5 program (Hall, 1999) and aligned by using the SINA webaligner (http://www.arb-silva.de/) (Pruesse et al., 2007) for the 16S rRNA genes, and using ClustalX (Larkin et al., 2007) for the *mcrA* amino acid sequences. The alignments were then manually checked using ARB for the 16S rRNA sequences (Ludwig et al., 2004). Phylogenetic trees were calculated using the neighbor-joining method in MEGA4.0.2 (Tamura et al., 2007). Robustness of the inferred topology was tested by bootstrap resampling (1000 replicates). Rarefaction curves were calculated using the RarFac program (http://www.icbm.de/pmbio/) and a 97% similarity cutoff value for sequence based operational taxonomic units (OTUs). Gene library coverage (C) was calculated using the following formula: $C=[1-(n_1/N)]\times100$, where n_1 is the number of unique OTUs and N is the number of clones in the library (Singleton et al., 2001). The sequence data reported here will appear in the GenBank nucleotide sequence database under the accession numbers JX097099 to JX097186 for the archaeal 16S sequences, JX097268 to JX097358 for the bacterial 16S sequences, and JX097187 to JX097267 for the *mcrA* sequences.

V.4. RESULTS

V.4.1. Formation of hydrocarbons from selected C-2 and C-3 substrates

Substrate	Incubation days	Product of major interest		Concentration (µmol L^{-1} slurry) of other hydrocarbons as products		
		Name	Concentration (µmol L^{-1} slurry)	Methane	Ethylene	Propylene
Ethylene	76	Ethane	1.813 (0.439)	2868 (281)	-	BD
Ethanol	76	Ethane	BD	2287 (48)	BD	BD
Ethanethiol	76	Ethane	0.082 (0.003)	1658 (175)	0.047 (0.012)	BD
Propylene	76	Propane	BD	1811 (95)	BD	-
Propanol	76	Propane	BD	2042 (68)	BD	0.012 (0.004)
Propanethiol	76	Propane	0.029 (0.003)	2089 (109)	BD	0.057 (0.003)
Acetate	63	Ethane Propane	BD BD	3410 (111)	BD	BD

Table V.1. Concentration of hydrocarbons in 1:10 sediment slurries supplemented with different substrates after 63-76 days of incubation. Results are presented as the means and 50% of ranges of duplicate incubations. BD: below detection.

Table V.1 summarizes the results of substrate tests. Ethylene and ethanethiol were the two substrates that resulted in significant accumulation of ethane. Ethane became detectable after 30 days of incubation with ethylene (Fig. V.1) and after 50 days with ethanethiol. After 76 days of incubation, the yield of ethane (1.8 µmol L^{-1} slurry) from ethylene was 22-fold higher than the yield of ethanethiol-derived ethane (0.08 µmol L^{-1} slurry; Table 1). No ethane was found in the sediment supplemented with ethanol or acetate. To compare the alkane-producing potential of different substrates at the same concentration level, we calculated the conversion efficiency, defined as the final amount of C-2 or C-3 alkane divided by the initial amount of added substrate. It should be noted that the measured ethylene concentrations (2.5 µmol L^{-1} slurry; Fig. V.1) at time zero were much lower than the theoretical value of 12.4 µmol L^{-1} slurry, probably due to adsorption of ethylene on sediment (Witt and Weber, 1975) or on the interior of sample tubes. Using the theoretical initial concentration of ethylene, we obtained a conservative estimate of 15% (38% in the isotopic fractionation experiment) for the conversion efficiency of ethylene, which is much higher than the value for ethanethiol (0.01%). Among all the tested C-2 and C-3 substrates,

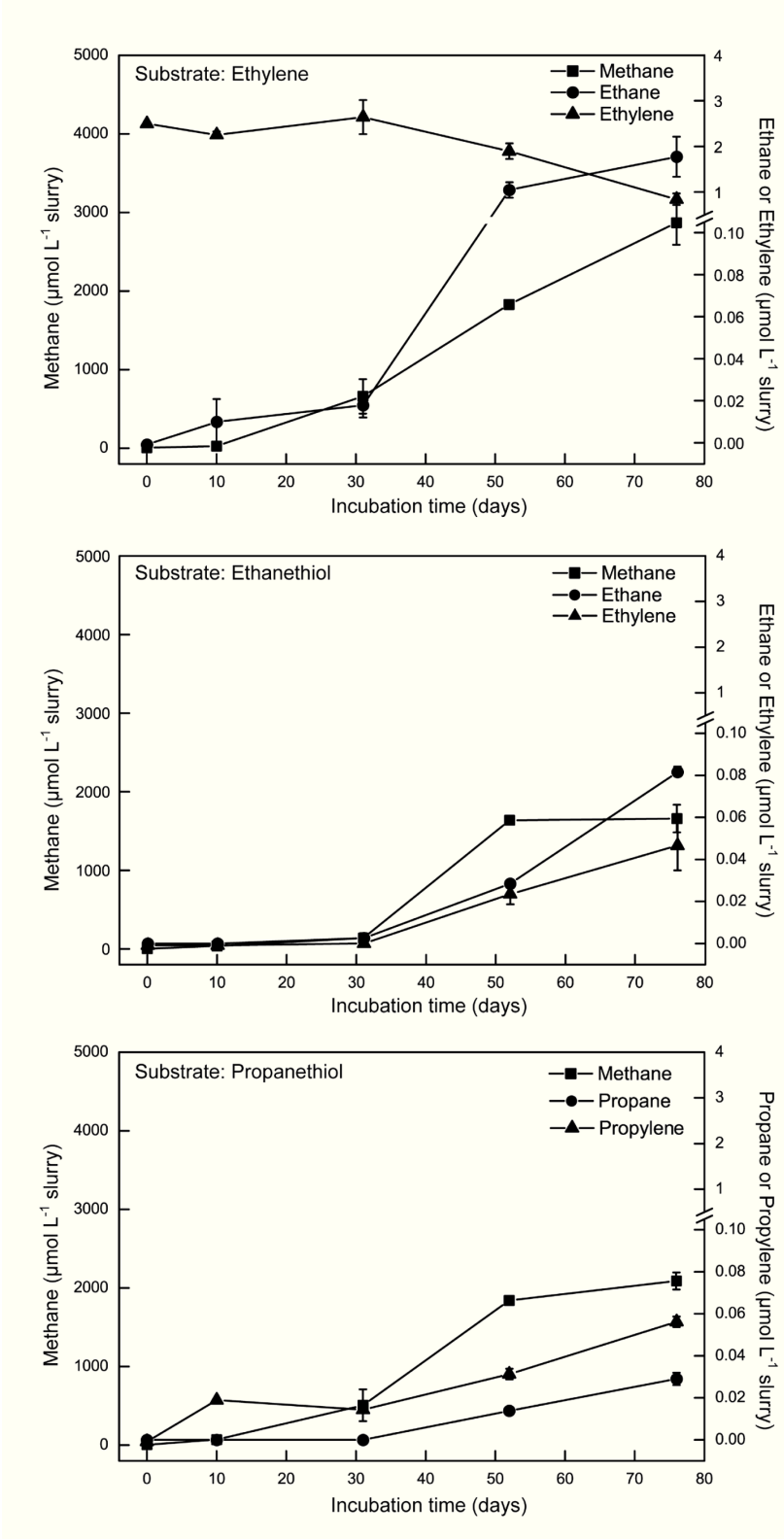

Fig. V.1. Concentrations of hydrocarbons in the 1:10 sediment slurries supplemented with 0.025% ethylene, 1 mM ethanethiol and 1 mM propanethiol, respectively. Results are presented as the average and standard error of duplicate tubes.

	Substrate	Incubation days	Product of major interest		Concentration (µmol L^{-1} slurry) of other hydrocarbons as products		
			Name	Concentration (µmol L^{-1} slurry)	Methane	Ethylene	Propylene
Autoclaved	Ethylene	76	Ethane	BD	5.3 (0.5)	-	BD
	Ethanethiol	76	Ethane	BD	4.2 (1.3)	0.019 (0.007)	BD
	Propanethiol	76	Propane	BD	2.9 (0.3)	BD	0.008 (0.001)
+ BES	Ethylene	76	Ethane	BD	26.4 (4.5)	-	BD
	Ethanethiol	76	Ethane	BD	26.2 (4.2)	0.056 (0.011)	BD
	Propanethiol	76	Propane	BD	25.7 (3.1)	BD	0.009 (0.001)
+ NO_3^-	Ethylene	76	Ethane	BD	34.6 (6.5)	-	BD
	Ethanethiol	76	Ethane	BD	31.9 (2.1)	0.017 (0.021)	BD
	Propanethiol	76	Propane	BD	33.9 (2.5)	BD	0.007 (0.001)

Table V.2. Effects of autoclave, 2-bromoethanesulfonic acid (BES) and nitrate (NO_3^-) on the formation of hydrocarbons in 1:10 sediment slurries supplemented with different substrates after 76 days of incubation. Results are presented as the means and 50% of ranges of duplicate incubations. BD: below detection.

propane was detected only in propanethiol-treated slurries at a concentration of 0.03 µmol L^{-1} slurry and a conversion efficiency of 0.003% after 76 days of incubation. Propylene, propanol, and acetate did not lead to detectable propane accumulation. There is no evidence of ethane or propane consumption based on the concentration data.

Besides ethane and propane, other hydrocarbon products were also observed (Table V.1). Methane was the most abundant hydrocarbon gas in all sediment slurries, with concentrations ranging from 1.7 mmol L^{-1} slurry in the ethanethiol-supplemented slurries to 3.4 mmol L^{-1} slurry in the acetate-supplemented slurries after 63-76 days of incubation. Accumulation of methane was generally detectable before accumulation of ethane or propane, as exemplified for ethylene additions (Fig. V.1). In slurries that were supplemented with C-2 and C-3 thiols, ethylene and propylene were apparently formed, respectively (Table V.1). The ratios of produced alkene to alkane in thiol supplementation were 1:2 for ethanethiol and 2:1 for propanethiol. Unlike thiols, alcohol-to-alkene conversion was only observed for propanol.

V.4.2. Effects of autoclaving, BES, and nitrate

To determine whether the observed ethano- and propanogenesis from ethylene, ethanethiol and propanethiol (Table V.1) is a biological process and whether methanogens are involved, the three substrates were added separately into sediment slurries that were either sterilized or added with chemicals inhibitory to methanogenic activities (Table V.2). Methane concentrations were consistently low (2-6 μmol L^{-1} slurry) in the sterilized samples. After addition of BES or nitrate, methane was less than 40 μmol L^{-1} slurry after 76 days incubation, translating to >98% of inhibition when the concentrations were compared to those of samples without these chemicals (Tables V.1 and V.2). Concentrations of ethane and propane were all below the limit of detection in the samples that were sterilized or supplemented with inhibitory chemicals.

V.4.3. Effects of H_2 partial pressure

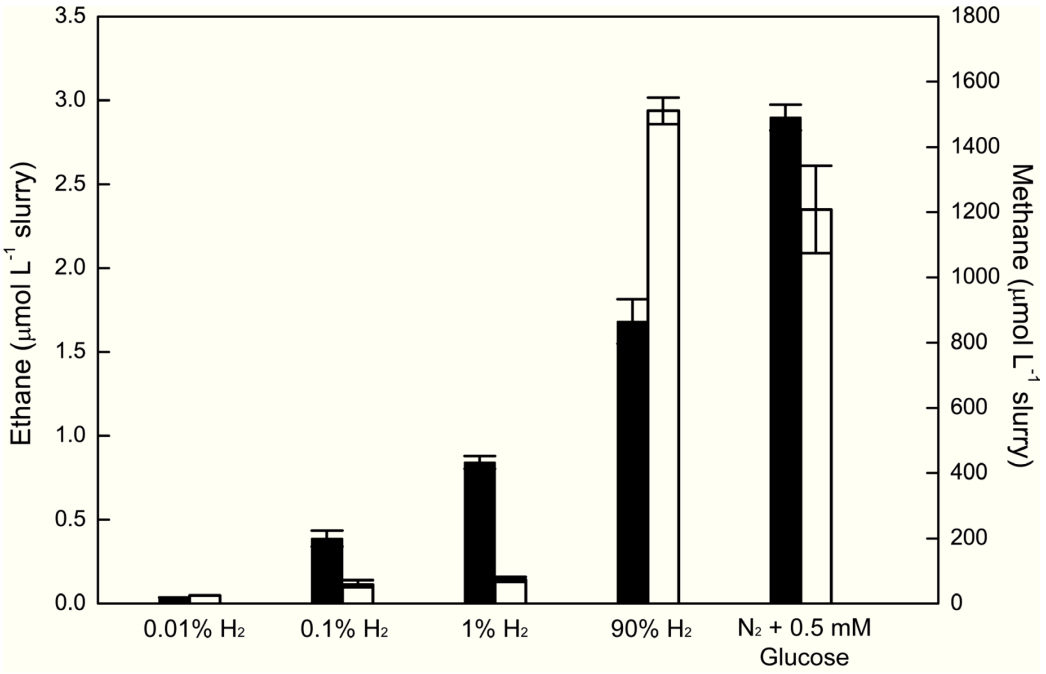

Fig. V.2. Concentrations of methane and ethane in 1:10 sediment slurries supplemented with 0.025% ethylene under different initial H_2 partial pressure after 67 days of incubation. H_2 was added either directly as a headspace gas component or indirectly via fermentation of glucose. Results are presented as the means and ranges of duplicate tubes.

Further geochemical and microbiological experiments were only performed with the substrate ethylene, which gave the highest yield of non-methane hydrocarbon gas among all the tested substrates (Table V.1). We first examined the effects of H_2 partial pressure on ethanogenesis from ethylene. Ethane was detected in all the samples after 67 days of incubation, and the concentrations increased from 0.04 to 1.7 μmol L^{-1} slurry with increasing initial H_2 partial pressure (Fig. V.2). Nevertheless, the highest amount of ethane (2.9 μmol L^{-1} slurry) was obtained in ethylene-amended sediment slurries with 0.5 mmol glucose L^{-1} slurry under a N_2 headspace. The variation in methane concentration follows a similar pattern to that of ethane: higher initial H_2 partial pressure resulted in a higher yield of methane. However, unlike the case with ethane, methane in the glucose additions was less abundant than in the sample with 90% initial H_2 partial pressure (Fig. V.2).

V.4.4. Isotopic composition of ethane in the ethylene additions

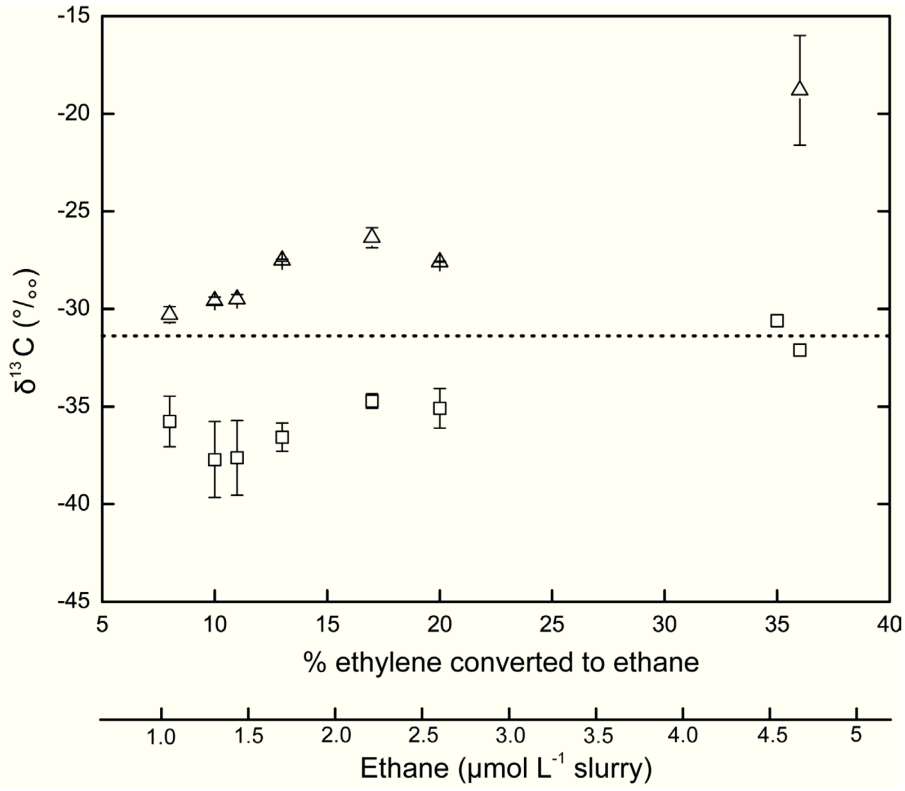

Fig. V.3. Stable carbon isotope compositions of ethylene (triangles) and ethane (squares) complied from enrichments with different dilutions. The dashed line represents the $\delta^{13}C$ of ethylene from the stock gas container. Results are presented as the means and standard errors of duplicate measurements. Note that the conversion efficiencies in some dilutions were higher than the 14% reported for the preliminary 1:10 dilution.

Because of varying incubation durations and dilution factors, the concentrations of ethane ranged from 1.1 to 4.7 μmol L^{-1} slurry, equivalent to conversion efficiencies of 9-38% (Fig. V.3). Ethane was constantly more ^{13}C-depleted than ethylene; the apparent isotope fractionations between the concurrent ethylene and ethane ($\varepsilon_{ethane/ethylene}$) were on average -8.6±2.4 ‰. The $\delta^{13}C$ values of ethane became increasingly positive with elevated ethane concentrations and, at the highest substrate conversion, approached the isotopic value of ethylene from the stock gas container ($\delta^{13}C$ = -31.4‰; Fig. V.3). These observations are consistent with a biologically induced fractionation in a closed system, in which isotopically depleted precursor molecules are preferentially utilized but with the progression of the reaction, $\delta^{13}C$ values of the product gradually approach that of the precursor (Mariotti et al., 1981).

V.4.5. Diversity of mcrA genes, archaeal and bacterial 16S rRNA genes in the ethanogenic enrichment

Percent coverage of clone libraries was 87.6, 98.9, and 84.6% for the *mcrA*, archaeal and bacterial 16S rRNA gene libraries respectively. Rarefaction curves all showed saturation (Fig. V.S1). The *mcrA* gene library yielded sequences affiliated with methanogens (Fig. V.4) with the majority (91.4%) belonging to the *Methanomicrobiales* order. Within the *Methanomicrobiales*, one sequence was close to the genus *Methanogenium*, and three sequences were distantly affiliated to the genus *Methanoplanus*. Most of the *Methanomicrobiales*-affiliated sequences (86.4% of the total *mcrA* gene library) were closest to the genus *Methanospirillum* via the NCBI BLASTN search (with 93% identity, Table V.S1), although these sequences did not branch with the genus *Methanospirillum* in the *mcrA* phylogenetic tree (Fig. V.4). Furthermore theses sequences did not branch with any known methanogenic *mcrA* sequences. The remaining six sequences were affiliated with the nutritionally versatile genus *Methanosarcina* within the order *Methanosarcinales*.

The archaeal 16S rRNA gene library yielded 63.6% of sequences affiliated with known methanogenic clades (Fig. V.5). Within these methanogens, four sequences were affiliated with the genus *Methanosarcina*, one with the genus *Methanogenium* and 85.7% of the methanogen sequences were closely affiliated (99% identity) with the genus *Methanocalculus* within the *Methanomicrobiales* (Table V.S2). Intriguingly, 34.1% of the archaeal sequences were affiliated with the DHVE-8 group (Deep sea Hydrothermal Vent Euryarchaeota group 8), belonging to the

DHVE II group. The DHVE groups were an uncultured archaeal lineage, first discovered in hydrothermal fields in Japan (Takai and Horikoshi, 1999). Indeed Reysenbach et al. (2006) isolated a member of the DHVE-2 (belonging to the DHVE I group), an obligate thermo-acidophilic sulfur- or iron-reducing heterotroph. Many of the closest relatives, for both the *mcrA* and the archaeal 16S rRNA gene sequences, were found in hypersaline alkalic environments or in oil reservoirs (Tables V.S1 and V.S2).

The bacterial 16S rRNA gene library displayed the highest diversity (Fig. V.6). Half of the sequences (50.5%) were closely affiliated with the homoacetogenic genus *Acetobacterium* (Table V.S3). This is consistent with the detection of 7.5 ± 0.7 mmol acetate L^{-1} slurry in the enrichments upon the harvest. Five sequences were also affiliated with the acetogen genus *Clostridium* sp. The second largest group of sequences was affiliated with the sulfate-reducing genus *Desulfovibrio* (14.3%). The other sulfate-reducer detected was close to *Desulfotignum toluenicum*, first isolated form an oil reservoir model column (Ommedal and Torsvik, 2007). Like the *mcrA* and archaeal 16S rRNA gene libraries, many closest relatives of the bacterial 16S rRNA gene sequences were found in oil reservoirs (Table V.S3).

Fig. V.4. Distance tree showing the affiliations of ethane-producing enrichment MCR amino acid sequences. Boostrap values (in percent) are based on 1000 replicates and are indicated at nodes for branches values ≥50% boostrap support. Gene sequences from this study are in boldface type. Numbers in bracket indicate the number of analyzed clones that have more than 97% sequence identity. The bar indicates 5% estimated phylogenesis divergence.

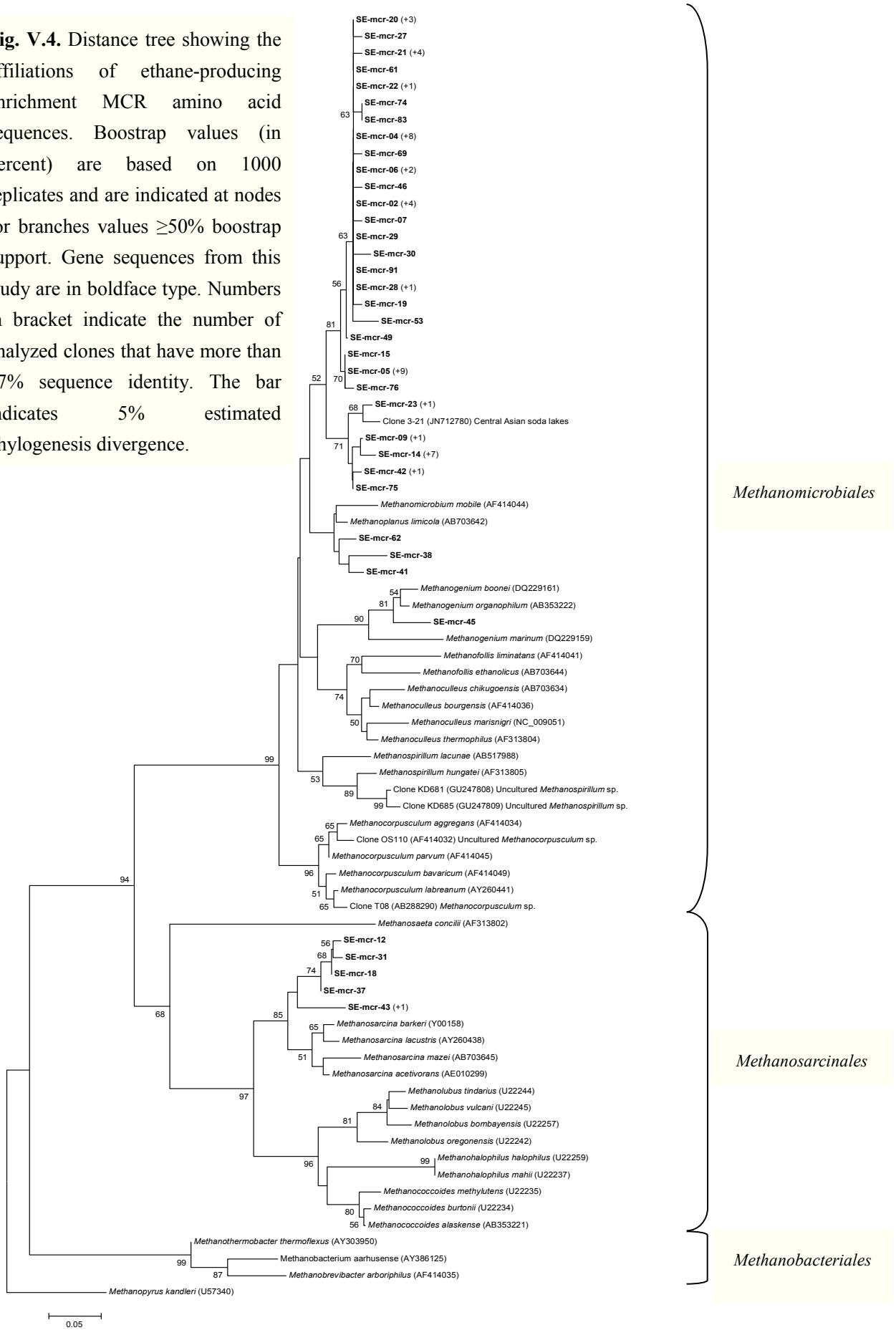

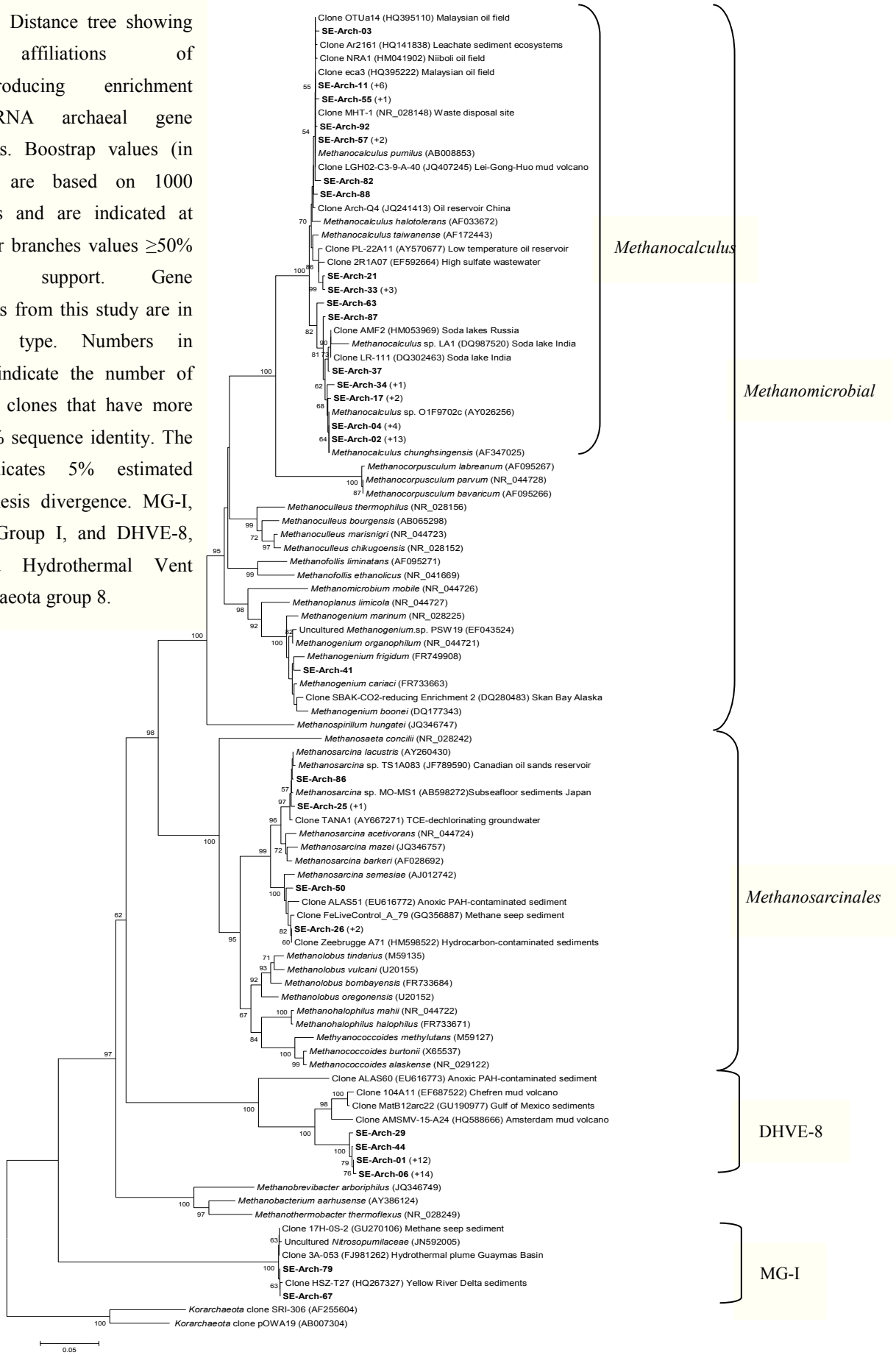

Fig. V.5. Distance tree showing the affiliations of ethane-producing enrichment 16S rRNA archaeal gene sequences. Boostrap values (in percent) are based on 1000 replicates and are indicated at nodes for branches values ≥50% boostrap support. Gene sequences from this study are in boldface type. Numbers in bracket indicate the number of analyzed clones that have more than 97% sequence identity. The bar indicates 5% estimated phylogenesis divergence. MG-I, Marine Group I, and DHVE-8, Deep-sea Hydrothermal Vent Euryarchaeota group 8.

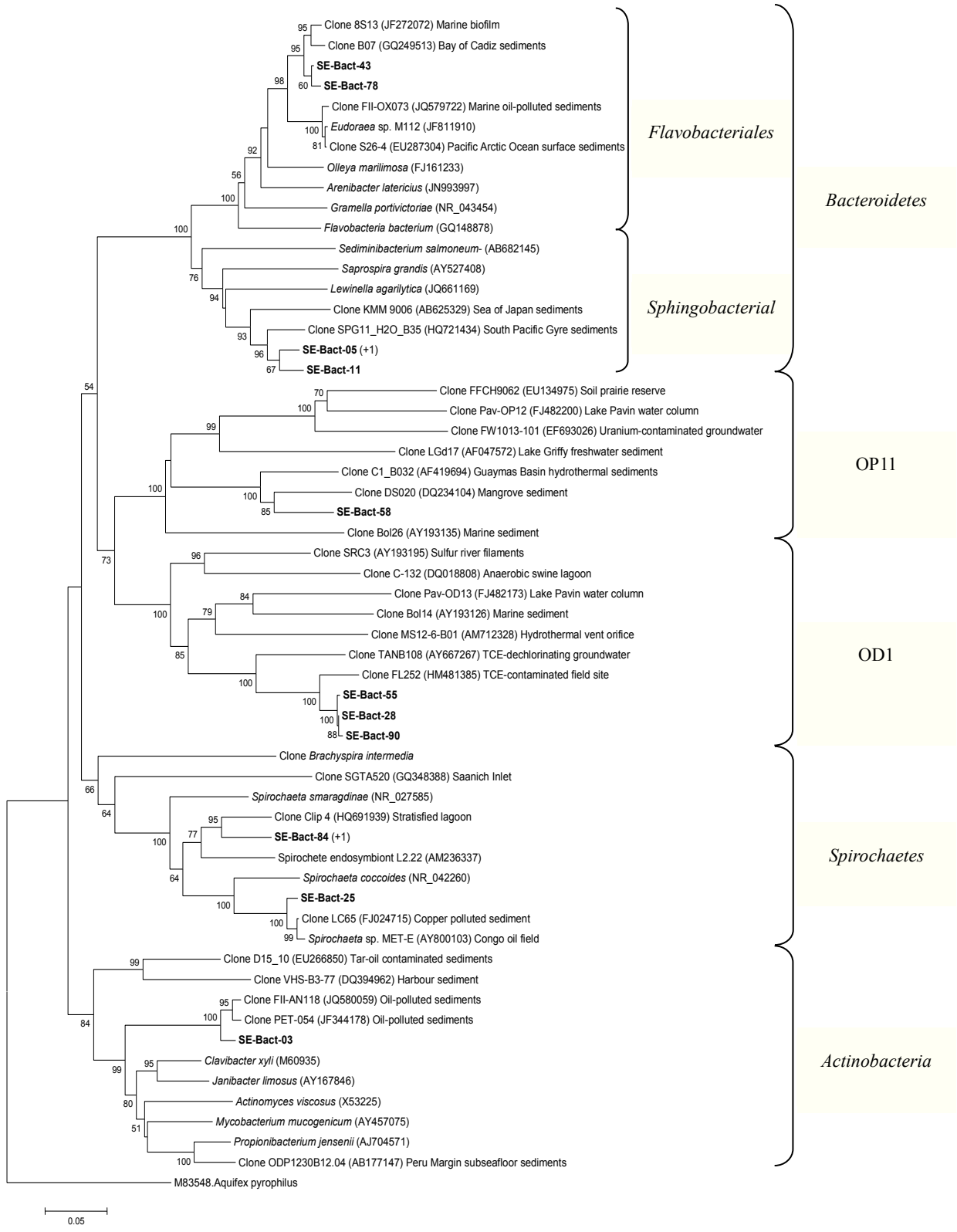

Fig. V.6. Distance tree showing the affiliations of ethane-producing enrichment 16S rRNA bacterial gene sequences. Boostrap values (in percent) are based on 1000 replicates and are indicated at nodes for branches values ≥50% boostrap support. Gene sequences from this study are in boldface type. Numbers in bracket indicate the number of analyzed clones that have more than 97% sequence identity. The bar indicates 5% estimated phylogenesis divergence.

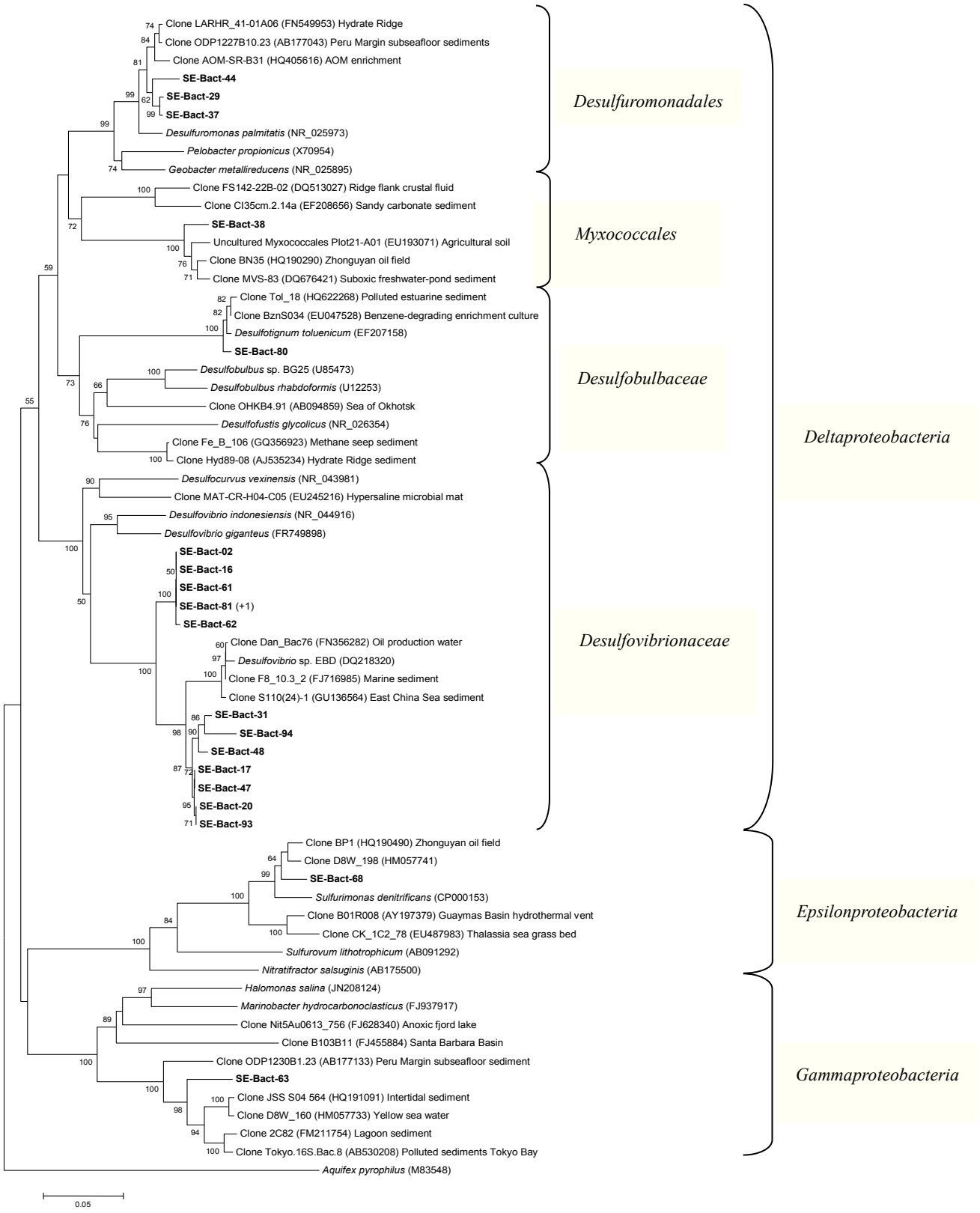

Fig. V.6. (continuted).

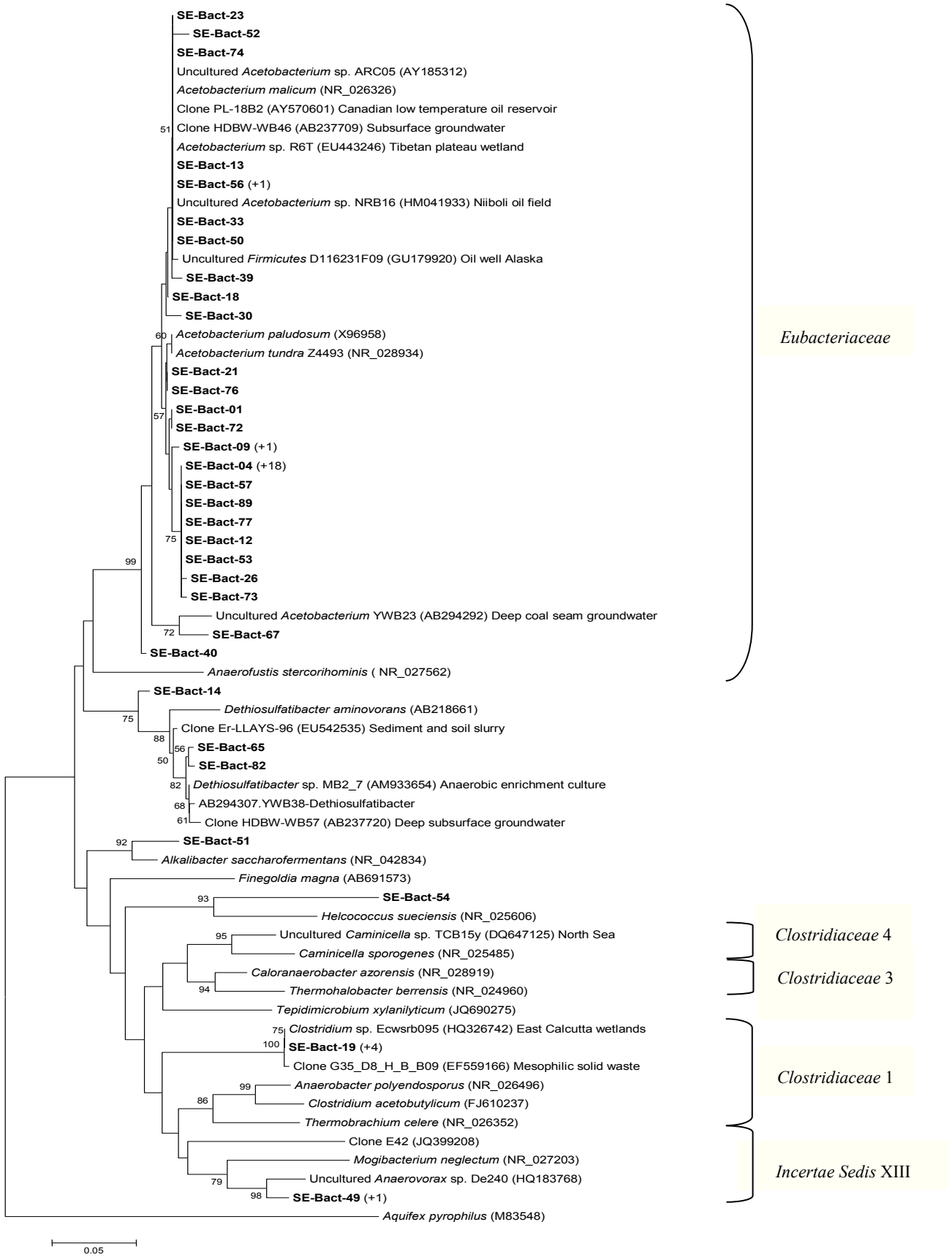

Fig. V.6. (continued).

V.5. DISCUSSION

V.5.1. Ethane-producing potential of tested substrates

This is the first study to compare the alkane-producing potential of C-2 and C-3 substrates with different functional groups in anoxic marine sediment. Ethane formation was found only in sediment incubated with ethylene or ethanethiol, with higher yields for the former substrate (Table V.1). Tests with sterilized sediment slurries, BES, and nitrate were negative to ethane and methane production, indicating that the ethane was of biological origin (Table V.2). The inhibitory effect of nitrate on ethane formation suggests that microorganisms requiring highly reduced conditions were involved in the process. In addition to methanogenesis, BES also inhibits reductive dechlorination of chloroethenes (Löffler et al., 1997), another process that requires highly reduced conditions. However, reductive dechlorination by pure cultures does not generate ethane but rather terminates at ethylene as an end product (Bradley, 2003). Accordingly, the results from BES were interpreted to infer the involvement of methanogenesis in ethane formation. Production of ethylene was observed together with ethanogenesis from ethanethiol, a result consistent with the observation of Oremland et al. (1988). Conversion of ethanethiol to ethylene (up to 0.05 μmol L^{-1} slurry) was also observed in sterilized and inhibited samples, suggesting that either abiotic processes and/or microbes other than methanogens can mediate this process. Given the high conversion efficiency of ethylene to ethane, we propose that ethylene, produced by non-biological and/or biological reactions from C-2 precursor molecules, is an important intermediate during transformation of ethanethiol to ethane. The conversion efficiencies of up to 38% for ethylene and 0.01% for ethanethiol are lower than or equal to those reported in previous studies using the same substrate concentrations: Koene-Cottaar and Schraa (1998) demonstrated quantitative transformation of ethylene to ethane in a freshwater enrichment, whereas the results in Oremland et al. (1988) are equivalent to conversion efficiencies ranging form 0.01% to 0.6% for ethanethiol to ethane in anoxic lake and estuary sediments.

In contrast, no ethane was detected in ethanol- and acetate-supplemented samples. The poor ethane-producing potential of ethanol is in agreement with the results of Oremland et al. (1988), who showed that 1 mM of ethanol barely stimulated ethane formation. Although a pure culture of *Methanosarcina barkeri* has been shown to convert ethanol to ethane (Belay and Daniels, 1988), the required concentrations of ethanol were high (>89 mM) and are unrealistic for most marine environments. Moreover, our results do not support the hypothesis of Claypool (1999) and

Hinrichs et al. (2006): the simultaneous presence of H_2 and acetate at high concentrations did not stimulate production of ethane, which would theoretically serve as an efficient sink for both intermediates of fermentation. The elevated concentrations of methane in acetate-supplemented slurries (Table V.1) indicate that instead of ethane, acetate was metabolized to methane and CO_2. However, our experiments were not performed under high methane partial pressure, which makes acetoclastic methanogenesis a thermodynamically less favorable reaction. Methane saturation is typical for many deep subseafloor sediments with which Hinrichs et al. (2006) made their observations. Future work that aims at testing this hypothesis would require the employment of high-pressure incubation equipments to simulate methane-rich settings.

V.5.2. Propane-producing potential from the selected substrates

All the selected C-2 and C-3 substrates have a poor potential for propane production. Like the case of ethanogenesis, our data do not support the hypothesis of Hinrichs et al. (2006) that condensation of DIC to C-2 compounds (acetate or related intermediates) leads to biogenic propane. Propanethiol was the only substrate that resulted in detectable propane production (Table V.1). The conversion efficiency (0.003%) was comparable to that of lake sediments (0.002%; Oremland et al., 1988) at the same propanethiol concentration. Despite this low yield, propane production from propanethiol was clearly suppressed by sterilization, BES, and nitrate (cf. Table V.2), suggesting that propanogenesis from propanethiol is a biological process that requires highly reduced conditions with the redox potential comparable to that for methanogenesis or reductive dechlorination.

Propanethiol, like its C-2 counterpart, resulted in formation of propylene in non-sterilized, sterilized, and inhibited samples. The yields of propylene from propanethiol in sterilized and inhibited samples (0.009 μmol L^{-1} slurry) were an order of magnitude lower than in non-sterilized samples (0.06 μmol L^{-1} slurry; Table V.1), suggesting biological enhancement of propylene production. However, conversion of propylene to propane was not observed. We conclude that in our case study, (i) propylene is an unlikely intermediate during the conversion from propanethiol to propane, and (ii) the enzymatic system involved in the conversion of ethylene to ethane does not mediate an analogous reaction involving propylene.

V.5.3. The role of H_2

One important question that follows the demonstration of alkane-producing potential is the relevance of these processes in natural environments. On the one hand, the in situ concentrations of the potential precursors need to be constrained. However, addressing the issue would require analytical solutions for detecting trace levels of low-molecular-weight compounds and is beyond the scope of the present work. On the other hand, the H_2 partial pressure used to stimulate the reactions is substantially higher than in nature (Hoehler et al., 1998; Lin et al., 2012). We therefore tested the effect of varying H_2 partial pressure on ethane formation from ethylene, the reaction that had the highest alkane-producing potential in our substrate tests (Table V.1).

Our results (Fig. V.2) showed that the minimal H_2 partial pressure required to stimulate ethanogenesis from ethylene in our slurry could be as low as 0.01% H_2 (equivalent to 120 nmol dissolved H_2 L^{-1} slurry). Given that ethane formation appeared to commence later in the incubation than methanogenesis (Fig. V.1), the actual minimal H_2 requirement at the inception of ethanogenesis from ethylene was probably lower than 0.01% in the headspace, as a substantial fraction of H_2 had already been consumed by methanogenesis and/or acetogenesis. The inferred mid-to-low nanomolar range of H_2 required for ethanogenesis is in the range of H_2 concentrations reported for some sedimentary environments (Hoehler et al., 1998, 1999; Lin et al., 2012), suggesting that high H_2 concentrations (80%-90%) used in typical laboratory incubation are not required for microbes to produce ethane from ethylene. Elevated initial H_2 partial pressure did enhance the ethane yield, but not in a linearly proportional way (Fig. V.2). In fact, the proportion of H_2 fueling ethylene reduction decreased from 0.6% under 0.01% initial H_2 to 0.004% under 90% initial H_2, suggesting that the marginal effect of H_2 diminished quickly. The proposition that microbial ethylene reduction does not require high H_2 concentrations is further supported by the high ethane yields in the glucose-supplemented slurries (Fig. V.2), in which H_2 would have been first generated via fermentation, consumed by microorganisms (e.g., Nüsslein and Conrad, 2000), and finally kept at low concentrations (Hoehler et al., 1998). It is unlikely that the carbon from glucose contributed directly to ethane via C-2 fermentation intermediates; otherwise, the addition of ethanol or acetate, two common products from glucose fermentation, should have resulted in ethane production. In summary, we conclude that ethylene reduction is feasible in natural sedimentary environments from the perspective of H_2 requirement; the main limiting factor for its relevance in nature is probably the availability of ethylene rather than H_2.

V.5.4. Gas ratios and isotopic fractionation

The gas ratio and isotopic compositions of gases from our ethylene-added slurries are not distinct from those reported for thermogenic natural gas. In our incubations, the ratio of $C_1/(C_2+C_3)$ was between 270 and 36,000, i.e., a range typically interpreted as mixed signals of biogenic and petroleum-derived gas (Bernard et al., 1976; Whiticar, 1999). This value is still higher than those reported for some cold, near-surface marine sediments (Bernard et al., 1976, Kvenvolden, 1988), suggesting either that methanogenic ethane production alone is not sufficient to explain the common existence of ethane in these environments, or that methane is selectively consumed in these environments, leading to the reported low $C_1/(C_2+C_3)$. The apparent isotope fractionation from ethylene to ethane ($\varepsilon_{ethane/ethylene}$ = -8.6±2.4‰) was small compared to reductive methanogens ($\varepsilon_{CO2/methane}$ = 39~95‰) based on the fractionation data reported in Whiticar (1999). Based on this observation, ethylene would have to be ^{13}C-depleted if ethylene reduction were an explanation for the isotopically light ethane (in a range between -70‰ and -44‰) reported in several anoxic marine sediments (Waseda and Didyk, 1995; Seifert et al., 1999; Paull et al., 2000). To our knowledge, there is no isotopic value reported for ethylene in cold, marine sediment.

V.5.5. Microbial ethanogenesis from ethylene

Our experimental data suggest that ethylene can be an effective precursor for biogenic ethane: it has the highest conversion efficiency among all the selected substrates. Very low H_2 concentration (as low as 120 nmol H_2 L^{-1} slurry) are adequate for ethanogenesis. Additionally, various reconnaissance studies have already demonstrated the wide occurrence of ethylene in cold marine environments (Hunt, 1974; Bernard et al., 1978; Kvenvolden and Redden, 1980; Whelan et al., 1980; Vogel et al., 1982; Kvenvolden, 1988; Seifert et al., 1999). There are at least two natural sources of ethylene. In soils and fresh water, microorganisms including fungi (Lindberg et al., 1979), cyanobacteria (Hodges and Campbell, 1998), and other bacteria (Nagahama et al., 1992; Fukuda et al., 1993) are found to produce ethylene, with aerobic degradation of methionine being the most common pathway. Our tests confirmed that addition of methionine also caused ethylene accumulation in the Wadden Sea sediment in the presence of oxygen (data not shown). Although this process only takes place aerobically, the swift variation in oxygen penetration at the depth scale of a few centimeters in the upper tidal flat of the German Wadden Sea (Jansen et al., 2009) may create conditions under which a fraction of ethylene generated via methionine decomposition

escapes aerobic degradation (Shennan, 2006) and is later involved in ethane formation. The second source comes from volatile chlorinated C-2 compounds, which can be produced naturally or anthropogenically (Bradley, 2003) and are present extensively in seawater (Gribble, 1994). Reductive dechlorination is a well documented process that converts chloroethenes into ethylene and other products under anoxic conditions (Bradley, 2003). However, the concentrations of chloroethenes in sediment appear to be rather low (Roose et al., 2001; Bravo-Linares and Mudge, 2007). Given the widespread occurrence of ethylene in deep subseafloor sediment (cf. Janus Web Database, http://www-odp.tamu.edu/database/) that is far away from the oxic zone of marine sediment, there might be other unknown pathways that produce ethylene under anoxic conditions.

In this study we sought to identify the microbial community present in the ethane-producing enrichments using molecular methods. Both *mcrA* and archaeal 16S rRNA gene libraries yielded a majority of sequences affiliated with the methanogenic order *Methanomicrobiales*. Most of the *mcrA* sequences were affiliated with an unknown methanogen belonging to the *Methanomicrobiales*, whereas a majority of the archaeal 16S rRNA gene sequences belonging to the methanogens were affiliated with the genus *Methanocalculus* within the *Methanomicrobiales*. It is therefore likely that the *mcrA* sequences that we recovered in this study belong to the genus *Methanocalculus*. Springer et al. (1995) and Luton et al. (2002) have previously compared the topology of the *mcrA* and the archaeal 16S rRNA gene phylogenetic trees, in order to assess the use of *mcrA* genes for the study of methanogenic community diversity. Unfortunately, both phylogenetic trees in this study do not show strong correlations regarding the genera within the order *Methanomicrobiales*. This has been previously observed, as the taxonomy of this order is complex (Luton et al., 2002).

In their study of a freshwater ethane-producing enrichment that was originally enriched via addition of *cis*-1,2-dichloroethene, Koene-Cottaar and Schraa (1998) observed via microscopy three different microorganisms, two of which were methanogens. One of these microbes was *Methanospirillum*-like and was considered a candidate responsible for ethanogenesis. This observation could be related to our *mcrA* sequences close to *Methanospirillum*, and the archaeal 16S rRNA gene sequences belonging to *Methanocalculus*. The first representative of the genus *Methanocalculus* was the species *Methanocalculus halotolerans*, isolated from a saline subsurface oil-producing well (Ollivier et al., 1998). This hydrogenotroph produces methane from H_2+CO_2 or formate, and requires acetate to grow. Since ethylene reduction to ethane is a hydrogenotrophic reaction, we consider the methanogen genus *Methanocalculus* a candidate carrying out

ethanogenesis. However, given the fact that ethanogenesis is a minor process in our incubation, the involvement of other methanogenic groups in our clone libraries cannot be ruled out.

The bacterial 16S rRNA gene clone library yielded a majority of sequences affiliated with the homoacetogenic genera *Acetobacterium* and *Clostridium* belonging to the *Firmicutes* phylum. Homoacetogens catalyze the formation of acetate. They grow with H_2 plus CO_2 as energy sources. This again is in accordance with the study of Koene-Cottaar and Schraa (1998), who observed one group of microorganisms capable of producing acetate from H_2 and CO_2. Sulfate-reducers, being the second-most frequently detected bacterial group in our methanogenic enrichment, could be sequences derived from earlier microbial generations during pre-incubation. An alternative but less probable explanation would be that sulfate salts were still present in the 100-fold diluted sediment slurry, supporting sulfate reducing bacteria that could survive at lower sulfate concentrations.

From the enzymatic point of view, ethylene is to some extent compatible with the enzymes and cofactors of the methanogenic pathways. The final step of methanogenesis is catalyzed by the methyl-coenzyme M reductase, and involves the coenzyme M (CoM) co-factor (Balch and Wolfe, 1979). This co-factor CoM is usually present in methanogens as mercaptoethanesulfonic acid (HS-CoM) or methylthioethanesulfonic acid (CH_3-S-CoM). Gunsalus et al. (1978) showed that the methyl-coenzyme M reductase complex present in the methanogen *Methanobacterium thermoautotrophicum* is able to use ethylthioethanesulfonic acid (ethyl-S-CoM) as a structural analog of CH_3-S-CoM to produce ethane from ethylene. Furthermore, Oremland (1981) also showed that ethyl-S-CoM could serve as a precursor for ethane production. However, the reason why methanogens produce ethane is not fully clear. Based on the toxicity of ethylene to methanogens, Koene-Cottaar and Schraa (1998) suggested that ethanogenesis is a detoxification mechanism for methanogens to adapt to the presence of ethylene before ethylene accumulates to inhibitory levels (>0.1%, Koene-Cottaar and Schraa, 1998; >5%, Oremland and Taylor, 1975). Although Koene-Cottaar and Schraa (1998) further reported that such a mechanism was not observed in a few selected methanogen isolates cultured under freshwater conditions, our results showed that it can be easily activated in anoxic estuarine sediment. Therefore, it is likely that the ability of reducing ethylene is more common in methanogens inhabiting marine environments.

V.6. CONCLUSIONS

1. Ethylene was the substrate that gave the highest yield of alkane production. Ethanethiol and propanethiol also stimulated production of ethane and propane, respectively, but with much lower conversion efficiencies than ethylene.

2. Methanogens were probably involved in the process of alkane production from ethylene, ethanethiol, and propanethiol.

3. The H_2 partial pressure required to stimulate ethanogenesis from ethylene was lower than 0.01% H_2 (120 nmol L^{-1} slurry), a concentration prevailing in some sedimentary environments.

4. The apparent isotope fractionations from ethylene to ethane ($\varepsilon_{ethane/ethylene}$) were -8.6±2.4‰. Therefore, if the isotopically light ethane in some geological records is to be explained by ethylene reduction, a depletion in ^{13}C of naturally occurring ethylene would be expected.

5. Molecular analysis of ethane-producing enrichments detected two main groups of sequences within the bacteria and the archaea. The first was affiliated with homoacetogenic bacteria responsible for the production of acetate. The second was affiliated with the methanogenic genus *Methanocalculus* within the archaea, and is a potential candidate for mediating ethanogenesis using ethylene as a substrate.

V.7. ACKNOELEDGEMENTS

This study is funded by the Deutscher Verband Flüssiggas (DVFG) and the State of Bremen through the project ″Ökologiefonds/Förderprogramm Angewandte Umweltforschung″. SX is funded by the China Scholarship Council; YSL is funded by the Deutsche Forschungsgemeinschaft through the Cluster of Excellence/Research Center MARUM; CL is funded through the Advanced Grant DARCLIFE by the European Research Council. We thank X. Prieto-Mollar for technical support and Gao Chen for the help with enrichments and Verena B. Heuer for assistance in determining concentrations of acetate.

V.8. REFERENCES

Akunna JC, Bernet N, Moletta R (1998) Effect of nitrate on methanogenesis at low redox potential. *Environ Technol* **19**: 1249-1254.

Altschul SF, Gish W, Miller W, Myers EW, Lipman DJ (1990) Basic local alignment search tool. *J Mol Biol* **215**:403-410.

Balch WE, Wolfe RS (1979) Specificity and biological distribution of coenzyme M (2-mercaptoethanesulfonic acid). *J Bacteriol* **137**: 256-263.

Belay N, Daniels L (1987) Production of ethane, ethylene and acetylene from halogenated hydrocarbons by methanogenic bacteria. *Appl Environ Microbiol* **53**:1604-1610.

Belay N, Daniels L (1988) Ethane production by *Methanosarcina barkeri* during growth in ethanol supplemented medium. *Antonie Van Leeuwenhoek* **54**: 113-125.

Bernard BB, Brooks JM, Sackett WM (1976) Natural gas seepage in the Gulf of Mexico. *Earth Planet Sci Lett* **31**:48-54.

Bernard BB, Brooks JM, Sackett WM (1978) Light hydrocarbons in recent Texas continental shelf and slope sediments. *J Geophys Res* **83**: 4053-4061.

Bradley PM (2003) History and Ecology of Chloroethene Biodegradation: A Review. *Bioremediat J* **7**: 81-109.

Bravo-Linares CM, Mudge SM (2007) Analysis of volatile organic compounds (VOCs) in sediments using in situ SPME sampling. *J Environ Monit* **9**: 411-418.

Casamayor EO, Schäfer H, Bañeras L, Pedrós-Alió C, Muyzer G (2000) Identification of and spatio-temporal differences between microbial assemblages from two neighboring sulfurous lakes: Comparison by microscopy and denaturing gradient gel electrophoresis. *Appl Environ Microbiol* **66**: 499-508.

Casamayor EO, Massana R, Benlloch S, Øvreås L, Díez B, Goddard VJ, Gasol JM, Joint I, Rodriguez-Valera F, Pedrós-Alió C (2002) Changes in archaeal, bacterial and eukaryal assemblages along a salinity gradient by comparison of genetic fingerprinting methods in a multipond solar saltern. *Environ Microbiol* **4**: 338-348.

Claypool GE (1999) Biogenic ethane-Where does it come from? *In* Abstr.AAPG Hedberg Res. Conf.: Natural gas formation and occurrence, 27-29. Durango, CO.

Crozier TE, Yamamoto S (1974) Solubility of hydrogen in water, seawater, and NaCl solutions. *J Chem Eng Data* **19**: 242-244.

Davis JB, Squires RM (1954) Detection of microbially produced gaseous hydrocarbons other than methane. *Science* **119**: 381-382.

Egorov AV, Ivanov MK (1998) Hydrocarbon gases in sediments and mud breccia from the central and eastern part of the Mediterranean Ridge. *Geo-Mar Lett* **18**:127-138.

Friedrich MW (2005) Methyl-coenzyme M reductase genes: Unique functional markers for methanogenic and anaerobic methane-oxidizing Archaea. *Methods Enzymol* **397**: 428-442.

Fukuda H, Ogawa T, Tanase S. 1993. Ethylene production by micro-organisms. *Adv. Microb. Physiol.* **35**: 275-306.

Garcia J-L, Patel BKC, Ollivier B (2000) Taxonomic, phylogenetic, and ecological diversity of methanogenic *Archaea*. *Anaerobe* **6**: 205-226.

Gribble GW (1994) The Natural Production of Chlorinated Compounds. *Environ Sci Technol* **28**: 310A–319A.

Gunsalus RP, Romesser JA, Wolfe RS (1978) Preparation of coenzyme M analogues and their activity in the methyl coenzyme M reductase system of Methanobacterium thermoautotrophicum. *Biochemistry* **17**: 2374-2377.

Hales BA, Edwards C, Ritchie DA, Hall G, Pickup RW, Saunders JR (1996) Isolation and identification of methanogen-specific DNA from blanket bog peat by PCR amplification and sequence analysis. *Appl Environ Microbiol* **62**: 668-675.

Hall TA (1999) BioEdit: a user-friendly biological sequence alignment editor and analysis program for Windows 95/98/NT. *Nucleic Acids Symp Ser* **41**: 95-98.

Hallam SJ, Girguis PR, Preston CM, Richardson PM, DeLong EF (2003) Identification of methyl coenzyme M reductase A (*mcrA*) genes associated with methane-oxidizing Archaea. *Appl Environ Microbiol* **69**:5483-5491.

Heuer V, Elvert M, Tille S, Krummen M, Mollar XP, Hmelo LR, Hinrichs K-U (2006) Online $\delta^{13}C$ analysis of volatile fatty acids in sediment/porewater systems by liquid chromatography-isotope ratio mass spectrometry. *Limnol Oceanogr Methods* **4**: 346-357.

Hinrichs K-U, Hayes JM, Bach W, Spivack AJ, Hmelo LR, Holm NG, Johnson CG, Sylva SP (2006) Biological formation of ethane and propane in the deep marine subsurface. *Proc Natl Acad Sci USA* **103**: 14684-14689.

Hodges CF, Campbell DA (1998) Gaseous hydrocarbons associated with black layer induced by the interaction of cyanobacteria and *Desulfovibrio desulfuricans*. *Plant Soil* **205**: 77-83.

Hoehler TM, Alperin MJ, Albert DB, Martens CS (1998) Thermodynamic control on hydrogen concentrations in anoxic sediments. *Geochim Cosmochim Acta* 62: 1745-1756.

Hoehler TM, Albert DB, Alperin MJ, and Martens CS (1999) Acetogenesis from CO_2 in an anoxic marine sediment. *Limnol Oceanogr* 44: 662-667.

Hunt JM (1974) Hydrocarbon geochemistry of Black Sea. *In* The Black Sea-Geology, Chemistry and Biology (ed. Degens ET, Ross DA), 499-504. American Association of Petroleum Geologists, Tulsa, Okla.

Jansen S, Walpersdorf E, Werner U, Billerbeck M, Böttcher ME, de Beer D (2009) Functioning of intertidal flats inferred from temporal and spatial dynamics of O_2, H_2S and pH in their surface sediment. *Ocean Dynam* **59**: 317-332.

Koene-Cottaar FHM, Schraa G (1998) Anaerobic reduction of ethene to ethane in an enrichment culture. FEMS Microbiol Ecol **25**: 251-256.

Krummen M, Hilkert AW, Juchelka D, Duhr A, Schlüter HJ, Pesch R (2004) A new concept for isotope ratio monitoring liquid chromatography/mass spectrometry. *Rapid Commun Mass Spectrom* **18**: 2260-2266.

Kvenvolden KA, Redden GD (1980) Hydrocarbon gas in sediment from the shelf, slope, and basin of the Bering Sea. *Geochim Cosmochim Acta* **44**: 1145-1150.

Kvenvolden KA (1988) Hydrocarbon gas in sediment of the Southern Pacific Ocean. *Geo-Mar Lett* **8**: 179-187.

Lane DJ (1991) 16S/23S rRNA sequencing. *In* Nucleic acid techniques in bacterial systematics (ed. Stackebrandt E, Goodfellow M), 115-175. John Wiley and Sons, New York, NY.

Larkin MA, Blackshields G, Brown NP, Chenna R, McGettigan PA, McWilliam H, Valentin F, Wallace IM, Wilm A, Lopez R, Thompson JD, Gibson TJ, Higgins DG (2007) Clustal W and Clustal X version 2.0. *Bioinformatics* **23**: 2947-2948.

Lin Y-S, Heuer VB, Goldhammer T, Kellermann MY, Zabel M, Hinrichs K-U (2012) Towards constraining H_2 concentration in subseafloor sediment: a proposal for combined analysis by two distinct approaches. *Geochim Cosmochim Acta* **77**:186-201.

Lindberg T, Granhall U, Berg B (1979) Ethylene formation in some coniferous forest soils. Soil Biol Biochem **11**: 637-643.

Löffler FE, Ritalahti KM, Tiedje JM (1997) Dechlorination of chloroethenes is inhibited by 2-bromoethanesulfonate in the absence of methanogens. Appl Environ Microbiol **63**: 4982-4985.

Ludwig W, Strunk O, Westram R, Richter L, Meier H, Yadhukumar, Buchner A, Lai T, Steppi S, Jobb G, Förster W, Brettske I, Gerber S, Ginhart AW, Gross O, Grumann S, Hermann S, Jost R, König A, Liss T, Lüßmann R, May M, Nonhoff B, Reichel B, Strehlow R, Stamatakis A, Stuckmann N, Vilbig A, Lenke M, Ludwig T, Bode A, Schleifer K-H (2004) ARB: a software environment for sequence data. *Nucleic Acids Res* **32**: 1363-1371.

Luton PE, Wayne JM, Sharp RJ, Riley PW (2002) The *mcrA* gene as an alternative to 16S rRNA in the phylogenetic analysis of methanogen populations in landfill. *Microbiology* **148**:

3521-3530.

Mariotti A, Germon JC, Hubert P, Kaiser P, Letolle R, Tardieux A, Tardieux P (1981) Experimental determination of nitrogen kinetic isotope fractionation: Some principles; illustration for the denitrification and nitrification processes. *Plant Soil* 62: 413-430.

Nagahama K, Ogawa T, Fujii T, Fukuda H (1992) Classification of ethylene-producing bacteria in terms of biosynthetic pathways to ethylene. *J Ferment Bioeng* **73**: 1-5.

Nüsslein B, Conrad R (2000) Methane production in eutrophic Lake Plußsee: seasonal change, temperature effect and metabolic processes in the profundal sediment. *Arch Hydrobiol* **149**: 597-623.

Ollivier B, Fardeau M-L, Cayol J-L, Magot M, Patel BKC, Prensier G, Garcia J-L (1998) *Methanocalculus halotolerans* gen. nov., sp. nov., isolated from an oil-producing well. *Int J Syst Bacteriol* **48**: 821-828.

Ommedal H, Torsvik T (2007) *Desulfotignum toluenicum* sp. nov., a novel toluene-degrading, sulphate-reducing bacterium isolated from an oil-reservoir model column. *Int J Syst Evol Microbiol* **57**: 2865-2869.

Oremland RS, Taylor BF (1975) Inhibition of methanogenesis in marine sediments by acetylene and ethylene: Validity of the acetylene reduction assay for anaerobic microcosms. *Appl Environ Microbiol* **30**: 707-709.

Oremland RS (1981) Microbial formation of ethane in anoxic estuarine sediments. *Appl Environ Microbiol* **42**: 122-129.

Oremland RS, Whiticar MJ, Strohmaier FE, Kiene RP (1988) Bacterial ethane formation from reduced, ethylated sulfur compounds in anoxic sediments. *Geochim Cosmochim Acta* 52: 1895-1904.

Paull CK, Lorenson TD, Borowski WS, Ussler III W, Olsen K, Rodriguez NM (2000) Isotopic composition of CH_4, CO_2 species, and sedimentary organic matter within samples from the Black Ridge: Gas source implications. *Proc Ocean Drill Prog Sci Results* **164**: 67-78.

Pruesse E, Quast C, Knittel K, Fuchs BM, Ludwig W, Peplies J, Glöckner FO (2007) SILVA: a comprehensive online resource for quality checked and aligned ribosomal RNA sequence data compatible with ARB. *Nucleic Acids Res* **35**: 7188-7196.

Roose P, Dewull J, Brinkman UAT, Langenhove HV (2001) Measurement of volatile organic compounds in sediments of the Scheldt Estuary and the Southern North Sea. Water Res **35**: 1478-1488.

Sassen R, Curiale JA (2006) Microbial methane and ethane from gas hydrate nodules of the Makassar Strait, Indonesia. *Org Geochem* **37**: 977-980.

Seifert R, Delling N, Richnow HH, Kempe S, Hefter J, Michaelis W (1999) Ethylene and methane in the upper water column of the subtropical Atlantic. *Biogeochemistry* **44**: 73-91.

Shennan JL (2006) Utilisation of C_2-C_4 gaseous hydrocarbons and isoprene by microorganisms. *J Chem Technol Biotechnol* **81**: 237-256.

Singleton DR, Furlong MA, Rathbun SL, Whitman WB (2001) Quantitative comparisons of 16S rRNA gene sequence libraries from environmental samples. *Appl Environ Microbiol* **67**: 4374-4376.

Springer E, Sachs MS, Woese CR, Boone DR (1995) Partial gene sequences for the A subunit of methyl-coenzyme M reductase (*mcrl*) as a phylogenetic tool for the family Methanosarcinaceae. *Int J Syst Bacteriol* **45**: 554-559.

Swinnerton JW, Lamontagne RA (1974) Oceanic distribution of low-molecular-weight hydrocarbons baseline measurements. *Environ Sci Technol* **8**: 657-663.

Takai K, Horikoshi K (1999) Genetic diversity of Archaea in deep-sea hydrothermal vent environments. *Genetics* **152**: 1285-1297.

Tamura K, Dudley J, Nei M, Kumar S (2007) MEGA4: Molecular evolutionary genetics analysis (MEGA) software version 4.0. *Mol Biol Evol* **24**: 1596-1599.

Vogel TM, Oremland RS, Kvenvolden KA (1982) Low-temperature formation of hydrocarbon gases in San Francisco Bay sediment (California, U.S.A.). *Chem Geol* **37**: 289-298.

Waseda A, Didyk BM (1995) Isotope compositions of gases in sediments from the Chile continental margin. *Proc Ocean Drill Prog Sci Results* **141**: 307-312.

Whelan JK, Hunt JM, Berman J (1980) Volatile C_1-C_7 organic compounds in surface sediments from Walvis Bay. *Geochim Cosmochim Acta* **44**: 1767-1785.

Whiticar MJ (1999) Carbon and hydrogen isotope systematics of bacterial formation and oxidation of methane. *Chem Geol* **161**: 291-314.

Widdel F, Bak F (1992) Gram-negative mesophilic sulfate-reducing bacteria. *In* The Prokaryotes, 2nd (ed. Balows A, Trüper HG, Dworkin M, Harder W, Schleifer K.-H), 3352-3378. Springer-Verlag, New York, NY.

Witt WW, Weber JB (1975) Ethylene Adsorption and Movement in Soils and Adsorption by Soil Constituents. *Weed Sci* **23**: 302-307.

V.S1. SUPPORTING TABLES

Table V.S1. Closest relatives of representative clones from the *mcrA* gene library from ethane producing enrichments.

Phylogenetic affiliation	Clone name	Closest relative (accession number) and origin	Sequence identity (%)
Methanospirillum sp.	SE-mcr-01	3-21 McrA (JN712780) Haloalkaliphilic methanogens in Central Asian soda lake sediments, Kulunda steppe, Russia	93
	SE-mcr-02 (=47/89/60/03)	3-21 McrA (JN712780) Haloalkaliphilic methanogens in Central Asian soda lake sediments, Kulunda steppe, Russia	93
	SE-mcr-04 (=52/55/65/13/44/11/92/93)	3-21 McrA (JN712780) Haloalkaliphilic methanogens in Central Asian soda lake sediments, Kulunda steppe, Russia	93
	SE-mcr-05 (=58/84/66/67/71/86/70/50/57)	3-21 McrA (JN712780) Haloalkaliphilic methanogens in Central Asian soda lake sediments, Kulunda steppe, Russia	93
	SE-mcr-06 (=82)	3-21 McrA (JN712780) Haloalkaliphilic methanogens in Central Asian soda lake sediments, Kulunda steppe, Russia	93
	SE-mcr-07	3-21 McrA (JN712780) Haloalkaliphilic methanogens in Central Asian soda lake sediments, Kulunda steppe, Russia	93
	SE-mcr-09 (=10)	3-21 McrA (JN712780) Haloalkaliphilic methanogens in Central Asian soda lake sediments, Kulunda steppe, Russia	93
	SE-mcr-14 (=26/17/25/36/85/54/63)	3-21 McrA (JN712780) Haloalkaliphilic methanogens in Central Asian soda lake sediments, Kulunda steppe, Russia	93
	SE-mcr-15	3-21 McrA (JN712780) Haloalkaliphilic methanogens in Central Asian soda lake sediments, Kulunda steppe, Russia	93
	SE-mcr-19	3-21 McrA (JN712780) Haloalkaliphilic methanogens in Central Asian soda lake sediments, Kulunda steppe, Russia	93
	SE-mcr-20 (=39/51/68)	3-21 McrA (JN712780) Haloalkaliphilic methanogens in Central Asian soda lake sediments, Kulunda steppe, Russia	93
	SE-mcr-21	3-21 McrA (JN712780)	93

(=35/77/34/33)	Haloalkaliphilic methanogens in Central Asian soda lake sediments, Kulunda steppe, Russia	
SE-mcr-22 (=73)	3-21 McrA (JN712780) Haloalkaliphilic methanogens in Central Asian soda lake sediments, Kulunda steppe, Russia	93
SE-mcr-23 (=81)	3-21 McrA (JN712780) Haloalkaliphilic methanogens in Central Asian soda lake sediments, Kulunda steppe, Russia	93
SE-mcr-27	3-21 McrA (JN712780) Haloalkaliphilic methanogens in Central Asian soda lake sediments, Kulunda steppe, Russia	93
SE-mcr-28 (=59)	3-21 McrA (JN712780) Haloalkaliphilic methanogens in Central Asian soda lake sediments, Kulunda steppe, Russia	93
SE-mcr-29	3-21 McrA (JN712780) Haloalkaliphilic methanogens in Central Asian soda lake sediments, Kulunda steppe, Russia	93
SE-mcr-30	3-21 McrA (JN712780) Haloalkaliphilic methanogens in Central Asian soda lake sediments, Kulunda steppe, Russia	93
SE-mcr-42 (=87)	3-21 McrA (JN712780) Haloalkaliphilic methanogens in Central Asian soda lake sediments, Kulunda steppe, Russia	93
SE-mcr-46	3-21 McrA (JN712780) Haloalkaliphilic methanogens in Central Asian soda lake sediments, Kulunda steppe, Russia	93
SE-mcr-49	3-21 McrA (JN712780) Haloalkaliphilic methanogens in Central Asian soda lake sediments, Kulunda steppe, Russia	93
SE-mcr-53	3-21 McrA (JN712780) Haloalkaliphilic methanogens in Central Asian soda lake sediments, Kulunda steppe, Russia	93
SE-mcr-61	3-21 McrA (JN712780) Haloalkaliphilic methanogens in Central Asian soda lake sediments, Kulunda steppe, Russia	93
SE-mcr-69	3-21 McrA (JN712780) Haloalkaliphilic methanogens in Central Asian soda lake sediments, Kulunda steppe, Russia	93
SE-mcr-74	3-21 McrA (JN712780) Haloalkaliphilic methanogens in Central Asian soda lake sediments, Kulunda steppe, Russia	93

	SE-mcr-75	3-21 McrA (JN712780) Haloalkaliphilic methanogens in Central Asian soda lake sediments, Kulunda steppe, Russia	93
	SE-mcr-76	3-21 McrA (JN712780) Haloalkaliphilic methanogens in Central Asian soda lake sediments, Kulunda steppe, Russia	93
	SE-mcr-83	3-21 McrA (JN712780) Haloalkaliphilic methanogens in Central Asian soda lake sediments, Kulunda steppe, Russia	93
	SE-mcr-91	3-21 McrA (JN712780) Haloalkaliphilic methanogens in Central Asian soda lake sediments, Kulunda steppe, Russia	93
Methanoplanus sp.	SE-mcr-38	*Methanoplanus petrolearius* DSM 11571 (NR_028240) Off shore oil field from Gulf of Guinea	85
	SE-mcr-41	*Methanoplanus petrolearius* DSM 11571 (NR_028240) Off shore oil field from Gulf of Guinea	87
	SE-mcr-62	*Methanoplanus petrolearius* DSM 11571 (NR_028240) Off shore oil field from Gulf of Guinea	87
Methanogenium sp.	SE-mcr-45	McrA2 (EU681934) Shallow sediments of the Pearl River Estuary, Southern China	94
Methanosarcina sp.	SE-mcr-12	TopMcrA32 (EU681941) Shallow sediments of the Pearl River Estuary, Southern China	96
	SE-mcr-18	TopMcrA32 (EU681941) Shallow sediments of the Pearl River Estuary, Southern China	95
	SE-mcr-31	TopMcrA32 (EU681941) Shallow sediments of the Pearl River Estuary, Southern China	95
	SE-mcr-37	TopMcrA32 (EU681941) Shallow sediments of the Pearl River Estuary, Southern China	95
	SE-mcr-43 (=79)	NTm2 (AB283003) Deep-sea sediment cores, Nankai Trough deep-sea sediment	94
	SE-mcr-90	aSm14 (GU322049) Wetland soil ecosystem	93

Table V.S2. Closest relatives of representative clones from the archaeal 16S rRNA gene library from ethane producing enrichments.

Phylogenetic affiliation	Clone name	Closest relative (accession number) and origin	Sequence identity (%)
Euryarchaeota			
Methanocalculus sp.	SE-Arch-02 (=18/35/58/75/91/13/66/74/09/31/46/73)	AMF2 (HM053969) Haloalkaliphilic methanogens from soda lakes in Kulunda Steppe, Altai, Russia	99
	SE-Arch-03	OTUa14 (HQ395110) Biodegraded Malaysian oil Reservoir, oil reservoir fluids	99
	SE-Arch-04 (=66/89/65/39/19)	AMF2 (HM053969) Haloalkaliphilic methanogens from soda lakes in Kulunda Steppe, Altai, Russia	99
	SE-Arch-11 (=12/15/20/30/27/36)	OTUa14 (HQ395110) Biodegraded Malaysian oil Reservoir, oil reservoir fluids	99
	SE-Arch-17 (=51/42)	AMF2 (HM053969) Haloalkaliphilic methanogens from soda lakes in Kulunda Steppe, Altai, Russia	99
	SE-Arch-21	PL-22A11 (AY570677) Waters of a low-temperature biodegraded Canadian oil reservoir	99
	SE-Arch-33 (=43/45/49)	PL-22A11 (AY570677) Waters of a low-temperature biodegraded Canadian oil reservoir	99
	SE-Arch-34 (=71)	AMF2 (HM053969) Haloalkaliphilic methanogens from soda lakes in Kulunda Steppe, Altai, Russia	98
	SE-Arch-37	AMF2 (HM053969) Haloalkaliphilic methanogens from soda lakes in Kulunda Steppe, Altai, Russia	99
	SE-Arch-55 (=64)	OTUa14 (HQ395110) Biodegraded Malaysian oil Reservoir, oil reservoir fluids	99
	SE-Arch-57 (=61/76)	OTUa14 (HQ395110) Biodegraded Malaysian oil Reservoir, oil reservoir fluids	99
	SE-Arch-63	LGH02-C3-9-A-40 (JQ407245) Lei-Gong-Huo mud volcano of eastern Taiwan	98
	SE-Arch-82	OTUa14 (HQ395110) Biodegraded Malaysian oil Reservoir, oil reservoir fluids	99
	SE-Arch-87	AMF2 (HM053969) Haloalkaliphilic methanogens from soda lakes in	99

		Kulunda Steppe, Altai, Russia	
	SE-Arch-88	Arch-Q4 (JQ241413)	96
		Chinese production water from oil reservoirs	
	SE-Arch-92	OTUa14 (HQ395110)	99
		Biodegraded Malaysian oil Reservoir, oil reservoir fluids	
Methanosarcina sp.	SE-Arch-25 (=28)	TS1A083 (JF789590)	99
		Canadian oil sands reservoir containing severely biodegraded oil	
	SE-Arch-26 (=81/83)	ALAS51 (EU616772)	99
		Anoxic PAH-contaminated sediment near Gwangyang bay	
	SE-Arch-50	ALAS51 (EU616772)	99
		Anoxic PAH-contaminated sediment near Gwangyang bay	
	SE-Arch-86	TS1A083 (JF789590)	99
		Canadian oil sands reservoir containing severely biodegraded oil	
Methanogenium sp.	SE-Arch-41	*Methanogenium cariaci*	97
		type strain DSM1497T (FR733663)	
DHVE-8	SE-Arch-01	AMSMV-15-A24 (HQ588666)	93
	(=05/08/10/22/23/40/	Amsterdam mud volcano sediment, East Mediterranean	
	59/69/77/84/90/47)	Sea	
	SE-Arch-06	AMSMV-15-A24 (HQ588666)	93
	(=14/16/52/53/78/07/	Amsterdam mud volcano sediment, East Mediterranean	
	54/60/62/38/70/85/68/	Sea	
	94)		
	SE-Arch-29	AMSMV-15-A24 (HQ588666)	93
		Amsterdam mud volcano sediment, East Mediterranean Sea	
	SE-Arch-44	AMSMV-15-A24 (HQ588666)	93
		Amsterdam mud volcano sediment, East Mediterranean Sea	
Crenarchaeota			
MG-I	SE-Arch-67	HSZ-T27 (HQ267327)	99
		Mud Wedge Sediments From Yellow River Delta; China	
	SE-Arch-79	HSZ-T27 (HQ267327)	99
		Mud Wedge Sediments From Yellow River Delta; China	

Table V.S3. Closest relatives of representative clones from the bacterial 16S rRNA gene library from ethane producing enrichments.

Phylogenetic affiliation	Clone name	Closest relative (accession number) and origin	Sequence identity (%)
Acetobacterium sp.	SE-Bact-01	NRB16 (HM041933) Crude-oil, large-insoluble-particle and formation-water components of the reservoir fluid from a non-flooded high-temperature petroleum reservoir, Japan	94
	SE-Bact-04 (=64/06/79/69/27/86/91/22/32/35/92/75/34/60/15/07/70/24)	Z 4493 (NR_028934) Tundra soil, Russia:Polar Ural	97
	SE-Bact-09 (=10)	F8_10.3_2 (FJ716985) Arenicola marina L. (lugworm) Bioturbated Mesocosm marine sediment from Cullercoats, Northumberland, United Kingdom	87
	SE-Bact-12	NRB16 (HM041933) Crude-oil, large-insoluble-particle and formation-water components of the reservoir fluid from a non-flooded high-temperature petroleum reservoir, Japan	97
	SE-Bact-13	PL-18B2 (AY570601) Waters of a low-temperature biodegraded Canadian oil reservoir	98
	SE-Bact-18	ARC05 (AY185312) Contaminated site, USA: MI, Montague	93
	SE-Bact-21	ARC05 (AY185312) Contaminated site, USA: MI, Montague	90
	SE-Bact-23	NRB16 (HM041933) Crude-oil, large-insoluble-particle and formation-water components of the reservoir fluid from a non-flooded high-temperature petroleum reservoir, Japan	98
	SE-Bact-26	NRB16 (HM041933) Crude-oil, large-insoluble-particle and formation-water components of the reservoir fluid from a non-flooded high-temperature petroleum reservoir, Japan	97
	SE-Bact-30	YWB23 (AB294292) Deep coal seam groundwater of northern Japan	89
	SE-Bact-33	NRB16 (HM041933) Crude-oil, large-insoluble-particle and formation-water components of the reservoir fluid from a non-flooded	99

	high-temperature petroleum reservoir, Japan	
SE-Bact-39	Z 4493 (NR_028934) Tundra soil, Russia:Polar Ural	97
SE-Bact-40	NRB16 (HM041933) Crude-oil, large-insoluble-particle and formation-water components of the reservoir fluid from a non-flooded high-temperature petroleum reservoir, Japan	91
SE-Bact-46	ARC05 (AY185312) Contaminated site, USA: MI, Montague	99
SE-Bact-50	R6T (EU443246) Acetobacterium zoigenese sp. nov., a new psychrophilic acetogenic bacterium from zoige wetland soil	99
SE-Bact-52	NRB16 (HM041933) Crude-oil, large-insoluble-particle and formation-water components of the reservoir fluid from a non-flooded high-temperature petroleum reservoir, Japan	97
SE-Bact-53	PL-18B2 (AY570601) Waters of a low-temperature biodegraded Canadian oil reservoir	98
SE-Bact-56 (=66)	R6T (EU443246) Acetobacterium zoigenese sp. nov., a new psychrophilic acetogenic bacterium from zoige wetland soil	99
SE-Bact-57	NRB16 (HM041933) Crude-oil, large-insoluble-particle and formation-water components of the reservoir fluid from a non-flooded high-temperature petroleum reservoir, Japan	97
SE-Bact-67	Z 4493 (NR_028934) Tundra soil, Russia:Polar Ural	90
SE-Bact-72	NRB16 (HM041933) Crude-oil, large-insoluble-particle and formation-water components of the reservoir fluid from a non-flooded high-temperature petroleum reservoir, Japan	93
SE-Bact-73	PL-18B2 (AY570601) Waters of a low-temperature biodegraded Canadian oil reservoir	98
SE-Bact-74	NRB16 (HM041933) Crude-oil, large-insoluble-particle and formation-water components of the reservoir fluid from a non-flooded high-temperature petroleum reservoir, Japan	98
SE-Bact-76	NRB16 (HM041933) Crude-oil, large-insoluble-particle and formation-water	93

		components of the reservoir fluid from a non-flooded high-temperature petroleum reservoir, Japan	
	SE-Bact-77	Z 4493 (NR_028934) Tundra soil, Russia:Polar Ural	97
	SE-Bact-89	PL-18B2 (AY570601) Waters of a low-temperature biodegraded Canadian oil reservoir	96
Clostridium sp.	SE-Bact-19 (=42/36/41/45)	G35_D8_H_B_B09 (EF559166) Microbial functional groups in a mesophilic anaerobic solid waste digestor	93
Dethiosulfatibacter sp.	SE-Bact-14	Er-LLAYS-96 (EU542535) Dechlorination of coplanar PCBs in sediment slurries, Taiwan	97
	SE-Bact-65	B-58 (HQ860702) Marine sediment and Qinghai lake	99
	SE-Bact-82	MB2_7 (AM933654) Enrichment of a dioxin-dehalogenating *Dehalococcoides* species in two-liquid phase cultures	96
Anaerovorax sp.	SE-Bact-49 (=59)	E42 (JQ399208) Xiao River receiving treated oxytetracycline production wastewater	99
Alkalibacter sp.	SE-Bact-51	OXIC-069 (JF344339) Marine oil-polluted sediments affected after the Prestige oil spill (Galicia, Spain)	92
Helcoccocus sp.	SE-Bact-54	CK06-06_Mud_MAS1B-28 (AB369171) Riser drilling mud fluid, Offshore the Shimokita Peninsula, Japan	99
Sphingobacteriales	SE-Bact-05 (=08)	SPG11_H2O_B35 (HQ721434) Oligotrophic abyssal marine sediments at the southern edge of the South Pacific Gyre	91
	SE-Bact-11	Asc-w-9 (EF632712) Contrasting aquatic environments of the high altitude Andean Altiplano (northern Chile)	97
Flavobacteriales	SE-Bact-43	8S13 (JF272072) Natural marine biofilms	98
	SE-Bact-78	S26-4 16S (EU287304) Surface sediments from the Pacific Arctic Ocean	99
Actinobacterium sp.	SE-Bact-03	PET-054 (JF344178) Marine oil-polluted sediments affected after the Prestige oil spill (Galicia, Spain)	92
Spirochaeta sp.	SE-Bact-25	LC65 (FJ024715)	95

		Sediments exposed to copper mining residues	
	SE-Bact-84 (=85)	Clip 4 (HQ691939)	92
		Unique stratified lagoon, the Clipperton atoll (N Pacific)	
OP11	SE-Bact-58	DS020 (DQ234104)	92
		Danshui river estuary of Northern Taiwan	
OD1	SE-Bact-28	FL252 (HM481385)	96
		Reductive dechlorination at a TCE-contaminated site	
	SE-Bact-55	FL252 (HM481385)	96
		Reductive dechlorination at a TCE-contaminated site	
	SE-Bact-90	FL252 (HM481385)	96
		Reductive dechlorination at a TCE-contaminated site	
Desulfovibrio sp.	SE-Bact-02	F8_10.3_2 (FJ716985)	99
	(=61/62)	Arenicola marina L. (lugworm) Bioturbated Mesocos marine sediment from Cullercoats, Northumberland, United Kingdom	
	SE-Bact-16	F8_10.3_2 (FJ716985)	99
		Arenicola marina L. (lugworm) Bioturbated Mesocos marine sediment from Cullercoats, Northumberland, United Kingdom	
	SE-Bact-17	S110(24)-1 (GU136564)	95
		Marine sediment, China: East China Sea, ShangHai	
	SE-Bact-20	F8_10.3_2 (FJ716985)	96
		Arenicola marina L. (lugworm) Bioturbated Mesocos marine sediment from Cullercoats, Northumberland, United Kingdom	
	SE-Bact-31	F8_10.3_2 (FJ716985)	89
		Arenicola marina L. (lugworm) Bioturbated Mesocos marine sediment from Cullercoats, Northumberland, United Kingdom	
	SE-Bact-47	S110(24)-1 (GU136564)	93
		Marine sediment, China: East China Sea, ShangHai	
	SE-Bact-48	35_EDB1 (AM882609)	93
		Hydrocarbon contamination gradient in a coastal sediment	
	SE-Bact-81 (=87)	F8_10.3_2 (FJ716985)	100
		Arenicola marina L. (lugworm) Bioturbated Mesocos marine sediment from Cullercoats, Northumberland, United Kingdom	
	SE-Bact-93	F8_10.3_2 (FJ716985)	96
		Arenicola marina L. (lugworm) Bioturbated Mesocos marine sediment from Cullercoats, Northumberland,	

		United Kingdom	
	SE-Bact-94	F8_10.3_2 (FJ716985) Arenicola marina L. (lugworm) Bioturbated Mesocos marine sediment from Cullercoats, Northumberland, United Kingdom	88
Desulfuromonadales	SE-Bact-29	LARHR_41-01A06 (FN549953) Sediment-free enrichment mediating the anaerobic oxidation of methane with sulfate (AOM) originating from the Hydrate Ridge, Coast of Oregon	97
	SE-Bact-37	LARHR_41-01A06 (FN549953) Sediment-free enrichment mediating the anaerobic oxidation of methane with sulfate (AOM) originating from the Hydrate Ridge, Coast of Oregon	92
	SE-Bact-44	LARHR_41-01A06 (FN549953) Sediment-free enrichment mediating the anaerobic oxidation of methane with sulfate (AOM) originating from the Hydrate Ridge, Coast of Oregon	99
Myxococcales	SE-Bact-38	BN35 (HQ190290) Bacterial diversity of Zhongyuan oil field, China	90
Desulfotignum sp.	SE-Bact-80	Tol_18 (HQ622268) Anoxic layer of a polluted microbial mat from Wadi Gaza, Palestine	98
Epsilonproteobacteria	SE-Bact-68	BP1 (HQ190490) Bacterial diversity of Zhongyuan oil field, China	93
Gammaproteobacteria	SE-Bact-63	JSS S04 564 (HQ191091) Coastal, intertidal sediment, German Wadden Sea	92

V.S2. SUPPORTING FIGURES

Fig. V.S1. Rarefaction analysis of the *mcrA* (closed circles), archaeal 16S rRNA (open circles), and bacterial 16S rRNA and genes from ethane producing enrichments, by using the RarFac program.tree (Fig. V.4). Furthermore theses sequences did not branch with any known methanogenic *mcrA* sequences. The remaining six sequences were affiliated with the nutritionally versatile genus *Methanosarcina* within the order *Methanosarcinales*.

Chapter VI

Concluding Remarks and Outlook

VI.1. SUMMARY AND CONCLUSIONS

This PhD thesis investigated microbial lipids and carbon flows in oxygen-deficient oceanic water and marine sediment in order to get a better understanding of the distribution, activity and turnover of microorganisms inhabiting in these environments.

Intact polar membrane lipids (IPLs) are ubiquitous as membrane constituents of every living organism. Due to rapid degradation after cell decay (White et al., 1979; Harvey et al., 1986), IPLs are used as biomarkers for living biomass and have been successfully applied in a variety of surface ecosystems, while the core lipids (hydrolysis of polar head groups from IPLs) represent fossil biomarkers of their source organisms. In the oxygen minimum zone (OMZ) of the Eastern Tropical North Pacific Ocean (ETNP), the distributions of eukaryotic, bacterial and archaeal lipids were investigated. IPLs were predominant by eukaryotic and bacterial IPLs. Intact polar isoprenoid glycerol dialkyl glycerol tetraethers (IP GDGTs), the biomarker for living Archaea, were detected after purification of the total lipids extract (TLE) using preparative HPLC. Highest concentrations of eukaryotic and bacterial IPLs (300~1400 ng/L) were found in the euphotic zone, and secondary peaks in concentration (15~40 ng/L) were observed within the OMZ, mimicking the zones of phototrophic and chemoautotrophic production in surface waters and the OMZ, respectively. Ten major eukaryotic and bacterial IPL classes were identified in the OMZ of the ETNP: monoglycosyldiacylglycerol (MGDG), diglycosyldiacylglycerol (DGDG), sulfoquinovosyldiacylglycerol (SQDG), glycosylceramides (Gly-Cer), phosphatidylethanolamine (PE) and its methylated derivatives (phosphatidyl-(N)-methylethanolamine (PME) and phosphatidyl-(N,N)-dimethylethanolamine) (PDME), phosphatidylglycerol (PG), phosphatidylcholine (PC), and betaine lipids (BL). Glycolipids, MGDG, DGDG and SQDG, dominated in the surface layer. Phospholipids (PE, PME, PDME, PG and PE) and BL became dominant (60%~100%) in the OMZ and deep oxycline layers where prokaryotes had elevated concentration (Podlaska et al., 2012). This zonation distribution of IPLs indicates that distinct microbial communities dominate in different water environments. The dominant fatty acid compositions for each IPL class were variable throughout the water column indicating distinct biological sources for each IPL group in each horizon. Due to similar biochemical functions and same ionic charge at physiological pH, SQDG and BL are known as substitute lipids for PG and PC, respectively. Under phosphorus-deficient conditions, these phospholipids were found to be substituted with their respective non-phosporous containing counterparts for eukaryotic

phytoplankton, cyanobacteria and anoxygenic phototrophs both in the lab and in the environment (Benning et al., 1993; 1995; Van Mooy et al., 2009; Popendorf et al., 2011). In the OMZ of the ETNP, SQDG/PG and BL/PC were calculated in water samples up to 1000 m water depth. High ratios were observed at depths where phosphate were abundant, which suggests that enrichment of substitute lipids is not be only impacted by phosphate limitation but also microbial community inhabiting in the oceanic water. Archaeal IP GDGTs, including mono- and diglycosidic isoprenoid glycerol dialkyl glycerol tetraethers (1Gly-GDGTs and 2Gly-GDGTs) were most abundant in the upper layers of the OMZ, and secondary abundance were observed in the deeper layers of the OMZ. Crenarchaeol dominated IP GDGTs indicates marine mesophilic Crenarchaeota as their prominent source. Highest abundance of Crenarchaeota and Euryarchaeota were detected in the euphotic zone and depths below OMZ (Podlaska et al., 2012), where IP GDGTs were hardly detected or with very low concentration. Secondary peaks in abundance of Crenarchaeota and Euryarchaeota were presented in the OMZ of the ETNP, where IP GDGTs were abundant.

In addition to IPLs, a series of glycerol ether core lipids were also presented in the OMZ of the ETNP. Nine groups of glycerol ether core lipids were present, namely, isoprenoid GDGTs (core iso-GDGTs), isoprenoid glycerol dialkanol diethers (iso-GDDs), branched glycerol dialkyl glycerol tetraethers (branched GDGTs), hydroxylated isoprenoid GDGTs and GDDs (OH-GDGTs and OH-GDDs), overly branched GDGTs (OB-GDGTs), sparsely branched GDGTs (SB-GDGTs), hybrid isoprenoid/branched GDGTs (IB-GDGTs) and a tentatively identified H-shaped GDGT (H-1020). Core iso-GDGTs were the most abundant components among all the glycerol ether core lipids, with an average relative abundance of 89%, followed by iso-GDDs (4%), branched GDGTs (2%) and OH-GDGTs (1%), and other four compounds with the concentration by one to three orders of magnitude lower than core iso-GDGTs were accounted as minor components in the OMZ of the ETNP. The maximum core iso-GDGTs were observed below the peak of corresponding IP GDGTs, suggest downward export and degradation of archaeal biomass within the OMZ. The high abundance of branched GDGTs in the OMZ is likely in-situ production rather than terrestrial input, due to the 400-600 km distance of the study area from the coast. IP GDGTs, OH-GDGTs and OH-GDDs exhibited higher abundances in the upper OMZ while the other glycerol ether core lipids were more enriched in mid OMZ, which suggests that IP GDGTs, OH-GDGTs and OH-GDDs might represent living signal, but the other core lipids were exported downward and accumulated in the mid OMZ with a longer residence time due to the presence of a permanent pycnocline and deep low-salinity intermediate waters. Alternatively, distinct origin of

IP GDGTs, OH-GDGTs and OH-GDDs from other glycerol ether lipids could also result in different depth profiles of these lipids. IP GDGTs were hydrolyzed by acid and analyzed for core composition. TEX_{86} were calculated for both IP GDGTs and core iso-GDGTs. Depth profiles of TEX_{86} values of core iso-GDGTs and IP GDGTs were similar throughout the water column, but only temperature estimated from TEX_{86} at surface waters could reflect in situ temperature.

Although archaeal IPLs are applied as biomarkers in a variety of environments, their application in low-activity subseafloor sediment remains controversial (cf. Lipp and Hinrichs, 2009; Schouten et al., 2010, Logemann et al., 2011). A radiotracer experiment combined with a modeling work were performed under conditions relevant to low-activity subsurface sediments to investigate the application of IPLs as biomarker in the deep biosphere, and further help us to better understand the turnover and activity of the benthic life. A synthesized archaeal model IPL (head group ^{14}C-labeled), ^{14}C-glucosyl-diphytanylglyceroldiether (GlcDGD), was used to examine the degradation kinetics of archaeal IPLs in anoxic marine sediments. In general, degradation rate constant of GlcDGD were by one to two orders of magnitude lower than bacterial phospholipids (Logemann et al., 2011) in the top 1 km of sediment column at a typical continental margin site. Comparing microbial community turnover times (1.6 to 73 kyrs) with half-life of archaeal IPL (20 to 310 kyrs), a substantial proportion of benthic archaeal IPL are fossil lipids (50%-84%). The combination of observed concentration profiles of subseafloor archaeal IPLs and degradation kinetics provide insight on the rates of archaeal lipid production and thus growth. Concentration profiles require that archaeal IPL synthesis rates to 1000 pg ml^{-1} yr^{-1} at the surface to 0.2 pg ml^{-1} yr^{-1} at 1 km depth to balance decay, equivalent to production of 7×10^5 to 140 archaeal cells ml^{-1} sediment yr^{-1}. Due to more than 80% archaeal IPLs are fossil fraction, previous estimates of community size in the deep biosphere might be overestimated. Based on IPL analysis alone, it is difficult to distinguish whether archaea or bacteria is more dominant in the deep biosphere.

Ethane and propane are widely detected in the anoxic cold marine sediments and considered as biological products of microbial metabolism (e.g. Oremland et al., 1988; Koene-Cottaar et al., 1998; Hinrichs et al., 2006). In this thesis, ethane- and propane-producing potential of a series of substrates, including alkenes, alcohols, thiols, and carboxyl acids with C-2 or C-3 skeleton, were firstly compared in the anoxic sediment collected from the German Wadden Sea. Ethane production was observed in the sediment supplemented with ethylene and ethanethiol, and propane formation was found in the propanethiol added sample. Among all the substrates that

gave a positive response for alkane production, ethylene had maximum conversion efficiency (up to 38%). Experiments with sterilized sediment or chemicals inhibitory to methanogenesis suggested that methanogens were involved in the processes of alkane generation. The H_2 concentration required for ethanogenesis from ethylene was lower than 0.01% H_2 (equivalent to 120 nmol dissolved H_2 L^{-1} slurry). In addition, an ethane-producing enrichment with ethylene as the substrate was used for molecular characterization. The Homoacetogens *Acetobacterium* and *Clostridium* were the most abundant in the bacterial 16S rRNA gene library, whereas *Methanocalculus* and sequences belonging to the *Methanomicrobiales* were the dominant groups in the archaeal 16S rRNA gene library and the *mcrA* gene library. *Methanocalculus* is a candidate responsible for ethanogenesis from ethylene, but other methanogens detected in the gene libraries cannot be ruled out.

VI.2. OUTLOOK

This thesis targeting the distribution and turnover of microbial lipids, as well as carbon flows in oxygen-deficient oceanic water and marine sediment, gave us a better understanding of composition ecology and activity of microbial communities under suboxic or anoxic conditions. However, some new topics focused on questions raised up by our conducted studies need to be demonstrated in future works.

In the OMZ of the ETNP, high ratios between phosphorous-containing lipids and their corresponding non-phosphorous-containing substitute lipids, were observed at depths where phosphate were abundant. To investigate whether it is a common phenomenon or only restricts to the OMZ of the ETNP, more water column samples (especially deep depths) are required to be analyzed for the substitute lipids composition. If enough filter samples could be obtained in the future expeditions, sugar cleavage (Lin et al., 2010) could be performed on 1Gly- and 2Gly-GDGTs after purification. Analyzing stable carbon isotopic composition of sugar head group could provide further information on biological sources of the IP GDGTs in the open ocean.

The biological sources and environmental importance of the minority glycerol ether core lipids, such as branched GDGTs, OH-GDGTs, OH-GDDs, OB-GDGTs, IB-GDGTs, SB-GDGTs and H-1020, still remain unknown. Environmental samples with higher abundance of these lipids could be used for incubation experiment in order to get microbial enrichment. Further analysis target on the enrichment, such as IPL analysis to check the presence of intact forms of these core

lipids and phylogenetic analysis, could give us a better understanding of the biological origin of these core lipids.

According to our modeling results of the IPL degradation, a distinction between archaeal and bacteria dominance is different in the deep biosphere, and other biomolecular tools such as DNA (e.g., Dell'Anno and Danovaro, 2005; Corinaldesi et al., 2011) and cell wall components (Lomstein et al., 2012) will likely face similar problems as IPL. And therefore, other alternative approaches are proposed to examine deep biosphere, such as separating cellular and extracellular lipids to investigate the proportion of living biomass (Braun, 2011), or using labile but less abundant IPLs to provide useful information on the activity of the deep biosphere.

Our results of biological ethane and propane-producing suggest that ethylene can be an effective precursor for biogenic ethane in anoxic estuarine sediment. The sediment supplemented with acetate or both acetate and inorganic carbon did not produce ethane and propane, which disagrees with the previous studies of deep marine sediments (Claypool, 1999; Hinrichs et al., 2006). Further incubations could be performed with potential precursors under conditions relevant to deep subsurface sediment, e.g. low temperature and higher pressure, to investigate precursors for ethane and propane formation in the deep biosphere.

VI.3. REFERENCES

Benning C, Beatty JT, Prince RC, Somerville CR (1993) The sulfolipid sulfoquinovosyldiacylglycerol is not required for photosynthetic electron transport in *Rhodobacter sphaeroides* but enhances growth under phosphate limitation. *Proc Natl Acad Sci USA* **90**: 1561-1565.

Braun S (2011) Master thesis (University of Bremen, Bremen, Germany)

Claypool GE (1999) Biogenic ethane-where does it come from? *In* Abstr. AAPG Hedberg Res, 27-29. Conf.: Natural gas formation and occurrence, Durango, CO.

Corinaldesi C, Barucca M, Luna GM, Dell'Anno A (2011) Preservation, origin and genetic imprint of extracellular DNA in permanently anoxic deep-sea sediments. *Mol Ecol* **20**: 642-654.

Dell'Anno A, Danovaro R (2005) Extracellular DNA plays a key role in deep-sea ecosystem functioning. *Science* **309**: 2179.

Harvey HR, Fallon RD, Patton JS (1986) The effect of organic matter and oxygen on the

degradation of bacterial membrane lipids in marine sediments. *Geochim Cosmochim Acta* **50**: 795-804.

Hinrichs K-U, Hayes JM, Bach W, Spivack AJ, Hmelo LR, Holm NG, Johnson CG, Sylva SP (2006) Biological formation of ethane and propane in the deep marine subsurface. *Proc Natl Acad Sci USA* **103**:14684-14689.

Koene-Cottaar FHM, Schraa G (1998) Anaerobic reduction of ethane to ethane in an enrichment culture. *FEMS Microbiol Ecol* **25:** 251-256.

Lin YS, Lipp JS, Yoshinaga M, Lin SH, Elvert M, Hinrichs K-U (2010) Intramolecular stable carbon isotopic analysis of archaeal glycosyl tetraether lipids. *Rapid Commun Mass Spectrom* **24**: 2817-2826.

Lipp JS, Hinrichs K-U (2009) Structural diversity and fate of intact polar lipids in marine sediments. *Geochim Cosmochim Acta* **73**: 6816-6833.

Logemann J, Graue J, Köster J, Engelen B, Rullkötter J, Cypionka H (2011) A laboratory experiment of intact polar lipid degradation in sandy sediments. *Biogeosciences* **8**: 2547-2560.

Lomstein BA, Langerhuus AT, D'Hondt S, Jørgensen BB, Spivack AJ (2012) Endospore abundance, microbial growth and necromass turnover in deep sub-seafloor sediment. *Nature* **484**: 101-104.

Oremland RS, Whiticar MJ, Strohmaier FE, Kiene RP (1988) Bacterial ethane formation from reduced, ethylated sulfur compounds in anoxic sediments. *Geochim Cosmochim Acta* **52:** 1895-1904.

Podlaska A, Wakeham SG, Fanning KA, Taylor GT (2012) Microbial community structure and productivity in the oxygen minimum zone of the eastern tropical North Pacific. *Deep Sea Res I* **66**: 77-89.

Popendorf KJ, Tanaka T, Pujo-Pay M, Lagaria A, Courties C, Conan P, Oriol L, Sofen LE, Moutin T, Van Mooy BAS (2011). Gradients in intact polar diacylglycerolipids across the Mediterranean Sea are related to phosphate availability. *Biogeosciences* **8**: 3733-3745.

Schouten S, Middelburg JJ, Hopmans EC, Sinninghe Damsté JS (2010) Fossilization and degradation of intact polar lipids in deep subsurface sediments: A theoretical approach. *Geochim Cosmochim Acta* **74**: 3806-3814.

Van Mooy BAS, Fredricks HF, Pedler BE, Dyhrman ST, Karl DM, Koblížek M, Lomas MW, Mincer TJ, Moore LR, Moutin T, Rappé MS, Webb EA (2009) Phytoplankton in the ocean

use non-phosphorus lipids in response to phosphorus scarcity. *Nature* **458**: 69-72.

White DC, Davis WM, Nickels JS, King JD, Bobbie RJ (1979) Determination of the sedimentary microbial biomass by extractible lipid phosphate. *Oecologia* **40**: 51-62.

ACKNOWLEDGEMENTS

The deepest thanks certainly go to my supervisor, Prof. Dr. Kai-Uwe Hinrichs. I would like to thank him for providing me this PhD position and gave me an opportunity to enter the exciting world of IPL and the deep biosphere. I feel very fortunate to have the opportunity to work under his supervision. Thanks for his guidance by inspiring ideas and fruitful discussion, and I especially appreciate his trust, encouragement, patient and continuous support throughout years.

I would like to thank Prof. Dr. Stuart G. Wakeham for giving me an opportunity to work with him. Three years ago when we first met in Bremen, he patiently introduced me the OMZ literatures and answered my questions, although I was a student without any experience in working with water column samples at that time. Thanks for his encouragement, support and discussions during last years. Many thanks to Timothy G. Ferdelman for introducing me to the radiotracer world and let me work in his lab. I also would like to thank Prof. Dr. Gesine Mollenhauer for agreeing to be my second supervisor. Many thanks to my PhD committee for reviewing my thesis.

All of my work would not have been possible without generous support of Dr. Julius S. Lipp, Dr. Florence Schubotz, Dr. Yu-shih Lin and Dr. Xiao-Lei Liu. I would like to thank them for teaching me so many big and small things, e.g. experiment design, the basic lab working procedures, data processing and writing. Thanks a lot for helpful suggestions and comments on my works. Thank Flo and Julius inviting me to their apartment for dinner when I was first in Bremen. I still remember the delicious lasagna and duck that Flo cooked. I would like to thank Yu-shih, who encouraged me a lot when I was depressed. Thank her both for helping me preparing my first presentation, and also for sharing interesting detective novels and TV plays with me. I particularly want to thank Xiao-Lei for his help not only as a colleague in the lab but also as a friend. I will never forget the things that he helped me, e.g., finding apartment, picking up me at the airport, helping me carrying my heavy luggage and so on. I could not remember how many questions I asked him during the last four years, but he is always patient with me.

I would like to thank Dr. Marcus Elvert for teaching me interpretation of GC-MS data when I first started to work in the lab. I must thank our excellent lab technician Xavier Prieto-Mollar for keeping the instruments running and organizing the lab in a good order. I would like to thank Jenny Wendt and Jessica Arndt for ordering lab staff and all the other support in the lab. Many thanks to our secretary, Birgit Schmincke, who is very patient and helped me with all the administrative stuff. I still remember the scenes that she took me to the international office for registration and introduced our campus in 2008. I would like to thank Evert Kramer for his assistance in computer and software issues.

I must thank Dr. Gunter Wegener for his helpful suggestions for my work. He patiently showed me how to use "CuO oven" in his lab. I benefit a lot from the pleasant collaboration with Dr. Cassandre Sara Lazar. She is a very kind and patient lady, and always replied my email quickly even when she was on vacation. Dr. Arne Leider kindly

helped me translate thesis abstract into German. Dr. Verena Heuer kindly provided her sediment sample, and taught me processing of acetate isotopic data. Dr. Matthias Kellermann and Dr. Marcos Yoshinaga taught me lipid extraction at the beginning of my PhD, and their good suggestions for my work. Dr. Travis Meador helped me to interpret PCA results and answer my questions about writing in English. Jan Schröder voluntary informs us newest publications. Dr. Eoghan P. Reeves helped me to measure gas samples on his GC machine. Rong Zhu generously shared snacks during late night work hours in the office. Guangchao Zhuang patiently taught me how to use refractometer. Dr. Lars-Peter Wörmer showed me how to install and use our data processing software. I am lucky to work in a friendly and lovely lab with all the present and former group members, Dr. Frauke Schmidt, Dr. Chun Zhu, Becker Kevin, Raika Himmelsbach, Dr. Marshall Bowles, Dr. Martin Könneke, Dr. Gerard Versteegh, Bernhard Viehweger, Susanne Alfken, Nadine Broda, Wolf Dummann, Nadine Goldenstein, Gina Kuippers, Franziska Pfeifer, Nadine Smit, Tim Stoltmann, Christopher Dibke, Stefan Braun, Felix Elling, Dr. Solveig Bühring, Dr. Pamela Rossel, Dr. Lars Hoffmann, Dr. Tobias Ferdinand Ertefai, Marlene Bausch and Dr. Julio Sepúlveda.

I would like to thank my friends, Mingming, Yixian, Chenjian, Liping, Joana, Miao，Guodong and Pengfei for chatting, cooking and a lot of fun in our spare time. Thank Haiyan for taking care of my parents in Munich. I need to thank Ursula for teaching me German, although I was not a good student. Min Hui shared her apartment when I did not find a new place. Thank Gao Chen for his help with enrichment.

A special thanks to Bremen, the city where I met my husband Dongchao Hou. Thank you for your support and invaluable help for my PhD study. Thank you for sharing so much laughter, sadness and happiness in our life, and the most importantly for coming into my life, loving me, taking care of me and making me smile every day.

感谢毕彩丰教授，范玉华教授多年来对我的教育，培养，关心与出国留学的支持。感谢我的好朋友们：小五，丁小玲，贾丽，璐璐，老大，秀秀，娜娜，是你们真挚的友情，让我一路有爱陪伴。

谢谢爸爸妈妈二十九年来对我无私的爱与坚定的支持，使我成为最幸福的女儿。感谢舅舅舅妈待我如女儿般的关心与呵护。谢谢爷爷，姑姑，姑父一直以来对我的爱。谢谢哥哥，大任，陈瀚在学业上的相互鼓励，你们的乐观与支持陪伴我开心的成长。感谢所有的家人这些年来对我的爱护。

感谢国家留学基金委(CSC)为我提供四年奖学金。

最后谢谢所有关心，帮助过我的人。谢谢大家。